Oscillations in the cerebral cortex: mechanisms of control and alterations in a transgenic model of Down syndrome

Marcel Ruiz Mejías

IDIBAPS

Universitat de Barcelona

OSCILLATIONS IN THE CEREBRAL CORTEX: MECHANISMS OF CONTROL AND ALTERATIONS IN A TRANSGENIC MODEL OF DOWN SYNDROME

Doctoral Thesis

Marcel Ruiz Mejías

2013

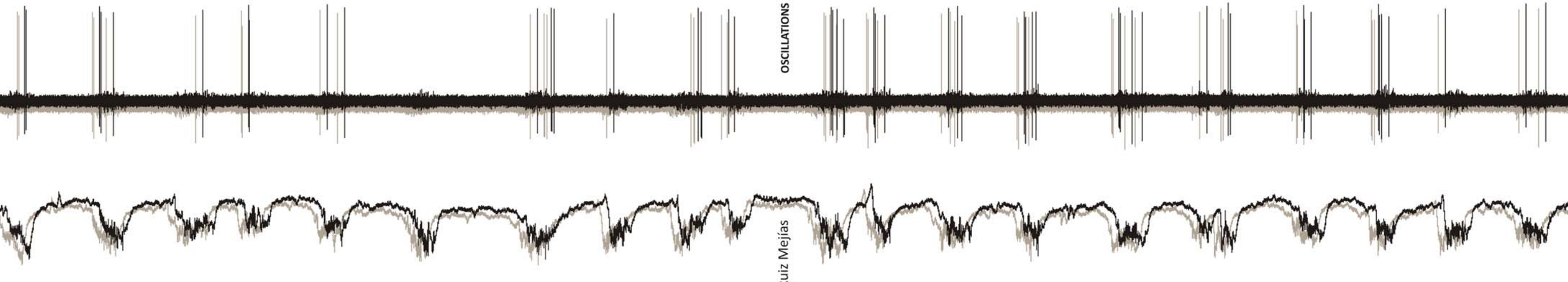

Director: María Victoria Sánchez-Vives

OSCILLATIONS IN THE CEREBRAL CORTEX: MECHANISMS OF CONTROL AND ALTERATIONS IN A TRANSGENIC MODEL OF DOWN SYNDROME

2013 Marcel Ruiz Mejías

Universitat de Barcelona
Institud d'Investigacions Biomèdiques August Pi i Sunyer
Programa de Doctorado en Biomedicina

OSCILLATIONS IN THE CEREBRAL CORTEX: MECHANISMS OF CONTROL AND ALTERATIONS IN A TRANSGENIC MODEL OF DOWN SYNDROME

Área: Neurociencias clínicas y experimentales
Grupo: Redes Corticales
Línea de investigación: Neurofisiología y computación en sistemas corticales

Doctorando:

Marcel Ruiz Mejías

Directora de tesis:

María Victoria Sanchez Vives

A mis padres

"I count him braver who overcomes his desires than him who conquers his enemies; for the hardest victory is over self"

Aristotle

ACRONYMS AND ABBEVIATIONS

AHP: Afterhyperpolarization current
ANOVA: Analysis of variance
ATP: Adenosin tri-phosphate
AP: Anteroposterior (axis)
APP: Amyloid-precursor protein
APV: D-(-)-2-Amino-5-phosphonopentanoic acid
BAC: Bacterial artificial chromosome
BSA: Bovin serum albumin
CRG: Crentre de Regulació Genòmica
CSD: Current source density
CV: Coeficient of variation
DLPFC: Dorsolateral prefrontal cortex
CNQX: 6-Cyano-7-nitroquinoxaline-2,3-dione
DSCR: Down syndrome critical region
DYRK1A: dual-specificity tyrosine-(Y)-phosphorylation regulated kinase 1A
EC50: Effective concentration 50
ECoG: Electrocorticogram
EEG: Electroencephalogram
ESD: Extreme studentized deviate
EPSP: Excitatory post-synaptic potential
IDIBAPS: Institut d'Investigacions Biomèdiques August Pi i Sunyer
I_{NaP}: Persistent sodium current
IPSP: Inhibitory post-synaptic potential
fPSP: field post-synaptic potential
$GABA_{A-B}$: gamma-aminobutyric acid receptor A-B
LFP: Local field potential
LORETA, e/sLORETA: (exact/standard) Low Resolution Electromagnetic Tomography
LTCP: Low treshold calcium potential
MEG: Magnetoencephalogram
mRNA: messenger ribonucleic acid
mPFC: medial prefrontal cortex
L: Lateral (axis)
M1: Primary motor cortex
MUA: Multiunit activity
NMDA: N-Methyl-D-aspartate
NRT: *nucleus reticularis talami*
Non-REM: Non-rapid eye movement
PBS: Phosphate buffered saline
PCA: Principal component analysis

PETH: Peri-event time histogram
PV: Parvalbumin
PYR: Pyramidal
PRBB: Parc de Recerca Biomèdica de Barcelona
REM: Rapid eye movement
S1: Primary somatosensory cortex
SD: Standard deviation
SEM: Standard error of mean
SWS: Slow wave sleep
TSM: Transcranial magnetic stimulation
VPM: Ventral postero-medial thalamus
V1: Primary visual cortex
YAC: Yeast artificial chromosome
YFP: Yellow fluorescent protein

INDEX

LIST OF FIGURES

FOREWORD

Entender la función del cerebro a través de su actividad rítmica es lo que me hizo interesarme en el laboratorio de Mavi Sánchez-Vives. El modo como empecé a trabajar en este laboratorio, que fue unos días después de que Mavi me propusiera asistir a un experimento de registro de oscilaciones lentas *in vitro* –al que fui el mismo día después de una breve conversación que mantuvimos cuando le quise preguntar qué hacían en el laboratorio- aseguró la oportunidad única que me fue brindada para adentrarme en los capos de la neurociencia de sistemas. Por todo esto, me gustaría agradecer a Mavi por darme esa oportunidad y por creer en mí.

Entre esos primeros días en el laboratorio, Mavi me propuso embarcarme en un proyecto para estudiar la función cortical en ratones genéticamente modificados que presentaban aspectos de las disfunciones cerebrales en el síndrome de Down, los ratones TgDyrk1A. A parte de todo el aprendizaje que obtuve con este estudio, este proyecto también supuso una colaboración muy enriquecedora con María Martínez de Lagrán y Mara Dierssen, postdoc y investigadora principal, respectivamente, del laboratorio de Neurobiología Celular y de Sistemas en el Centro de Regulación Genómica de Barcelona. Este fue de hecho el pretexto para descubrir el complejo mundo 'oscilante' que hay detrás de la función cortical, donde tuve la oportunidad de poner mi granito de arena.

Una vez en el laboratorio, me sorprendió encontrar a los compañeros con los que he tenido la oportunidad de trabajar. Ramón y Vanessa, que fueron miembros iniciales del laboratorio, no dudaron en mostrarme cómo funcionaba el laboratorio –difícil para mí al principio- y a responder generosamente y de modo preciso todas mis dudas. Salvador tuvo paciencia infinita cuando le interrumpía mientras hacía experimentos *in vivo*. Esos años Juan mostraba su rectitud y responsabilidad a la vez que Thomas se quejaba de quién cogió la lidocaína. A pesar de ello, Thomas se lo montó para crear un ser precioso, Amélie, y Juan hizo lo mismo casi un año más tarde, trayendo al mundo al pequeño Leo. María, que nos marcó a todos, puso la mayor parte del sentimiento –a veces más fuertemente de lo que creíamos- a estos años, ciertamente recordándome también que no soy un ingeniero de señales. En los descansos, Diego, Lorena y Núria –y también los otros- eran responsables a menudo de que mantuviéramos conversaciones excitantes que iban desde la ciencia al surrealismo –y vuelta- con el necesario contenido político y filosófico. A Xavi, Lucila y Daniel, que no se acostumbraron al laboratorio pero que contribuyeron con carácter y estilo, nunca los olvidaremos. Un estilo que sólo ha podido ser sobrepasado por el de Bea –fue genial compartir jamón de Extremadura y pizza durante los experimentos *in vitro*!-. En el presente, una de las últimas adquisiciones del laboratorio, Patricia, tuvo algunos problemas al comienzo para entender que hacíamos aquí, pero finalmente se ha convertido en una incansable productora de datos y también disertaciones de todo tipo –sí Patricia, eres locuaz…- Julia, otra de las nuevas, parece que haya estado haciendo experimentos de rodajas desde el colegio. Y Mattia: gracias por mostrarnos a todos como disfrutar de un buen café!. Gracias a todos por vuestro compañerismo.

Fue especialmente agradable trabajar lado a lado con aquellos de vosotros que colaboraron en llevar a cabo el análisis de los datos de esta Tesis: Laura, quien hizo una gran parte del análisis –aún estoy tratando de acostumbrarme a tu partida-, María –que ha contribuido con su extensa experiencia a desarrollar y llevar a cabo buena parte del análisis-, y en los últimos tiempos Lorena –no sé que más decirte, me das paz, se que algún día todo tu esfuerzo será compensado-. También Maurizio, del Intituto Superiore di Sanitá en Roma, con quien aún mantenemos una colaboración estimulante y fructífera, aunque aún tengo que aprender mucho de la propagación. Quisiera agradecer aquí especialmente a María y Mara, con quien mantenemos una bonita colaboración, su dedicación y experiencia: es un placer para mí trabajar en el mismo proyecto, y los mejores deseos para tu nueva vida, María!

A parte de todos los nombrados hasta ahora, mucha otra gente se ha visto envuelta emocionalmente en esta tesis, ya sea porque nos hemos conocido en este mundillo o porque les cuento las penas en el bar. Juanma y Núria, compañeros de la Universidad y amigos muy cercanos –nunca olvidaré nuestras charlas sobre aventuras de doctorado al lado de una Buena cerveza- y Enrique, que colaboró a abrir mi mirada con buenas discusiones y gran amistad. Ciertamente, hay mucha otra gente especial que han sido parte de mi vida durante todos estos años: Raúl, Carol, Rafa, Vane, Itziar, Sergio, Laura, Marc, Saki, Anna, Mariona, Mercè, Andrés… Gracias a todos y a todos los que harían que esta línea fuera bastante más larga por acompañarme.

Valoro especialmente el amor y confianza de mis padres y el amor incondicional de mis abuelas, que son felices porque tengo un trabajo. Ellos siempre han estado ahí, y de ellos obtuve siempre el apoyo necesario.

Finalmente, quisiera expresar mi gratitud a dos personas que han sido de una importancia vital para mí: una me dio todo el apoyo, energía y amor para este largo viaje, y el otro hizo lo mismo en este último año –aunque no se dio cuenta, supongo-: son Gemma y el pequeño Gerard, con quienes oscilo en la misma onda.

INTRODUCCIÓN

La actividad espontánea durante el sueño y algunos tipos de anestesia se caracteriza por actividad oscilatoria a diferentes frecuencias. El principal patrón rítmico del sueño No-REM es la oscilación lenta (~1Hz). Existen otros patrones, como las ondas delta (1-4 Hz), husos de sueño (7-14 Hz) y frecuencias rápidas beta-gamma (15-90 Hz). Por otro lado, el sueño REM se caracteriza por el ritmo theta (4-12 Hz) además de oscilaciones rápidas.

La oscilación lenta consiste en una alternancia de estados 'activos' e 'inactivos' que llamamos estados UP y DOWN, y compone uno de los distintivos de la actividad espontánea de la corteza cerebral. Los mecanismos de generación y mantenimiento de la actividad espontánea de la corteza en forma de ondas lentas todavía son objeto de debate. Entre los mecanismos propuestos, la propia recurrencia excitatoria cortical sería la encargada de generar y mantener la actividad de ondas lentas (Compte et al. 2003; Sanchez-Vives and McCormick 2000). Otras teorías defienden el inicio de los estados UP por el tálamo (Crunelli and Hughes 2010), o por la suma de potenciales sinápticos miniatura (Timofeev et al. 2000) o la existencia en la corteza de neuronas 'marcapasos' que empujarían a la red a generar los estados activos y mantener la actividad rítmica (Le Bon-Jego and Yuste 2007). Además, la conductancia de sodio lenta, o corriente persistente de sodio, ha sido encontrada en otras neuronas marcapasos de otras áreas (McCrimmon et al. 2001; Tazerart et al. 2008a) y ha sido postulada como uno de los mecanismos encargados de generar la actividad oscilatoria lenta cortical (Hill and Tononi 2005; Le Bon-Jego and Yuste 2007), participando en la generación y mantenimiento de los estados UP. Siendo la oscilación lenta una actividad cortical (Sanchez-Vives and McCormick 2000), su generación y mantenimiento respondería tanto a mecanismos intrínsecos de las neuronas (corrientes persistentes de sodio) como sinápticos (recurrencia excitatoria) (Bazhenov et al. 2002; Compte et al. 2003; Steriade et al. 1993c) .

Existen oscilaciones rápidas beta-gamma (15-90 Hz) acopladas a los estados UP en las oscilaciones lentas (Steriade 2006). En las últimas dos décadas existe un interés especial por estas oscilaciones rápidas beta-gamma debido que varias evidencias apuntan su participación en procesos cognitivos. Se ha encontrado que estas oscilaciones están presentes en estados de alerta y atención (Lopes da Silva et al, 1970, Bouyer, et al 1980, Desmedt and Tomberg, 1994) evocadas por estímulos externos (Gray et al 1989, Singer and Gray 1995, Jones and Barth, 1997) en el neocórtex, incluso en los sueños de la fase REM, relacionados con el rendimiento cognitivo (Llinas and Ribary, 1993).

Así, muchos estudios ponen en evidencia en los últimos diez años la importancia de entender los mecanismos y la dinámica de la actividad oscilatoria, ya que relacionan

los patrones oscilatorios dañados con diferentes trastornos cerebrales. Por citar algunos ejemplos, una disfunción de sincronización en oscilación gamma existe en procesos patológicos que estan relacionados con discapacidades cognitivas, como la esquizofrenia (revisado en Uhlhaas and Singer 2010) o la enfermedad de Alzheimer (Koenig et al. 2005).

En esta dirección, los trabajos en ratones genéticamente alterados han generado datos importantes sobre las características de estos patrones oscilatorios dañados –o otros aspectos funcionales- en trastornos neurobiológicos. En general, estos modelos murinos exhiben típicamente un fenotipo parcial, o en diferentes extensiones, comparado con la enfermedad humana, permitiendo el desenmarañamiento de características particulares del desorden cerebral, facilitando su estudio. Uno de los desordenes neurobiológicos que se estudian también a través de estos modelos es el síndrome de Down (DS), la causa más común de discapacidad intelectual (Shin, 2009). Entre otras características, el DS se ha relacionado directamente con una disfunción de la corteza prefrontal (Jernigan et al. 1993; Raz et al. 1995; Wisniewski 1990). A pesar de ello, queda por determinar la unión entre las bases neurofisiológicas de esta alteración y las disfunciones cognitivas y en el comportamiento descritas.

El gen *DYRK1A* se ha propuesto como un candidato principal para generar el fenotipo cognitivo del DS, debido a su localización en la DSCR (Región Crítica del Síndrome de Down) en el cromosoma 21 de los humanos, y a su sobreexpresión en la corteza de fetos y adultos con DS (revisado en Dierssen et al. 2006). Este gen juega papeles clave en la proliferación y supervivencia celular, diferenciación neuronal, plasticidad sináptica y neurodegeneración (Park et al. 2009; revisado en Tejedor and Hammerle 2011).

Se ha visto que la sobreexpresión de DYRK en ratones genera daños cognitivos y en el comportamiento (Ahn et al. 2006; Altafaj et al. 2001) y reduce la complejidad de la morfología piramidal cortical (Martinez de Lagran et al. 2012), pero el impacto de esta sobre-expresión en la función cortical no se ha establecido todavía. Esta última idea está en total relación con el objetivo principal de esta tesis; el estudio de patrones oscilatorios corticales en diferentes sistemas es el hilo conductor de este trabajo. Este estudio pretende dar una visión de cómo se expresan los patrones oscilatorios corticales en diferentes redes corticales *in vitro* e *in vivo* y en un modelo *in vivo* de red cortical alterada –la de ratones TgDyrk1A, un modelo transgénico de síndrome de Down-, centrándose en algunos mecanismos que implican el control de la actividad persistente y el origen de una función cortical alterada.

OBJETIVOS

1. Determinar el rol de la corriente persistente de sodio en la generación y mantenimiento de los estados UP y de las oscilaciones lentas *in vitro*.

2. Describir y caracterizar los patrones de actividad rítmica espontánea en la corteza cerebral de ratones *in vivo* anestesiados.

3. Comparar la actividad oscilatoria espontánea emergente de la corteza de ratones *wild type* con la que existe en ratones TgDyrk1A, un modelo de síndrome de Down.

RESULTADOS

Estudio de la dependencia de los ritmos corticales de la corriente persistente de sodio

Teniendo en cuenta que la corriente persistente de sodio se mantiene a lo largo de todo el estado UP, se ha generado la hipótesis de que si la corriente persistente de sodio contribuyera al mantenimiento los estados UP, su bloqueo los acortaría. Para comprobarlo hemos llevado a cabo un trabajo en el último año en la preparación de rodajas de corteza visual de hurón en solución ACSF (líquido cefalorraquídeo artificial) que generan actividad oscilatoria espontánea de ondas lentas. En estas rodajas oscilatorias se ha bloqueado la corriente persistente de sodio con fenitoína en concentraciones crecientes (40, 60 y 80 µM en la solución de baño), para saber en qué medida las oscilaciones lentas y la generación y mantenimiento de estados UP dependen de esta conductancia. El resultado es que, en la mayoría de casos, en presencia de alta concentración de fenitoína (80 µM), seguían apareciendo estados UP, aunque a una frecuencia mucho menor y con una duración más larga. Además, se realizaron experimentos de bloqueo de la corriente persistente con un bloqueo previo parcial de transmisión excitatoria, es decir, se bloquearon los receptores NMDA y AMPA con APV 10 µM y CNQX 2 µM respectivamente, suficiente para reducir la recurrencia excitatoria. En estas condiciones, el bloqueo con fenitoína 80 µM no consiguió alargar los estados UP en promedio, de modo que el alargamiento de los estados UP depende de la recurrencia excitatoria, es decir, del nivel de excitabilidad de la red.

Sorprendentemente, el disparo de las neuronas en los estados UP también se vio aumentado de manera paramétrica con el bloqueo progresivo. Para comprobar este efecto a nivel de neurona única, se llevaron a cabo experimentos de registro

extracelular 'single unit' conjuntamente con registro extracelular LFP mientras se bloqueaba con una concentración de 80 µM de fenitoína. El resultado fue que el número de potenciales de acción por estado UP, así como la frecuencia de disparo (número potenciales dividido entre duración del estado UP), aumentaban con el bloqueo, confirmando así los resultados de los experimentos iniciales. Así, al bloquear la corriente persistente la excitabilidad de la red aumenta. Esto es paradójico debido a que se esperaría que la frecuencia de disparo bajara, teniendo en cuenta el bloqueo del sodio entrante. Este hecho debería contribuir a la hiperpolarización de las neuronas, y en consecuencia a la disminución de la excitabilidad y frecuencia de disparo, como se vio anteriormente en otras preparaciones sin actividad espontánea (Lampl et al. 1998). Además se calculó el espectro de potencia mediante la transformada de Fourier de los estados UP y DOWN (por separado), y se vio que las frecuencias beta-gamma (altas frecuencias) estaban aumentadas con el bloqueo, indicando un aumento de sincronía en estas frecuencias, que en definitiva es compatible con un aumento de la actividad sináptica que la genera, producido por el aumento de excitabilidad: más frecuencia de potenciales significa más eventos sinápticos capaces de ser sincronizados en frecuencias beta-gamma (revisado en Buzsaki and Wang 2012).

Hemos visto que el alargamiento de los estados UP correlaciona significativamente con el aumento de excitabilidad. Para demostrar que el alargamiento depende precisamente de un aumento de la recurrencia excitatoria al bloquear la corriente persistente de sodio, se registraron oscilaciones lentas en rodajas mientras se estimulaba la red cortical, evocando estados UP intercalados entre la generación de estados UP espontáneos por un fenómeno de reclutamiento sináptico. Se vio entonces que al bloquear con 80 µM de fenitoína, la red era capaz de generar estados UP evocados aun cuando se reducían los estados UP espontáneos por el efecto del bloqueante, por lo que daba la idea de que la red realmente estaba más excitable, y podía generar UPs evocados por reclutamiento sináptico de manera eficiente, que se mantenían durante un tiempo similar a los estados UP espontáneos. Para estudiar el efecto de la corriente persistente de sodio sobre la generación de estados UP, se realizaron experimentos de estimulación en los que se dieron pulsos a 0.25 Hz en condiciones control y con fenitoína, tanto perfundida en el baño (80 µM) o liberada localmente (800 µM). El resultado fue que bajo el efecto de la fenitoína, que como se ha visto disminuía la frecuencia de generación de estados UP, los estímulos eran capaces de generar estados UP completos (evocados). Además, las respuestas evocadas en control eran más pequeñas en duración y amplitud que los estados UP evocados en fenitoína. Esto demostró que la corriente persistente de sodio es crítica para la generación de estados UP de manera espontánea, pero no para su

mantenimiento, pues una vez se consige iniciar un estado UP, tanto espontaneo como evocado, se desarrolla completamente.

Estos resultados llevaron a la conclusión de que el rol de la corriente persistente de sodio consistiría en regular la excitabilidad de la red para evitar que se re-entrara de manera excesiva en los bucles excitatorios que generarían y mantendrían los estados UP, de modo que las oscilaciones lentas dependen en la misma medida de mecanismos sinápticos e intrínsecos, estando relacionados los unos con los otros y siendo los dos críticos para la expresión fisiológica de la oscilación, aunque la corriente persistente de sodio no es crítica para el mantenimiento de los estados UP. De un modo similar, la corriente persistente de sodio amortiguaría la generación de ondas rápidas, evitando que aumentaran demasiado debido al exceso de actividad sináptica.

Caracterización de patrones oscilatorios en diferentes areas corticales

La segunda parte consiste en describir y caracterizar los patrones de actividad rítmica en el córtex cerebral de ratones anestesiados. Para ello se ha realizado un estudio de la actividad oscilatoria en ratones anestesiados *wild type* (WT) de la cepa C57Bl6/SJL. Mediante la aplicación de anestesia con ketamina y medetomidina y una bomba de infusión de anestesia de mantenimiento de ketamina, se estudiaron los patrones oscilatorios emergentes que imitan el sueño de onda lenta.

En primer lugar, se estudiaron las oscilaciones Lentas mediante la obtención de registros extracelulares de Local Field Potential (LFP) en capas corticales profundas y en las condiciones descritas en cuatro áreas corticales, incluyendo 3 áreas primarias: visual, somatosensorial y motora; y una área superior: corteza prefrontal.

A través de la aplicación de un algoritmo de análisis que detecta los estados de activación de la red modelando el disparo de la red a través de su actividad *Multi Unit Activity* (MUA), se detectaron los estados UP de los registros de LFP, a partir de lo cual se calcularon nueve parámetros para caracterizar la onda lenta, que se han comparado entre las cuatro áreas de la corteza. Los parámetros son: frecuencia de la oscilación lenta, duración de los estado UP, duración de los estados DOWN, pendiente de la transición de estado DOWN a UP, pendiente de la transición de estado UP a DOWN, frecuencia máxima de disparo relativa de la red entre estado UP y DOWN, Coeficiente de Variación de los estados UP, Coeficiente de Variación de los estados DOWN, Coeficiente de Variación del periodo UP+DOWN. Los resultados obtenidos nos muestran diferencias significativas en la corteza prefrontal respecto las otras áreas en parámetros relativos al disparo de la red (transiciones y frecuencia de disparo máxima) y regularidad en la duración de los estados activos (CV de los estados UP). Estas diferencias pueden ser explicadas en parte por las diferencias estructurales entre áreas

primarias, que compartirían similitudes, y el área prefrontal, que además cuenta con mayor riqueza de conectividad recíproca con otras regiones subcorticales como la amígdala, hipocampo, tálamo o subículum (Elston 2003 en monos búho; Hoover and Vertes 2007 en ratas; revisado en Ongur and Price 2000 entre especies; revisado en Yeterian et al. 2012 en monos). Estos cambios son compatibles también con una mayor conectividad y recurrencia de neuronas excitatorias en la corteza prefrontal. El descubrimiento de mayor cantidad de espinas en la corteza prefrontal (Elston 2000; Elston et al. 2001) indica también una mayor conectividad sináptica en esta zona.

Seguidamente se realizó un análisis de la propagación de la oscilación lenta en la corteza del ratón mediante la obtención de registros con electrodos multicanal. Este análisis reveló que la oscilación lenta viaja principalmente de la parte anterior de la corteza a la posterior, a una velocidad entre 6 y 75 mm/s. Además, este análisis demuestra la existencia de patrones de propagación más complejos que se sobreponen al patrón principal de adelante hacia atrás. Estos resultados son compatibles con los resultados de otros trabajos en propagación de ondas en capas supragranulares de ratones (Petersen et al. 2003a) y humanos (Massimini et al. 2004), aunque la velocidad de propagación en humanos que se encontró en el primer estudio citado es de 1.2-7m/s, una velocidad mucho más rápida que en el presente estudio, que podría reflejar la mayor conectividad de largo alcance. En rodajas de hurón, por otra parte, la velocidad registrada fue de 10 mm/s, presumiblemente debido a la falta de conectividad de larga distancia (Sanchez-Vives and McCormick 2000). De esta manera, la actividad oscilatoria de onda lenta parece ser principalmente generada en la corteza frontal y viaja hacia atrás, aunque se ha visto en los estudios citados que aparte también se puede generar en otros puntos de la corteza.

A continuación nos centramos en el estudio de las frecuencias generadas por la corteza durante los estados de activación, en los que hay una prominente ocurrencia de oscilaciones en el rango de beta-gamma (entre 15 y 90 Hz), que han sido relacionadas con capacidades cognitivas y atención durante el estado despierto. En este análisis, se ha observado que la corteza prefrontal genera patrones oscilatorios en estas frecuencias de manera más prominente que en las otras áreas analizadas. Una mayor ocurrencia de frecuencias beta-gamma reflejan redes implicadas de interneuronas de disparo rápido o lazos excitatorias-inhibitorias (Compte et al. 2008; Freund 2003; Hasenstaub et al. 2005; Paik et al. 2009; Tamas et al. 2000; Whittington et al. 1995). Esta sincronización en estas frecuencias podría estar regulada por el estado cerebral, p. ej. Dormido, anestesiado, despierto o durante procesos de atención. Por otra parte, este comportamiento de la corteza prefrontal concuerda con el origen de las influencias top-down en tareas perceptivas, de atención o memorísticas.

Otros resultados obtenidos en esta parte del proyecto se basan en la observación de los patrones de disparo de neuronas aisladas. Se vio que las neuronas de áreas primarias como la corteza motora y somatosensorial disparan potenciales de acción mayoritariamente durante todos los periodos de activación de la oscilación lenta, y lo hacen con pocos potenciales de acción (6 o menos). Además, un análisis del disparo a lo largo de cada estado UP revela que existe un aumento de la frecuencia de disparo hacia el centro del estado UP, independientemente de la duración de este. Estos patrones de disparo son comparables a los encontrados en estudios previos en ratón (Erchova et al. 2002; Luczak et al. 2007). A diferencia de la corteza primaria, la corteza prefrontal genera mayor número de potenciales de acción por estado UP y mayor porcentaje de estados UP con potenciales, demostrando el aumento de frecuencia de disparo encontrado en los registros de LFP. Estas neuronas disparan mayoritariamente hacia el inicio del estado UP, a diferencia de lo encontrado en neuronas de cortezas primarias.

Comparación de los patrones oscilatorios corticales y el balance excitación-inhibición en la corteza prefrontal y somatosensorial de ratones wild type y TgDyrk1A

Para estudiar las bases neurofisiológicas relacionadas con la sobreexpresión de DYRK, se han estudiado ritmos corticales como las ondas lentas y rápidas (beta-gamma)**,** de modo similar al apartado anterior. En primer lugar, se ha realizado la comparación de los 9 parámetros de las ondas Lentas obtenidos en LFP de corteza prefrontal y somatosensorial de ratones WT con los obtenidos en TgDyrk1A. El principal resultado obtenido es que la corteza prefrontal es menos excitable en ratones TgDyrk1A, que muestran valores más bajos en las transiciones DOWN a UP y una frecuencia de disparo de red máxima menor en el estado UP. Además, las frecuencias gamma de 60 a 90 Hz, relativas a procesos cognitivos y que en el ratón anestesiado se encontrarían en su estado basal, se muestran disminuidas en el ratón TgDyrk1A. Las alteraciones de frecuencias gamma en los dos hemisferios correlacionan positivamente con la frecuencia de disparo de la población en los ratones WT, mientras que en los TgDyrk1A esta relación no existe, mostrando coeficientes de Pearson bajos y siendo no significativa.

La propagación de las oscilaciones Lentas a lo largo de la corteza también se ve alterada en ratones TgDyrk1A, aunque no en la corteza prefrontal, donde se generarían principalmente. Los cambios en propagación aparecen y son más severos cuanta más distancia hay en el eje rostrocaudal respecto la corteza prefrontal, siendo la propagación más lenta en los ratones TG, lo cual es compatible con una mayor inhibición de la corteza (Sanchez-Vives et al. 2010).

Al ser el gen Dyrk1A crítico en la neurogénesis y basándonos en la hipótesis de inhibición aumentada, se han contado subpoblaciones de interneuronas (parvalbumina-positivas, calretinina-positivas y somatostatina-positivas), pero no se encontraron cambios en estos contajes. Contrariamente, la conectividad cortical en la corteza prefrontal sí se encuentra alterada: el ratio de terminales presinápticas excitatorias/inhibitorias (Vglut1/Vgat) es significativamente más alto en TgDyrk1A debido a un número significativamente reducido de vesículas presinápticas inhibitorias. A nivel post-sináptico no se detectaron cambios.

Finalmente, se realizaron experimentos analizando el número de conexiones sinápticas contactando el soma (sinapsis perisomáticas) en subpoblaciones de neuronas piramidales excitatorias (PYR) e interneuronas parvalbúmina-positivas (PV, 80% de las interneuronas). En estos experimentos se ha visto que el mecanismo por el cual existen los cambios en la función de la red (disminución de frecuencia de disparo, disminución de frecuencias gamma 60-90 Hz) es una disminución de la conectividad perisomática de interneuronas PV sobre ellas mismas (se han mirado sinapsis de PV sobre PV, sinapsis de PV sobre PYR, sinapsis de PYR sobre PV y sinapsis de PYR sobre PYR), por lo que el sustrato de la red sobre el que emergerían las deficiencias cognitivas responderían a una mayor inhibición de la red debido a la desinhibición de las neuronas inhibitorias, que generaría esta actividad gamma alterada (relación entre inhibición perisomática y frecuencias gamma revisada en Buzsaki and Wang 2012).

Por otra parte, experimentos de estimulación en tálamo VPM con registro de potenciales post-sinápticos de campo (fPSPs) en corteza somatosensorial han revelado cambios en el balance excitación-inhibición de la corteza que apuntan hacia una mayor inhibición cortical, debido a una actividad sináptica inhibitoria evocada aumentada. Esta actividad está mediada por conductancias inhibitorias rápidas asociadas a receptores $GABA_A$ (Agmon and Connors 1991; Gil and Amitai 1996; Silberberg and Markram 2007). En la corteza somatosensorial no se han detectado cambios en los parámetros del LFP ni en las frecuencias beta-gamma. Además, se ha detectado una disminución del número de interneuronas parvalbúmina-positivas, que indica que la neurogénesis inhibitoria está alterada, y una disminución del número y tamaño de terminales postsinápticas inhibitorias, que indicarían mecanismos compensatorios para regular el nivel de excitabilidad de la red.

Todo esto ha corroborado la alteración en el balance entre excitación e inhibición que se había hipotetizado en la corteza de los ratones TgDyrk1A. Los experimentos de inmunohistoquímica y comportamiento han sido realizados por la Dra. María Martinez de Lagrán, bajo la dirección de la Dra. Mara Dierssen, con quien hemos mantenido una colaboración.

DISCUSIÓN GENERAL

En esta tesis se demuestran algunos aspectos mecanísticos que controlan la emergencia de patrones rítmicos de circuitos corticales, poniendo énfasis en mecanismos que controlan la excitabilidad o la conectividad que subyace las ocilaciones en circuitos corticales. Primeramente, este estudio presenta en qué medida los ritmos lentos y rápidos dependen de un mecanismo intrínseco de las neuronas que gobierna las oscilaciones corticales como es la corriente persistente de sodio. También se presenta el rol de la excitabilidad cortical en la expresión de estos ritmos en diferentes áreas corticales. Finalmente, este estudio muestra las alteraciones de la actividad oscilatoria de red en un modelo de síndrome de Down, donde se han visto disminuidas tanto la excitabilidad de la red como las oscilaciones rápidas en la corteza prefrontal, que se pueden explicar por un aumento de inhibición de la red. En las secciones siguientes se presenta una discusión acerca de estos temas.

Comparación de la expresión de los ritmos lentos y rápidos entre redes corticales de acuerdo con sus componentes celulares y conectividad *in vivo*.

Del trabajo de esta tesis, se desprende un papel fundamental de la conectividad cortical que sostiene la actividad oscilatoria. Más concretamente, aquí se presentan los elementos celulares y su conectividad que se ha mostrado que son críticos para la expresión de las oscilaciones rapidas, que es la inhibición perisomática mediada por las interneuronas parvalbúmina-positivas (PV, revisado en Buzsaki and Wang 2012). En los capítulos 3.3 y 3.4 se muestra el efecto de los cambios en esta conectividad en las oscilaciones rápidas *in vivo*, y cómo estos cambios afectan directamente a la función cognitiva. Un punto crítico es que las oscilaciones rápidas se expresan de modo diferente entre áreas de la corteza, así como en redes corticales alteradas.

En primer lugar, las diferencias en expresión de las oscilaciones rápidas pueden ser explicadas por la composición neuronal distinta, siendo el caso lo que ocurre entre corteza prefrontal y somatosensorial (la corteza somatosensorial muestra una densidad de PV de ~3.10^{-4} *vs* ~2.10^{-4} cells/μm^2 en la corteza prefrontal). La proporción de cada subclase de interneuronas, así como la densidad de neuronas, especialmente PV, puede ser la primera clave para entender la aparición de oscilaciones rápidas con características especiales dependiendo del área. Así, una mayor densidad en la población de interneuronas además de diferencias en la conectividad de terminales excitatorios (115 *vs* 185 terminales de media por campo en la capa 5 de las cortezas somatosensorial y prefrontal, respectivamente, ver figura en apartado *DISCUSSION*) e inhibitorios (200 vs 270 en somatosensorial y prefrontal, ver figura en apartado

DISCUSSION) explicarían el diferente grado de excitabilidad, como ocurre en la corteza somatosensorial respecto la prefrontal. Además, la corteza prefrontal presenta una conectividad especial en comparación a las cortezas primarias, en la que se ha encontrado un número superior de espinas neuronales (Elston 2001). Finalmente, la inhibición perisomática mediada por PV, tanto sobre neuronas piramidales como otras PV, se encuentra expresada de manera diferente entre ratones wild type y TgDyrk1A en la corteza prefrontal. Estos tres argumentos pueden explicar por qué las oscilaciones Lentas y rápidas en la corteza prefrontal de ratones wild type son distintas de las de los transgénicos. En la corteza somatosensorial, los cambios en neurogénesis de interneuronas, actividad sináptica aumentada en capa 4 y las terminales postsinápticas estructurales reducidas en número y tamaño no provocaron cambios en los patrones rítmicos corticales de la capa 5, aunque muestran indicios de mecanismos compensatorios de la red.

En referencia al balance excitación-inhibición y su desajuste en la red cortical alterada

El estudio *in vitro* presentado aquí muestra la dependencia de los patrones oscilatorios corticales de mecanismos intrínsecos de las neuronas como las corrientes persistentes de sodio. Aquí se propone un posible rol para esta conductancia, que es la participación en el control de la excitabilidad de la red, de manera que evitaría la actividad excitatoria recurrente excesiva, haciendo que la red no entre de manera excesiva en los bucles excitatorios que generan y mantienen los estados UP. Desde este punto de vista, la corriente persistente de sodio colabora a mantener el balance entre excitación e inhibición en un punto regulado, ya que este delicado equilibrio es lo que mantiene la correcta expresión de la oscilación lenta. Además de la regulación de las oscilaciones lentas, las corrientes persistentes de sodio también amortiguan otros ritmos corticales como las oscilaciones rápidas beta-gamma, controlando la expresión de los ritmos corticales de onda lenta (Bazhenov et al. 2002) y frecuencias rápidas (Oke et al. 2010).

Otro aspecto que se desprende de los hallazgos de este estudio es la comparación del desarrollo de la oscilación lenta entre redes corticales fisiológicas y alteradas *in vivo*. Los resultados expuestos aquí en ratones *wild type* muestran que las oscilaciones lentas y rápidas son diferentes entre áreas corticales dependiendo en gran medida del grado de conectividad y de la inhibición perisomática, como se ha expuesto anteriormente.

Por lo tanto aquí se presentan evidencias, aunque indirectas, de que podría existir una relación entre excitación e inhibición en cada area cortical de modo independiente

que subyace la generación de los patrones rítmicos corticales necesarios para la función de cada área.

El hallazgo de que las ondas lentas y rápidas estén alteradas en la corteza prefrontal en un modelo de síndrome de Down como resultado de cambios en la conectividad e inhibición perisomática destaca su papel crítico en la aparición de las oscilaciones de las diferentes redes corticales, fisiológicas o alteradas (Freund and Katona 2007; Molaee-Ardekani et al. 2010). También, en la corteza somatosensorial, el desbalance se demuestra por los incrementos en inhibición sináptica, aunque no se pudo resolver si es debido a un contacto talámico excitatorio incrementado o actividad sináptica inhibitoria cortical aumentada, aunque esto no alteró los patrones oscilatorios corticales. Esto puede ser explicado por cambios compensatorios, como una conectividad excitatoria sináptica aumentada, de los cuales se presenta evidencia en este estudio.

Así, una red balaceada es crucial para la expresión de los patrones corticales y evita actividad oscilatoria aberrante, que puede llevar a una función alterada de las oscilaciones lentas y rápidas para su rol propuesto en función cognitiva en sueño y vigilia.

Finalmente, en el apartado final de la discusión de la tesis se describen perspectivas acerca de tratamientos para trastornos del cerebro que incluyen la estimulación magnética transcranial (TMS) y sus potenciales beneficios para la función cognitiva.

CONCLUSIONES

Objetivo 1, sobre el rol de la I_{Nap} las oscilaciones lentas

1. La corriente persistente de sodio es crítica para el correcto desarrollo de la actividad espontánea, y es necesaria para la generación de estados UP a una frecuencia y duración fisiológicas, pero no para el mantenimiento del UP state.

2. Paradójicamente, el bloqueo de esta conductancia provoca aumento de la frecuencia de descarga y de la sincronía de frecuencias beta/gamma, sugiriendo un aumento de excitabilidad potencial.

3. La corriente persistente de sodio regula el nivel de excitabilidad de la red que generan y mantienen los estados UP.

Conclusiones del Objetivo 2, sobre la línea base de la actividad oscilatoria en ratones WT

4. La corteza prefrontal muestra propiedades de disparo de la red únicas y diferentes al resto de cortezas primarias analizadas, mostrando una frecuencia de disparo mayor de la red y de neuronas aisladas. Además muestra mayor regularidad en la duración de los estados UP.

5. La corteza prefrontal genera patrones oscilatorios en el rango de frecuencias beta/gamma 15-90 Hz) de mayor potencia que en las áreas corticales primarias analizadas, compatible con su rol en señalización top-down, donde las oscilaciones gamma se pueden regular hacia un incremento para construir ensamblajes cognitivos.

6. Ls oscilaciones se propagan principalmente desde la parte frontal hacia zonas posteriores, y viajan a través del cortex motor a velocidades de entre 6 y 75 mm/s, aunque contienen patrones de propagación de mayor complejidad.

Conclusiones del Objetivo 3, sobre la actividad oscilatoria alterada en la corteza de ratones TgDyrk1A

7. Los ratones TgDyrk1A muestran alteraciones cognitivas relacionados con la corteza prefrontal en tareas de comportamiento que implican solución de problemas.

8. La frecuencia de disparo de la red y la pendiente de la transición de estado DOWN a UP están disminuidas en la corteza prefrontal de los ratones TgDyrk1A. Esto indica que la cortexa prefrontal en ratones TgDyrk1A es menos excitable.

9. Las frecuencias rápidas beta-gamma en corteza prefrontal están disminuidas. Además, la potencia de las ondas gamma en la banda baja (30-60 Hz) y alta (60-90 Hz) no esta correlacionada con el pico máximo de frecuencia de disparo de red la corteza prefrontal de ratones TgDyrk1A.

10. Hay un descenso de la velocidad de propagación de las ondas lentas en el ratón TgDyrk1A, a medida que se alejan de la corteza prefrontal. Este punto junto las dos conclusiones anteriores es compatible con una mayor inhibición de la red y supondría una posible explicación para los déficits cognitivos observados en comportamiento.

11. La disminución de la excitabilidad y de potencia de frecuencias gamma en la corteza prefrontal de ratones TgDyrk1A se pueden explicar por un descenso de la conectividad inhibitoria perisomática sobre neuronas inhibitorias, que provocarían un aumento de inhibición de la red.

12. La inhibición sináptica está aumentada en la corteza somatosensiorial de los ratones TgDyrk1A evocada por resultado de estimulación talámica, mientras que la actividad sináptica excitatoria resulta inalterada. Esto demuestra que existe una altreación del balance excitación-inhibición en la capa 4 en este modelo.

13. Los patrones oscilatoruios emergentes de la red somatosensorial de ratrones TgDyrk1A no están alterados. Esto sugiere la existencia de mecanismos compensatorios relativos a un proceso homeostático.

1. INTRODUCTION

Neurons are cells capable of transmitting information to other neurons through contacts called synapses. In the brain –and in neocortex- two main populations of those cells are present: excitatory neurons, which are mainly pyramidal neurons, and inhibitory neurons or interneurons. These cells, as all others, have an outer membrane which is composed by a lipidic bilayer impermeable to electric charges, and ion channels, which are proteins that allow the flow of ions between inside and outside the cell. Neuronal membranes have the particularity of being electrically excitable, a phenomenon that is happening in the brain constantly.

The expression of the flow of information through connected neurons are fluctuations of the membrane voltage –or membrane potential, *Vm*- of each neuron, if we understand a neuronal membrane as a model circuit where a resistance –the ion channels that control the flux of ions across the membrane- and a capacitor -the lipidic membrane that accumulates ion charges at both sides- are connected in parallel. The fluctuations of the membrane voltage are the elements that we can record as electric signals, either in intracellular or extracellular unitary recordings –from a single cell-, or extracellular local field potentials (LFP), which express a wide range of voltage fluctuations from a neuronal population (origin of LFP reviewed in Buzsaki et al. 2012). Other population signals such as the electroencephalogram (EEG) allow the recording of population activity in a non invasive manner, which is widely used in humans. Extracellular signals allow for example the study of spontaneous activity of the neocortex, i.e. in absence of external stimuli, like the case in sleep.

Spontaneous activity during sleep and some kinds of anesthesia is characterized by oscillatory activity at different frequencies (Fig. 1). The main rhythmic pattern of Non-REM sleep is the slow oscillation. Other patterns are also present, such as delta waves (1-4 Hz), spindles (7-14 hz) and fast beta-gamma frequencies (15-90 Hz). REM sleep is characterized by oscillations in the theta rhythm (4-12 Hz) and fast oscillations as well. The study of spontaneous oscillations is critical because they may reflect intrinsic features of the underlying circuit and show alterations when this circuit presents abnormalities.

It is postulated that synchronization in oscillations allows communication of neocortex with other brain regions. While theta rhythm seems to be engaged by hippocampus/prefrontal interplay, beta-gamma activity is postulated to mediate intracortical bottom-UP and top-down communications between prefrontal and sensory cortices (reviewed in Benchenane et al. 2011) related to cognitive function. Cortical slow wave sleep, as well, has been postulated to display a key role in memory consolidation, through the orchestration of rhythms coming from other brain areas, such as thalamus or hippocampus (Molle and Born 2011).

A special attention in beta-gamma oscillations has been paid in the last two decades, as many evidences highlight their involvement in cognitive processes. Such beta-gamma activity is reported to be present during alertness and attention (Bouyer et al. 1980; Desmedt and Tomberg 1995; Lopes da Silva et al. 1970) or triggered by external stimuli (Gray and Singer 1989; Jones and Barth 1997; Singer and Gray 1995) in the neocortex, even in dreams during REM sleep related to cognitive performance (Llinas and Ribary 1993).

Many studies in the last ten years evidenced the importance of the understanding of the mechanisms and dynamics of oscillatory activity, as they related impaired cortical patterns to different brain disorders. As examples, a dysfunction in gamma synchronization is present in pathological processes which are related to cognitive disabilities, such as schizophrenia (reviewed in Uhlhaas and Singer 2010) or Alzheimer disease (Koenig et al. 2005).

In this direction, work in genetically altered mice reported important data about the features of those impaired oscillatory patterns -or other structural or functional aspects- in neurobiological disorders. In general, these models typically exhibit a partial phenotype to different extents compared of the human disease, allowing the disentangling of particular characteristics of the brain disorder, and thus facilitating its study (Altafaj et al. 2001; Boutajangout et al. 2010; Colas et al. 2004; Dragomir et al. 2010; Verret et al. 2012). This last idea is well related to the aim of this Thesis: the study of cortical oscillatory patterns in different systems is the conducting wire of this work. Our study pretends to give a view about how cortical oscillatory patterns are expressed across *in vitro* and *in vivo* cortical networks and in an *in vivo* model of impaired cortical network –the TgDyrk1A mice, a mouse model of Down Syndrome-, focusing on some mechanistic aspects which involve the control of persistent activity and the origination of altered cortical function.

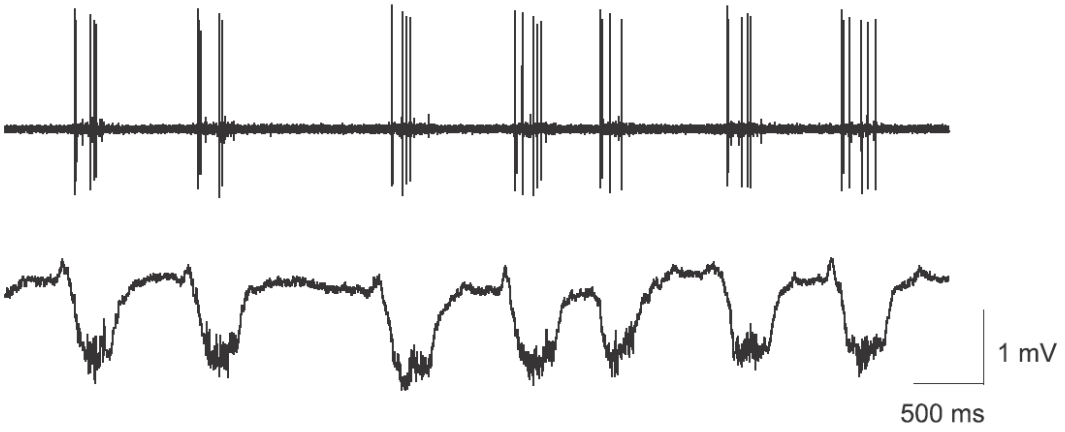

Figure 1. Slow oscillations in the mouse prefrontal cortex under ketamine-medetomidine anesthesia. Top: extracellular single unit recording which shows a neuron's firing in the UP states. Bottom: extracellular LFP recording which shows the alternation of UP and DOWN states at a frequency of ~1Hz.

1.1. Slow oscillations

Cortical activity has often been studied in response to sensory stimuli. But in absence of external input, neocortex undergoes an oscillatory activity which is characteristic of rest or non-REM sleep states and that is also observed under several types of anesthesia, the so called slow waves (~1 Hz). This oscillatory activity was characterized in detail by Mircea Steriade and collaborators in 1993. (Steriade et al. 1993a; Steriade et al. 1993b, c). In those studies, three main ideas, among others, came off from extracellular and intracellular cortical recordings in cats: the oscillation was an alternation of 'active' depolarized and 'inactive' hyperpolarized states at a frequency below 1 Hz; it was maintained by synaptic activity of excitatory and inhibitory components of the network; the oscillation contained other rhythms such as spindles (7-14 Hz) or (beta) gamma oscillations (15-90 Hz) related to the 'active' states (Fig. 2). Other authors have used UP and DOWN terminology to refer to the 'active' and 'inactive' states, although both are commonly used nowadays.

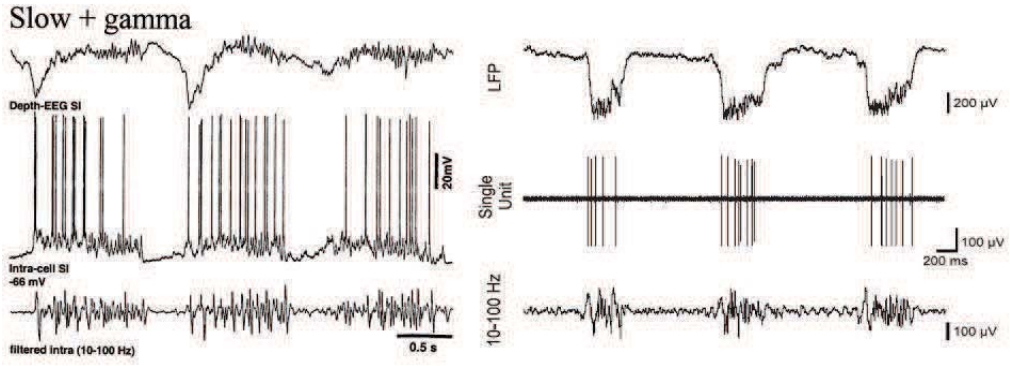

Figure 2. Slow oscillations contain other rhythms such as gamma oscillations.
Left: cat cortical slow oscillations recorded extracellularly (upper trace) and intracellularly (middle trace). Lower trace: filtered intracellular that shows gamma activity within the 'active' depolarized states (taken from Steriade, 2006). Right: mouse cortical slow oscillations (modified from Ruiz-Mejias et al. 2011) recorded extracellularly in a LFP recording (UPper trace) or single unit (middle trace). Lower trace: filtered extracellular LFP recording showing gamma activity within the UP state.

These early studies highlighted the relevance of the interplay of excitatory and inhibitory components of the neocortical networks, finely balanced in the generation of emerging oscillatory patterns such as the slow rhythm. Since the disclosure of this oscillation, several studies have focused on the mechanisms that generate and terminate UP states, the maintenance of the activity, the possible participation of different brain areas, its propagation across the cortex, as well as its biological meaning.

1.1.1. Mechanisms of initiation, maintenance and termination of UP states with emphasis on persistent sodium current

Several mechanisms are proposed to generate, maintain and terminate UP states. Among them, the combination of excitatory and inhibitory postsynaptic events of recruitment and synchronization combined with intrinsic conductances of neocortical cells such as the persistent sodium current was the first to be proposed (Steriade et al. 1993c). A model including some of the same authors years after pointed out to the summation of spike-independent miniature EPSPs resulting from the fusion of single vesicles -which would synchronize and subsequently activate the persistent sodium current- as the responsible mechanisms that initiate UP states (Timofeev et al. 2000). Despite the different details of the mechanisms, both defended the slow rhythm to be an emergent property of neocortical circuits, as thalamic lesions left intact the cortical slow oscillation (Steriade et al. 1993c), and was confirmed afterwards in deafferented cortical slabs (Timofeev et al. 2000).

In contrast to that, some studies pointed out to a key role of the thalamus in generating and controlling activation of UP states through intrinsic conductances of thalamic neurons (Crunelli and Hughes 2010) or synaptic activity coming also from the thalamus (Rigas and Castro-Alamancos 2007). These works defended the principal role of thalamus in generating the slow oscillation. Indeed, many studies give rise to the significant implication of thalamocortical circuits in physiological sleep and slow oscillations (Bazhenov et al. 2002; Poulet et al. 2012; Steriade 2003; Timofeev and Chauvette 2011), but researchers still debate about the role of the thalamus on this oscillation.

Conclusively, a study performed in spontaneously active cortical slices which generated the slow rhythm demonstrated that it emerged from cortical circuits without the input of any other brain area (Fig. 3; (Sanchez-Vives and McCormick 2000). In the study of Sanchez-Vives and McCormick, as well as in a neocortical network model (Compte et al. 2003) the authors postulated that the spontaneous excitatory activity of neocortical cells amplified by a recurrent network of excitatory connections is the responsible mechanism of generate and maintaining UP states (Figure 5).

Specifically, these studies demonstrated that the initiation of UP states occurs in the layer 5 of the cortical column. In the work of Sanchez-Vives and McCormick, the authors give evidences supporting the generation of UP states in layer 5 pyramidal neurons, and further propagation to deeper and more superficial layers (Sanchez-Vives and McCormick, 2000). A previous study reported that this layer is sufficient to generate rythmicity in pyramidals due to intrinsic membrane properties such as sodium conductances (Silva et al. 1991). Other posterior studies converged in

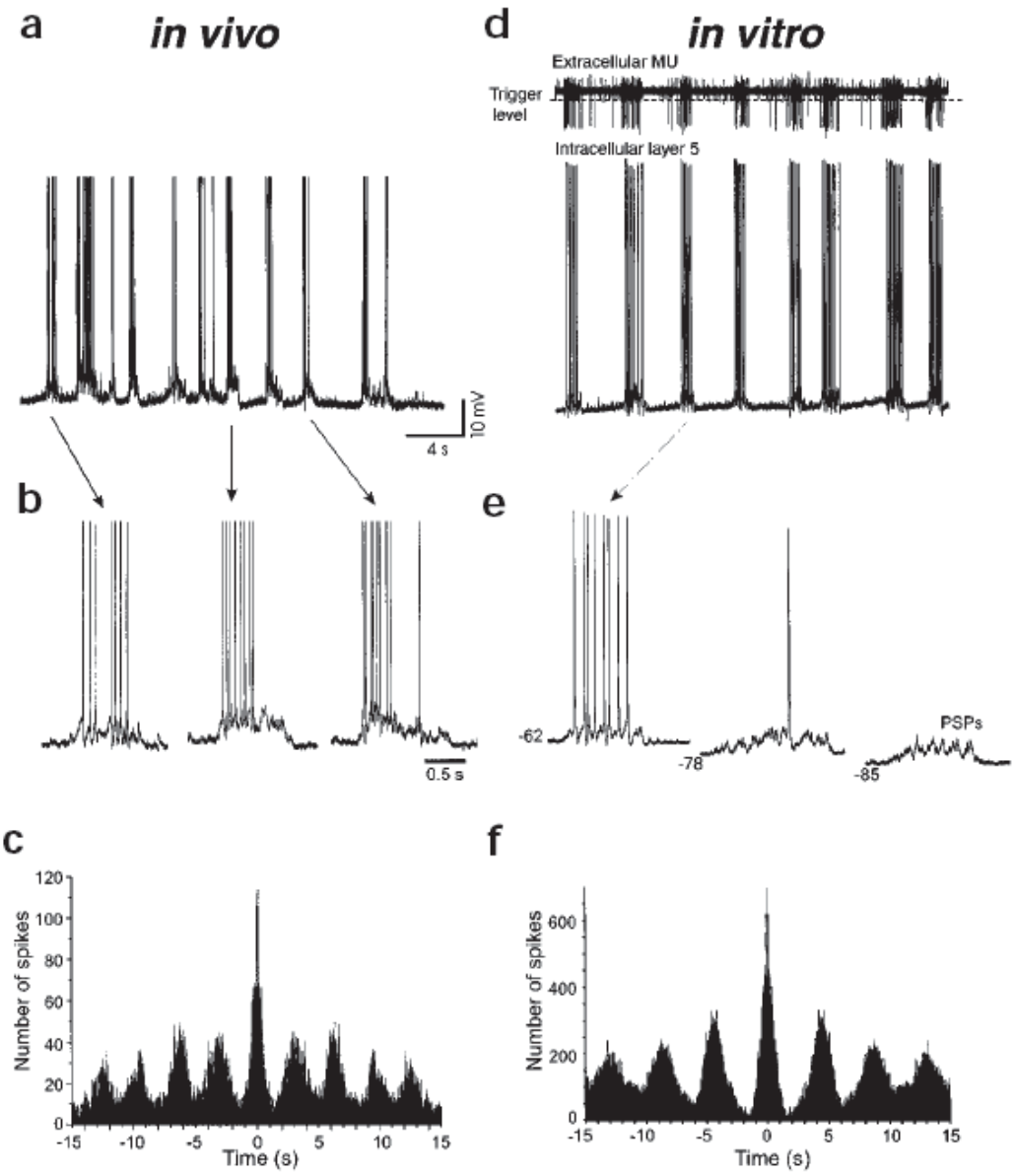

Figure 3. Slow oscillations *in vivo* and *in vitro* show common features.
Slow wave oscillatory activity in an halotane-anesthetized cat (a,b) and in ferret slices (d,e). a, Intracellular traces which show depolarizations and hyperpolarizations of the alterning UP and DOWN states *in vivo*. b. Example of depolarizations in a. d, intracellular traces with an extracellular Multiunit activity recording (top trace) *in vitro*. e. Example of depolarizated state at three membrane potentials, f. Autocorrelograms of the intracellular traces, which show periodicity of the oscillation in one cycle each three seconds *in vivo* (c) and one in each four seconds *in vitro* (f). Taken from Sanchez-Vives and McCormick, 2000).

the hypoThesis of the involvement of layer 5 in the initiation of slow wave activity in sleeping and deeply anesthetized animals from several species like cats or mice (Beltramo et al. 2013; Chauvette et al. 2010; Sakata and Harris 2009; Shu et al. 2003). A study in humans that combined laminar local field potentals and unit recodings found a major involvement of supragranular layers in the genesis of slow wave activity (Csercsa et al. 2010), showing a clear difference in the mechanisms that originate slow waves with respect to other species.

With respect to the variety of connectivity present in the neocortex, a recent study with whole-cell recording in submerged enthorinal cortex slices from neonate mice provided evidence that specific connectivity between different kinds of pyramidal and interneurons differently contribute to the generation of the oscillation. They observed that from 5 types of interneurons, only fast-spiking contribute with a high amount of spiking activity during slow oscillations, and that the persistent activity in the UP state is mainly due to recurrent interactions between pyramidal and fast-spiking interneurons. The study also supported the hypoThesis of prevalent intracortical synaptic mechanisms in the generation of this rhythm and (Tahvildari et al. 2012).

As mentioned in the beginning of this section, the initiation of UP states may involve the activation of persistent sodium currents (Bazhenov et al. 2002; Compte et al. 2003; Hill and Tononi 2005; Steriade et al. 1993c; Timofeev et al. 2000). These currents would consist on late openings of the voltage-gated fast sodium channels, which could switch into different modes of gating (Alzheimer et al. 1993). It is characterized by a slow inactivation (Fleidervish et al. 1996; Fleidervish and Gutnick 1996), and would be activated all along the UP state.

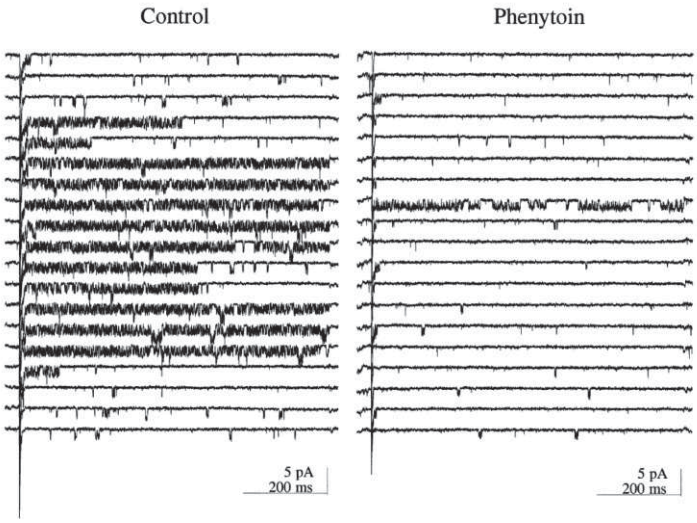

Figure 4. Effect of phenytoin on persistent sodium current.
Left: Single channel recording showing late currents trough sodium channels. Right: Application of 60 μM of phenytoin in bath reduces those late currents. Taken from Siegel and Douglas, 1997.

This conductance is thought to be involved in burst firing of neocortical neurons (Brumberg et al. 2000; Guatteo et al. 1996), and has properties that are layer specific (Aracri et al. 2006). Regarding the blockers, riluzole (Kononenko et al. 2004; Le Bon-Jego and Yuste 2007) and phenytoin (Chao and Alzheimer 1995; Colombo et al. 2013; Segal and Douglas 1997) have been shown to efficiently block this conductance (Fig. 4). A recent work argues that phenytoin may act rather during the inactivation of the channel rather than blocking the gating (Colombo et al. 2013), although some authors described unspecific effects on voltage-gated fast sodium and calcium channels (Stefani et al. 1997b). Despite that, Is not yet clear whether persistent sodium currents result from the different gating of the same channel type as transient sodium currents.

Other studies pointed out that persistent sodium currents may be critical for supporting spontaneous activity with persistent firing in a reduced number of cortical 'pacemaker' cells (Le Bon-Jego and Yuste 2007) that may engage ensembles of small number of neurons and entrain the network in an active state (Cossart et al. 2003).

Altogether, those studies opened the debate about the participation of intrinsic and synaptic mechanisms in the generation and maintenance of UP states. Together with some evidence presented in the next part of the introduction -about the mechanisms of maintenance of persistent activity- the question of whether the persistent sodium current is strictly necessary for the ocurrence of slow oscillatory activity and UP state generation and maintenance arises, a hypoThesis experimentally tested in the present work, and that will be further exposed and discussed in the following chapters of this Thesis.

Regarding UP state termination, several studies reported distinct evidences to the mechanisms that terminate UP states. Initially, and as mentioned above, Steriade proposed the concrete interplay of EPSPs and IPSPs to be the responsible in the generation and termination of the slow waves. The study of Sanchez-Vives and McCormick proposed that the slow afterhyperporarization potassium (AHP) currents, which are dependent on the cumulated sodium and calcium within the depolarized state, to be the responsible of terminating UP states. Similar to this finding but supporting a metabolic theory, some work defended the terminating potassium current to be dependent on ATP, as both potassium conductances share similar time courses (Cunningham et al. 2006). Also in Sanchez-Vives and McCormick work, the terminating process is proposed to be mostly related to excitatory activity in the neocortex, as the slow AHP was typically expressed in excitatory neurons -although in certain conditions such as long stimulations, slow AHP appears also in inhibitory neurons (Descalzo et al. 2005)-, and was expressed as the inability of the network of maintaining a self-activated state, which may be overcomed by the negative Na^+ and Ca^+-activated outward K^+ conductances (Compte et al. 2003; Sanchez-Vives and

McCormick 2000). Those findings were also simulated in the cortical network model mentioned above (Fig5; (Compte et al. 2003).

Other work pointed out to synaptic 'fatigue' or depression to be the dominant mechanism (Contreras et al. 1996) or contribute to the termination of UP states (Hill and Tononi 2005; Rigas and Castro-Alamancos 2009), suggesting that the depletion of readily releasable pools of vesicles are limiting UP state length. In contrast to this, a recent biophysical model based on experimental data about the impact of oscillatory activity on short-term synaptic depression (Reig et al. 2006; Reig and Sanchez-Vives 2007) found that the mutual interactions between synaptic depression and ongoing oscillatory activity are critical to determine the mechanisms that modulate cortical emerging patterns, and that an increase in synaptic depression is in fact elongating the UP states (Benita et al. 2012).

Other mechanisms of termination have been proposed, such as GABA(B)-mediated inhibition, which would be triggered from layer 1 of the neocortex (Mann et al. 2009). Finally, recordings from multiple cells suggested a large-scale network mechanism external to intrinsic and synaptic properties of individual cells to the initiation of silent states, as distance between recorded cells and cell type did not affect the precision in silent state synchronization (Volgushev et al. 2006). A recent work proposes this synchronization in the termination of UP states to be mediated by inhibition and intrinsic hyperpolarizing conductances (Chen et al. 2012).

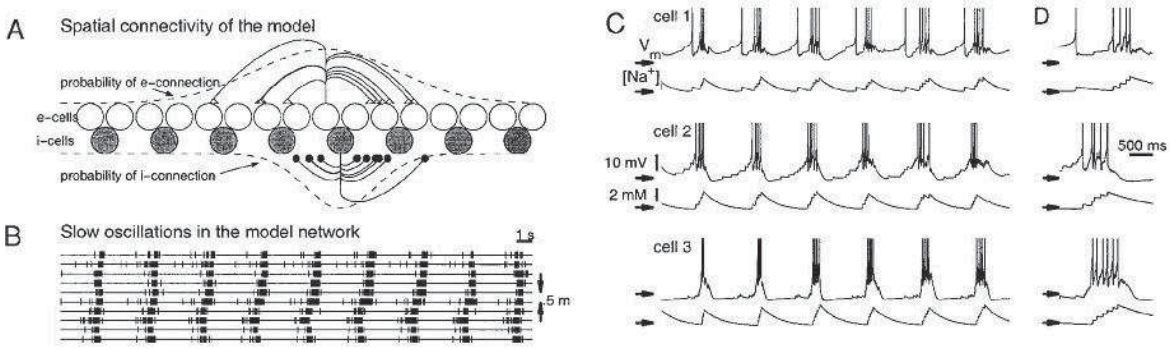

Figure 5. A model combines synaptic and intrinsic mechanisms for the generation of slow waves.
A. Schematic spatial connectivity of the model. E-cells: excitatory cells; i-cells: inhibitory cells. B. Slow oscillations in function of groups of 5 units per site, 500 µm between sites. Propagation can be observed. C. examples of firing of 3 pyramidal cells during slow oscillations, with the intracellular Na^+ concentration. D. Detail of a depolarized episode of the cells in C (taken from Compte et al. 2003).

1.1.2. Mechanisms of maintenance of the slow oscillation

Persistent oscillatory cortical activity, understood as slow waves developing in long lasting periods at a frequency ~1 Hz, requires of a mechanism (or more), which would be derived from intrinsic or synaptic properties of cells participating in the oscillation, and that would be capable of maintaining the rhythmicity. In the work of Sanchez-Vives and McCormick, the authors postulated a mechanism in that alternation of UP and DOWN states was determined largely by a balance between excitation and inhibition in the neocortex (Compte et al. 2009). The authors expressed the hypoThesis as the inability of the network of maintaining a self-activated state, which may be overcomed by the negative Na^+ and Ca^+-activated outward K^+ conductances that persist and hyperpolarize the network. Then, because the activity associated with the UP state ceases or decreases dramatically during the down state, the slow afterhyperpolarization slowly decreases in amplitude, allowing the network to again generate another UP state (Sanchez-Vives and McCormick 2000). This mechanism was also supported by a cortical network model (Compte et al. 2003). In this direction, other work supports the hypoThesis that a balanced excitation and inhibition is maintaining the slow oscillations, where excitation contribution is more prevalent at the onset and end of the UP state (Haider et al. 2006), being pyramidals and fast spiking interneurons and their recurrent connectivity the main generators, as mentioned above (Tahvildari et al. 2012).

On the other hand, and as mentioned above, some authors provided data supporting a major role of thalamus –and reticular thalamic nucleus- in 'pacemaking' slow oscillations which is mediated by low-threshold calcium potentials (LTCP) through T-type channels in thalamic neurons (Crunelli et al. 2006 for a review; Hughes et al. 1999). In following studies, the authors give a striking importance of cortico-thalamo-cortical connectivity in a context in which three different but not exclusive oscillators interplay in the generation and maintenance of slow oscillations: a synapticaly-based oscillator from cortical origin, and two intrinsic conditional oscillators, i.e. thalamocortical and *nucleus reticularis thalami* (NRT) neurons, being the condition the sustained activation of post-synaptic thalamic mGluR1a receptors, which are active by cortical input. The authors propose in their work that the thalamic 'pacemaking' activity is able to generate UP states in the triple oscillator scenario and transmit them to the cortex (Crunelli and Hughes 2010), at least in a small percentage.

As mentioned in the previous section of the introduction, some authors reported evidence that support the existence of cortical 'pacemaker' cells (Llinas 2001; Llinas 1988), which would sustain rhythmic activity by means of certain intrinsic conductances, such as persistent sodium current (Le Bon-Jego and Yuste 2007), a

conductance that is present in other 'pacemaker' neurons outside the cortex, e.g. in cerebellum (Solinas et al. 2007) or spinal cord (Tazerart et al. 2008b).

Together with the hypoThesis of persistent sodium current to be sufficient to trigger an UP state in a cortical network model or to participate in the maintenance of the oscillation (see 1.2.1) –this last was already proposed in the first description of the slow rhythm, in Steriade et al. 1993-, the above exposed detaches the debate about which are the responsible mechanisms for maintaining slow oscillatory activity, and opens the question of what is the concrete role of this current in UP state generation and maintenance. Experimental evidence on this topic is reported and discussed in the following chapters of this Thesis.

1.1.3. Propagation of the slow oscillation

Slow waves have been shown to propagate within the vertical and horizontal direction of the neocortex (Fig. 6; (Sanchez-Vives and McCormick 2000). Thus, the horizontal propagation property of these oscillations is what we refer to as 'travelling waves', although this term is also used to describe propagation of other rhythms such as 'splindles' (Hughes et al. 1995). Certainly, the earlier evidences of slow wave horizontal propagation came off from the work of Steriade in the 90's (Amzica and Steriade 1995), where time lags between pairs of recorded neurons in cat neocortex increased with distance.

A description of vertical and lateral propagation of the *in vitro* slow wave was originally provided in the work of Sanchez-Vives and McCormick, where oscillations travelled without any external input from outside of the cortex, demonstrating that propagation in within the neocortex is a synaptic property which only requires cortico-cortical short-range connectivity. In this study, the horizontal speed of propagation was slower to that suggested in Amzica and Steriade work, 10 vs 100 mm/s, presumably because of the lack of long range cortical connectivity *in vitro*, as the authors proposed.

Further work on wave propagation showed with means of voltage sensitive dye imaging that the propagation of depolarization-dependent activity in the cortical layer II-III of anesthetized mice was also ranging between 10 to 100 mm/s (Petersen et al. 2003b), with similar results reported with intracortical recordings in deep layers (Ruiz-Mejias et al. 2011). Another EEG study in humans showed how sleep slow oscillations travelled from front to back in the neocortex (Massimini et al. 2004) at much higher speeds than observed before in animals, a fact that was also related to increased to longer-range cortico-cortical connectivity. In a quite recent work, propagation of sow waves over the cortical surface of anesthetized mice was detected also with voltage sensitive dye imaging (Mohajerani et al. 2010), which gave instantaneous velocities of

a single peak of activity ranging around 10-80 mm/s, although a systematic quantitative study on speeds and dynamics was not provided. Also *in vivo*, a recent study reported a mean speed of propagation of slow waves of 37 mm/s, this time measured by means of calcium imaging (Stroh et al. 2013).

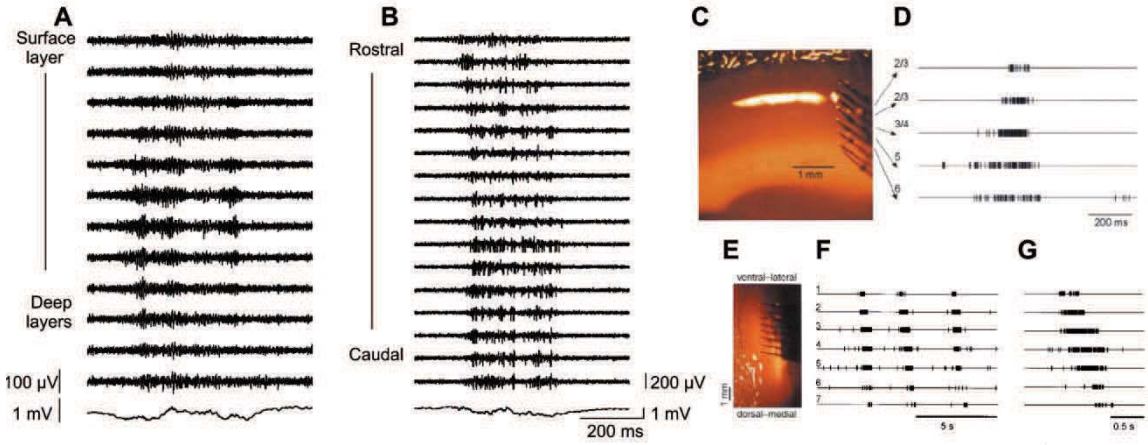

Figure 6. Propagation of slow waves *in vivo* and *in vitro*.
A,B. *In vivo* vertical (A) and horizontal (B) propagation of UP states within the mouse cortex. Extracellular MultiUnit traces (above 200 Hz) with the corresponding raw LFP at the bottom, both with electrode site spacing of 100 µm. C-F. *In vitro* ferret cortical oscillations in which UP states are also propagated vertically across layers (C-D) and horizontally within a layer (C-G is taken and modified from Sanchez-Vives and McCormick, 2000). Note propagation *in vivo* is faster (smaller time lags between electrode sites).

Those previously cited studies highlight the importance of studying slow wave oscillations as travelling waves and disclose their biological function –if any-, their dynamics and the mechanisms which allow their propagation in this Thesis. Experiments in anesthetized mice have been carried out to address some of these questions, and results are provided and discussed in further chapters. In the Results section data about direct electrophysiological intracortical field potential recordings of travelling slow oscillations is reported with quantitative information of speed and functional dynamics of slow wave propagation.

1.2. Fast oscillations

The cerebral cortex is able to display other oscillatory patterns, in addition to slow oscillations, such as beta-gamma waves (15-90 Hz), also called fast oscillations (Figure 2). The first evidence of this rhythmic activity appeared in surface EEG recordings made by Bremer and collaborators (Bremer 1960), where these oscillations were referred as a "synchronized activity". Early studies also observed fast oscillations in EEG and EMG recordings during cognitive performance (Loring and Sheer 1984). The cellular mechanisms of this fast oscillatory activity, at that time called 40 Hz waves, are represented as depolarizations of neurons in the neocortex (Llinas et al. 1991) or in the thalamus (Nunez et al. 1992; Pedroarena and Llinas 1997). These waves involve synaptic and intrinsic mechanisms and are modulated in the cortex and thalamus by cholinergic input coming from the brainstem (Steriade 1992). Steriade proposed that beta and gamma rhythms can interchangeably be termed *fast* because neurons may pass from beta to gamma oscillation in very short periods of time, 0.5–1 s, with slight depolarization (Steriade et al. 1996).

Since their description, fast oscillations suscited increasing interest, as many studies related cortical beta-gamma oscillations to cognitive processes such as attention, as firstly described in monkeys or cats (Bouyer et al. 1981; Fries et al. 2007; Rougeul et al. 1979). In this direction, several studies suggested gamma synchrony between neural assemblies to play a role in integration of sensory information (Gray and Singer 1989; Siegel et al. 2008). In addition to this, work in humans also related gamma oscillations to cognitive processes in different areas of the neocortex (Morgan et al. 2011; Muthukumaraswamy et al. 2009; Palva et al. 2002; Tallon-Baudry 2009; Uhlhaas and Singer 2010). In the last decade, researchers made a special point of interest in those rhythms since several studies related impairments in fast activity related to different diseases such as schizophrenia (Uhlhaas and Singer 2010 for a review), Alzheimer disease (Koenig et al. 2005), autism (Wilson et al. 2007) among others (reviewed in Uhlhaas and Singer 2006).

1.2.1. Cortical connectivity and mechanisms that generate fast oscillations

It is generally assumed that there are two main circuits that can sustain synchronized activity at fast frequencies: one is a circuit that involves inhibitory-inhibitory connectivity; the other involves pyramidal-interneuron feedback loops. Both network mechanisms are present in the cerebral cortex, one arising above the other depending on the relative strengths of the two. Valuable information is extracted from computational models, which as far as possible are supported with experimental evidences. The cellular and network mechanisms which involve fast rhythms are an issue that is extensively being addressed in the last two decades.

In the inhibitory-inhibitory circuit, kinetics of synaptic activity of different GABA receptors may allow the synchronization of activity at different frequencies: while $GABA_B$ receptor-mediated synapses (τ_{syn}~100 ms) may play a role in synchronization at low frequencies of a few Hertz, $GABA_A$ receptor-mediated synapses (τ_{syn}~5-10 ms) have time constants which fit for the synchronization at gamma frequencies. In a network model of GABAergic interneurons, spike firing frequency of individual neurons can be varied in a broad range, e.g., by changing the mean external drive or the strength of synaptic interactions among neurons in the network, yet the synchrony is high only in the gamma frequency band (Wang and Buzsaki, 1996). The first experimental evidence of an inhibitory-inhibitory circuit that generated gamma oscillations at 40 Hz was obtained by blocking fast excitatory glutamate AMPA and NMDA receptors and network was stimulated through metabotropic glutamate receptors (Whittington et al. 1995). Thus, networks of inhibitory cells provide a mechanism for synchronous fast oscillations. Evidence of beta-gamma oscillations emerging from interneuronal connectivity and involving $GABA_A$ conductances is also reported in an *in vitro* study, where the application of thiopental, a $GABA_A$ receptor modulator which prolongues its openings, reduced peak frequency of beta-gamma oscillations (Compte et al. 2008; Compte et al. 2003).

The other network mechanism that sustains fast oscillations is pyramidal-interneuron connectivity. In an early model, oscillations would emerge from reciprocal interactions, where there is strong presence of recurrent connections and inhibition has slower time constants and delayed relative to excitation (Wilson and Cowan 1972). Here, an oscillatory cycle begins when fast excitation drives UP neural firing in a positive feedback, until slower inhibition is recruited to eventually bring down population activity. As the excitatory drive to interneurons diminishes, the network recovers from inhibition and a new cycle starts, leading to rhythmic behavior (Hansel and Mato 2003; Paik et al. 2009).

In contrast to the synchrony at the population level, synchronization can be understood as spike-to-spike synchrony, where coherent oscillations are generated among a population of GABAergic cells, and pyramidal neurons are presumably synchronized by inhibitory inputs to produce a population rhythm. Experimental data that used optogenetic tools for selective stimulation of cell populations demonstrated that photoactivation of channelrodopsin-2 -a cation channel that depolarizes the cell when photostimulated- in fast spiking interneurons led to entrainment of pyramidal cells preferentially at gamma frequencies in mouse frontal (Sohal et al. 2009) and somatosensory cortex (Cardin et al. 2009).

In addition to those mechanisms, a special role of a particular localization of inhibitory synapses has been proposed, being that beta-gamma activity has been found to be inextricably tied to perisomatic inhibition (reviewed in Buzsaki and Wang 2012)

Finally, an extracortical mechanism has been proposed for the generation of fast oscillations, where high-frequency peripheral (retinal, lemniscal or cerebelar) oscillations could impose peripheral fast activities onto thalamocortical system (reviewed in Timofeev and Chauvette 2011).

The mechanisms of beta-band oscillations have been much less studied but may be generated by a similar circuit mechanism as gamma rhythm. For example, some experimental and computational models of interacting pyramidal neurons and interneurons exhibit network oscillations either in the beta or gamma band (Compte et al. 2008; Compte et al. 2003). The time scale of beta rhythmicity is comparable to the spike afterhyperpolarization lasting for 30–100 ms. Wang argues in his review in 2010 that at present is not fully understood what are the circuit properties required to quantitatively explain the observed relative phase lag between excitatory and inhibitory cells during gamma and beta rhythms (reviewed in Wang 2010).

1.2.2. Fast oscillations related to cognitive processes in neocortex

As mentioned in the beginning of this introduction, fast oscillations have been extensively related to cognitive function in the neocortex. Firstly, a role of gamma oscillations in attention has been extensively demonstrated (Bouyer et al. 1981; Rougeul et al. 1979). But also, interplay of different areas involved in multisensory processing has been found to be mediated by gamma oscillations. As an example, in a study (Ghazanfar et al. 2008) where the authors investigated binding of a vocalized sound and its associated mouth movement in monkeys, the presentation of a auditory stimulus displayed a peak in the gamma band in the LFP of auditory cortex. Coherence

in the gamma band was also present between auditory cortex and superior temporal sulcus (STS) when a face was also presented.

Gamma oscillations may also play a role in selective attention and its modulation by top-down signaling. For example, in a work in epileptic patients (Ray et al. 2008) the authors recorded subdural electrocorticography (ECoG) when the subjects were asked to pay attention to either auditory stimuli or vibrotactile stimuli. ECoG in the auditory and somatosensory cortical areas showed an early and a late component of event-related gamma band activity. The early component was localized in modality specific cortical areas, and not modulated by attention. In contrast, the late component (400 ms after the target stimulus onset) is larger in the somatosensory (respectively auditory) cortex when subjects attended vibrotactile (respectively sound) stimuli. Moreover, at electrode sites in the prefrontal cortex, ECoG gamma activity was negligible when a stimulus was presented in an unattended modality, but large in response to the presentation of an attended stimulus regardless of whether it was auditory or vibrotactile. These observations suggest that gamma-band oscillations in a sensory area are enhanced by selective attention, involving top-down signals from the prefrontal cortex.

Layered structure of the neocortex also may play an important role in signaling, which is tightly related to fast frequencies. While gamma oscillations are commonly enhanced under conditions that involve cognitive control, top-down signaling itself may be particularly associated with beta-band neural activity. Interplay between gamma and beta ocillations has been proposed in top down signaling. In this scenario, supragranular layers would mainly oscillate at gamma frequencies, whereas infragranular layers would do it al lower frequencies, in the beta range. Beta oscillations would interact with gamma oscillations as infragranular layers of a ‘higher order’ area in signal processing exert they top-down influence over supragranular layers of the ‘lower’ area (reviewed in Wang 2010).

Gamma oscillations have been also related to other cognitive processes such as working memory or learning. These oscillations have been recorded in frontal, parietal and other cortical areas in MEG and EEG recordings related to working memory tasks (Howard et al. 2003; Jensen et al. 2007; Reinhart et al. 2012; Roux et al. 2012). Coupling of theta and gamma rhythms seem to play a key role in learning (Kendrick et al. 2011; Zhang et al. 2012), while beta-gamma oscillations also seem to configure a cognitive mechanism involved in reward expectation (Lima et al. 2011; Zhang et al. 2012).

1.2.3. Assembly of beta-gamma oscillations within slow waves

During slow wave activity, both in slow wave sleep or under anesthesia, several rhythms have been shown to be superimposed to the slow oscillation. Among them, beta-gamma oscillations have a particular distribution within the slow waves: fast oscillations occur in a more prominent way within the depolarized states (UP states, (Chauvette et al. 2011; Collins et al. 2001; Compte et al. 2008; Steriade 2006; Steriade et al. 1996; Valderrama et al. 2012). In human sleep, spontaneous gamma oscillations have been described to be coupled to slow waves across the cortex, associated to the depolarized states, but also an oscillatory activity of less amplitude was present in the silent states (Valderrama et al. 2012). In anesthetized animals, slow waves show gamma oscillations associated to UP states (Chauvette et al. 2011; Collins et al. 2001; Steriade et al. 1996) but the study of Chauvette and collaborators, in which the oscillatory activity is compared between sleeping and anesthetized cats, showed that gamma activity is more prominent when coupled to anesthesia induced slow oscillations, thus suggesting an increase in synchrony of oscillations during anesthesia compared to sleep.

Also in spontaneously active cortical slices where slow oscillations emerged beta-gamma oscillations were recorded, probably sharing mechanisms of those observed *in vivo*, indicating that local cortical connectivity is sufficient for the generation of these rhythmic patterns (Compte et al. 2008).

1.3. An altered cortical network: the Down syndrome

Down syndrome (DS) is the most common cause of intellectual disability with a prevalence of aproximately 1 over 700 cases in the world (Parker et al, 2010). It consists on a chromosomic alteration with total or partial triple copy –aneuploidy- of human chromosome 21 (Hsa21). The syndrome was firstly described by Jean-Étienne Dominique Esquirol in 1838 and some years after by Edouard Seguin, in 1844. It took the name from John Langdon Down, who published a description of the syndrome in 1866, and was characterized as a trysomy-21 by Jérôme Lejeune in 1958. This genic overdosage confers a characteristic morphological phenotype with a wide variety of physical affections, including a specific neuropsychological profile. The average IQ of individuals with DS ranges 40-50, with cognitive disabilities affecting spatial learning, aspects of language acquisition and comprehension, and memory (Abbeduto et al. 2007; Chapman and Hesketh 2000; Nadel 2003; Pennington et al. 2003). Brain structural alterations are present in DS indviduals which comprise reduced cerebral and cerebellar hemispheres and smaller frontal lobe and hippocampal formation, among other changes ((Pinter et al. 2001; Raz et al. 1995). In the last decades, cognitive impairment in DS humans is quantified in several studies (Caltagirone et al. 1990; Haxby 1989; Menghini et al. 2011; Rowe et al. 2006; Velikova et al. 2011).

1.3.1. Candidate genes to generate cognitive disability in DS

A hypoThesis by Hardy and collaborators states that genes in Down Syndrome Critical Region (DSCR) region, when triplicated, are responsible for the majority of DS phenotype and may cause the disease (Hardy et al. 1989). Within DSCR, a major candidate gene proposed to underlie the cognitive disability in DS is *DYRK1A*. This gene, homologous to *minibrain* in drosophila, is expressed during the neurodevelopment and has a critical role in neurogenesis and neuronal differentiation. In this direction, several data supported that the over-expression of this gene would have a major impact in cognitive performance in DS (reviewed in Tejedor and Hammerle 2011). The DYRK1A protein belongs to the dual-specificity tyrosine phosphorylation-regulated kinase family, which interacts with a wide range of substrates and proteins implicated in different processes at cellular and molecular level, including synaptic function (Chen-Hwang et al. 2002; Huang et al. 2004; Murakami et al. 2006; Wegiel et al. 2004), and is expressed mainly in cortex, cerebellum and hippocampus (Guimera et al. 1999; Guimera et al. 1996).

Other candidates to generate cognitive disability in DS are *OLIG1* and *OLIG2* genes, which code for oligodendrocitic transcription factors, also related to neuronal proliferation and neurogenesis. Work in trisomic mice -Ts65Dn mice, a model of DS that includes a triple copy of the DSCR, among other genes- demonstrated that returning *OLIG1* and *OLIG2* over-expression to euploid levels leaded to normalized neurogenesis and inhibitory neuronal production in cortex and hippocampus (Chakrabarti et al. 2010). Despite that, triplication of *OLIG1* and *OLIG2* may not be sufficient to generate cognitive deficits in DS, because evidence of synaptic failure was found in mice with triplicated DSCR –Ts1Rhr mice- (Belichenko et al. 2009), and hippocampal performance is identical to control animals when DSCR is returned to euploid levels in models with triple copy of genes external to this region, which include *OLIG1-2* genes (Olson et al. 2007).

1.3.2. DS mouse models

For the study of the neurobiology of Down syndrome, genetically engineered animals provide a useful tool to disentangle the mechanisms which underlie the phenotype of DS individuals. These mouse models reproduce different features of DS, allowing the analysis of structural, functional, and behavioral aspects of cognitive deficits in DS. These models present modifications which range from a single gene to a complete chromosome triplication. Other models not included there are *knock-out* for a single gene or monosomic for a region of genes, which are also used in study of DS.

Among the DS mouse models, trisomic models present triplications or translocations –changes of genetic material between chromosomes- of a wide chromosomic region which include a large amount of genes (Fig. 7) upon the triplication of a whole chromosome. Thus, trisomic models of DS are: Tc1; aneuploid for whole Hsa21 (O'Doherty et al. 2005); Ts16 (Epstein et al. 1985) carry a trisomy of MMU16; Ts65Dn (Davisson et al. 1993), which are trisomic for a segment of MMU16 including the DSCR; Ts1Rh mice –trisomic for just the DSCR- and MTs1Rh/T65Dn –euploid for DSCR but other regions triplicated- (Olson et al. 2007), Ts1Cje and Ts2Cje (Sago et al. 1998; Villar et al. 2005); Ms1Ts65 (Sago et al. 2000), trisomic for the region by which Ts1Cje and Ts65Dn differ; Dp(10)1Yey/+; Dp(16)1Yey/+ and

Dp(17)1Yey/+ mice (Yu et al. 2010), with full triplications of syntenic cromosomes MMU10, MMU16 and MMU17 respectively –which are the murine chromosomes which contain the genes of human chromosome 21 (Hsa21)- and Ts1Yah, that carries genes of the MMU17 that is syntenic of a telomeric region in Hsa21 (Pereira et al. 2009).

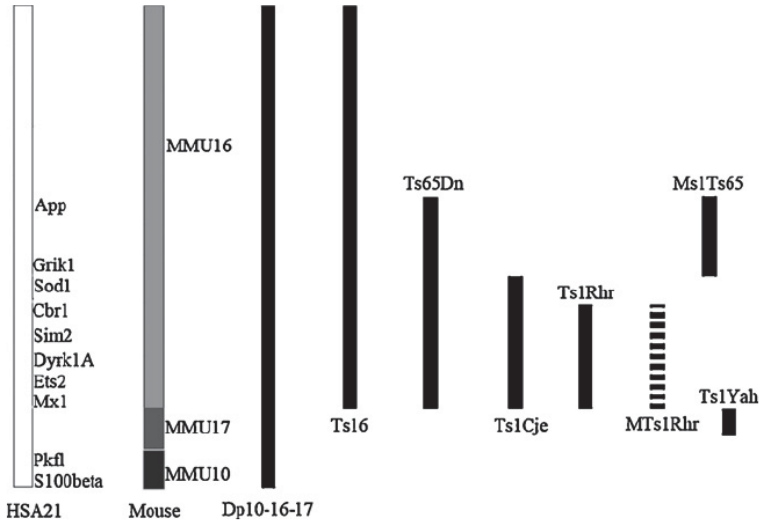

Figure 7. Trisomic mouse models of DS.
Scheme where is representated the extension of triplicated genes in different trisomic mouse models of Down syndrome. Taken from Gotti et al.(2011), that was partially modified from Seregaza et al. (2006) and Roubertoux and Carlier (2010).

Models with a few extragenomic genes or a single gene expressed in artificial chromosomes are: YAC152F7 -containing the genes *PIGP*, *TTC3*, *DSCR9*, *DSCR3*, *DYRK1A*- and YAC141G6 -containing the genes *DSCR6*, *PIGP*, *TTC3*, *DSCR9*, *DSCR3*, both expressed in a yeast artificial chromosome (Branchi et al. 2004; Sebrie et al. 2008); hAPP-YAC, expressing a single copy of human APP protein in a yeast artificial chromosome (Lamb et al. 1993), DYRK1A BAC -which contains a single copy of DYRK1A gene in an external bacterial artificial chromosome- (Ahn et al. 2006); and transgenic mice, each of them carrying one or more extra copies of one of the following genes –present in Hsa21- in their genome: *DYRK1A*, (TgDyrk1A mice, (Altafaj et al. 2001), *SIM2* (Ema et al. 1999), *S100beta* (TghuS100B mice, (Friend et al. 1992), SOD1 (Epstein et al. 1987), *APP* (Tg2576 mice, Tg6209 mice, (Hsiao 1998). Other models are double-transgenic mice, such as the APP-SOD1 mice (Borg and Chereul 2008; Xue et al. 2002). The motivation to generate single gene models is to generate an alteration only related to a single gene. Nonetheless, as longer is the triplicated genotype it typically produces a greater effect (Chabert et al. 2004).

In most of these models, impaired cognitive performance in different behavioral tasks is observed. Tasks are those related to visuo-spatial learning and working memory –Morris water maze, new object recognition tasks and others- or operant

conditioning, involving both cortex and hippocampus depending on the task (reviewed in Roubertoux and Carlier 2010). However, most of them were performed in Ts65Dn and Ts1Cje mice, although some behavioral tasks have been performed in single-gene transgenic mice (Altafaj et al. 2001).

1.3.3. The TgDyrk1A as a mouse model of DS

To allow the analysis of cognitive function alterations –and others- that might produce the *Dyrk1A* gene triplication, TgDyrk1A mice were generated.

In the first characterization of the model, TgDyrk1A mice have been shown to present cognitive impairment related to hippocampal and prefrontal cortex function, with altered visuospatial learning and cognitive flexibility, as well as motor abnormalities and neurodevelopmental delay (Altafaj et al. 2001; Martinez de Lagran et al. 2004), all of these present in DS humans. The phenotype is also spread to cerebellum, where TgDyrk1A presents increased expression of NR2A subunits of NMDA channels and altered decay of NMDA–induced calcium transients (Altafaj et al. 2008). Thus, as *DYRK1A* is expressed in the cortex, it would be rather possible that over-expression of *DYRK1A* produced alterations in neocortex in TgDyrk1A mice as previous data suggested (Altafaj et al. 2001; Martinez de Lagran et al. 2004). This is why in this Thesis this mouse model of Down syndrome is proposed as a model of an altered cortical network. However, behavioral data in this model that provide evidence of clear implications of prefrontal cortex in cognition in neocortex-dependent tasks were missing. These data have been obtained by María Martínez de Lagrán from Mara Dierssen lab, and will be presented in the results part of this Thesis.

1.3.4. Cortical and sleep alterations in DS individuals

Neocortex in DS individuals presents a wide range of structural alterations: a decrease in the number and depth of sulci, an irregular neocortical laminar formation, neuronal heterotopias –which are alterations in neuronal migration-, a delayed myelination of cortical fibers, and reduced spine density and dendrytic branching (Becker et al. 1991; Coyle et al. 1986; Golden and Hyman 1994; Suetsugu and Mehraein 1980; Takashima et al. 1989). In addition, fetal DS cortex show reductions in the levels of GABA, but not in glutamate (Whittle et al. 2007), whereas in adult a decrease in glutamate has been described (Reynolds and Warner 1988; Risser et al. 1997), suggesting an impaired balance between excitatory and inhibitory system. Other neocortical alterations found in recent studies are a reduction of 40% in the number of neurons and 30% of glial cells in DS individuals (Karlsen and Pakkenberg

2011). Among the associated pathologies, aging DS individuals develop neuropathological changes similar to those in Alzheimer disease in virtually all cases by the age of 40 years (Mann and Esiri 1989) and dementia prevalence is 77% between 60 and 69 years (Visser et al. 1997)

Cortical alterations are also expressed as changes in sleep architecture of DS individuals. Early polysomnographic studies showed that, in addition to the morphological changes, altered patterns in REM and non-REM sleep were present in DS individuals. These alterations include decreased REM sleep, altered durations of non-REM sleep stages, and an increase in body movements and awakening during sleep were present in DS humans (Castaldo 1969; Clausen et al. 1977; Fukuma et al. 1974; Hamaguchi et al. 1989; Petre-Quadens and Jouvet 1967). In some of these studies, increases or decreases in different sleep stages were observed, often reporting contradictory results (and Fukuma et al. 1974; see Petre-Quadens and Jouvet 1967), but all found alterations in sleep patterns in DS humans.

1.3.5. Cortical alterations in DS mouse models

As mentioned above, cortical alterations in DS humans are modeled to different degrees with genetically engineered mice. The following are studies in which different aspects of cortical deficits are found in mouse models of DS.

In isolated cortical neurons from fetal Ts16 mice, alterations of calcium currents have been detected (Acuna et al. 2012). Also in isolated neurons from Ts16 mice, endosomal trafficking dysfunctions were present related to amyloid precursor protein when neurons were treated with cholesterol (Acuna et al. 2012), and apoptosis was found to be related to the intracellular accumulation of amiloyd protein (Arriagada et al. 2007). Ts16 mice show in addition disrupted sequence of neurodevelompental formation of neocortex (Cheng et al. 2004).

In the Ts65Dn mouse, the most widely studied model of DS, several cortical alterations have been reported. At structural level, increased size of presynaptic and postsynaptic contacts in dendrites of neocortical –and hippocampal- neurones has been reported in this model (Belichenko et al. 2004). A previous study showed significantly less (30%) asymmetric synapses (typically excitatory) in the temporal cortex of Ts65Dn mice than in controls, whereas the density of symmetric synapses (typically inhibitory) remained unaltered. In addition, the mean synaptic apposition lengths of both asymmetric and symmetric synapses were significantly larger in Ts65Dn mice than in controls (Kurt et al. 2000). Increased number of dendritic branches, length of dendritic branches, spine densities and number of spines in the basal dendritic arbors of neocortex layer III pyramidal cells were also reported in Ts65Ds mice (Dierssen et al. 2003). From the molecular point of view, an increase in

proteins related to active inhibitory synapses has been detected in somatosensory cortex, that point out to an increase in inhibitory synaptic activity in the neocortex (Perez-Cremades et al. 2010). Whith this hypoThesis, a recent multidisciplinary work by Chakrabarti and collaborators in Ts65Dn mice found a direct link between gene triplication and defects in neuron production during embryonic development. These neurogenesis defects led to an imbalance between excitatory and inhibitory neurons and to increased inhibitory drive in the Ts65Dn forebrain. In the same work, as mentioned above, the authors show that normalizing *OLIG1* and *OLIG2* gene overdosage rescued the inhibitory phenotype in trisomic mice. In a more recent work regarding mRNA transcripts, the authors found cortical splicing aberrations in neocortex of Ts65Dn mice and also in a Dyrk1A over-expression model derived from mRNA pools from TgDyrk1A mice (Toiber et al. 2010). Other work showed reduced neuropeptide expression in neocortex, (Hernandez et al. 2012). Accumulations of amyloid precursor protein (APP) were found in parietal cortex –and hippocampus- at 13-16 months of age, suggesting a link to the development of degenerative processes resembling those of Alzheimer disease (Hunter et al. 2003). At functional level, a study found alterations in visual-evoked potentials recorded in visual cortex in this model that demonstrate visual deficits in those mice (Scott-McKean et al. 2010). Another substance that may play a role in mental retardation in DS individuals, myo-inositol, was also elevated in several areas of the brain in Ts65Dn mice including frontal cortex with respect to controls (Shetty et al. 2000).

Other studies were performed in Ts1Cje mice demonstrating oxidative stress, mitochondrial dysfunction and hyperphosphorylation of tau protein, all of which may play critical roles in the pathogenesis of mental retardation in DS (Shukkur et al. 2006). Altered regulation of tau phosphorylation was also observed in Tc1 mice (Sheppard et al. 2011).

In transgenic models, little data about cortical alterations is available from any model compared to what is found in trisomic Ts65Dn and Ts16 mice, but several cortical alterations at different levels have been described in the different monogenic models. At molecular level, a study in mice that overexpressed human *SOD1* gene, proteasome activity was reduced in neocortex of (Le Pecheur et al. 2005). Another study also demonstrated that hAPP-YAC transgenic mice have an UP-regulation in the frontal cortex of the ubiquitin-proteasome system similar to AD and DS patients (Seo and Isacson 2010). In another study with double transgenic mice, an enhanced accumulation of phosphorylated alpha-synuclein was found, which modeled the same findings present in DS and Alzheimer disorders (Kurata et al. 2007). As described above, pools of mRNA coming from TgDyrk1A mice presented splicing aberrations (Toiber et al. 2010). And Tg2576 mice, which overexpress human APP protein, show beta-amyloid plaques in neocortex (Sarsoza et al. 2009). At structural level, a MRI

study of transgenic APP and SOD1 and double-transgenic APP/SOD1 mice, showed pronounced alterations in gray matter volume were observed in 1-year-old double APP/SOD1 transgenic mice. Entorhinal, and cingulate cortex –and hippocampus- volumes were decreased by 8% to 25%. In contrast, mice homozygous for SOD1 exhibited atrophy specifically in cortex regions (cingulate, retrosplenial, and temporoparietal cortex), but no significant modification was found in the hippocampus region. None of these alterations was seen in single APP transgenic mice (Borg and Chereul 2008). The characterization of spontaneous oscillatory patterns emerging from neocortical circuits in a model of a triplication of a single gene, the TgDyrk1A mice, is one of the aims of this Thesis, providing data about functional aspects of the neocortex in this mouse model.

1.3.6. EEG oscillatory activity in DS humans and mouse models

First descriptions of oscillatory activity in DS humans were performed by O. Vergani and T. Beley in the 50's, and later by T. Hirai and E.L. Gibbs in the 60's in EEG studies. Altered sleep patterns in DS humans were firstly observed by O. Petre-Quardens in 1967 and V. Castaldo in 1969, with means of polysomnographic recordings. Other posterior studies in the 70's, combined EEG recording with power spectrum analysis in different frequency bands to study oscillatory activity in DS individuals in different sleep stages (Clausen et al. 1977). In later studies EEG signals were combined with other techniques, such as the measure of cognitive performance, localization of current sources, among others. Other initial studies described how DS brain responded to external stimuli in form of evoked potentials in the 60's and early 70's (Barnet and Lodge 1967; Barnet et al. 1971; Bigum et al. 1970), while work in the 60's with EEG recordings described as well the increased occurrence of epilepsy in DS humans (Borselli and Sferlazzo 1963; Seppalainen and Kivalo 1967). Despite that, the following are studies which relay on the interictal altered EEG sleep and oscillatory and patterns in DS individuals.

As mentioned above, one of the first studies of oscillations in sleeping humans with DS combined power spectrum analysis in EEG recordings to evaluate oscillatory activity across sleep stages (Clausen et al. 1977). The authors reported increasing power of frequencies between 1 and 20 HZ in all stages of sleep with exception to a narrow band of 8-13 Hz corresponding to alpha waves. The differences in power were more prominent in stages 1, REM sleep and waking state. In the waking state, a peak that appeared in controls was not present in DS humans, but the absolute power difference remained non-significant. A posterior study in DS children with similar techniques but no power spectrum analysis provided evidence that DS children have some degree of lag of maturation of EEG-sleep patterns. In addition to a low incidence

of quiet sleep (non-REM) in the first three months, DS children had less spindles and later disappearance of frontal sharp waves, which are common during fist stages of development (Hamaguchi et al. 1989).

Those initial studies, together with the characterization of the neuropsychological of DS, led to the study of oscillatory activity in the waking period. Work in DS EEG oscillatory activity found a correlation between alpha wave activity, cognitive performance and age. In this study, the authors EEGs, psychometric testing, quantitative computed tomography, and positron emission tomography with fludeoxyglucose –that provides a measure of brain metabolism- in 19 young DS subjects, 9 older DS subjects and 13 healthy control subjects. Results were that all the control subjects, 13 young adult patients with DS, and 5 older patients with DS had normal EEG backgrounds. In comparison with the age-matched patients with DS with normal alpha background, older patients with DS with decreased alpha background had dementia, fewer visuospatial skills, decreased attention span, larger third ventricles, and a global decrease in cerebral glucose utilization with parietal hypometabolism. In the young patients with DS, the EEG background did not correlate with psychometric or positron emission tomographic findings, but the third ventricles were significantly larger in those with abnormal EEG background. The young patients with DS, with or without normal EEG background, had positron emission tomographic findings similar to those of the control subjects (Devinsky et al. 1990).

A study in 1996 showed that alpha band power ratio in waking EEG of DS humans in the occipital area between closed-eyes and open-eyes recording was substantially increased compared to controls. The authors also showed that the degree of changes correlated with neuropsychological test scores of DS subjects, indicating changes that affected more than vision (Partanen et al. 1996).

Parallel work in DS individuals explored the occurrence of oscillatory activity in aging. In a former study, frequencies of occipital alpha waves decreased with age in DS individuals. In older individuals, the author show that slowing was accompanied with an increase of activity in 6-8 Hz, but didn't correlate with cognitive performance in the daily life (Ono 1993). In a study in the same year, the authors related a slowing in EEG oscillatory activity that significantly correlated with and an age-related decline of cognitive functions in DS humans (Soininen et al. 1993). In addition to this, a study in aging DS individuals showed that a slowing in frequency of oscillatory activity in EEG recordings was present in DS compared to controls during aging (Murata et al. 1994), where a mean frequency of EEG power in delta, theta1-3, alpha1-4 and beta1-2 bands was 9.37 at 20's in DS individuals, 9.17 at 30's and 8.76 at 40's, whith significant changes between them, while in controls differences were non-significant between individuals in their 20's and 60's. Posterior work on this topic compared EEG peaks of alpha waves in DS individuals and control healthy persons as well as in those with

mentally retardation except the Down syndrome (non-DS mental retardation) across aging. Here, resting EEGs from the frontal, central and occipital regions were examined through power spectrum in groups of subjects in intervals of 5 years. The number of subjects with DS who showed dominant component within 8 Hz band of the basic rhythm reached maximum in its appearance rate at 40±44 years of age in the occipital area, while in healthy subjects the presence of this 8 Hz rhythm was in a minority of cases. Confirming previous results, a slowing in this basic rhythm progressed already at 30±34 years in DS subjects. In contraposition, in non-DS mental retardation, the number of subjects who showed dominant component at 8 Hz reached maximum at 45±49 years of age, and this slowing of the basic rhythm was not as clear as in DS. In a parallel follow-UP study, EEGs were recorded repeatedly once a year during 8 or 9 years in persons with DS and with non-DS mental retardation. The result was that although the lowering in EEG frequency to 8 Hz took place in various years of age individually, earlier distinct decrease of the frequency was commonly noticed in DS subjects (Katada et al 2000). The authors in both studies hypothesized that the earlier slowing could be a senile sign and be related to the decline of brain function referring to Alzheimer disease.

One of the issues in the study of oscillatory activity in DS humans is its different consolidation during development. In this direction, work in DS individuals which ranged from 9 months to 26 years studied EEG coherence between areas. This was computed for five groups of electrode pairings: 1) anterior-to-posterior, 2) posterior-to-anterior, 3) posterior-temporal, 4) anterior-temporal and 5) interhemispheric. The results showed that EEG coherence strongly and consistently discriminated between DS and control groups (McAlaster 1992). A more recent study of EEG that used 21 electrodes in frontal, central, parietal, occipital and temporal areas in DS children provided evidence of a decrease in alpha waves during REM sleep -while beta, theta and delta bands did not differ significantly between the groups-, confirming differences during development in oscillatory activity of DS individuals (Smigielska-Kuzia et al. 2005).

Despite all this work on oscillatory activity, the present Thesis is focused on alterations of gamma rhythm during slow waves of a Down syndrome mouse model. So, here are presented the most relevant findings in humans regarding fast oscillations: Babiloni and collaborators tested the hypoThesis that inter-hemispheric directional functional coupling of eyes-closed resting EEG rhythms is abnormal in adolescents with DS. They studied power of EEG rhythms, which was evaluated by FFT for control purposes, whereas interhemispheric directional EEG functional coupling was computed by directed transfer function (DTF). EEG rhythms of interest were delta (2-4 Hz), theta (4-8 Hz), alpha 1 (8-10.5 Hz), alpha 2 (10.5-13 Hz), beta 1 (13-20 Hz), beta 2 (20-30 Hz) and gamma (30-40 Hz). Results were that alpha, beta, and gamma

power was widely higher in young controls than young DS subjects, whereas the opposite was true for delta power. As a novelty, DTF (directionality) values globally prevailed from right to left occipital areas in normal young subjects and in the opposite direction in DS patients (Babiloni et al. 2009).

Further work focused in the identification of the current sources which underlie differences in wave activity. A study in adults by Babiloni and collaborators that appeared one year after the previous exposed consisted in a study combining EEG recording with LORETA technique (Low Resolution Electromagnetic Tomography), which allowed the correlation of EEG signals to the Current Source density representations in three dimensions. Here, the authors separated power spectrum in the same frequency bands as in the previous work. Both techniques and power spectrum analysis showed central, parietal, occipital, and temporal cortical sources of resting alpha and beta rhythms were lower in amplitude in the DS than control subjects, whereas the opposite was true for occipital delta cortical sources (Babiloni et al. 2010). The authors argued that this result in alpha cortical source is consistent to what is typically found in Alzheimer's disease. In another study a year after, EEG was also combined with e/sLORETA technique (exact/standard Low Resolution Electromagnetic Tomography) and provided correlation with cognitive performance. They calculated absolute and relative power in delta (1–3 Hz), theta (4–7 Hz), alpha1 (8–9 Hz), alpha2 (10–12 Hz), beta1 (13–18 Hz), beta2 (19–21 Hz) and beta3 (22–30 Hz) frequency bands. When compared with controls, DS showed increased CSD in theta, alpha1 and beta1 classical bands and in individual alpha peak frequency-adjusted bands -which were alpha1, alpha2 and theta bands-, while relative alpha2 was decreased. A negative correlation between cognitive performance and theta/alpha CSD in the right frontal lobe and right posterior cingulate cortex was also found (Velikova et al. 2011).

In summary, while the awake oscillatory activity appears to be altered in alpha, beta and gamma waves, which are decreased, and theta oscillations, that are increased in some areas in DS humans, sleep studies described increased oscillatory activity in a wide range of frequencies across sleep stages in DS individuals except in the alpha band, which is consistent with that alpha waves are an oscillatory pattern related to awake activity. Despite all those results, it has to be mentioned that is difficult to extract high frequency components from the EEG signals due to filtering by tissue between cortex and recording electrodes and possible limitations in sampling frequency of multiple channels together.

In parallel to the last work in humans, EEG signals have also been obtained in several mouse models of Down syndrome, in which EEG-sleep patterns have been studied. Two studies describe the work, one performed in transgenic models overexpressing human SOD1 and human APP and the other in trisomic models –

Ts65Dn and TsjCe mice-, both combining EEG recordings with power spectrum analysis In the former study, the authors found that baseline records presented unchanged parameters in slow wave sleep and waking, whereas REM sleep episode numbers were decreased and REM latency increased after lights off in hSOD mice versus controls. In contrast, hAPP mice exhibited no change in REM sleep but an increase in waking and a decrease in slow wave sleep before light transition as well as an increase in theta-power in REM and waking. In addition, sleep deprivation affected differently both models: while hSOD mice did not experience slow wave sleep or REM sleep rebounds after sleep deprivation but EEG activity in the delta-SWS activity was enhanced, hAPP mice exhibited slow wave sleep and REM sleep rebounds as well as enhancement of delta-slow wave activity (Colas et al. 2004). In the other study, the authors studied similar features in the trisomic models. They found increased waking amounts at the expense of non-REM sleep, increased theta power during sleep and a delayed sleep rebound after sleep deprivation in Ts65Dn mice. In contrast, Ts1Cje had limited sleep and EEG abnormalities, showing only a delayed sleep rebound after sleep deprivation and no difference in theta power (Colas et al. 2008). As a hypoThesis extracted from those studies, where theta oscillations were altered in hAPP and Ts65Dn mice, the authors suggested a possible correlation between APP over-expression and changes in hippocampal theta oscillations. However, none of those studies in DS mouse models provided a systematic characterization of slow and foast oscillatory activity, or gave a network mechanism explaining how emergence of cortical patterns is impaired.

2. METHODS

2.1. Experiments *in vitro*

2.1.1. Slice preparation.

Ferrets (2-12 month old, either sex) were anesthetized with sodium pentobarbital (34 mg/kg) and decapitated. The entire forebrain was rapidly removed to oxygenated cold (4-10^{o}C) bathing medium. Coronal slices (0.4 mm thick) from the occipital cortex containing primary and secondary visual cortical areas (areas 17, 18, and 19 (Innocenti et al. 2002) were used.

A modification of the sucrose-substitution technique developed by (Aghajanian and Rasmussen 1989) was used to increase tissue viability. During preparation of slices, the tissue was placed in a solution in which NaCl was replaced with sucrose while maintaining an osmolarity of 307 mOsm. After preparation, slices were placed in an interface style recording chamber (Fine Sciences Tools, Foster City, CA). For the first 15 minutes cortical slices were superfused with an equal mixture in volume of the normal bathing medium and the sucrose-substituted solution. Following this, normal bathing medium was switched into the chamber and superfused the slices for 1-2 hours, then modified slice solution were used throughout the rest of the experiment. Bath temperature was maintained at 34.5-36^{o} C.

The normal bathing medium contained (in mM): NaCl, 126; KCl, 2.5; $MgSO_4$, 2; NaH_2PO_4, 1.25; $CaCl_2$, 22; $NaHCO_3$, 26; dextrose, 10, and was aerated with 95% O_2, 5% CO_2 to a final pH of 7.4. The modified solution had the same ionic composition except for different levels of (in mM) KCl, 3.5; $MgSO_4$, 1 and $CaCl_2$, 1-1.2 (Sanchez-Vives and McCormick 2000). Electrophysiological recordings started after allowing at least 2 hours recovery.

2.1.2. Local Field Potential, single unit and stimulation

Extracellular LFP recordings were obtained with 2-4 MΩ tungsten electrodes (FHC, Bowdoinham, ME) in L5 of visual cortex slices. Single units were recorded with glass electrodes (8-15 MΩ) pulled on a Sutter Instruments P-97 micropipette puller (Novato, CA) from medium-walled glass. Single unit electrodes were also placed in L5 of the visual cortex. A tungsten electrode similar to those described previously was placed nearby the glass electrode in single unit experiments, at less than 200 μm, to obtain a recording from the local network in the vicinity. LFP recordings with triggered UP states were obtained by placing the tungsten electrode in L4 through stimulation of

white matter with a bipolar tungsten electrode. Stimuli were delivered at 0.25 Hz with a duration of 0.2 ms at 120 or 220 μA with a stimulus isolator triggered with Spike2 and a Master8 unit. Control recording started at least after 5 min of stabilization of evoked fPSP. Signals were amplified with a NeuroLog system (Digitimer, UK), digitized at 50 kHz for single unit recordings and 5 or 10 kHz using a CED board and Spike 2 software. Filtered LFP signals were obtained also with Spike 2 software.

2.1.3. Pharmacological agents.

Phenytoin (Combino Pharma, Spain) was applied in the bath at different concentrations. The slices were in an interface chamber during recordings and drug application. In this type of recording chamber reaching the final concentration of a drug in the bath takes around 20 minutes. We used phenytoin since it is a more specific blocker of INaP than riluzole and has less effect on the transient Na+ current (Chao and Alzheimer 1995; Stefani et al. 1997a). For extracellular LFP recordings, phenytoin concentrations were 40, 60 and 80 μM. For single unit recordings, concentration was 80 μM in 40 ml of ACSF also perfused in bath during at least 30 min. In the electrical stimulation experiments, 80 μM phenytoin was perfused in the bath also for at least 30 min (n=5). In 2 cases 800 μM phenytoin was locally applied through the pressure-pulse technique in which a brief pulse of pressure (50-75 ms; 200-300 kPa) was applied to the back of a broken microelectrode (1-4 μm diameter) to extrude around 1-20 pl solution. A mixture of CNQX (2 μM, RBI, USA) and APV (10 mM, Tocris, UK) in ACSF was used for the blockade of the excitatory recurrence. After 5 ml of perfusion with the blockers, 80 μM phenytoin was added to the bath solution. Slow oscillations were recorded until were completely blocked.

2.1.4. Data analysis.

UP state detection for calculation of network temporal and firing parameters was performed using an algorithm that estimates MUA as the power change in the Fourier components at high frequencies of extracellular recordings (Reig et al. 2010; Sanchez-Vives et al. 2010). All the MUA off-line estimates and analyses were implemented in MATLAB (The MathWorks Inc., Natick, MA).

Single unit recordings were analyzed using Spike2 software (Cambridge Electronic Design). The length of the analyzed periods for single units was 200 seconds, obtaining 4 periods during the recording: control in the first 300 seconds before drug application, period 1 in the first 300 seconds just after bath application of the drug, the middle period 2 at half time between first and last period, and period 3 at the last 20 % of the

time while recording the units. Full recording ended until all 40 ml were bath applied or oscillations were lost. The firing rate distribution analysis within the UP state was performed dividing the UP states in five segments and calculating firing rate for each independent segment using homemade scripts for Spike2. The segments of analysis were the same as for the analysis in the whole UP state.

In order to analyze the fast components of oscillations, UP states and DOWN states were detected and their respective power spectrums were calculated. The power spectral density (psd) of the original signal (local field potential) was calculated with Welch's method, which splits the data into overlapping segments: the original signal is divided segments of length M (0.1 sec), overlapping by 0.05 seconds. Each segment is windowed with a Hanning window. After that; the periodogram is calculated by computing the discrete Fourier transform, and then computing the squared magnitude of the result. Finally the resulting periodograms are averaged to produce the power spectral density estimate.

LFP recordings with evoked UP states were analyzed qualitatively, although a quantification of UP state duration and relative firing rate of evoked UP states was performed in presence of phenytoin. A section of the UP state was removed in order to avoid stimulus artifacts. Bath applications of phenytoin (80 µM) were computed together with local applications (800 µM) as we noted that the effect went in the same direction.

LFP analysis was performed in collaboration by María Perez, who also used the algorithms and scripts. Single Unit analysis was performed in collaboration with Laura Ciria, who made and used scripts.

2.1.5. Statistical analysis.

All comparisons between multiple means were performed using One-way ANOVA followed by Fischer *post-hoc* tests. Two-tailed paired T-tests were used to evaluate effects of local application of phenytoin with previous excitatory synaptic blockade with APV-CNQX or with evoked UP states. The outlier was removed using extreme studentized deviate (ESD) method. Values are reported as normalized mean or mean ± SD in the text and normalized mean or mean ± SEM in the plots.

2.2. Experiments *in vivo*

2.2.1. In vivo extracellular recordings.

Mice were cared for and treated in accordance with Spanish regulatory laws (BOE 256; 25-10-1990), which comply with the European Union guidelines on protection of vertebrates used for experimentation (Strasbourg 3/18/1986). All experiments were approved by the Ethics Committee from the Hospital Clinic (Barcelona, Spain). Adult C57BL6/SJL or TgDyrk1A mice 3–6 months old were used for extracellular recordings. Anesthesia was induced with intraperitoneal injection of ketamine (75 mg/kg) and medetomidine (1 mg/kg). Atropine (0.3 mg/kg) was administered to prevent respiratory secretions. Tracheotomy was performed to increase stability during recordings. After this procedure and administration of a maintaining dose of ketamine (37.5 mg/kg ip), the animal was placed in a stereotaxic frame and air enriched with oxygen was delivered through a thin silicon tube placed at 0.5–1 cm from the tracheal cannula. A continuous infusion of ketamine at 40 mg·kg_1·h_1 was delivered subcutaneously to maintain a constant level of anesthesia. Methylprednisolone (30 mg/kg) was also administered to prevent inflammation. Body temperature was maintained at 36–37.5°C. Bilateral craniotomies were made at 4 sites: AP 2.3 mm from bregma, L 0.4 mm or AP 2.5 mm, L 0.5 mm (medial prefrontal cortex); AP 0.5 mm, L 1.5 mm (primary motor cortex); AP -1.5 mm, L 2.5 mm (primary somatosensory cortex); and AP -2.5 mm, L 2.5 mm (primary visual cortex) (following Franklin and Paxinos 2008). Extracellular slow wave recordings were obtained with tungsten electrodes with impedances of 1–2 MΩ. Electrodes were placed in infragranular layers (0.4 lateral and 1.0 –1.2 mm deep in prefrontal cortex, 0.9 –1.1 mm in somatosensory cortex, 0.7– 0.9 mm in visual cortex, 1.0 –1.2 mm in motor cortex). Extracellular recordings were usually obtained bilaterally, amplified with either a NeuroLog (Digitimer) or a multichannel system (Multi Channel Systems). The signal was digitized at 20 KHz with a CED acquisition board and Spike 2 software (Cambridge Electronic Design).

2.2.2. In vivo slow wave propagation.

Arrays of M = 16 aligned electrodes separated by 100 µm (Neuronexus) were used to record activity propagation. We computed the speed of UP state propagation across the cortex, relying on the time lags between consecutive detected UP state onsets from multiunit activity (MUA) of different electrodes. We selected time series containing at least N=300 UP states. The average of the onset times of the same traveling UP state in the multielectrode array was taken as reference for each detected

UP state to compute the array of relative time lags. In other words, if *Ts,c* is the onset time of the *s*th UP state in the *c*th electrode, the array of relative time lags is $\Delta T_{s,c} = \sum_{c=1}^{M} Tsc/M$. Absolute values $\Delta T_{s,c} > 150$ ms were not considered, because these were very likely due to a failed UP state detection. We explored the possible existence of different patterns of activity propagation by sorting the time lag arrays ΔT_s of the detected UP states in the low-dimensional space resulting from principal component analysis (PCA) (Jackson 1991). We found that the first three principal components always represented >50% of the total variance. In this three-dimensional subspace each detected UP state is a point. We worked out the "principal axis" of the point cloud, minimizing in the least-squares sense the sum of the distances of the points from this axis. Finally, the points are projected on such a principal axis in order to associate a scalar quantity to each UP state and to rank them. Sorting $\Delta T_{s'}$ with such ranking, we found gradual but significant changes in the activity propagation patterns. We then pooled the UP states in five equally sized groups (at least 60 time lag arrays per group), such that the first pool was $\Delta T^{(1)} = \{ \Delta T_{s'} \}_{s'=1}^{N/5}$, the second pool was $\Delta T^{(2)} = \{ \Delta T_{s'} \}_{s'=\frac{N}{5}+1}^{2N/5}$, and so on. For each group of arrays we carried out the average time lag $\langle \Delta T_c^{(n)} \rangle = \sum_{s=1}^{N/5} \Delta T_{s,c}^{(n)}/(N/5)$ and its standard error (SE) for each electrode *c*. Finally, the speed was computed in those recordings showing a monotonic change with electrode position of the average time lag within each propagation pattern. It was carried out by dividing the distance $D(n)$ between the electrodes showing the maximum and minimum average time lags by their time lag difference: $D^{(n)}/[\max_c \langle \Delta T_c^{(n)} \rangle - \min_c \langle \Delta T_c^{(n)} \rangle]$.

Analysis of propagation was carried out by Maurizzio Mattia (Instituto Superiore di Sanitá, Rome).

2.2.3. In vivo single unit with extracellular recordings.

Glass recording electrodes (8–15 MΩ) were pulled on a Sutter Instruments P-97 micropipette puller (Novato, CA) from medium-walled glass and filled UP with saline. Electrodes were placed in the primary motor, medial prefrontal cortex, and somatosensory cortex. A tungsten electrode similar to those described above was placed nearby the glass electrode, at <200 µm, to obtain a recording from the local network in the vicinity. Signals were digitized and acquired at 50 kHz for single-unit recordings and at 10 kHz for extracellular recordings. Agar at 4% was used to prevent the cortex from desiccation and to stabilize electrophysiological recordings.

2.2.4. In vivo thalamocortical fPSP recordings.

Field postsynaptic potentials (fPSPs) were obtained at 0.6-0.7 mm deep in primary somatosensory cortex while stimulation was performed with a bipolar electrode placed in VPM thalamic area (AP -1.6-1.8, L 1.2-1.3, H 3.7-4.2), delivered at intensities that ranged 75 to 225 μA in increases of 25 μA. Stimuli had duration of 0.2 ms and were delivered at 0.33 Hz. The fPSP with the maximum peak of inhibitory response at 225 μA of intensity (positive component the peak value towards positive voltage within the first 100 ms from stimulus artifact.

2.2.5. Data analysis.

MUA was estimated as the power change in the Fourier components at high frequencies of the extracellular recordings (Reig et al. 2010; Sanchez-Vives et al. 2010). We assume that the normalized MUA spectrum provides a good estimate of the population firing rate, because normalized Fourier components at high frequencies have densities proportional to the spiking activity of the involved neurons (Mattia and Del Giudice 2002). MUAs were of fPSP from stimulus artifact) was selected from the recorded responses in barrel cortex (L 2.5 to 3.5) which were recorded with an horizontal silicon probe which spanned primary somatosensory cortex in the lateral axis (similar to the one used for propagation experiments described below). Latencies below 3 ms to the excitatory component were considered as monosynaptic, which were obtained to the onset of excitatory response. Excitatory components were quantified as the negative voltage value within the last 20% of the excitatory response but not the peak, at a fixed latency across stimulus intensities in each animal that ranged 1.9-2.8 ms across animals, which was set at 225 μA of intensity. Inhibitory responses were quantified as

logarithmically scaled in order to balance the large fluctuations of the nearby spikes. UP and DOWN states were singled out by setting a threshold in the log(MUA) time series. The threshold was set to 60% of the interval between the peaks in the bimodal distributions of log(MUA) corresponding to the UP and DOWN states. The peak related to the DOWN state was used as reference, setting there log(MUA) = 0. Singled-out sets of UP and DOWN state durations from each recording were used to estimate the nine parameters reported in Fig. 3. UP and DOWN state durations (Fig. 3, *B* and *C*) were the averages across such sets. Frequency in Fig. 3*A* was the inverse of the average duration of the whole UP-DOWN cycles. DOWN-to-UP and UP-to-DOWN transitions in Fig. 3, *D* and *E*, were estimated as the slope of the average profile of

log(MUA) around a small time interval around the transitions ([-10, 25] ms and [-25, 10] ms for Upward and Downward transitions, respectively). The maximum relative firing rate in Fig. 3*F* was the maximum average log(MUA) following the DOWN-to-UP transition. The coefficient of variation (CV) in Fig. 3, *G–I*, was the fraction between the standard deviation and the mean value of the durations of UP and DOWN states and of the whole UP-DOWN cycles singled out for each recording, respectively.

All of the MUA off-line estimates and analyses were implemented in MATLAB (The MathWorks, Natick, MA). Data are displayed as means ± SE in all error bars in plots. Single-unit recordings were analyzed with Spike2 software (Cambridge Electronic Design). Firing patterns were obtained through perievent time histograms (PETHs) triggered to the onset of UP states and a bin size of 20 ms. The length of the analyzed periods for the PETHs was 300 s. To analyze the fast components of oscillations, UP and DOWN states were detected and their respective power spectra were calculated. Power spectrum density analysis was carried out by Welch's method with 50% overlapped windows of 2,000 samples. To compare power, an average relative power was calculated by averaging within three frequency bands (beta 20–30 Hz, low gamma 30–60 Hz, and high gamma 60–90 Hz) resulting from the quotient between the power in the UP states and in the DOWN states.

LFP analysis was performed in collaboration with Laura Ciria and Lorena Perez, who also used the algorithms and scripts.

2.2.6. Statistical analysis.

Unless otherwise stated, all repeated measure comparison was performed with one-way ANOVA followed by Fischer least significant difference post hoc tests. Two population comparisons were performed by means of two tailed T tests. Correlations were assessed with Pearson coefficients and ANOVA tests for significance. Outliers in gamma quantification and correlations (see below) were removed with extreme studentized deviate method (ESD). Data are displayed as means ± SE in error bars in plots except in boxplots, and as means ± SD in the text. Statistical analysis was conducted using OriginPro 8.5 software.

2.3. Experiments in collaboration

These experiments were performed by María Martínez de Lagrán in the lab of Mara Dierssen (Center for Genomic Regulation, Barcelona).

2.3.1. Animals

The production of mice transgenic for Dyrk1A (TgDyrk1A) has previously been described (Altafaj et al. 2001) The transgene was inserted into C57BL/6JXSJL (Charles River, Barcelona, Spain) embryos and the stock is maintained by intercrossing wild type and transgenic mice derived from the original founder. The non-transgenic littermates of TgDyrk1A mice served as controls. To visualize cortical pyramidal neurons, we generated double transgenic mice (Thy-YFP/TgDYRK1A) crossing TgDyrk1A with overexpressing YFP under Thy1 promoter mice (strain B6.Cg-Tg(Thy1-YFPH)2Jrs/J nº 003782; The Jackson Laboratories). Same sex littermates were group-housed under a 12-h light/dark schedule (lights on at 0900 a.m.) in controlled environmental conditions of humidity (60%) and temperature (22 ± 2 ºC) with free access to food and water. Only males were tested in this study, so females could be spared for breeding purposes. Behavioral experiments were conducted during the light phase of the light/dark cycle between 10 am and 2 pm and were performed by trained observers blind to genotype. All experimental protocols involving the use of animals were performed in accordance to recommendations for the proper care and use of laboratory animals [local (law 32/2007) and European regulations (EU directive n° 86/609, EU decree 2001-486) and the Standards for Use of Laboratory Animals n° A5388-01 (NIH)] and were approved by the local ethical committee from PRBB and the Hospital Clinic of Barcelona.

2.3.2. Spontaneous Alternation Task in Y Maze

Individual mice were placed into a black Y-shaped maze (14 x 5 x 40 cm each arm), and allowed to explore freely through the maze for 8 min. The number of arm entries and the sequence of arms entered were recorded by using a computer-assisted data acquisition system (Smart, PANLAB, Spain). Non-performers with less than 10 arm entries throughout the entire 6 min observation period were excluded from the analysis. A correct alternation was scored when a sequence of three consecutive arm entries (a triplet) included entries into all three arms of the maze. Percent alternations were calculated as 100 × (number of correct alternations)/(total number of arm entires−2).

2.3.3. Puzzle box paradigm

Puzzle box paradigm is considered a problem-solving task that could reflect executive dysfunction. Mice are challenged with various interruptions of increasing difficulties to access to the goal arena and have to adopt different behaviors at the presentation of each new problem. The protocol was slightly modified from(Ben Abdallah et al. 2011). Briefly, arena consisted of a compartmented box (Fig. 1a), one lit (200 lux) start zone with white walls (55 cm long, 25 cm wide) and a smaller covered goal zone (15 cm long, 25 cm wide). Introduced into the start zone, mice were trained to move into the goal zone through a small opening (~4 cm wide), which communicated both compartments and challenged with impediments of increasing difficulty along the experiment (Fig.1a). Mice underwent a total of eleven trials (T1–T11) over 4 consecutive days. On day 1 (training), opening was unblocked allowing free access to the goal zone during T1. On T2 a swing plastic door was placed covering partially the entry. On day 2, T3 was identical to T2. On T4 and T5 an underground tunnel was located under the barrier. On day 3, T6 was a repetition of T4 and T5. However, on T7 and T8, mice were exposure to the underpass filled with sawdust and mice had to dig their way through. On last day, T9 was similar to T7 and T8. On T10 and T11, the underpass was obstructed by a piece of paper that mice had to pull with teeth and paws to enter the goal zone. This sequence allowed assessing problem solving ability (T4, T7 and T10), and learning/short-term memory for species-specific or instrumental responses (T5, T8, and T11), while the repetition on the next day provided a measure of long-term memory (T3, T6 and T9; Cowan, 2008). A trial started by placing the mouse in the start zone, and ended when the mouse entered the goal zone with all four paws, or after a total time of 4 min (T1-T6) or 5 min (T7-T11). Performance of mice in the puzzle box was assessed by measuring the latency to enter the goal zone.

2.3.4. Immunohistochemistry

Mice were anaesthetized and then perfused transcardially with 0.1M PBS, followed by chilled 4% paraformaldehyde in PBS. At least five animals were used per genotype. Brains were removed from the skull and postfixed in the same fixative for 24 h at 4ºC overnight. After rinsing in PBS, brains were cryoprotected in 30% sucrose and kept frozen at –80ºC. Coronal sections 40 μm thick were cut with a cryostat and maintained in cryoprotective solution at –20ºC until use.

Free floating coronal sections containing the medial prefrontal cortex (mPFC) cortex that includes cingulate1, prelimbic and infralimbic cortex (AP 2.10 to 2.58 mm) or primary somatosensory (AP -1.06 to -1.58 mm following Franklin and Paxinos, 2008)

were selected. Background staining was blocked with PBS containing 0.2% Triton X-100, 3% bovine serum albumin (BSA) 0.25% gelatine and 0.2M glycine by 1 h at room temperature. Sections were then incubated overnight at 4ºC with primary antibodies and subsequently, after several washes with 0.1M PBS, incubated for 1 h at room temperature with the corresponding fluorescence conjugated secondary antibodies (Alexa 488 or 594, 1:500, PROMEGA). Finally, sections were incubated 10 minutes with Hoechst solution (1:1000) for nuclei staining. Sections were mounted and coverslipped with mowiol reagent.

To characterize the different subpopulations of interneurons we used anti-parvalbumin (1:1500, SIGMA), anti-calretinin (1:1000, SIGMA), and anti-somatostatin (1:500, Millipore) antibodies. We also used anti-vesicular glutamate transporter (anti-VGLUT1, 1:200, Synaptic systems) and anti-vesicular GABA transporter (anti-VGAT, 1:200, Synaptic systems) antibodies to detect excitatory and inhibitory presynaptic vesicles, respectively. Excitatory and inhibitory postsynaptic sites were detected using anti-PSD95 (1:800, ABCAM) and anti-Gephryn (1:1000, Synaptic systems) antibodies respectively.

2.3.5. Confocal microscopy and image analysis

Images were acquired with a confocal Leica TCS SPE microscope and further analysed with Image J software. For the analysis of the different subpopulations of interneurons, microphotographies were taken from the medial prefrontal cortex (mPFC) or primary somatosensory cortex (S1) using a 10x lens. Images for studies of pre- and post-synaptic markers were obtained using a 63x lens with aa 5x zoom. Nissl-stained sections adjacent to the ones measured were used to determine the location of cortical layers. Excitatory-inhibitory balance was calculated as previously described (Blundell et al. 2009).

2.3.6. Statistical analysis

All comparisons between means were performed with two tailed Student's t or repeated measures ANOVA test. Data are displayed as means ± SE in error bars in plots and as means ± SD in the text. ANOVAs were followed by Student's t-test when only two groups were compared. Statistical analysis was conducted using SPSS 17.0 software.

OBJECTIVES

General aim

In the present Thesis, we aimed to study the neurobiological nature of cortical rhythms such as the slow oscillations and fast oscillations, their network mechanisms and their development in the normal cortex (*in vitro* and *in vivo*) and in an altered cortical network such as a Down syndrome mouse model, where we pretend to disclose the alterations of the network that may explain altered cortical patterns and cognitive dysfunction.

Objectives

1. To determine the role of persistent sodium current on UP state generation and maintenance of UP states within slow oscillations *in vitro*.

2. To describe and characterize the rhythmic activity patterns in different areas of the cerebral cortex of *in vivo* anesthetized mice, in order to have a baseline to compare with altered networks.

3. To compare the emergent cortical oscillatory activity of WT mice with the one present in TgDyrk1A mice, a model of Down syndrome.

3. RESULTS

3.1. RESULTS OF OBJECTIVE 1: STUDY OF THE DEPENDENCE OF CORTICAL RHYTHMS ON PERSISTENT SODIUM CURRENT

Local field potential recordings were obtained from layer 5 in 33 slices of ferret visual cortex. All these slices generated slow oscillations between 0.1 and 1 Hz (Fig. 8A, B). In order to study the effects of blocking I_{NaP} on the oscillations, phenytoin (Colombo et al. 2013; Lampl et al. 1998; McLean and Macdonald 1983) was added to the ACSF in increasing concentrations to 9 out of 33 slices.These slices generated slow oscillations at frequencies ranging between 0.25 and 0.68 Hz that averaged 0.37 Hz (Fig. 9 A). The rest of the slices were used for experiments described in the following sections.

3.1.1. Effects of blockade of I_{Nap} on the slow oscillations

Increasing concentrations of 40, 60 and 80 µM phenytoin were bath applied to the oscillatory slices, each concentration remaining for a minimum of 20 minutes (see Methods). IC50 of phenytoin has been reported to be between 34 to 78 µM in different preparations according to different authors (Chao and Alzheimer 1995, Lampl et al 1998). A recent study reported IC50 to be between 18 and 28 µM depending on the duration of an inactivating prepulse, having maximal inhibition of I_{NaP} around 25% at 100 µM (Colombo et al. 2013). We did not increase phenytoin concentration further

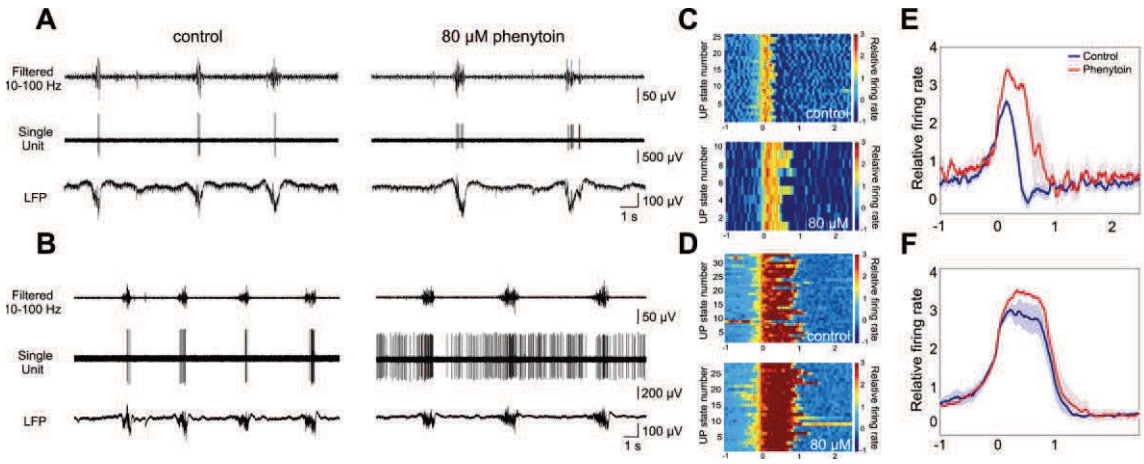

Figure 8. The blockade of I_{NaP} transforms slow oscillations.
A, B Left traces: Two examples of LFP spontaneous slow-wave activity with an extracellular single unit recording in control conditions and with direct bath application of phenytoin 80 µM. C, D: Raster plots with UP states ordered to their onset corresponding to the traces in A and B, respectively. UP state elongation can be observed. E, F: Waveform averages with network firing rate in UP states in control (blue traces) and in presence of 80 µM of phenytoin (red traces).

in order to avoid unspecific effects on transient sodium currents, as described in (Chao and Alzheimer 1995; Stefani et al. 1997a) and solubility problems (Colombo et al. 2013).

A striking effect of the application of phenytoin was the decrease in the frequency of the slow oscillation. This is illustrated for two single cases in Figure 8 A and B, and for the population average in Figure 9 A. Indeed, in 80 µM phenytoin the oscillations were almost completely blocked in 4 out of 9 slices, by "almost" meaning that some occasional UP state could still occur. For that reason, the average oscillatory frequencies illustrated in Figure 9 A understimate the decrease in frequency, since they refer only to the cases where the oscillations persisted (n=6) in 80 µM phenytoin, like the cases illustrated in Figure 8 A and B. In those, the frequency in 80 µM phenytoin had decreased to an average value of 0.07 Hz, while in control was 0.36 Hz. In 60 µM phenytoin, the oscillations were blocked in two cases. The decrease in the frequency of the slow oscillation was mainly the consequence of a progressive elongation of the DOWN states (Fig. 9 B, grey trace). In average, in the 6 slices that continued oscillating in 80 µM phenytoin, DOWN states where 6.6 times longer than in control conditions. However, not only DOWN states, were elongated. Six out of 9 slices displayed a consistent elongation of the UP states up to a duration that was in average 1.46 times longer than the control one (Fig. 2 B). In 2 out of 9 cases, the duration of UP states did not vary (1.02 times duration in 80 µM phenytoin), and in the remaining case the UP states were shortened to 0.52 times the control duration. Interestingly, the 6 slices that continued oscillating while in 80 µM phenytoin were the ones with an elongation of UP states.

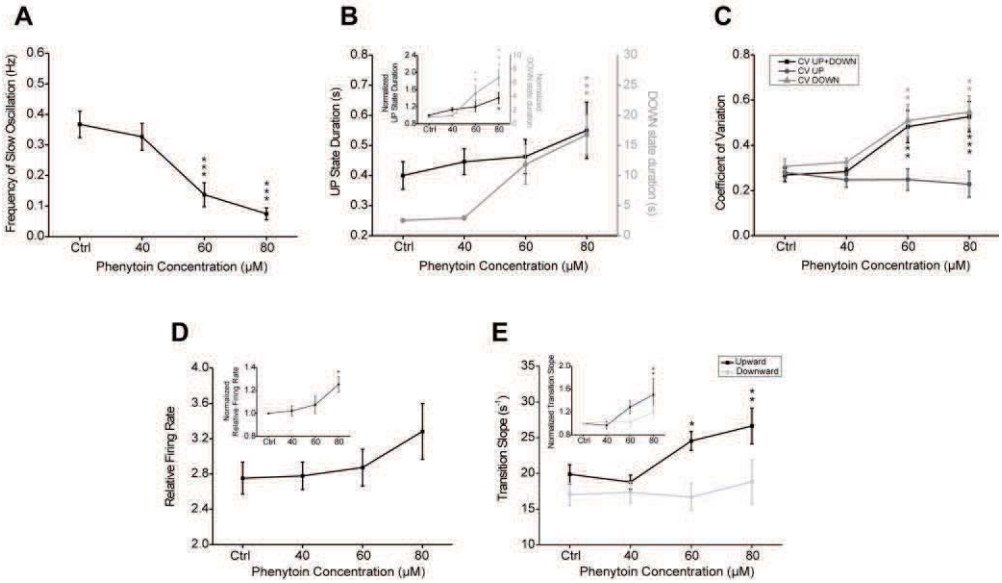

Figure 9. Temporal and firing parameters of slow oscillations in the presence of I_{NaP} blocker phenytoin. A: Frequency of oscillation averages in control, 40, 60 and 80 μM of phenytoin. B: UP state (black) and DOWN state (gray) duration averages in same conditions as A (inset: normalized to control values). For A and B: Frequency: F=11.5897, $P < 0.001$; UP state duration for normalized values: F=4.19744, $P < 0.05$; DOWN state duration: F=10.6775, $P < 0.001$. I: CV of UP states, DOWN states and UP-DOWN state cycle with increasing phenytoin concentration. CV UP-DOWN F=7.68208, $P < 0.001$; CV DOWN state F=6.21611, $P < 0.01$. *C*: Network firing rate averages in control and with bath application of 40, 60 and 80 μM of phenytoin (inset: normalized to control values). For normalized values: F=5.23387, $P < 0.01$. D: Upward (black) and Downward (grey) transition slope averages. For normalized values: F=5.23387, $P < 0.05$. For A to E: Control N=9; 40 μM: N=9, 60 μM: N=8; 80 μM: N=6. *$P < 0.05$, **$P < 0.01$, ***$P < 0.001$.

The elongation of the UP states in the presence of phenytoin was prevented by the partial blockade of the glutamatergic transmission (2μM CNQX and 10μM APV; n=7). Under these conditions, the duration and firing rate during UP states did not present signifficant changes while in phenytoin, while the frequency of UP states decreased (Fig. 10). The results demonstrate that the increase of UP state duration by effect of I_{NaP} blockade depends on the recurrency of the network.

Blocking I_{NaP} affected the regularity of the oscillation, which became progressively more irregular (Fig. 9 C). The coefficient of variation (CV) of the UP/DOWN state cycle and of the DOWN states duration increased with the concentration (to 1.79 and 1.63 times higher than control, respectively), revealing a decrease in oscillation regularity. The CV of UP state duration did not change though.

The results show a de-regulation in the oscillatory cycle demonstrating that I_{NaP} is critical for the correct development of the slow spontaneous activity, and that is necessary for the generation of UP sates at a physiological frequency. They also show that there is heterogeneity in the response to the blockade of the I_{NaP} current, although the most prevalent effect is that UP states are elongated and their frequency decreased but not completely blocked in 80 μM phenytoin. This trend was confirmed in the following experiments.

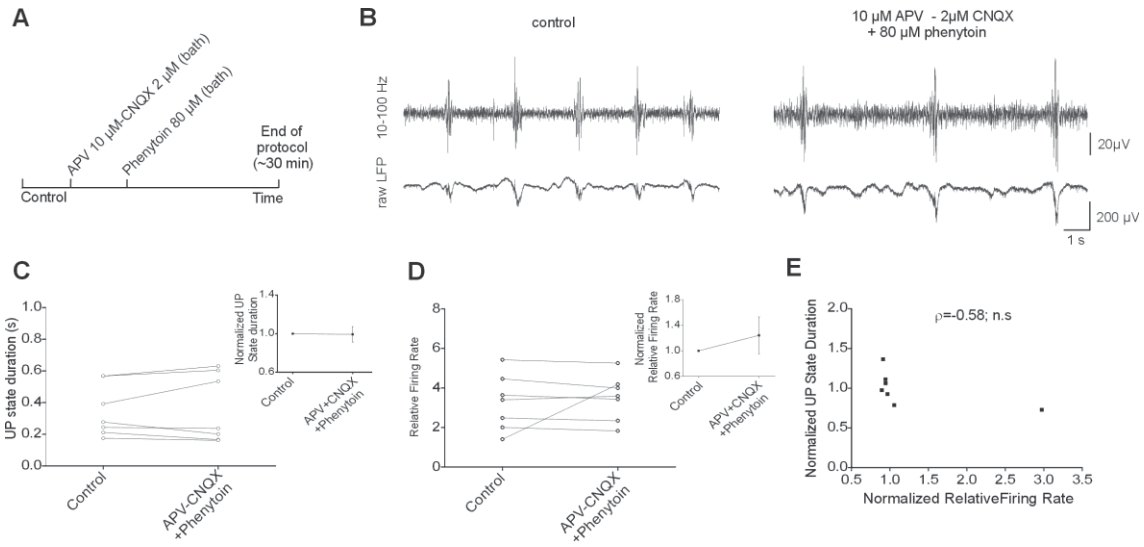

Figure 10. Recurrent excitability is critical for UP state elongation.
A: Scheme of the recording protocol. B: Examples of raw LFP and 10-100 Hz filtered traces showing UP state shortening in control (two upper traces) and after bath perfusion of phenytoin with previous blockade of excitatory synaptic transmission with CNQX 2µM and APV 10µM (two lower traces). C: Average of UP state durations in control and at the end of the protocol. Inset: normalized data. D: Average of network firing rate in control and at the end of the protocol Inset: normalized data. E: relationship between UP state durations and network firing rate at the end of the protocol (ρ=-0.58, *P* = 0.17). B-E: N=7.

3.1.2. Network and single neurons firing rates following the blockade of I_{NaP}

We analyzed network firing parameters as well as firing of single neurons while blocking $I_{NaP.}$ The population firing rate during UP states increased parametrically with the I_{NaP} blockade of the current (Fig. 9 D). The population firing rate in 80 µM phenytoin increased 1.30 times with respect to the control one (Fig. 8E, F and Fig. 9 E). This effect was observed in 5 out of 6 cases, with no change in the remaining one.

The slope of the Upward transition (from DOWN to UP state), that represents the recruitment of the local network, also increased 1.23 times with respect to the control value with phenytoin concentration (Figure 9 E, and Figure 8 E, F). On the other hand, the Downward transition (from UP to DOWN state), associated to the termination of the active states, did not show any statistically significant changes. These observations suggest that while the capability of the network to generate UP states is decreased, once one UP state occurs, the reverberance of activity is increased both in intensity and duration as a result of the I_{NaP} blockade.

We first explored to what extent the increased network firing rate corresponded to an increase in the firing rate of individual neurons (Fig. 11). With this purpose we extracellularly recorded from single neurons during slow oscillations and then bath applied 80 µM of phenytoin. Even when we did not applied increasingly larger

concentrations of phenytoin, the increase in the drug was not immediate as explained in the Methods, given that a interface chamber was used. Since the effect of 80 µM phenytoin was progressive, in Figure 11 we refer to it as periods 1, 2 and 3 (200 s each), for early and late effect of the drug respectively. Ten individual neurons were isolated in 10 slices, while a simultaneous LFP recording was obtained in close vicinity (less than 200 µm; Figs. 8 A, B; Fig. 11). In 9 out of 10 cases we detected a progressive increase in the number of spikes per UP state for increasing blockade of I_{NaP} (Fig. 8 B, C; n=10). In one particular case, the spike firing in the recorded neuron increased until eventually reached a continuous tonic firing that persisted through UP and DOWN states (Fig. 8 B). The firing parameters were not computed for this neuron in the grand average because it was classified as outlier. The firing rate of individual neurons was also increased during UP states with respect to controls. The mean value of the firing rate in individual neurons was 2.40 times higher in 80 µM than in the control condition (Fig. 11 C).

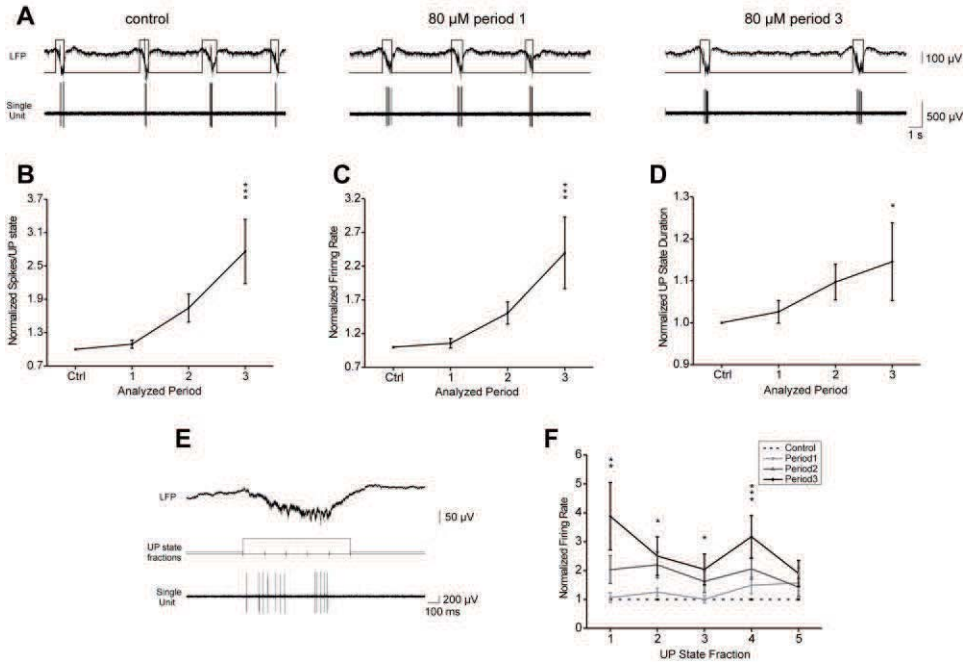

Figure 11. In the presence of I_{NaP} blocker also single neurons firing rate was increased.
A: Example of single unit trace with extracellular LFP signal in control (left traces) and in presence of 80 µM of phenytoin at an early time of perfusion (center traces) and at a late time of perfusion (right traces), reaching to the end. B, C: Number of spikes per UP state (B, normalized to control values) and Firing Rate (C, spikes divided by UP state duration, normalized to control values). N=10, Number of spikes F=7.10533, $P < 0.001$; in Firing rate F=5.86462, $P < 0.01$. G: UP state duration in this set of single unit experiments with direct bath application of 80 µM of phenytoin. In B-F, parameters were analyzed in control and three periods of the recording: at the beginning of the blocker application, at half time and at the end in N=9 neurons.F: Analysis of Firing Rate in 5 fractions in which UP states were divided, in control condition and in presence of 80 µM of phenytoin in same units as in E-G. N=10 for periods of analysis in control, 1 and 2; N=9 for period 3 (periods during drug application). Segment 1 F=4.83066, $P < 0.01$; segment 2 F=5.02155, $P < 0.05$; segment 3 F=2.42526, $P = 0.082$; segment 4 F=4.9093, $P < 0.01$; segment 5 N.S. 1 outlier removed in the fourth and fifth segments of UP states. *$P < 0.05$, **$P < 0.01$, ***$P < 0.001$.

Furthermore, UP states contained 2.75 times more spikes, including both the increase in firing rate and the significant elongation of the UP state duration (Fig. 11 D). These results were compatible with an increase in network excitability during UP states when I_{NaP} was blocked.

To better understand the changes in the firing rate of single units during UP states, additional analysis was performed to study the distribution of spikes during these periods. UP states were divided into 5 equal segments (Fig. 11 E). I_{NaP} blockade significantly raised the firing rate in the first four segments, the increase in the first segment of the UP state being the largest one (Fig. 11 F). The same panel illustrates also how the increase in the different segments was progressive with the blockade.

Finally we explored the relationship between two different variables reflecting excitability during UP states: network firing rate and duration of the UP states. These two variables are not necessarily related (e.g. Fig. 12 A), since the network firing rate does not refer to the mean firing rate during the UP state, but to the peak firing rate of the network (see Methods). While in control and in 40 µM phenytoin there was no relationship between both variables, in higher concentration phenytoin the correlation between both values became significant (Fig. 12 B-D). We observed a linear relationship between network firing rate and UP state duration at 60 and 80 µM phenytoin ($\rho_{Pearson}$=0.90, P<0.05 and $\rho_{Pearson}$=0.89, P<0.05 respectively, Fig. 12 C, D). This finding suggests an increased excitability during UP states with I_{NaP} blockade. In the only case where the UP state duration decreased, the peak network firing rate also decreased.

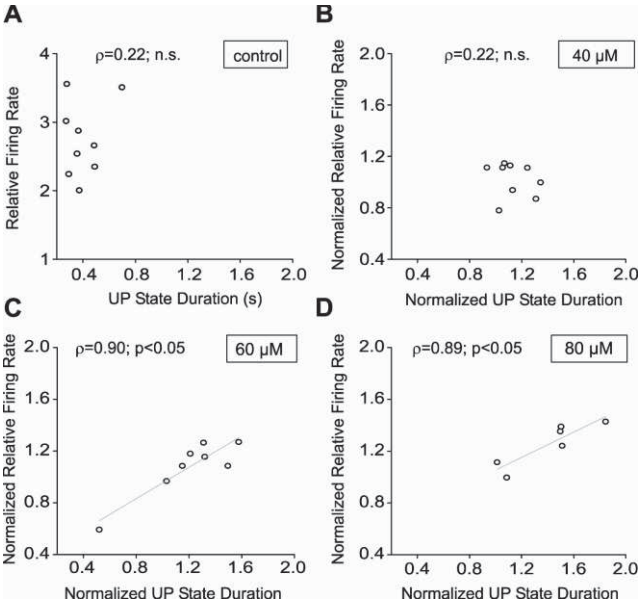

Figure 12. Correlation of UP state elongation and increase in network firing rate by I_{NaP} blockade.
A, B: UP state durations are uncorrelated to network firing rate in control conditions (A) and in presence of 40 µM of phenytoin (B). C, D: UP state elongations are correlated to network firing rate increases at 60 µM (C, ρ=0.90, p<0.05) and at 80 µM of phenytoin (D, ρ=0.89, p<0.05). A-D, control: N=9; 40 µM: N=9, 60 µM: N=8; 80 µM: N=6.

3.1.3. Effects of I_{NaP} blockade on beta and gamma frequencies

Given that both at the network and cellular level there was an increase in the firing rate during UP states, we explored whether this increase had a temporal structure. With that purpose, we carried out power spectrum density plots where we quantified average power in frequency bands in the range of beta (20-30 Hz) and gamma (30-90 Hz) waves (see Methods).

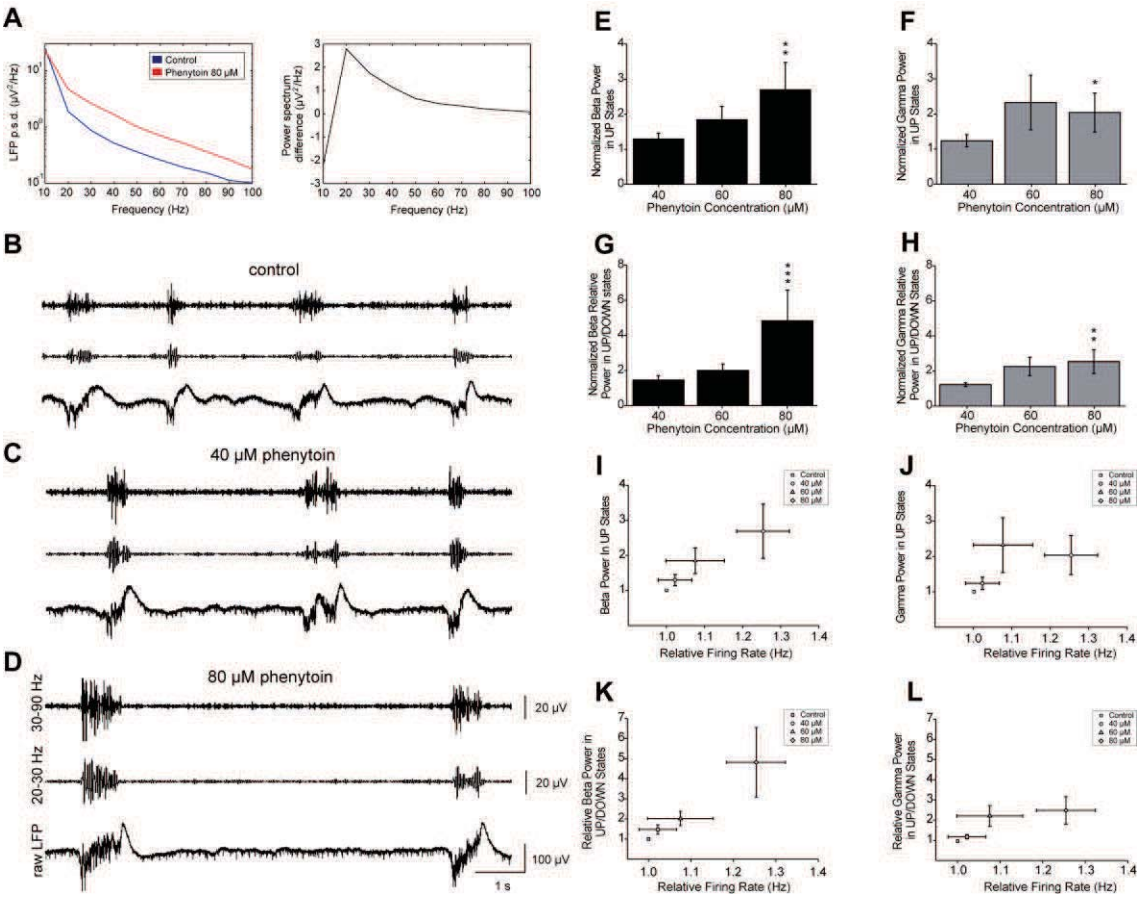

Figure 13. Fast oscillations during UP states are increased in the presence of phenytoin.
A left trace: Power spectrum density plots of detected UP states that show the increase in beta-gamma band by phenytoin. Right trace: subtraction of power spectrum plots in the left trace. B-D: Examples of traces of raw LFP and filtered LFP to 20-30 Hz (beta band) and 30-90 Hz (gamma band) in control (B) and increasing concentrations of phenytoin (B-D). B and D correspond to examples in periods where power spectums in A were calculated. E-H: Quantification of power in frequency bands in UP states and UP/DOWN states. Beta band in UP states: F=5.23865, $P < 0.01$; Gamma band in UP states: F=2.01741, $P = 0.13$, but post-hoc Fischer test $P < 0.05$ in 80 µM concentration. Beta band in UP/DOWN states: F=5.44103, $P < 0.05$; Gamma band in UP/DOWN states, F=4.06663, $P < 0.05$. I-L: plots where a relationship between the increases of beta-gamma power and network firing rate is present when power is calculated in UP states (F, G) and in the relative power in UP/DOWN states (H, I). In E to L: control: N=9; 40 µM: N=9, 60 µM: N=8; 80 µM: N=6, normalized to contol values. *$P < 0.05$, **$P < 0.01$, ***$P < 0.001$.

With the application of increasing concentrations of phenytoin, the power of both beta and gamma bands gradually increased (Fig. 13 A-D). This increase was true for both, the absolute beta and gamma frequencies in UP states (2.08 and 1.65 times respectively, Fig. 13 E, F), and also for the relative power with respect to DOWN states (3.26 and 2.08 times respectively, Fig. 13 G, H). The increase in high frequencies correlated in turn with the increase in the network firing rate (Fig. 13 I-L). These results revealed increases in fast frequencies within UP states that a functional I_{NaP} seems to be dampening.

3.1.4. Effects of of I_{NaP} blockade in evoked UP states

The experiments described so far revealed a network of increased excitability during UP states as a result of I_{NaP} blockade, while the frequency of spontaneously occurring UP states was critically decreased. To further explore the network state, we used electrical stimulation in the white matter right below layer 6 that evoked responses in L4 (n=7 slices). We had two main results in this set of experiments. First, that stimulus intensities (ca. 120 or 220 μA) that did not evoke UP states in control ACSF did evoke them in phenytoin, as phenytoin is decreasing the threshold in which UP states are full-blown triggered (Fig. 14 A, B). This was the case in all slices. Second, we observed that even when in phenytoin the frequency of spontaneous UP states was significantly decreased (Fig. 9 A), if electrical stimulation was provided to initiate UP states, UP states of the same duration could be evoked at the same frequency that the spontaneous ones in control condition. This suggests that the network resources to maintain UP states and normal frequencies are available, but the capacity to spontaneously initiate these UP states is deteriorated by the I_{NaP} blockade.

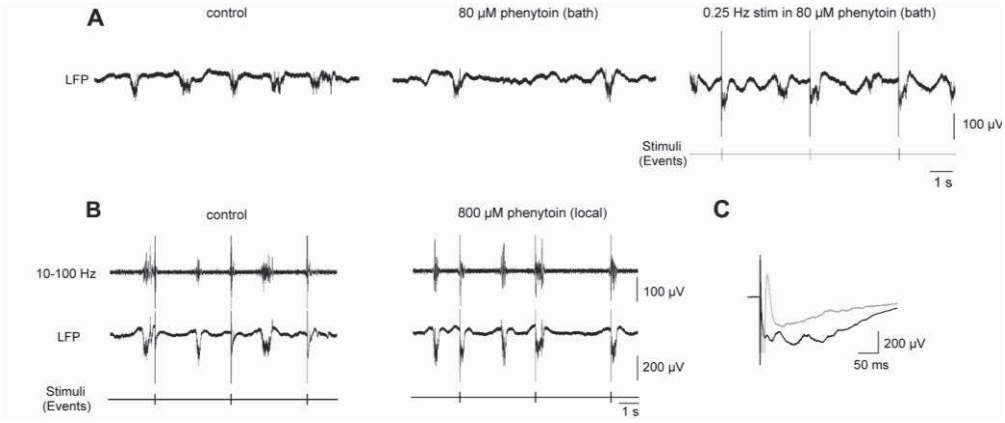

Figure 14. Network is more excitable when I_{NaP} is blocked.
A: Example of LFP showing the effect of 80 μM of phenytoin in the bath and also when we delivered stimulus at 0.25 Hz while in phenitoin. B: Examples of local application of 800 μM of phenytoin with a puffer. C: Waveform average of all the responses within 200 seconds in control (gray trace) and after local application of phenytoin (black trace).

3.2 RESULTS OF OBJECTIVE 2: CARACTERIZATION OF OSCILLATORY PATTERNS IN DIFFERENT CORTICAL AREAS

The spontaneous rhythmic activity generated in different regions of the mouse cortex (primary visual, somatosensory, and motor cortex and medial prefrontal) was recorded under ketamine anesthesia. Under these conditions, both slow oscillations and fast rhythms are generated in the thalamocortical network (Steriade et al. 1993, 1996). The slow oscillation (Fig. 16) consisted of periods of neuronal firing or UP states (Fig. 15 A, bottom) interspersed with rather silent periods or DOWN states. The recordings showed the low-frequency nature of the slow waves (<1 Hz). During UP states different frequencies were generated, including high frequency fluctuations (Fig. 15 A, top), as described in detail below. Such UP states propagate across the cortical tissue (Luczak et al. 2007; Massimini et al. 2004; Sanchez-Vives and McCormick 2000) and several parameters of these waves were analyzed to describe the features of these oscillations and to compare across different cortical areas.

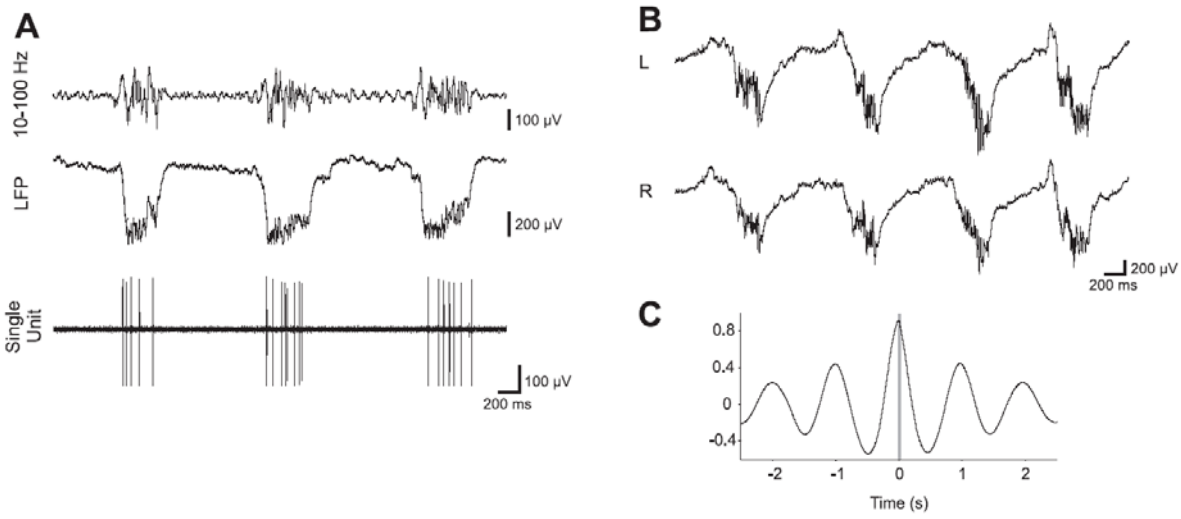

Figure 15. Oscillatory activity in the mouse cerebral cortex during ketamine anesthesia.
A, top: filtered signal of the recording (band pass 10–100 Hz) illustrating the occurrence of high frequencies in the UP state. Middle: local field potential (LFP) in the motor cortex. Bottom: single-unit recording of a neuron firing in the UP states. B: simultaneous bilateral extracellular recording in the prefrontal cortex. L, left hemisphere; R, right hemisphere. C: waveform cross-correlation of the 2 signals in B.

3.3.1. General description of slow oscillation in the anesthetized mouse.

To characterize the slow waves in the anesthetized mouse, extracellular recordings from primary visual, somatosensory, motor, and medial prefrontal cortex were obtained by means of tungsten electrodes placed in the deep cortical layers. The recordings were bilateral, and UP states usually occurred concurrently in both hemispheres with a small time lag measurable at the central peak of the waveform cross-correlation (Fig. 15, B and C). The distribution of time lags between left and right hemispheres is represented in Figure 16 (*n* = 29 bilateral recordings; *n*= 16 mice).

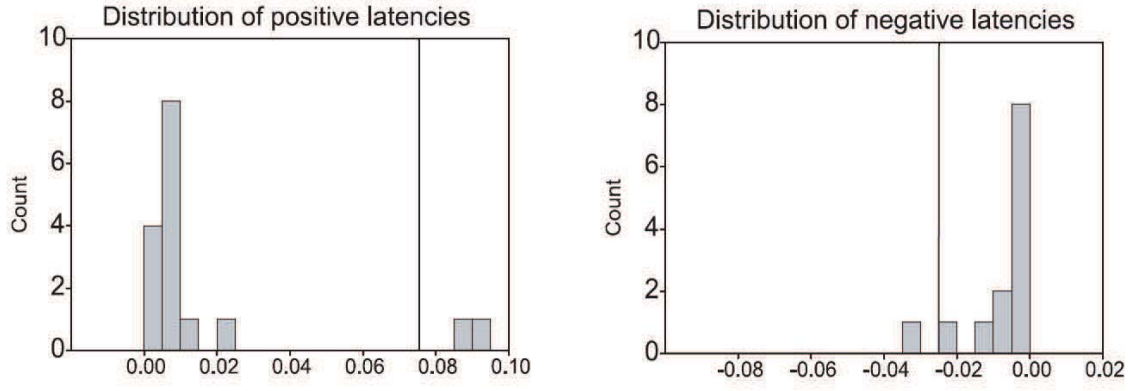

Figure 16. Distribution of latencies between bilateral recordings.

It illustrates that there was no significant bias toward one hemisphere to initiate the activity. The average absolute value of the time lag of the peak (mean ± SD) was 7.1 ± 10.9 ms in visual cortex (*n* = 7), 7.9 ± 9.4 ms in somatosensory cortex (*n* = 7), 5.0 ± 4.9 ms in motor cortex (*n* = 6) , and 6.4 ± 3.8 ms in prefrontal cortex (*n* = 9). To characterize the emergent rhythmic activity, nine parameters of the oscillatory activity were quantified as in Sanchez-Vives et al. (2010): frequency of oscillation, UP state duration, DOWN state duration, slope of DOWN-to-UP state transition, slope of UP-to-DOWN state transition, maximum relative firing rate, CV of the UP state duration, CV of the DOWN state duration, and CV of the UP state–DOWN state period. An operational definition of each one of these parameters is included in METHODS

Figure 17 illustrates representative recordings of all four recorded cortical areasand the analytical methods used to quantify their activity. We were interested in the comparative evaluation of these parameters across cortical areas, and therefore box plots were produced for primary visual (n = 7), primary somatosensory (n = 7), primary motor (n = 7), and medial prefrontal (n = 10), displaying the mean and median values (Fig. 18). These numbers of observations refer to the number of recordings included. Given that only one recording was obtained per area in each experiment, the number of recordings per area is equivalent to the number of animals. No significant differences in any of the analyzed parameters were found across hemispheres for the same cortical area.

The average oscillatory frequency of oscillation across all areas was 0.97 Hz; 54.8% of the recordings displayed frequencies frequencies between 0.6 and 1 Hz, while 45.8% oscillated at frequencies over 1 Hz. No significant differences across areas were observed between the average duration of either UP (Fig. 18 B; 0.28 s) or DOWN (Fig. 18 C; 0.8 s) states. Comparing across areas, prefrontal cortex was the area that exhibited larger differences ($P < 0.05$) compared with the other areas across a variety of parameters. The slope of DOWN-to-UP transitions in prefrontal recordings was significantly faster than in the other three cortical regions. The population firing rate was also higher in prefrontal cortex than in the other cortical areas (Fig. 18 F). Another property of the rhythm in the prefrontal cortex was the higher regularity in oscillations, reflected in a lower CV of the duration of UP states compared with the other three areas (Fig. 18 G).

Some other specific differences between areas were also detected, such as a faster transition from UP to DOWN state in motor and prefrontal cortex than in the two primary sensory areas. Further information about the statistics of this section is given in Figure 19.

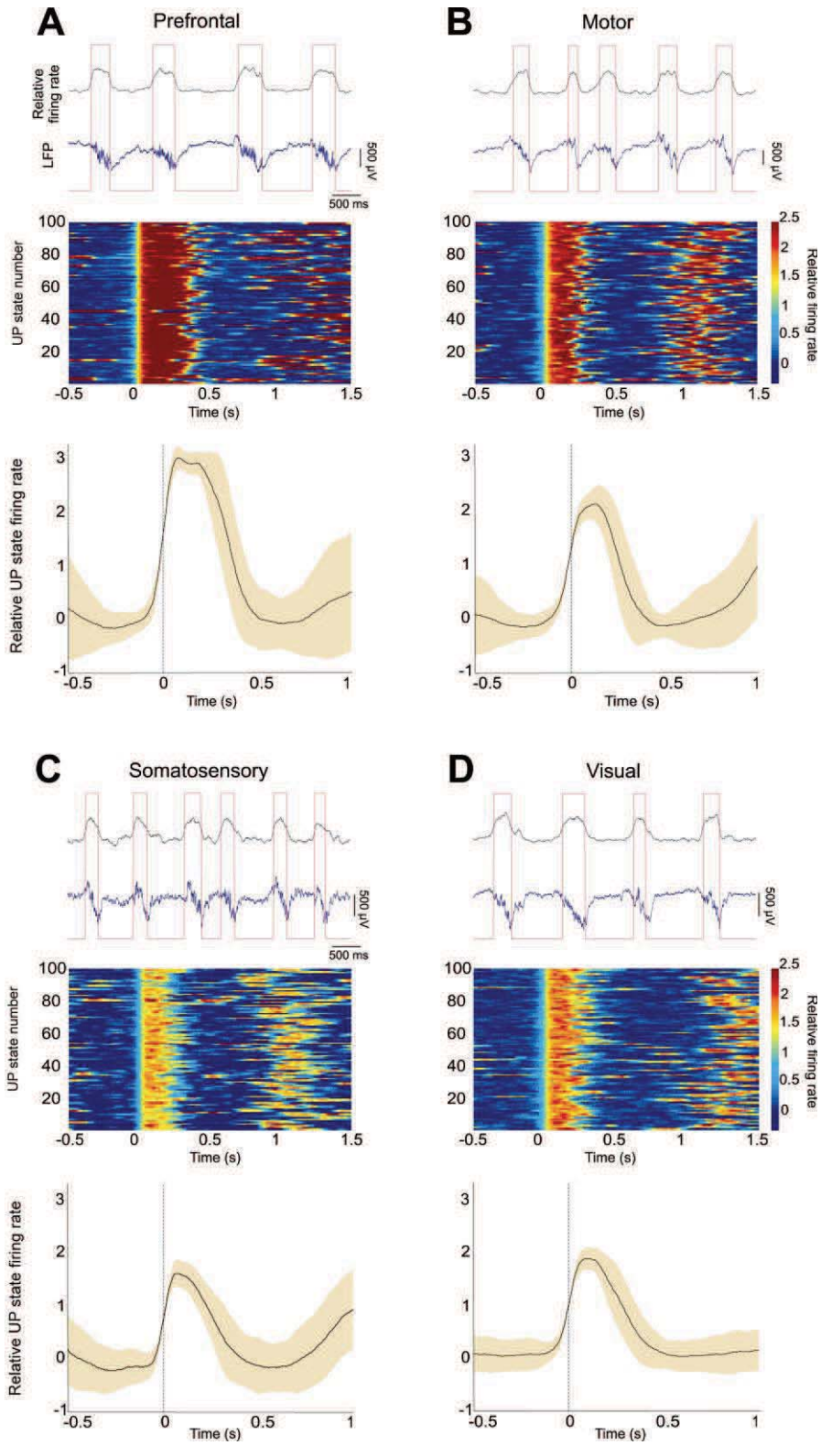

Figure 17. Analysis of population activity in 4 cortical areas.
A: prefrontal cortex: from top to bottom: relative firing rate, LFP, raster plots of 100 aligned UP states, and waveform average of the relative firing rate. This average is the one used for the calculation of the DOWN-to-UP and UP-to-DOWN slopes and the maximum firing rate of the analyzed periods. The shade corresponds to the SD. The red boxes represent the automatically detected UP and DOWN states. B–D: same as A but in motor, somatosensory, and visual cortices, respectively.

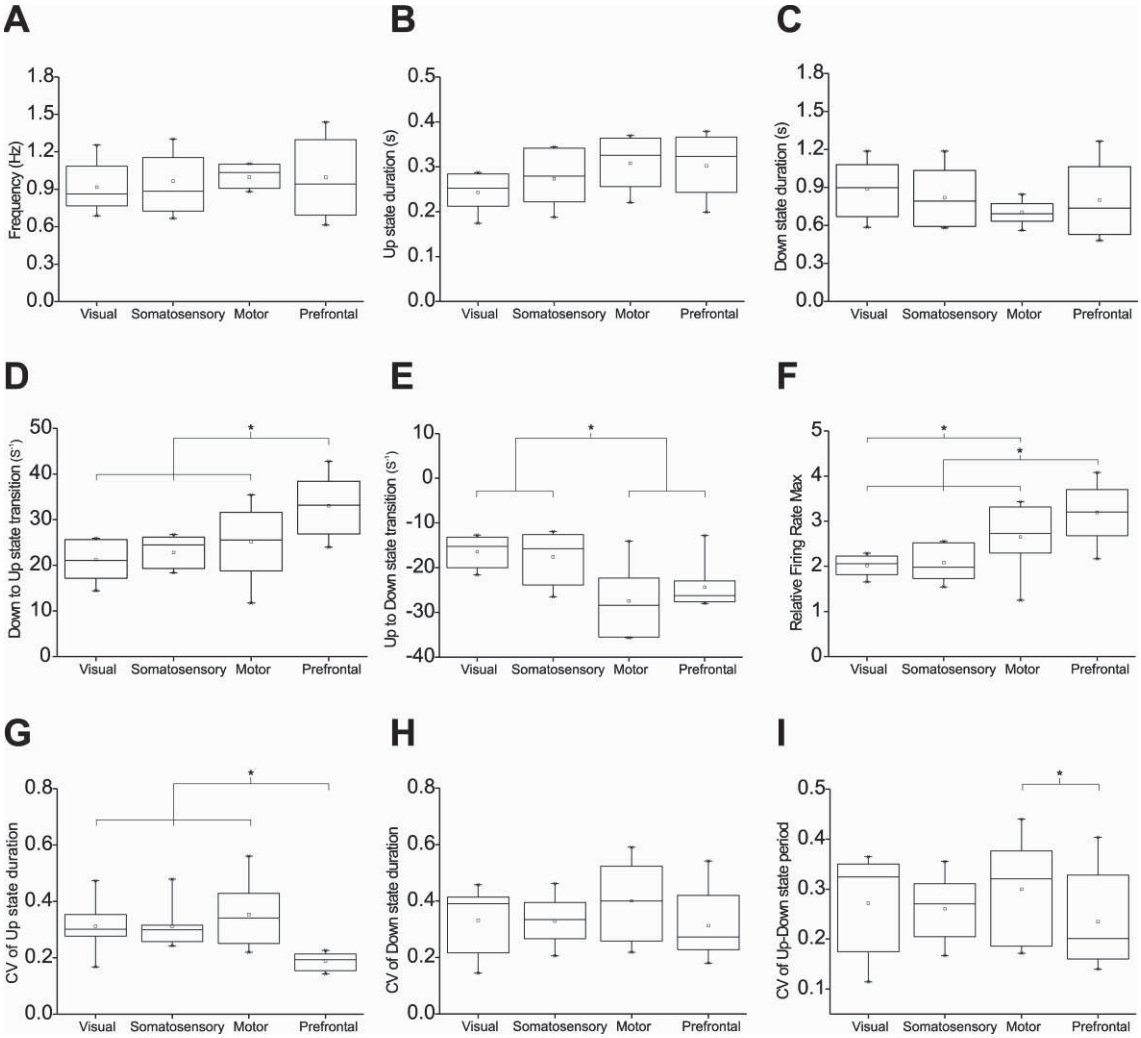

Figure 18. Box plots representing boxplots of the 9 parameters of the slow oscillations in visual, somatosensory, motor, and prefrontal cortex.

A: frequency of the oscillation. B: UP state duration. C: down state duration. D: DOWN-to-UP state transition slope. E: UP-to-DOWN state transition slope. F: peak of relative firing rate. G: coefficient of variation (CV) of up state duration. H: CV of down state duration. I: CV of the oscillatory period. Each box represents 50% of the data (from 25% to 75%), the small square inside depicts the mean, and the divisory line is the median. Whiskers represent the 5–95% interval of the data, and asterisks represent 1% and 99% values. Recordings from the right hemisphere were used for the averages.

A

Fischer test values			
	Frequency	Up state duration	Down state duration
Degrees of Freedom	3	3	3
F value	0.18828	0.76144	1.83611
Prob>F	0.90345	0.52557	0.16442
	Down-to-Up transition	Up-to-Down transition	Firing Rate Max
Degrees of Freedom	3	3	3
F value	6.94933	6.52562	3.33218
Prob>F	0.0013	0.00184	2.51586E-4
	CV Up states	CV Down states	CV period
Degrees of Freedom	3	3	3
F value	6.72707	0.44308	3.33218
Prob>F	0.00155	0.72413	0.03424

B

Fischer test p values			
	Frequency	Up state duration	Down state duration
mot pre	0.998	0.846	0.4
som pre	0.799	0.339	0.869
som mot	0.813	0.29	0.357
vis pre	0.501	0.056	0.447
vis mot	0.534	0.053	0.146
vis som	0.698	0.353	0.581
	Down-to-Up transition	Up-to-Down transition	Firing Rate Max
mot pre	0.012	0.28	0.047
som pre	0.0015	0.0205	2.4E-4
som mot	0.455	0.0028	0.058
vis pre	3.9E-4	0.0076	1.2E-4
vis mot	0.222	1E-3	0.034
vis som	0.627	0.701	0.803
	CV Up states	CV Down states	CV period
mot pre	3.6E-4	0.813	0.0046
som pre	0.0052	0.318	0.091
som mot	0.346	0.346	0.229
vis pre	0.0049	0.427	0.085
vis mot	0.358	0.605	0.242
vis som	0.982	0.846	0.974

Figure 19. Table showing One-way ANOVA statistical treatment for parameter calculation across areas.
A: General linear model. B: *post hoc* comparisons.

3.3.2. Firing properties of cortical neurons during slow waves.

Recordings of single units (Fig. 20) were obtained by singling out 37 single neurons from motor, 9 from somatosensory, and 43 from prefrontal cortex. Their firing patterns were analyzed with respect to the population activity in the same location recorded as the local field potential (LFP). Almost all spikes were found to occur during UP states, with a few exceptions that are described below. Figure 20*, A–D, illustrates* two different firing patterns that were observed: tonic firing during the whole duration of the UP state (mean firing rate 24.7 Hz; *n* = 19 neurons) versus a sparse firing (mean firing rate 5.2 Hz; *n* = 70).

We were interested to determine the number of spikes that single neurons fire per UP state. No differences were observed between neurons from motor and somatosensory cortex; thus we grouped them together. Of those 46 neurons, 52.2% fired in >90% of the UP states, while 37.0% fired in 50–90% of UP states and only 10.9% fired in <50% of active states (Fig. 20 F). On the other hand, most of the neurons had a sparse firing with <2 spikes per UP state in 47.8% of the neurons; 26.1% fired 2–6 spikes, and the same percentage had tonic firing and fired trains of >6 spikes during UP states (Fig. 20 E).

Neurons from prefrontal cortex showed some differences with neurons from primary cortices, and we report these separately. The difference was that prefrontal cortex neurons fired in more UP states and with more spikes per UP state. This is represented in Figure 20, G and H; 72% of prefrontal cortex neurons fired in all UP states, while only 3% fired in less than half the UP states. On the other hand, 50% of neurons had a discharge of 2–6 spikes per UP state. Taking all neurons together, we conclude that most of the neurons participate with a relatively sparse firing in most of the UP states when participating in slow oscillations.

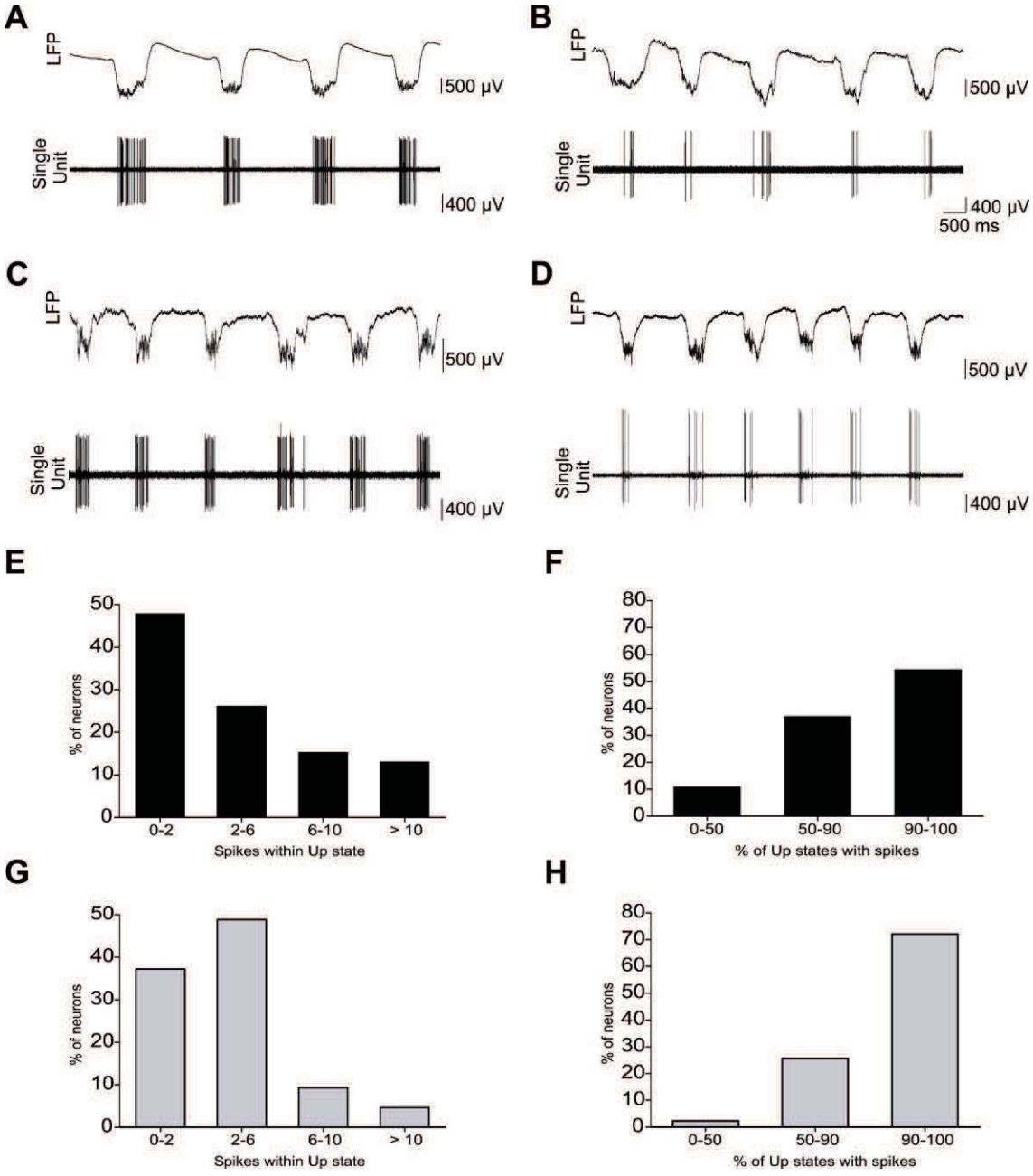

Figure 20. Firing of single units during UP states.
A: LFP (top) and single-unit recording from motor cortex (bottom) both obtained through closely located (>200 µm apart) tungsten and glass electrodes, respectively. B: recording from motor cortex from a different animal; rest same as in A. Neurons fired either tonically during UP states (e.g., A) or just a few spikes (e.g., B). C and D: as A and B, but the recording was obtained from prefrontal cortex. Note that the neuron in C fires more spikes per UP state than the neuron in D. E: histograms of single units from somatosensory and motor cortex according to the number of spikes fired within UP states. F: histograms of single units from somatosensory and motor cortex according to % of UP states where they displayed spike activity. G: histograms of single units from prefrontal cortex according to the number of spikes fired within UP states. H: histograms of single units from prefrontal cortex according to % of UP states where they displayed spike activity.

We were interested to know how the firing of individual neurons was distributed during UP states. Therefore, the firing rate of all 89 units was analyzed within UP states, and PETHs were built around the onset of UP states. We observed a different distribution of single units' firing during UP states between primary cortices and prefrontal cortex neurons, so they appear separated in the next considerations. The PETHs revealed two main groups of firing patterns: *1*) neurons with a maximum firing rate at the initiation of the UP state (primary cortices *n* = 15; prefrontal cortex *n* = 23) (Fig. 21, A and D) and *2*) neurons with the maximum firing rate toward the center of the UP state (primary cortices *n* = 28; prefrontal cortex *n* = 15) (Fig. 21, B and E).

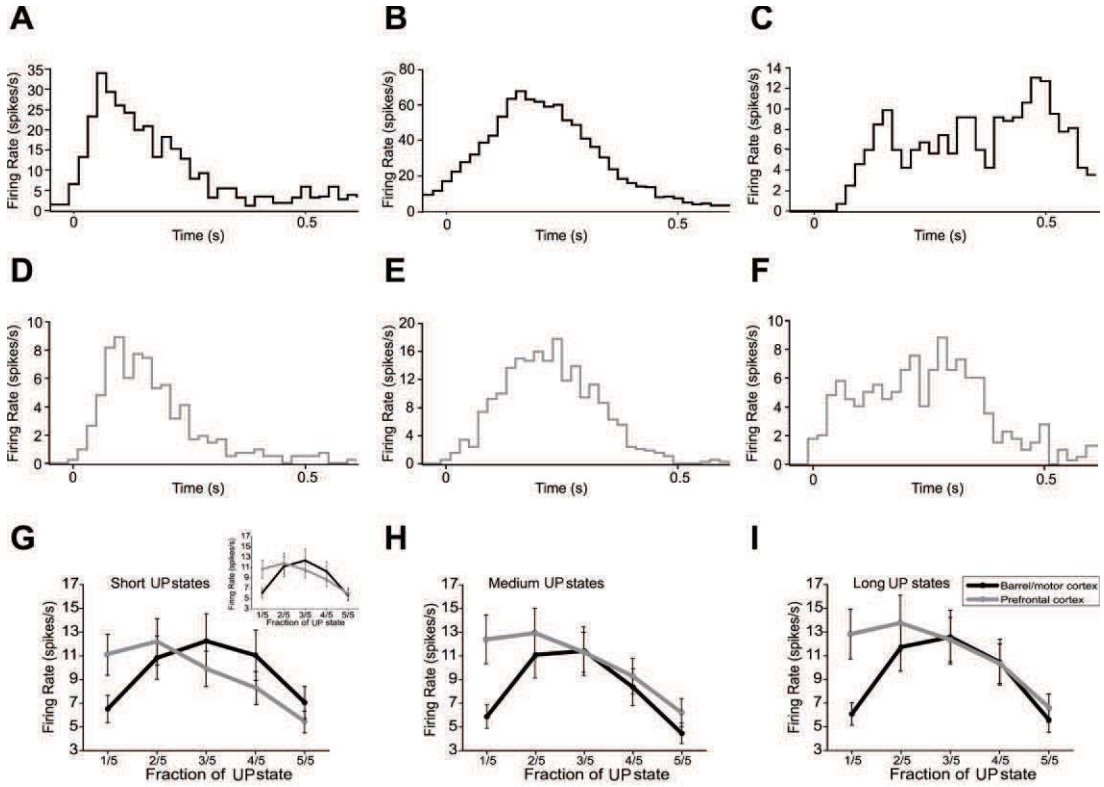

Figure 21. Distribution of single units' firing rate during UP states.
A: perievent time histogram (PETH) of a motoneuron with the firing rate peak toward the initiation of the up state. B: PETH of a motoneuron that reached the peak of its firing rate toward the center of the UP state. C: example of a motoneuron that fired rather tonically during the duration of the UP state, increasing its firing toward the end of the up state. In all cases 200 s has been analyzed and the firing rate in 100–200 UP states averaged for each neuron. D–F: same as A–C but for prefrontal cortex. G: distribution of single spikes during UP states for "short" (see below) UP states. Black, data corresponding to motor and somatosensory units; gray, data corresponding to prefrontal cortex units. Inset: grand average of the firing rate of single units (n = 46 for somatosensory and motor cortex, n = 43 for prefrontal cortex) after dividing each analyzed up state into 5 equal time windows. H: distribution of single spikes during UP states for "medium" (see below) UP states. I: distribution of single spikes during UP states for "long" (see below) UP states. UP states recorded for 200 s in each one of 46 neurons for somatosensory and motor cortex (gray traces) or 43 neurons in prefrontal cortex (black traces) were clustered in short, medium, and long durations (33.3% of analyzed UP states for each neuron were classified in each group). Error bars correspond to SE. Note that the distribution of firing rate of single neurons along the UP states was independent of their duration.

Of the remaining three neurons from primary cortices, one had a tonic firing evenly distributed during the duration of the UP state (e.g., Fig. 21 C) and two showed an increased firing rate preceding the termination of the UP state. Of the remaining prefrontal cortex single units, three fired at the end of UP states and two had rather a tonic discharge (Fig. 21 F).

To compare across neurons and to exclude the variations in UP state duration, UP states were divided into five even windows (Fig. 21, G–I), and the firing rate of the unit was estimated for each fifth of the UP state. In this way, a grand average of the PETHs for 46 neurons from primary cortices and 43 prefrontal cortex neurons was calculated (see Fig. 21 G, inset). The average distribution of somatosensory and motor single units' firing showed a preferential increase of firing rate toward the center of the UP state, given that the most common neuronal pattern was that in Figure 21 5 B and E. Prefrontal cortex single units fired toward the beginning of the UP state (Fig. 21 G, inset).

To further take into account differences in UP state duration, all the UP states recorded for each neuron (n = 100–200) were split into three groups according to length: short, medium, and large. When the firing rate distribution of single neurons was represented for these three groups (Fig. 21, G–I) it showed that the predominance of motor and somatosensory single-unit firing toward the center of the UP state was not dependent on the duration of the UP states. The same was the case for prefrontal cortex single units, which independently of the duration of UP states tended to fire toward the beginning of UP states (Fig. 21, G–I). In this way the single-unit firing rate distribution was evaluated in a total of 6,764 UP states in the case of the primary cortices and 7,695 in the case of the prefrontal cortex.

A small number of neurons (3 of 46) had spikes in the 50-ms window preceding UP states. These were the only spikes observed during DOWN states. When analyzing these spikes preceding UP states, we should take into account a number of possible sources of error. One of these is the fact that single units and LFP were analyzed with two closely located different electrodes. The maximum separation between the electrodes was 100 μm. If we consider that some UP states could be detected earlier in one electrode than in the other, and we consider the slowest detected propagation speed (10 mm/s), we conclude that it would take 10 ms to travel from one electrode to the other, so the firing occurring earlier than 10 ms has to be considered as preceding the UP state. Another possible source of error could be the method of detection of the UP state in the population. Any method of UP state detection requires the determination of a threshold. In the network, though, the UP state starts building UP before the threshold is reached. We estimate that on average we could consider that UP to 30 ms preceding the threshold there could be activity building UP. Thus, if we consider both confounds together, there can be a window of 40 ms during which the

firing of single units could be considered as occurring during UP states. Those occurring earlier are probably spikes actually preceding UP states. From this we conclude that the spikes detected in these two neurons that appear to precede up states are probably part of the building up of the activity.

3.3.3. Propagation of slow waves in the mouse cortex.

Wave propagation was evaluated with an array of 16 electrodes separated from each other by 100 µm. The electrode was placed at 1 ±0.2-mm depth and parallel to the midline in the motor cortex and orthogonal to the midline in the visual cortex (Fig. 22, A and B, top insets). We included in the analysis 20 recordings of wave propagation, 12 from motor and 8 from visual cortex, and the propagation of at least 300 consecutive UP states was evaluated.

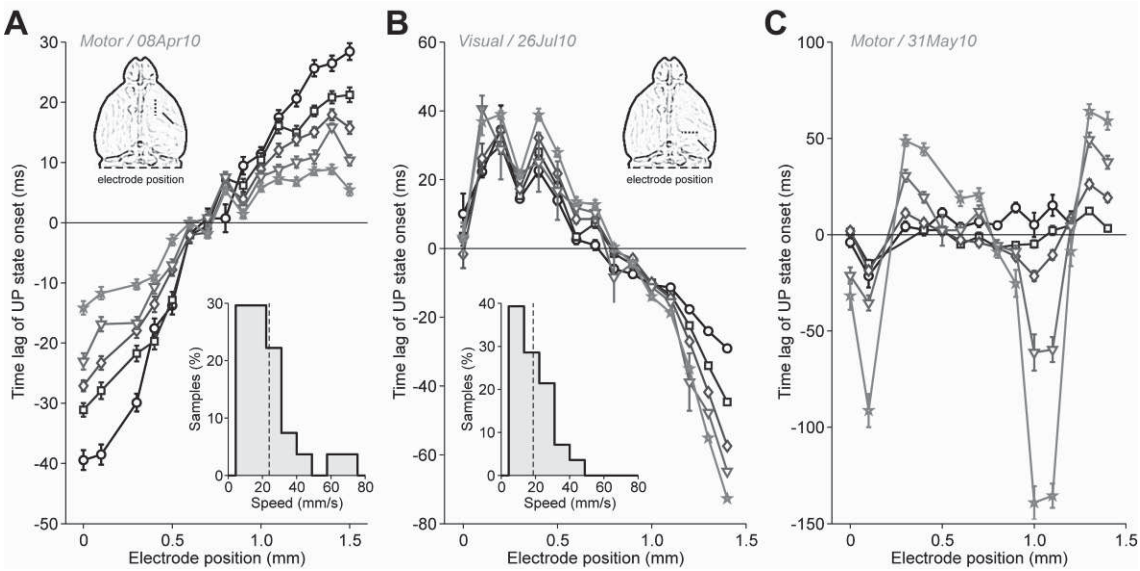

Figure 22. Speed of propagation of up state onsets in 2 cortical areas (motor and visual) of the mouse. A: average time lags of up state onsets recorded with arrays of 16 electrodes in primary motor cortex. Top inset: location and position of the recording array (discontinuous line). Time lags were grouped in 5 different pools with similar patterns of activity propagation (each with different symbols and gray levels) obtained with a principal component analysis (see text for details). Bottom inset: distribution of speeds estimated from the UP state pools with similar time lag patterns in the motor cortex recordings, illustrating a monotonic propagation from front to back (*n* = 27, 6 of 12 recordings). Vertical dashed line is the average propagation speed: 24 ± 3.12 mm/s. B: same as in A for recordings in the visual cortex. Note that in this cortical area the array was placed in the coronal plane (see *top inset*), thus orthogonal to that in A. Bottom inset: distribution of speeds for the visual cortex recordings showing a monotonic decrease of time lags from medial to lateral positions (*n* = 28, 6 of 8 recordings). Average speed: 18.72 ± 1.68 mm/s. C: another motor cortex example showing complex patterns of activity propagation.

UP states were detected with the same threshold algorithm for the spectral estimated MUA used previously to determine the properties of slow oscillatory activity (see METHODS for details; Sanchez-Vives et al. 2010). The relative time lags between UP state onsets singled out from the 16 electrodes were used to identify different patterns of activity propagation. Therefore, we performed a PCA that allowed the projection of the time lag patterns of different UP states into a subspace suitable for sorting them and capable of retaining the most variance. These ranked UP states were pooled into five equally sized groups. The average time lags within each group are shown in Figure 22 for three typical recordings: the different symbols and related connecting lines clearly display significantly different modes of propagation within the same recording session, which occur randomly in time.

Six of twelve cases showed a clear pattern of propagation from front to back in motor cortex, in agreement with the predominant direction of propagation of oscillations during slow-wave sleep in humans (Massimini et al. 2004). In visual cortex, the majority of cases (6 of 8) showed a monotonic variation of the average time lag along the multielectrode array.

While the direction of the propagation along the axis of the electrode array was constant, the estimated speed of different waves varied continuously within a range of 6.4–74.4 mm/s. This is illustrated for both motor and visual recordings in Figure 22, A and B. All 12 cases were highly similar to those illustrated here. The motor and visual distributions of velocities (Fig. 22, A and B, bottom insets) across time lag patterns and recordings are not significantly different (2-tailed Kolmogorov-Smirnov test, $P = 0.42$), although the two electrode arrays were placed in orthogonal positions. The remaining seven cases showed more heterogeneity in the direction of propagation (see, e.g., Fig. 22 C from a motor cortex recording). These patterns were compatible with waves propagating from other areas, e.g., with lateral propagation or with colliding waves coming from different directions. In these cases we could not confidently estimate the component of the speed of propagation along the axis of the electrode array.

3.3.4. Fast components of mouse neocortical slow oscillations.

The frequency content of the LFP in the recordings from the four studied cortical areas (visual, somatosensory, motor, and prefrontal cortex) was analyzed. Spectrogram analysis confirmed the presence of fast rhythms in the UP states (Fig. 23 A). To study frequency content during UP and DOWN states in a systematic manner, a power spectrum analysis was carried out on recordings from prefrontal cortex ($n = 10$ mice; Fig. 23, B and C) and somatosensory ($n = 7$; Fig. 23 E), motor ($n = 6$; Fig. 23 D), and visual ($n = 7$; Fig. 7*F*) areas. The analysis focused on the occurrence of fast rhythms that were divided into beta (15–30 Hz), low gamma (30–60 Hz), and high

gamma (60–90 Hz). The power of fast rhythms was significantly larger during UP than during DOWN states (Fig. 23, B and D–F). Interestingly, for all the studied frequency bands, beta, low gamma and high gamma, power was consistently higher in prefrontal cortex than in the rest of the areas (Fig. 24 A, B, and C, respectively). The absolute values of beta and gamma power in UP (Fig. 24, D–F) and DOWN (Fig. 24 G–I) states are illustrated in Figure 24 D–I, while the relative beta and gamma power in UP versus DOWN states is represented in Figure 24 A–C. Figure 24 shows that the higher beta and gamma power in prefrontal cortex is the result of a specific increase during UP states and not of other reasons like a lower power during DOWN states in prefrontal cortex. The beta band power was 3.5- to 7.2-fold higher in motor, somatosensory, and visual cortex in UP with respect to DOWN states.

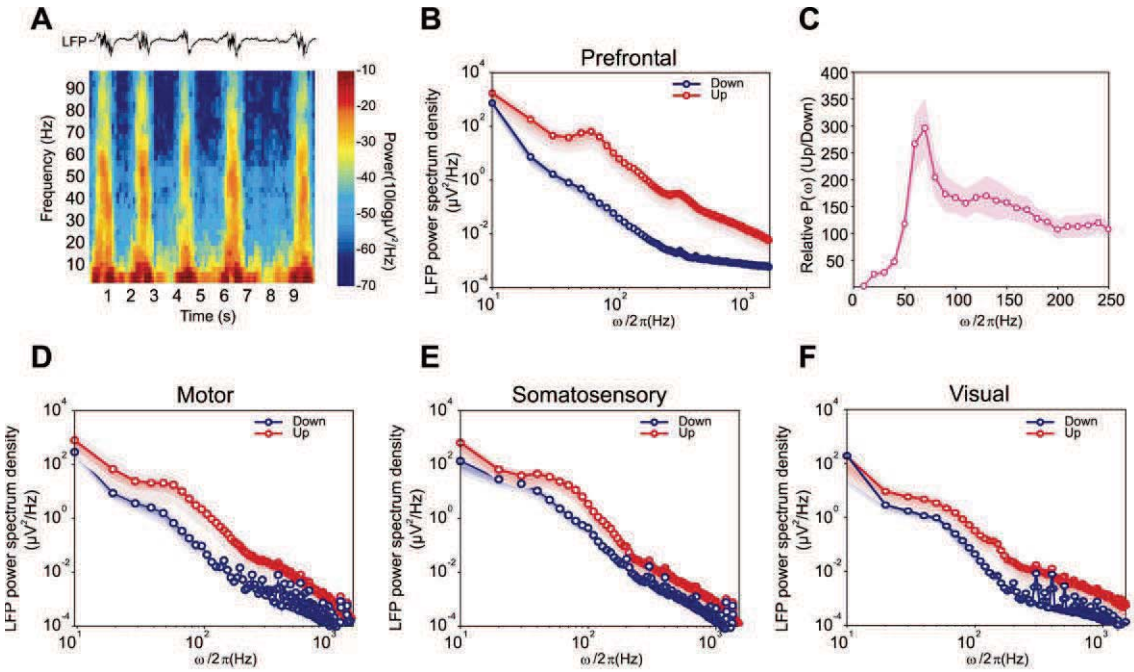

Figure 23. Oscillatory activity during slow waves in 4 (prefrontal, motor, somatosensory, and visual) cortical areas of the mouse.

A: spectrogram showing the occurrence of fast rhythms during the UP states in prefrontal cortex. B: power spectrum of activity in the prefrontal cortex after separating UP (red with circles) and DOWN (dark blue with circles) states. C: relative power in UP vs. DOWN states calculated from the power spectra. D–F: power spectra of oscillatory activity in motor, somatosensory, and visual cortex, respectively.

The beta power ratio was 13.2 times larger in prefrontal cortex ($P < 0.005$ with respect to motor cortex, $P < 0.0001$ with respect to somatosensory cortex, and $P < 0.0001$ with respect to visual cortex). Prefrontal cortex showed a markedly higher relative power in the gamma band (Fig. 23, B and C). We divided the gamma band into high gamma (60–90 Hz) and low gamma (30–60 Hz). In the low gamma range, the relative power in prefrontal cortex was 42.2, significantly larger than in other areas ($P < 0.001$ with respect to motor cortex, $P < 0.0001$ with respect to somatosensory cortex, and $P < 0.001$ with respect to visual cortex), where values ranged from 3.6 to 5.8. Finally, in the high gamma band prefrontal cortex showed a relative power value of 124, which was significantly different from motor ($P < 0.005$), somatosensory ($P < 0.005$), and visual ($P < 0.005$) cortices, where the values ranged from 8.9 to 14. Further information on the statistics of this section is given in Figure 25.

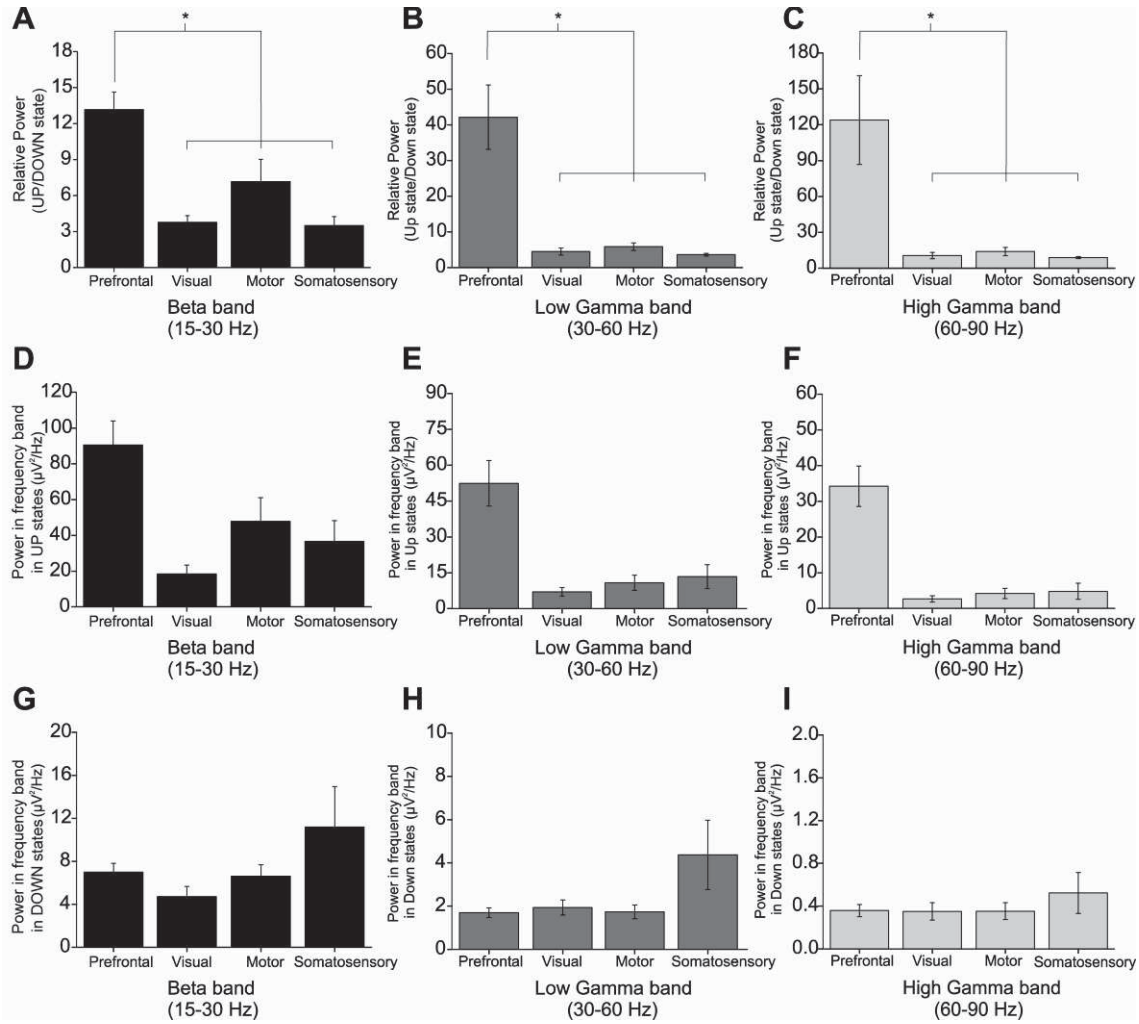

Figure 24. Fast rhythms in the mouse cerebral cortex during slow oscillations in 4 cortical areas.
A–C: comparison of relative power in 15–30 Hz (beta), 30–60 Hz (low gamma), and 60–90 Hz (high gamma) frequency bands across the 4 cortical areas (prefrontal, visual, motor, and somatosensory cortex). D–F: comparison of absolute power in UP states in the beta, low gamma, and high gamma frequency bands across cortical areas. G–I: comparison of absolute power across areas in DOWN states for the same frequency bands. Error bars are SE. *$P < 0.01$.

A

Fischer test values			
	Beta (15-30 Hz)	Low gamma (30-60 Hz)	High gamma (60-90 Hz)
Degrees of Freedom	3	3	3
F value	13.67706	10.96521	5.95757
Prob>F	1.50536E-5	7.77213E-5	0.00312

B

Fischer test p values			
	Beta (15-30 Hz)	Low gamma (30-60 Hz)	High gamma (60-90 Hz)
mot pre	0.00334	3.11776E-4	0.00494
som pre	1.01912E-5	9.20464E-5	0.00214
som mot	0.07838	0.81659	0.8683
vis pre	1.53471E-5	1.20106E-4	0.00268
vis mot	0.10219	0.88584	0.93024
vis som	0.88671	0.92666	0.93504

Figure 25. Table showing One-way ANOVA statistical treatment for beta-gamma band power calculation across areas.
A: General linear model. B: *post hoc* comparisons.

3.3 RESULTS OF OBJECTIVE 3: COMPARISON OF CORTICAL OSCILLATORY PATTERNS AND EXCITATORY-INHIBITORY BALANCE IN PREFRONTAL CORTEX OF WT AND TGDYRK1A MICE

3.3.1. TgDyrk1A mice showed behavioral deficits in cortical dependent tasks

First, we tested whether Dyrk1A overexpression could alter cognitive performance related to frontal cortex functioning. We started by analyzing spontaneous alternation, a prefrontal cortex-dependent behavioral task, which has been interpreted as an index of spatial working memory associated with cognitive function. No significant differences were observed in the total number of total entries in the Y-maze arms, indicating that locomotor activity was similar in both genotypes (Fig. 26 B). TgDyrk1A mice showed a reduced percentage of alternation with respect to controls (P <0.05, Fig. 26 C).

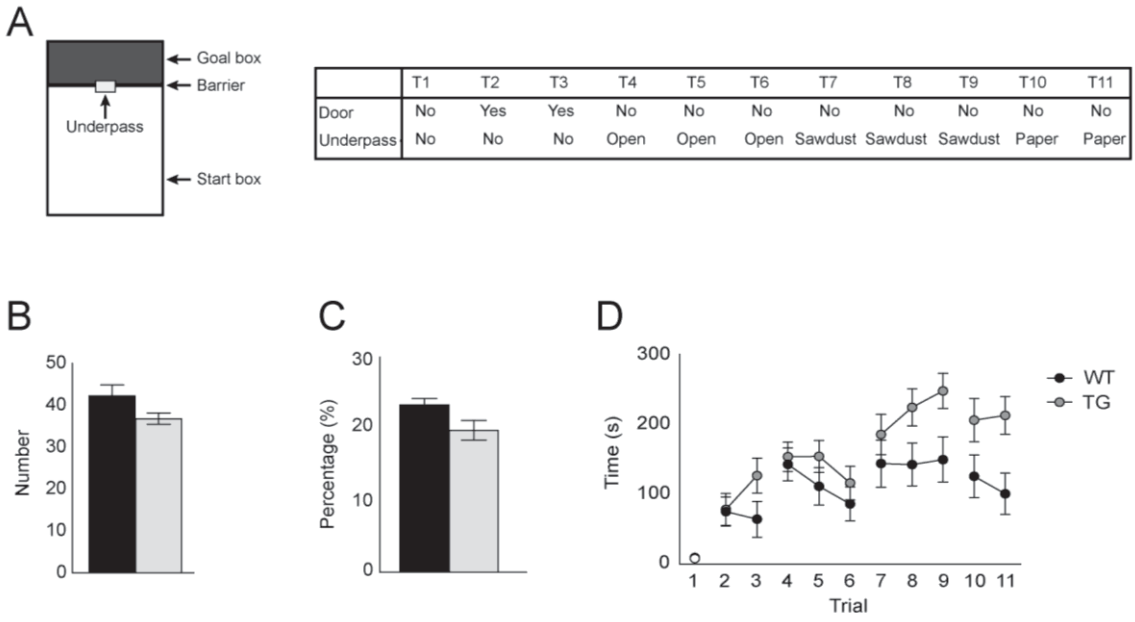

	T1	T2	T3	T4	T5	T6	T7	T8	T9	T10	T11
Door	No	Yes	Yes	No	No	No	No	No	No	No	No
Underpass	No	No	No	Open	Open	Open	Sawdust	Sawdust	Sawdust	Paper	Paper

Figure 26. Behavioral performance in frontal cortex dependent tasks.
A: Schematic representation of puzzle box arena and protocol (T = trial). B: TgDyrk1A mice performed similar number of arm entries in the Y-maze suggesting no alteration of locomotor activity. C: TgDyrk1A mice presented a significant reduction in spontaneous alternation in the Y-maze. D: TgDyrk1A mice presented deficits in problem-solving in the puzzle box. Black (WT mice) and grey (TgDyrk1A) symbols and bars represent mean ± SEM * P < 0.05.

The puzzle box (Ben Abdallah et al. 2011), provides information related to executive function necessary for problem-solving, which is known to require proficient prefrontal cortex functioning. Overall, differences were observed in the execution of the task between TgDyrk1A and control mice (ANOVA repeated measure, genotype effect, $P < 0.05$; Fig. 1 D). During the whole experiment TgDyrk1A mice showed significantly poorer performance (genotype-session interaction $P < 0.05$) than wild types. We can discard a lack of motivation of transgenic mice to reach to the goal zone by transgenic mice, since in the easier phase (T1) no differences between both genotypes were observed ($P = 0.72$). TgDyrk1A mice showed particularly higher latencies to reach to the goal zone with increasing difficulty of the task (genotype effect ANOVA repeated measure, underpass filled of sawdust (T7 to T9): $P = 0.06$, and underpass blocked with paper (T10 to T11): $P < 0.05$). In fact, while control mice learnt the task in the last phase of the experiment (T10-T11), TgDyrk1A mice showed increasing latencies indicating impaired learning. Interestingly, TgDyrk1A showed worst performance respect to control when long term memory was assessed (T3: $P = 0.094$, T8: $P = 0.05$), whereas not so marked impairment was observed at the presentation of a new problem (T2, T4, T7) with the exception of the most complicated task (T10: $P = 0.07$).

These behavioral findings demonstrate for the first time altered executive functions in a problem-solving task in Dyrk1A overexpressing mice that indicate frontal cortex dysfunction.

3.3.2. Firing rate and regularity of the slow rhythm are decreased in prefrontal cortex of TgDyrk1A mice.

Cortical emergent activity is the result of the integration of cellular and network properties. Spontaneous activity reflects features of the underlying network and thus shares spatiotemporal properties with the evoked activity (Tsodyks et al. 1999) as well as with the activity during wakefulness (Destexhe et al. 2007; Steriade and Timofeev 2003). Similarly to what happens in other mammals (Compte et al. 2008; Gray and McCormick 1996; Hasenstaub et al. 2005; Steriade and Amzica 1996), during anesthesia cortical activity is organized in spontaneous slow waves overridden with fast oscillations in the beta and gamma range in mouse (Compte et al. 2008; Gray and McCormick 1996; Hasenstaub et al. 2005; Ruiz-Mejias et al. 2011; Steriade and Amzica 1996), an activity comparable to that during slow wave sleep (Chauvette et al. 2011; Steriade 2006). Since the behavioral analysis pointed out to a prefrontal-dependent cognitive deficit in TgDyrk1A mice, we studied prefrontal emergent patterns during anesthesia with the aim to detect possible functional alterations.

We recorded slow oscillations in the medial prefrontal cortex (mPFC) of WT and TgDyrk1A mice. Unless the opposite is said, we processed and illustrated data from each hemisphere separately (see Fig. 27). Since we obtained all the recordings from both hemispheres, we find that it provides additional information on the consistency of the observations (e.g. Fig. 26). Both the mPFC from WT (n=15) and from TgDyrk1A (n=16) mice displayed consistent slow oscillations during anesthesia. Slow oscillations consisted of periods of activity or UP states interspersed with silent periods or DOWN states (Fig. 27 B-C). No differences existed in the frequency of oscillations, which was 0.88 Hz in both genotypes (Fig. 27 D, N= 15 WT and 16 TgDyrk1A, mean of both hemispheres). The duration of UP and DOWN states was as well preserved (UPs: 0.32±0.07 s and 0.33±0.08 s; Fig. 27 E; DOWNs: 0.93±0.36 s and 0.87±0.24 s in WT and transgenic mice respectively; Fig. 27 F, N= 15 WT and 16 TgDyrk1A, mean of both hemispheres). However, the coefficient of variation (CV) of the UP states duration was significantly increased in the mPFC of TgDyrk1A mice ($P < 0.01$, Fig. 27 G), meaning a decreased regularity in the UP states. This is relevant because prefrontal cortex has a characteristic regularity over other cortical areas (Ruiz-Mejias et al. 2011). No alterations were found in the CV of DOWN states duration (Fig. 27 H), or in the CV of the complete cycle (UP and DOWN states). Even larger significant differences emerged when we analyzed parameters relative to the firing rate of the network: the population firing rate during UP states was lower in TgDyrk1A mice than in controls (Fig. 27 I and K, L). The slope of the transition from DOWN to UP states of the firing rate (Upward transition slope) was lower in the TgDyrk1A mice, suggesting a slower recruitment of the network (Fig. 27 J). No changes were detected for the UP to DOWN transition (Fig. 27 K, L). The decreased firing during UP states would be compatible with a more inhibited network (see below), while the decrease in the regularity of UP states suggests a loss in the balance in the mPFC of TgDyrk1A mice.

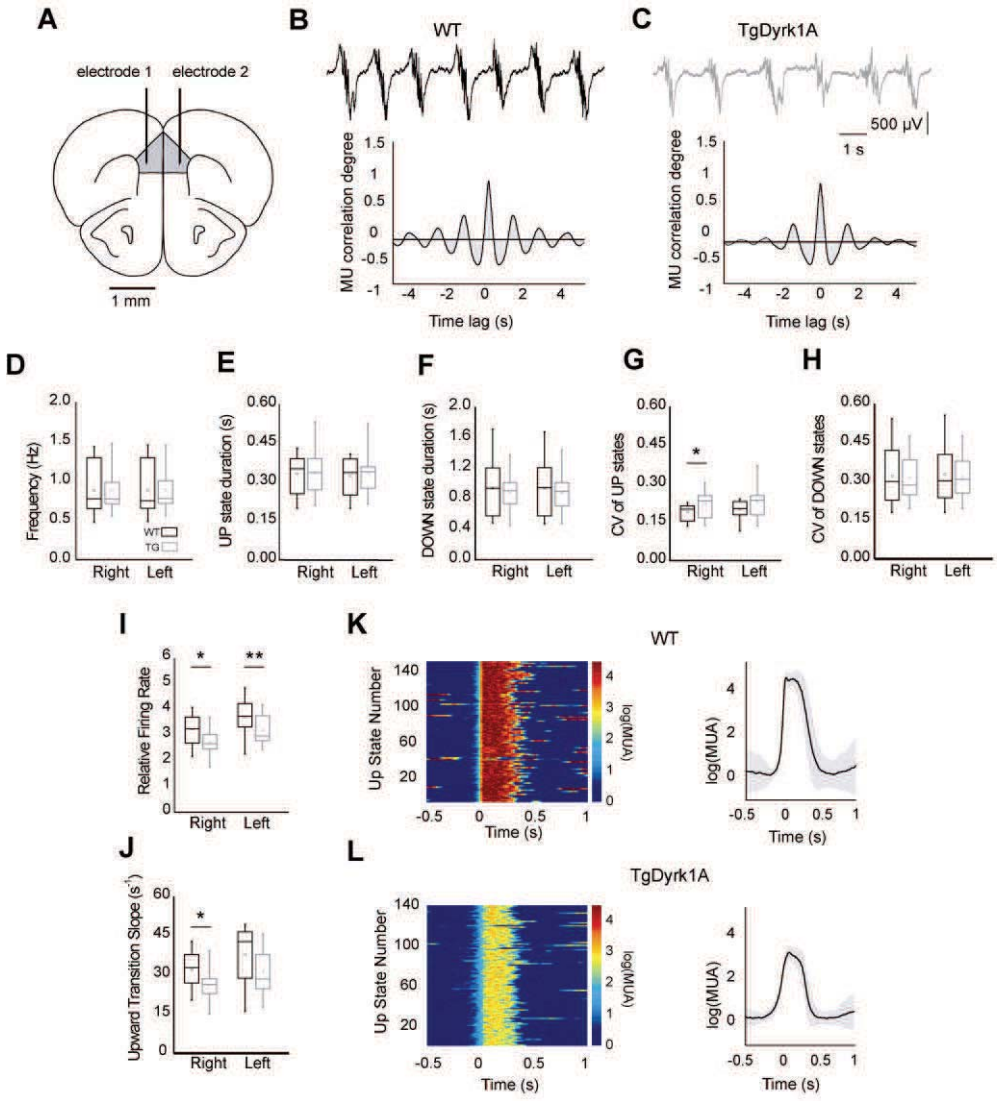

Figure 27. Characterization of slow waves in the mPFC in WT and TgDyrk1A mice.
A: Diagram depicting the recording arrangement to study mPFC network parameters. LFP was recorded typically bilaterally. B-C: Top black and gray traces: examples of the slow oscillation recorded in WT and TgDyrk1A mice, respectively. Bottom traces: Wave autocorrelations showing synchrony in LFP traces of both genotypes. D-H: Temporal parameters extracted from the analysis of LFP in WT and transgenic mice and in each hemisphere. A significant change was found in CV of UP states of I-L, Parameters regarding firing properties of mPFC network of both strains. J,L: raster plots showing an example of the decrease in network firing rate in TgDyrk1A mice. Left traces: example of waveform averages obtained with the algorithm to calculate firing parameters of the network. D-H,I,K: n=15 WT and n=16 TgDyrk1A mice per hemisphere. Boxes depict percentiles 25-75 with the median, the small squares inside represent mean values, whiskers correspond to values 5-95% and asterisks 1-99%. *$P < 0.05$; **$P < 0.01$.

3.3.3. Dyrk1A overdosage decreases gamma oscillations in the prefrontal cortex

During UP states the local cortical activity is synchronized in fast frequencies both in beta (15-30 Hz) and gamma (30-90 Hz) frequencies (Compte et al. 2008; Gray and McCormick 1996; Hasenstaub et al. 2005; Ruiz-Mejias et al. 2011; Steriade and Amzica 1996). To quantify the intensity of spontaneous high frequencies during slow oscillations we computed Fourier transform analysis in UP and DOWN states in transgenic mice and compared them to WT. We quantified high frequencies in three different frequency bands: beta (20-30 Hz), low gamma (30-60 Hz) and high gamma (60-90 Hz). We found that the average power in the relative power of the high gamma band (UP/DOWN state power, Fig. 28 A, B) was decreased in the TgDyrk1A mice in either right (94.41±64.92 vs 45.27±24.09, $P < 0.05$, Fig. 28 3 C, D) or left hemisphere (127.74±101.54 vs 64.48±42.21, $P < 0.05$, Fig. 28 E, F), while relative power in the low gamma band was decreased in the right hemisphere (41.81±24.62 vs 20.83±10.11, $p<0.01$, Figure 3 e), while the power in beta remained unaltered in both hemispheres.

We also detected a positive correlation between maximum network firing rate (multi-unit activity, MUA) during UP states and the relative power (Fig. 29 A, C), both in low gamma (right: $\rho_{Pearson}=0.60$, $P < 0.05$, Fig. 29 E; left: $\rho_{Pearson}= 0.62$, $P < 0.05$, Fig. 29 G) and high gamma bands (right: $\rho_{Pearson}=0.68$, $P < 0.01$, Fig 29 I; left: $\rho_{Pearson}=0.50$, $P = 0.056$, Fig. 29 K). This correlation that did not exist in TgDyrk1A mice neither in low gamma (right: $\rho_{Pearson}=0.23$, n.s., Fig. 29 F; left: $\rho_{Pearson}=-0.04$, n.s., Fig. 29 H) nor it high gamma (right: $\rho_{Pearson}=0.16$, n.s., Fig. 29 J; left: $\rho_{Pearson}=-0.07$, n.s., Fig. 29 L). Both, the decrease in the generation of gamma (60-90 Hz) and its uncoupling to the firing rate suggest that the network mechanisms generating high gamma frequencies are altered.

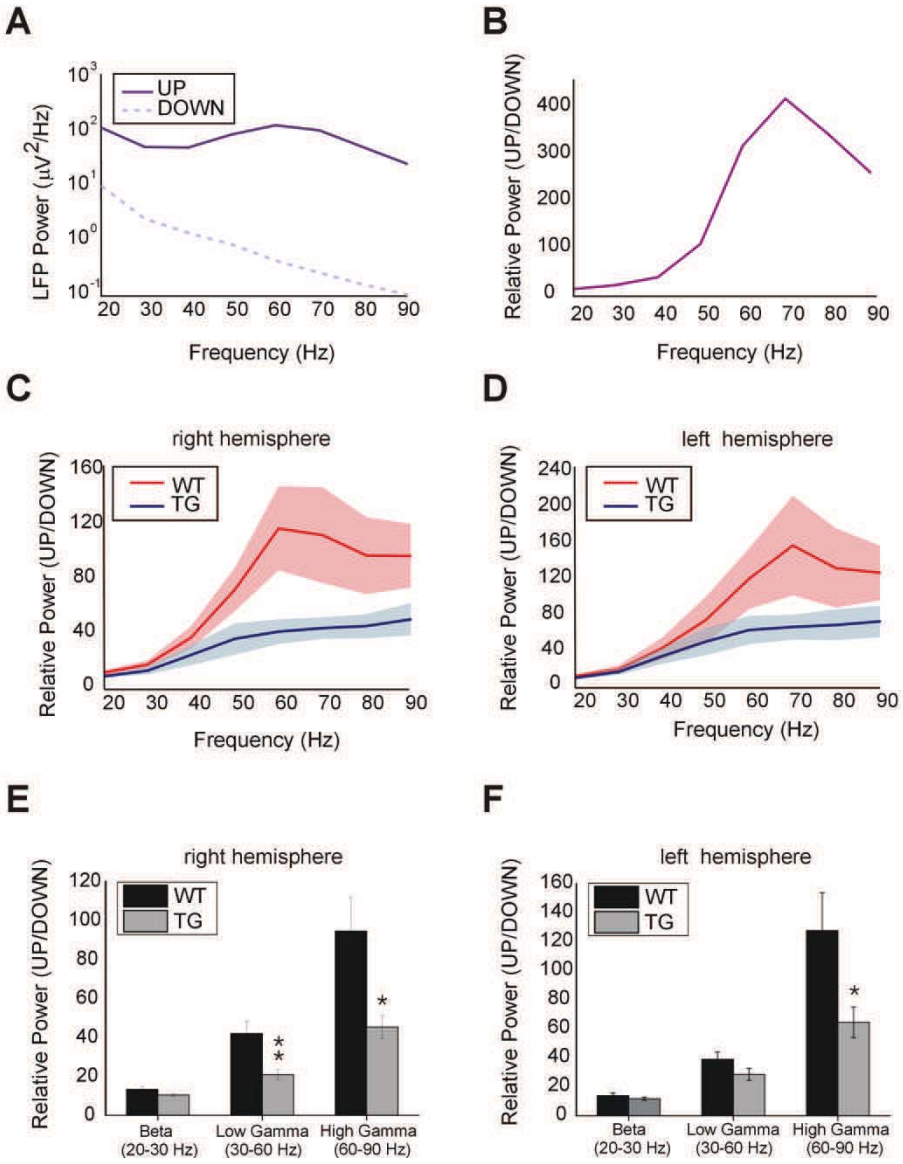

Figure 28. Characterization of fast rhythms in the mPFC of WT and TgDyrk1A mice.
A: Example of power spectrum density (p.s.d) plots calculated in the UP and DOWN state of a WT and a transgenic mouse. B: Example of relative power between UP and DOWN state from the p.s.d plots in a. C-D: Averages of relative power (UP/DOWN) of WT (black traces) and TgDyrk1A (grey traces) in either right (c) or left hemispheres (D). E-F: Averages of relative power in each frequency band in both genotypes in right (E) and left (F) hemispheres, were high gamma oscillations (60-90 Hz) were found to be decreased in both hemispheres ($P < 0.05$), while low gamma oscillations (30-60 Hz) were decreased in right hemisphere ($P < 0.01$). N=15 WT and 16 TgDyrk1A mice in both hemispheres for high gamma band. 4 outliers removed: 1 in low gamma, WT, right; 1 in low gamma, WT, left; 1 in low gamma, TG, left; 1 in high gamma, WT, right.

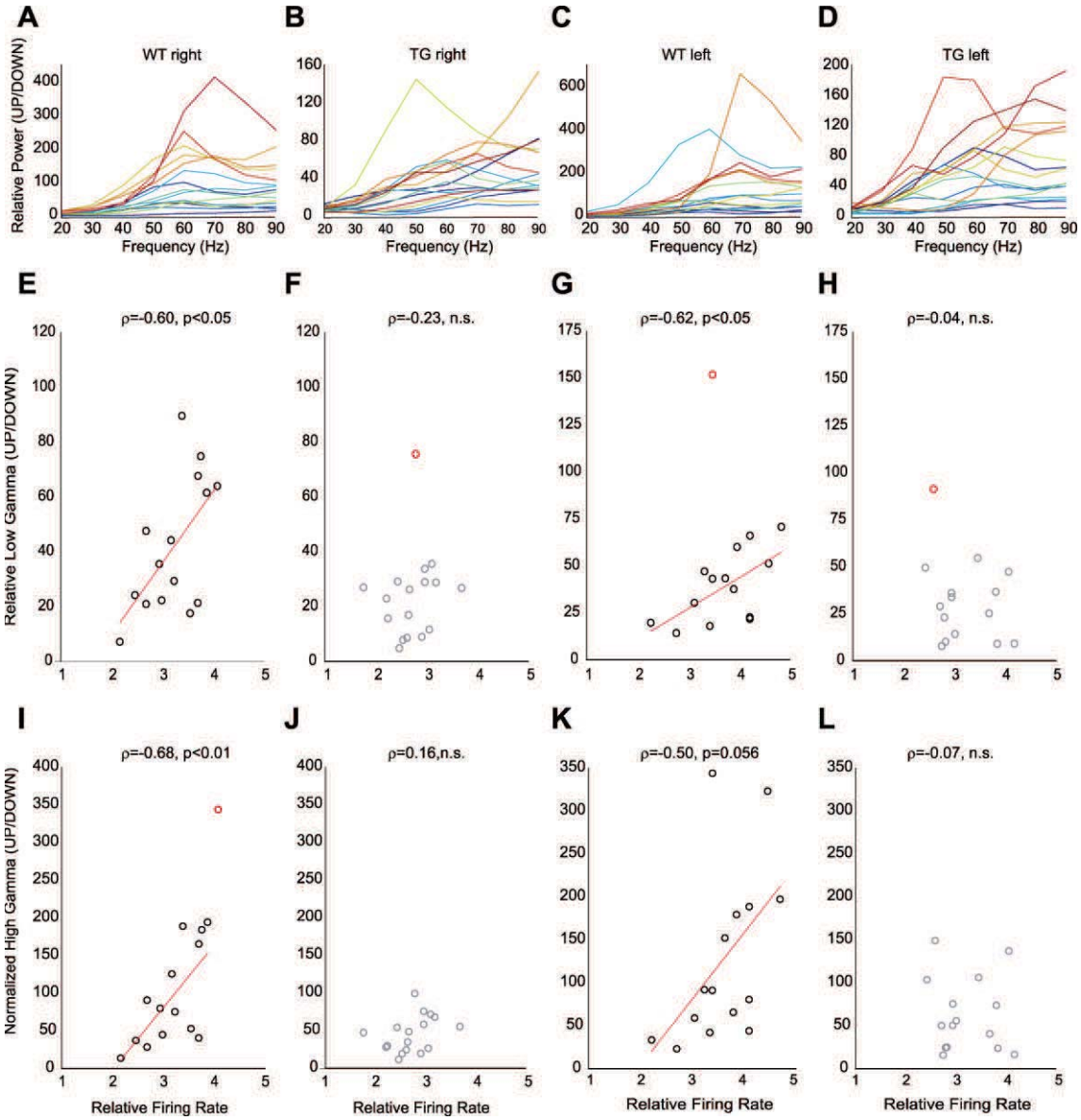

Figure 29. Correlation of network firing rate with gamma rhythms within UP states.
A-B: Plots where relative power (UP/DOWN) across animals is presented in WT mice (a) and TgDyrk1A (b) in the right hemisphere, ordered by color code of temperature with the network firing rate (dark blue, min value; deeP red, max value). C-D: Same as a-b, but for left hemisphere. E-F: Correlation of low gamma band (30-60 Hz) with network firing rate in the right hemisphere. G-H: Same as E-F but for the left hemisphere. I-J: Same as E-F but for high gamma band (60-90 Hz). K-L: Same as I-J but for high gamma band in the left hemisphere. F,H,J,L: Note that gamma frequency is uncorrelated to network firing rate in both hemispheres of the TgDyrk1a mice. E-L, Same 4 outliers removed as in Fig 3. Outliers are depicted as red circles in plots.

3.3.4. Propagation of slow waves is altered in the motor cortex of TgDyrk1A mice.

In humans, slow waves during sleeP are mainly generated in frontal cortex, travelling towards more posterior areas (Massimini et al. 2004; Murphy et al. 2009; Nir et al. 2011). Such preferred backward propagation of slow oscillations is observed also in anesthetized mice when probed both with multi-electrode recordings (Ruiz-Mejias et al. 2011) and voltage-sensitive dye imaging (Stroh et al. 2013). Travelling waves are an emergent property of spatially organized neuronal networks and can be affected by changes in the underlying circuitry, like alterations in the excitatory-inhibitory balance. Hence, we looked for differences of propagation features in mPFC and motor cortices of WT and transgenic mice, a wide frontal area where is likely to observe both onset and propagation of slow waves.

The passage of a wavefront across the area covered by the electrode array, appeared as a sequence of UP state onsets with progressively changing time lags δ_n (Fig. 30 A, B). Modes of propagation changed from one UP state to another, showing slow waves travelling both backward (increasing δ_n, Fig. 30 A bottom) and forward (decreasing δ_n, Fig. 30 A top) with respect to the anterior-posterior axis parallel to 16 aligned electrodes. Grouping similar patterns of activation onsets, mean and variability of inverse speeds (time over space) of propagation were computed for each of these groups (Fig. 30 B, C). Pooling all inverse speeds measured in motor cortex (Fig. 5 D) slow waves appeared to travel preferentially from front to back in both genotypes (positive speeds, Fisher's exact test $P<0.05$), while a preferred direction of propagation was not apparent in mPFC (Fig. 30 E). Such balance between positive (n=33) and negative (n=27) speeds in mPFC, further confirmed that slow waves initiate their journeys in a frontal region around electrode location. A progressive reduction of cortical excitability within and around mPFC confirmed by the significant reduction of backward propagation speed across motor cortex (Mann-Whitney U test, $P < 0.05$) in TgDyrk1A mice (17.7 ± 1.9 mm/s), compared to the one in control animals (24.8 ± 3.3 mm/s). The loss of excitability slowing the speed of propagation can be explained by an increase of inhibition in cortical networks, as discussed below.

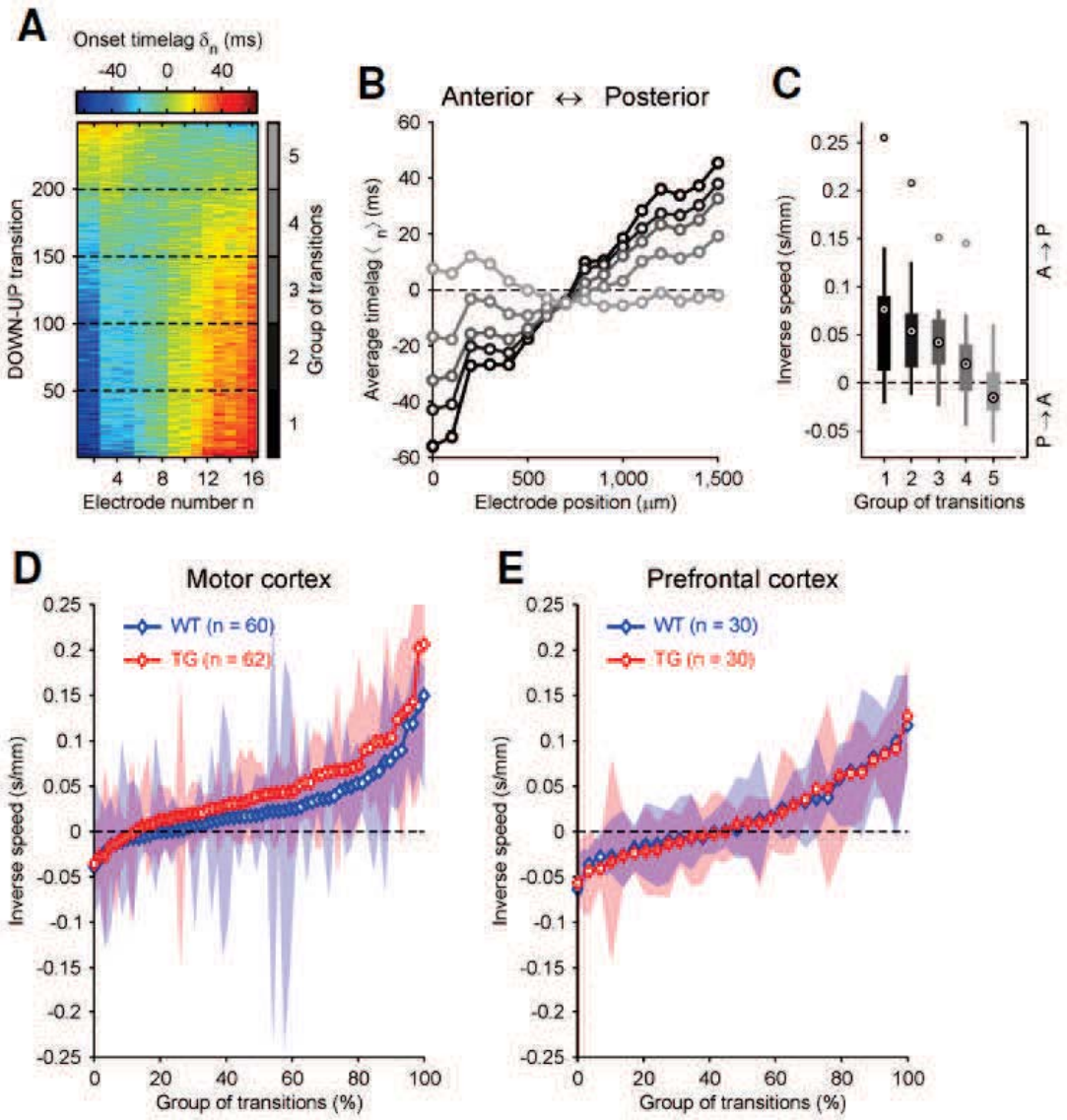

Figure 30. Slow wave propagation across frontal cortex of WT and TgDyrk1A mice.
A: Matrix of time lags δ_n of UP state onsets simultaneously detected in 16 aligned electrodes from an example recording in motor cortex. Matrix rows are different DOWN to UP transition, and colors code for δ_n. Principal component analysis is used to sort DOWN-UP transitions, bringing together similar modes of slow wave propagation (Ruiz-Mejias et al. 2011). B: UP state onsets are pooled in five equally sized groups of transitions (dashed lines in **a**) and group averaged δ_n are plotted for each of them (gray levels as in vertical color bar of A).C: Statistics of inverse local speeds in the five propagation modes in B. For each mode, the 15 inverse local speeds are the differences between average δ_n in nearby electrodes divided by their distance. Black circles with a dot, means of inverse speeds. Thick bars, second and third quartiles. Thin lines, extreme values. Gray circles, outliers. D-E**,** Mean inverse speeds in all groups of transitions detected in motor (D) and prefrontal (E) cortex of both WT (blue, n = 18) and TgDyrk1A (red, n = 20) mice. Shaded areas, second and third quartiles of inverse local speeds in each group of transitions. Propagation modes are sorted by inverse speeds. Symbols representing means are white filled if inverse speed of the propagation mode is significantly different from 0 (Wilcoxon's test, $P < 0.05$).

3.3.5. Deregulation of excitatory-inhibitory balance in TgDyrk1A prefrontal cortex

Our neurophysiological results suggested that Dyrk1A overexpression could lead to an overinhibited mPFC. However, we found no alterations in the number of cortical GABAergic neurons in the mPFC of TgDyrk1A (n=8) mice, compared to WT (n=8), as revealed by parvalbumin, calretinin and somatostatin immunostaining (Fig. 31 A). This did not rule out though the possibility that inhibition could be somehow enhanced. To investigate this, we analyzed the proportion of excitatory (Vglut1) *versus* inhibitory (Vgat) presynaptic puncta in the mPFC of transgenic and WT mice.

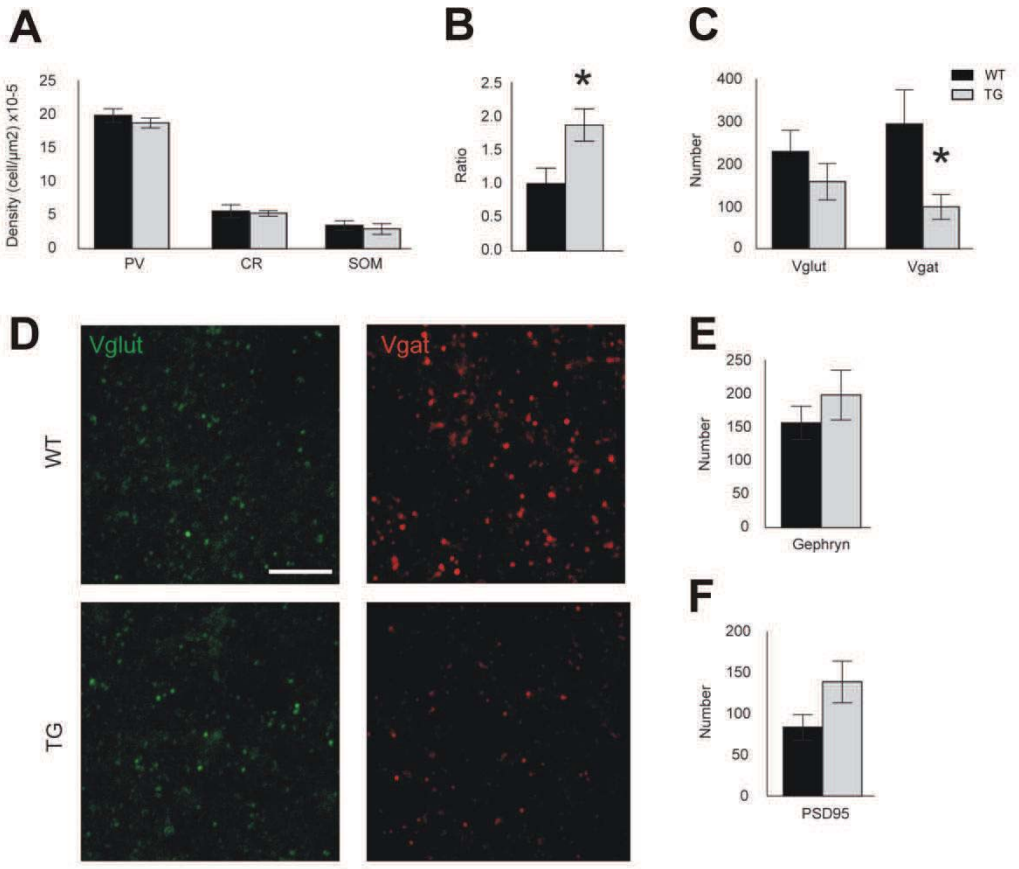

Figure 31. Histological analysis of the mPFC of WT and TgDyrk1A (1). A: Density of the different inhibitory neuronal populations represented by the parvalbumin (PV), calretenin (CR) and somatostatin (SOM) positive cells in the mPFC. B: Ratio of the vesicular Vglut1 (excitatory) versus Vgat (inhibitory) presynaptic markers as an index of the excitatory-inhibitory balance. C: Number of presynaptic inhibitory and excitatory puncta in the mPFC. D:**,** Confocal images showing Vglut (green) and Vgat (red) puncta in WT (upper panel) and TgDyrk1A (lower panel) mPFC and number of postynaptic E**,** inibitory (Gephryn) and F, excitatory (PSD95) sites**.**

Again, the results obtained did not explain our electrophysiological observations since TgDyrk1A mice showed a significantly increased Vglut1/Vgat ratio ($p < 0.05$, Fig. 31 B), due to a reduced number of presynaptic inhibitory puncta ($p < 0.05$, Fig. 31 C and D). However, no differences were found in the number of postsynaptic inhibitory sites stained with anti-geprhyn antibody (Fig. 31 E) in transgenic mice.

One possible explanation for these results could be that changes in excitatory–inhibitory balance affected differentially specific neuronal subpopulations. To explore this possibility we generated double transgenic mice crossing TgDyrk1A with mice overexpressing the yellow fluorescent protein (YFP) under the Thy1 promoter (Thy-YFP/TgDYRK1A). This strategy allowed us to directly visualize cortical pyramidal neurons, the most abundant neuronal population in mPFC, in TgDyrk1A. In the Thy-YFP/TgDYRK1A we could easily detect whether excitatory or inhibitory terminals (Vglut+ or Vgat+ puncta) contacted pyramidal neuron somas (Fig. 32 A and B). We did not observe differences in the density of the excitatory or inhibitory inputs received by pyramidal cells in Thy-YFP/TgDYRK1A mice overexpressing Dyrk1A (Fig. 32 A).

Since parvalbumin fast spiking interneurons modulate oscillatory activity in the gamma-range (see Bartos et al., 2007; Whittington et al., 2011 for reviews) and these oscillations were significantly reduced in TgDyrk1A mice, we specifically analysed the number of inhibitory and excitatory presynaptic terminals over the soma of parvalbumin inhibitory neurons. Importantly, mPFC parvalbumin positive neurons of TgDyrk1A received significantly fewer inhibitory terminals (Vgat+ puncta) compared to controls ($p < 0.05$, Fig. 32 C and 32 D), indicating a decreased inhibitory control of the main inhibitory population of prefrontal cortex. The density of excitatory presynaptic terminals (Vglut+ puncta) contacting parvalbumin positive neurons was though equal in both genotypes (Fig. 32 D). Thus, even though TgDyrk1A mice showed a significant increased Vglut1/Vgat ratio, overexpression of Dyrk1A leads to a reduction of the inhibitory synapses received by parvalbumin interneurons, what functionally results into a disinhibition of this inhibitory population and therefore a local over-inhibition of the neuronal network.

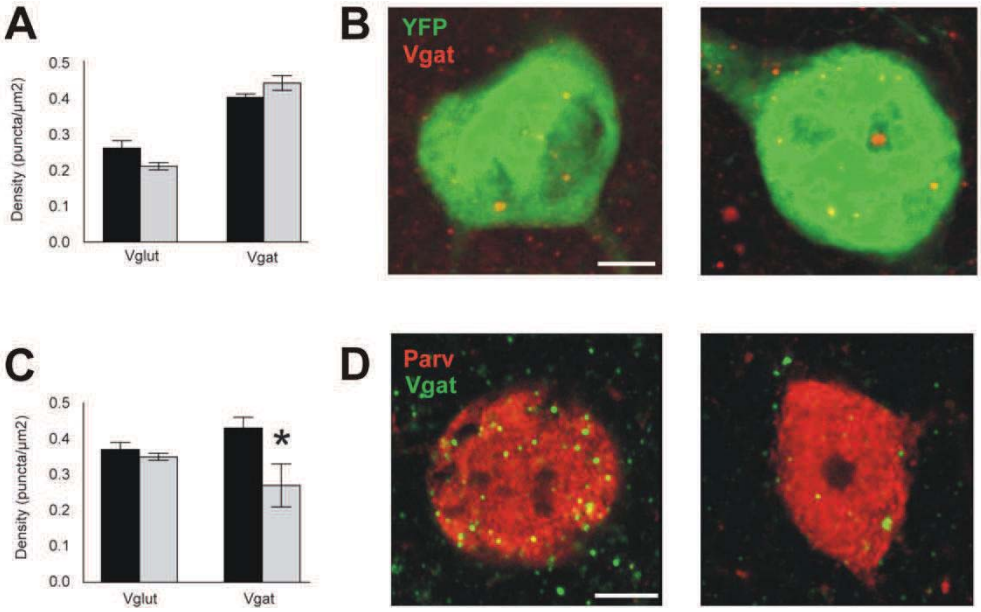

Figure 32. Histological analysis of the mPFC of WT and TgDyrk1A (2).
A: Density of excitatory and inhibitory terminals contacting with excitatory pyramidal neurons and B, single confocal images illustrating inhibitory terminals (red) contacting the soma of pyramidal neurons (green) in WT (left panel) and TgDyrk1A (right panel) mPFC. C: Density of excitatory and inhibitory terminals contacting with parvalbumin positive neurons and D:, representative micrographies of inhibitory perisomatic contacts (green) on parvalbumin positive neurons (red) of WT (left panel) and TgDyrk1A (right panel) mPFC. Bar scale = 5µm Black bars represented WT mice and grey bars TgDyrk1A ones. Data are represented as mean ± SEM; * $p < 0.05$.

3.4 RESULTS OF OBJECTIVE 3: COMPARISON OF CORTICAL OSCILLATORY PATTERNS AND EXCITATORY-INHIBITORY BALANCE IN SOMATOSENSORY CORTEX OF WT AND TGDYRK1A MICE

3.4.1. Increased fast inhibition in thalamocortically evoked fPSP of TgDyrk1A mice.

Thalamocortically-evoked extracellular field potentials were recorded at 0.6-0.7 mm from surface in somatosensory cortex (which corresponds to L4) while stimulating in ventral postero-medial thalamus (VPM) at different intensities. The analysis of positive and negative components of fPSP revealed an increase in the inhibitory component, which was determined to be the positive voltage deflection that peaked within the first 100 ms after stimulus artifact (Fig. 33 A).

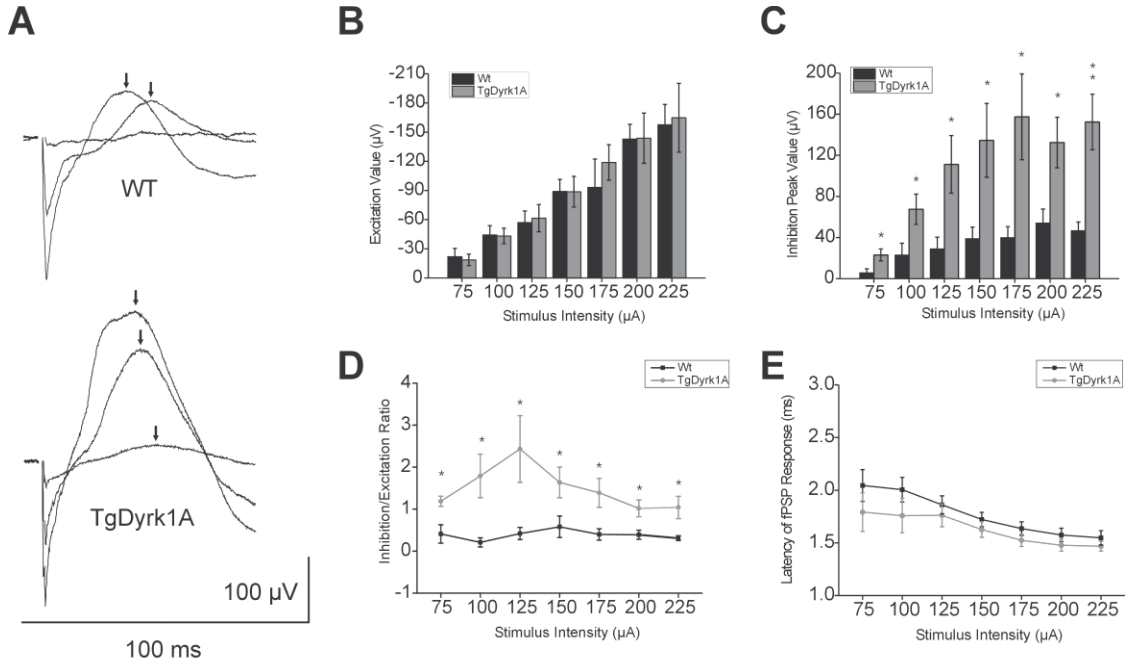

Figure 33. Synaptic inhibition is increased in TgDyrk1A mice.
A: Examples of fPSP evoked at 75, 150 and 255 µA of intensity. The stimulus had a duration of 0.2 ms and was delivered at a frequency of 0.33 Hz. B: Comparison of excitatory component values at all stimulus intensities. 75: N= 5 vs 6; 100: 6 vs 6; 125: 8 vs 7; 150: 8 vs 8; 175: 8 vs 8; 200; 8 vs 7; 225: 8 vs 7. C: Comparison of inhibitory component peak values at all stimulus intensities. 75: N= 5 vs 6; 100: 7 vs 5; 125: 8 vs 7; 150: 8 vs 8; 175: 8 vs 8; 200; 8 vs 7; 225: 8 vs 7. D: Ratio of inhibition/Excitation values at each intensity of stimulation. 75: N= 4 vs 4; 100: 7 vs 6; 125: 7 vs 6; 150: 8 vs 8; 175: 8 vs 8; 200; 8 vs 7; 225: 8 vs 7. Responses that had no inhibitory peak were not considered for ratios. Outliers removed. E: Comparison of ectitatory response latencies. 75: N= 4 vs 5; 100: 6 vs 6; 125: 8 vs 7; 150: 8 vs 8; 175: 8 vs 8; 200; 8 vs 7; 225: 8 vs 7. In B-E black: Wild type mice; grey: TgDyrk1A mice. 75: N= 5 vs 6; 100: 7 vs 5; 125: 8 vs 7; 150: 8 vs 8; 175: 8 vs 8; 200; 8 vs 7; 225: 8 vs 7. **P* < 0.05; ***P* < 0.01

The inhibitory peak resulted to be significantly higher in amplitude in TgDyrk1Amice than in controls in all stimulus intensities (Fig. 33 C). The time course of the evoked inhibition corresponded to the temporal kinetics of disynaptic inhibition associated to $GABA_A$ conductances (Agmon and Connors 1991; Gil and Amitai 1996; Silberberg and Markram 2007). Excitatory peaks across all stimulus intensities remained with no significant changes between the two genotypes. Ratios between excitatory and inhibitory peaks for each one of the stimulus intensites also showed the changes towards an increased fast inhibition (Fig. 33 D). Latencies of excitatory responses did not show any significant changes in the transgenic mice compared to wild types (Fig. 33 E).

3.4.2. Slow and fast oscillations are not changed in somatosensory cortex of TgDyrk1A mice.

We next aimed to study whether the increases in fast inhibition on oscillatory patterns which emerge from the cortical network, such as slow oscillations and fast beta-gamma activity, as that would mean changes in functional activity which may be the substrate of altered cortical processing (Fuchs et al. 2001; Matsuda et al. 2011; Morgan et al. 2011; Muthukumaraswamy et al. 2009; Uhlhaas and Singer 2006; Volman et al. 2011). LFP recordings were obtained bilaterally (Fig. 34 A, B). First, nine wave parameters were extracted from the analysis of LFP recordings performed in deep layers of somatosensory cortex, where UP states were detected. Parameters were the following: three that described temporal features of the slow waves (Frequency of oscillation, UP state duration, DOWN state duration); three representing variability of occurrence of network states (Coefficient of Variation (CV) of UP-DOWN cycle, CV of UP states and CV of DOWN states; and three which described firing properties of the network (Firing Rate of the network in UP states, slope of DOWN-to-UP state transition and slope of UP-to-DOWN state transition. Paradoxically, none of the nine parameters presented changes between genotypes (Figs. 34 F, G and Fig. 35), either in right or left hemisphere.

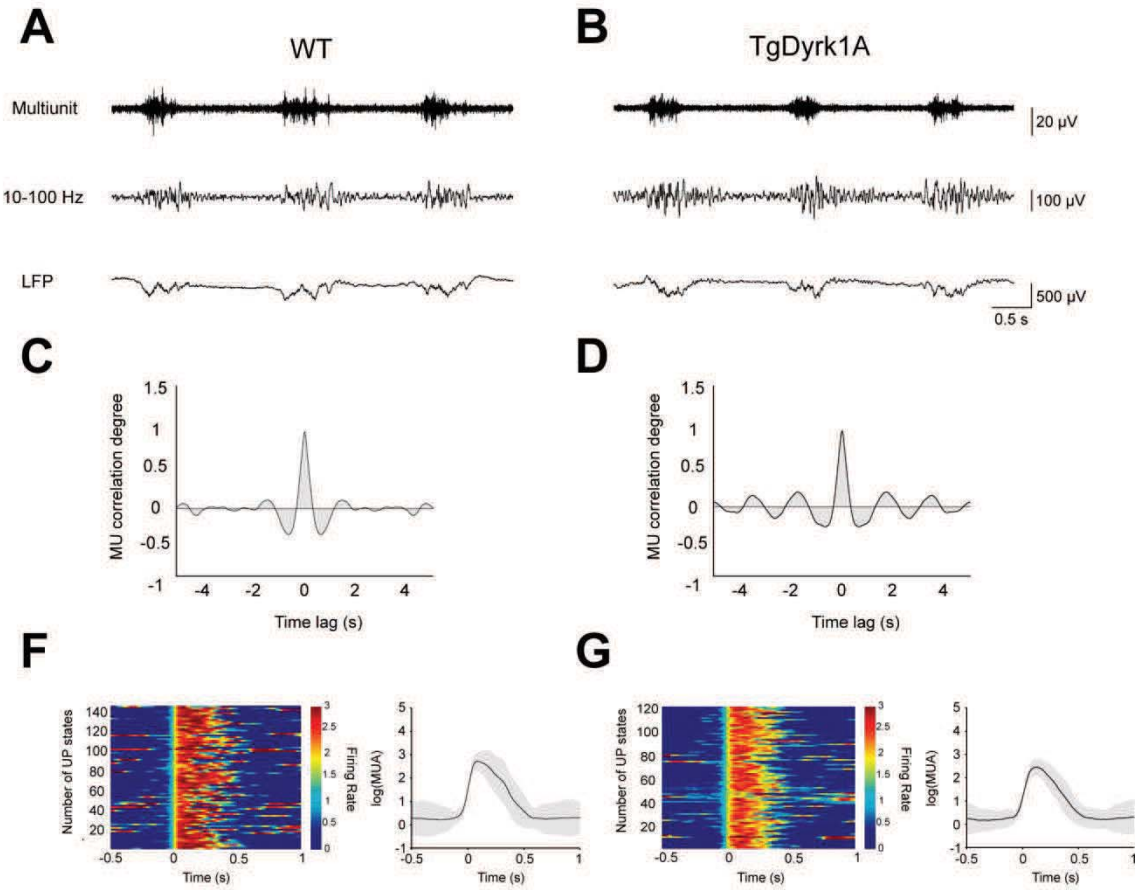

Figure 34. Slow oscillations in the somatosensory cortex of WT and TgDyrk1A mice.
A: Traces of MltiUnit, filtered to 10-100 Hz and row LFP of control and TgDyrk1A in somatosensory cortex. C, D: Autocorrelation of raw LFP signals in A and B, showing synchronization of Slow waves either in Wild type and TgDyrk1A mice. F, G: Raster plots and waveform averages showing temporal and firing properties of the LFP examples in A and B.

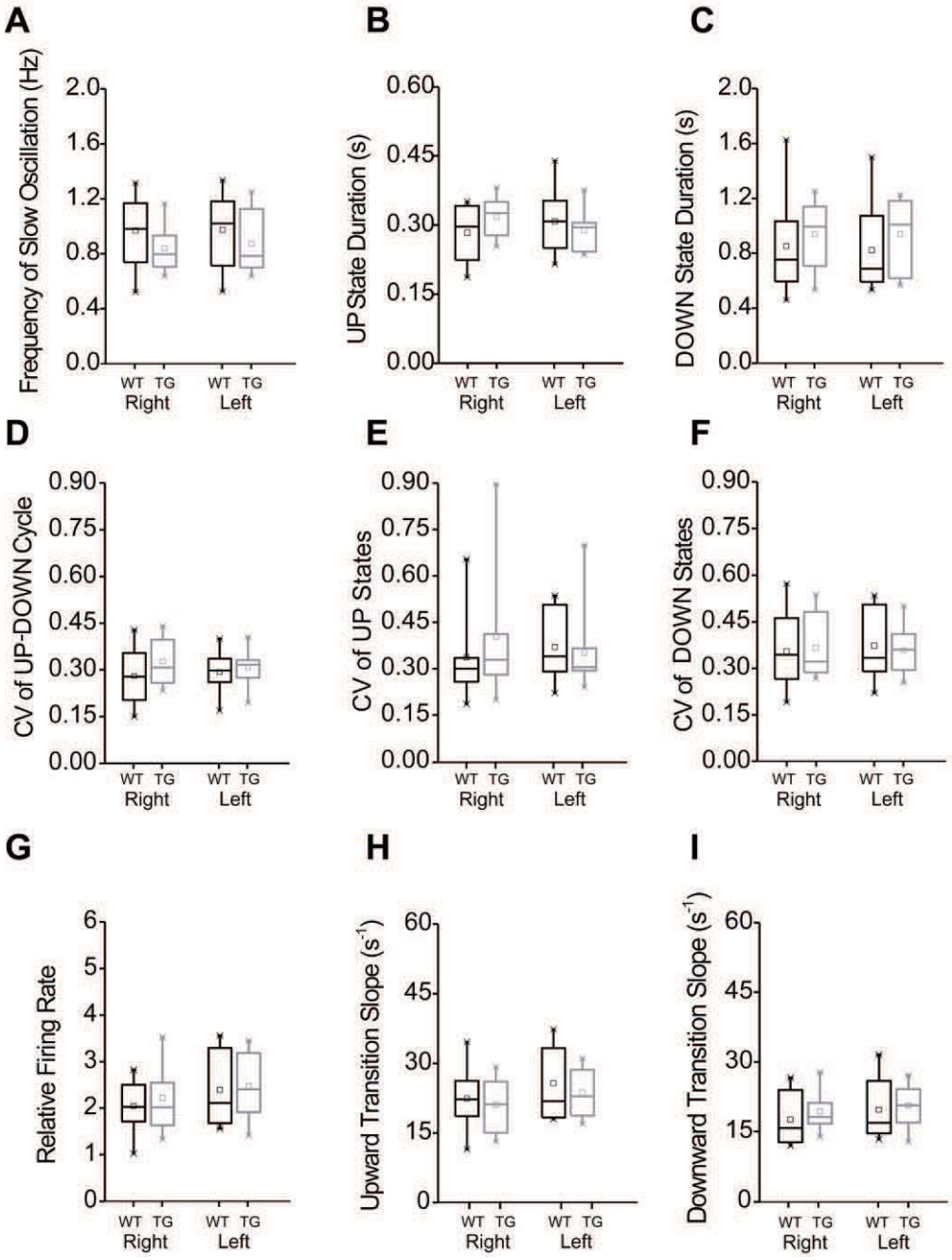

Figure 35. Quantification of Slow wave parameters in WT and TgDyrk1A mice.
Parameters are computed in WT mice (black boxes) or TgDyrk1A mice (grey boxes) in either right or left hemispheres. N=10 WT and 10 TgDyrk1A mice in each hemisphere.

To further investigate the emerging cortical oscillatory patterns in the somatosensory cortex in TgDyrk1A mice, an analysis was performed which estimated the average relative power between UP and DOWN states in three frequency bands of power spectrum density plots: beta (20-30 Hz), low gamma (30-60 Hz) and high gamma (60-90 Hz, Fig. 36). As in slow wave activity, no significant changes in any of the frequency bands were present in TgDyrk1A mice with respect to Wt mice, either in right (Fig. 36 E) or left hemisphere (Fig. 36 F), with mean values in controls and TgDyrk1A mice of 3.66 ± 2.68 vs 2.99 ± 1.22 in beta band, 4.57 ± 4.37 vs 3.62 ± 1.22 in low gamma and 13.89 ± 18.64 vs 8.60 ± 4.69 in high gamma band in the right hemisphere, and 4.11 ± 4.28 vs 3.21 ± 1.40 in beta band, 5.44 ± 7.20 vs 3.70 ± 1.49 in low gamma and 13.41 ± 19.00 vs 8.28 ± 3.48 in high gamma band in the left one (N=10 WT and 10 TgDyrk1A mice).

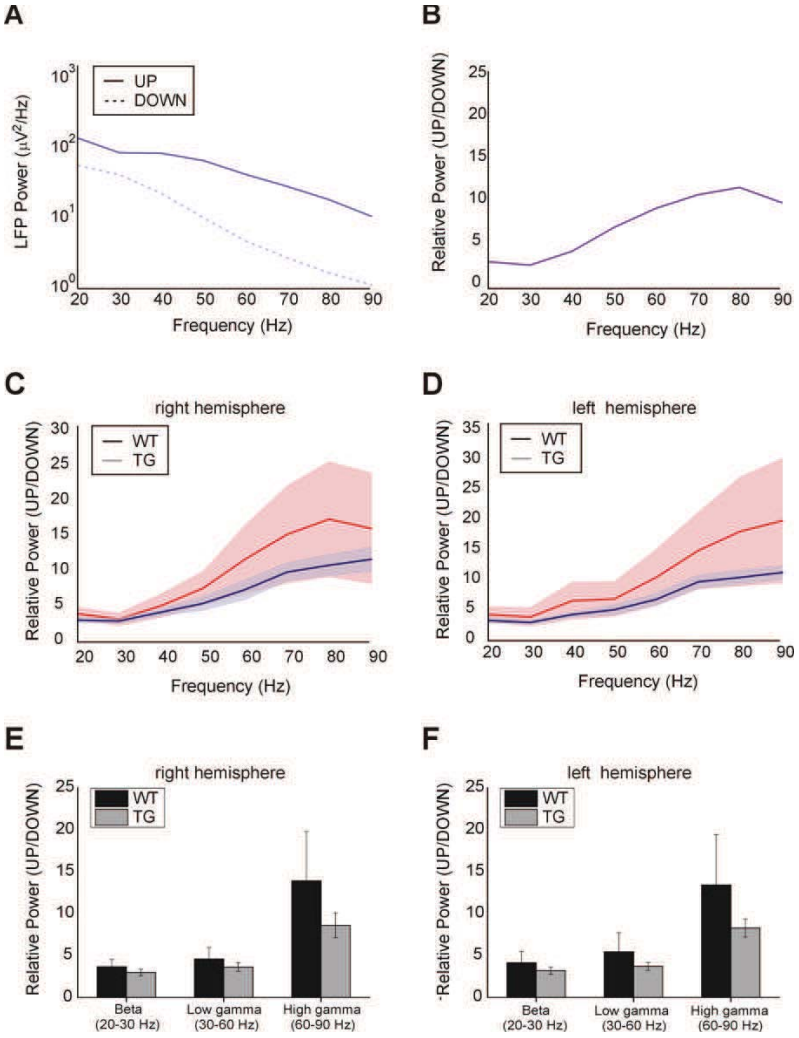

Figure 36. Characterization of fast rhythms in the somatosensory cortex of WT and TgDyrk1A mice.
A: Example of power spectrum density (p.s.d) plots calculated in the UP and DOWN state of a WT and a transgenic mouse. B: Example of relative power between UP and DOWN state from the p.s.d plots in a. C-D: Averages of relative power (UP/DOWN) of WT (black traces) and TgDyrk1A (grey traces) in either right (c) or left hemispheres (d). E-F: Averages of relative power in each frequency band in both genotypes in right (E) and left (F) hemispheres. N=10 WT and 10 TgDyrk1A mice in each hemisphere.

3.4.3. Inhibitory connectivity is down-regulated in somatosensory cortex of TgDyrk1A mice.

We next aimed to study the origin of increased inhibitory synaptic activity. For that purpose, we first studied the interneuron population proportion in somatosensory cortex. We initially carried out a general count of interneuronal population sub-classes, were we did not find any significant difference (Fig. 37 A), although parvalbumin-positive cells showed a nonsignifficant decrease. For that reason, we next explored layer-specific changes, aiming to the possibility of relate them to the observed increases in inhibitory synaptic activity observed 600-700 μm deep in the cortex (L4). Notably, we found a specific decrease of parvalbumin-positive interneurons in L4 ($P < 0.05$, Fig. 37 B) while in other layers –L3, L5- there were no changes in the number number of any subtype of interneurons. As there is no evidence of adult neurogenesis in the neocortex, we related those changes to neurogenesis during the neurodevelopment.

Then we aimed to analyze the proportion of excitatory and inhibitory contacts in the somatosensory network. We first studied the number of presynaptic terminals contacting neuronal populations in different layers (L3, L4, L5) by means of inmunofluorescence staining of Vglut and Vgat proteins, which are related to either excitatory and inhibitory presynaptic terminals, respectively. This analysis resulted in that none of both types of presynaptic contacts were significantly changed, although the ratio between them (Vglut/Vgat) showed a trend to be increased for excitatory terminals (Fig. 37 C). We next focused on the postsynaptic sites, where we analyzed PSD95 and gephyrin, which are scaffolding proteins in either excitatory or inhibitory post-synaptic terminals. Interestingly, the count of these post-synaptic sites showed a decreased number and size of gephyrin-positive terminals in L5 (number $P < 0.05$; size $P < 0.05$, Fig. 37 D, E). On the other hand, PSD95 remained unaltered although showing a trend to increase, which is in the same direction of the findings in the Vglut presynaptic contacts count (Fig. 37 I). Thus, the inhibitory post synaptic sites were decreased, highlighting a down-regulated inhibitory system on L5 of the somatosensory cortex of TgDyrk1A, and suggesting there might be compensatory mechanisms for the increased of inhibitory activity at the level of structural connectivity formation.

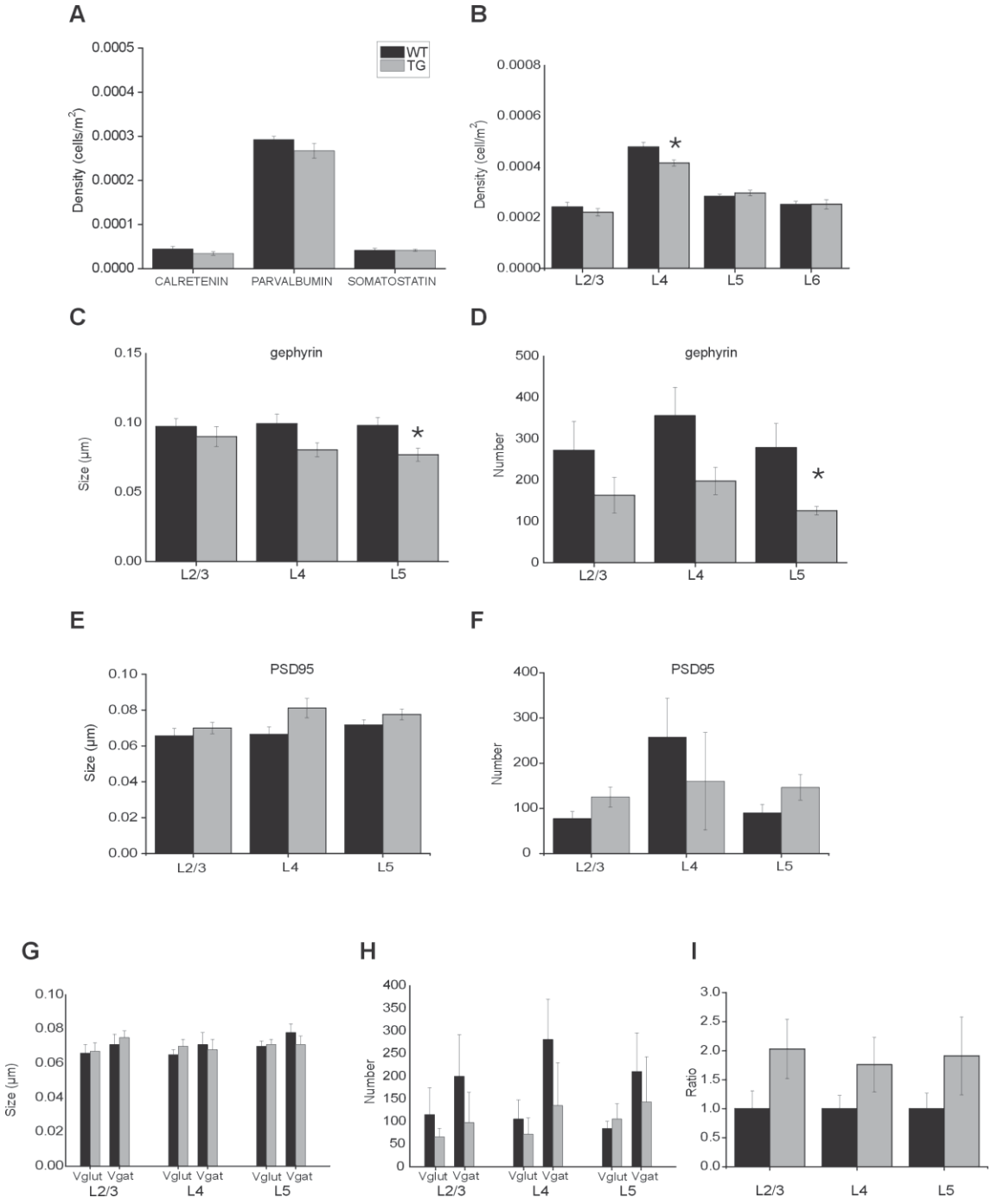

Figure 37. Histological analysis of the primary somatosensory cortex of WT and TgDyrk1A mice
A: Interneuron populations in the primary somatosensory cortex. B: parvalbumin-positive interneuron count across layers. C-D: Size and number of postsynaptic inhibitory terminals, stained for gephrin protein. E,F: Size and number of postsynaptic excitatory terminals, stained for PSD95 protein. G,H,I: Size, number and ratio of presynaptic excitatory and inhibitory terminals, stained for Vglut and Vgat proteins. *$P < 0.05$.

4. DISCUSSION

4.1. On the dependence of cortical oscillations on the persistent sodium current.

The aim of this work was to disclose the role of I_{NaP} on slow waves. In modeling studies, I_{NaP} has been proposed to be critical for UP state generation and maintenance along with pyramidal-to-pyramidal connectivity (Bazhenov et al. 2002; Hill and Tononi 2005). This idea was already proposed in the first experimental description of the mechanisms that govern of slow waves (Steriade et al. 1993c), while a critical role of synaptic excitatory recurrence in UP state generation and maintenance was proposed in (Sanchez-Vives and McCormick 2000). In the current study we find that the blockade of this current decreases the probability of occurrence of UP states, but those that occur are longer, presenting higher firing rates and higher power in beta and gamma frequencies. We discuss here whether these changes imply a role for I_{NaP} on the initiation of UP states, while it dampens high frequencies and contributes to regulating the duration of UP states.

The effect of phenytoin decreased the frequency of the oscillation and increased the variability of the wave cycles. Despite blocking with phenytoin at different concentrations (40, 60, 80 µM), slow waves did not disappear in all cases and UP states could still be generated. The EC50 for phenytoin is highly dependent on the preparation. EC50 has been found to be 34 µM for phenytoin in cell cultures (Chao and Alzheimer 1995), although other work in rat slices reported a EC50 value of 78 µM (Lampl et al. 1998) and cessation of firing was observed at 4 to 8 µM in mouse spinal cord neuronal cultures (McLean and Macdonald 1983). Importantly, blockade of persistent current shows a voltage dependency (Segal and Douglas 1997), where measures in Chao and Alzheimer were performed at -40 mV, and in Lampl et al were obtained with -60 mV pulses, being this a closer situation to the depolarized membrane potentials during UP states in our preparation (Sanchez-Vives and McCormick 2000). Note that in the studies of and Chao and Alzheimer and Lampl et al. the persistent current was totally blocked at concentrations of 100 µM or higher. Since the EC50 has not been calculated in our specific preparation, we cannot assure of the exact percentage of I_{NaP} that was blocked. We did not use higher phenytoin concentrations to avoid the unspecific blockade of sodium channels. The unspecific blockade of fast sodium channels, leading to the extinction of the activity in the network has been observed in several studies (Kuo and Bean 1994; Molnar and Erdo 1995; Segal and Douglas 1997; Stefani et al. 1997a). Our observed decrease in slow oscillations frequency during the I_{NaP} blockade would suggest a possible unspecific blockade of sodium currents. However, our next observation did not seem to support this decreased excitability.

Along with the decrease on slow frequency, we observed a significant elongation of UP states and increase in firing rate and high frequency generation. Those are all signs of increased excitability during UP states and do not seem to go along with an unspecific blockade of sodium channels. It does not rule out though that both effects may be concomitant, such that the increased excitability compensates for the sodium blockade. Nevertheless, despite that in their study neurons could not alternate between depolarized and hyperpolarized states as in our preparation, the effects in fast sodium currents observed in the study of Stefani and collaborators would be the closest case to our results at our knowledge. In our preparation, UP and DOWN states give rise to a bimodal distribution of membrane potential values with peaks at -68.7 and -61.2 in hyperpolarized and depolarized states respectively (Sanchez-Vives and McCormick 2000), while in the study of Stefani and collaborators the authors study the effect of phenytoin at depolarizing voltage pulses of -25 mV from an hyperpolarizing holding voltage of -70 mV. Unless the decreased frequency of UP states is due to the blockade of sodium channels, we can conclude that there seems to be a dependency of the slow oscillations on $I_{NaP,}$ being critical for the UP state occurrence at regular intervals and at physiological frequencies, but not for UP state maintenance.

A decrease in excitability following I_{NaP} blockade has been reported by other authors in recordings from neocortical neurons (Chao and Alzheimer 1995; Lampl et al. 1998; Segal and Douglas 1997). A decrease in induced excitability was found with I_{NaP} blockade with 20-200 µM phenytoin where firing rate of neurons decreased (Lampl et al. 1998). In studies of cultured spinal cord neurons started to lower the firing rate and bursting activity at 4 to 8 µM of phenytoin until become silent (McLean and Macdonald 1983) or in hippocampal cell cultures where single channel sodium openings were fewer in presence of 60 µM phenytoin (Segal and Douglas 1997). Previous work in ferrets showed reduced firing neurons when 120 µM of phenytoin was bath applied, and higher frequency bursts were present when I_{NaP} was potentiated with the sea anemone toxin ATX II (Brumberg et al. 2000).

How those general observations of decreased neuronal excitability with I_{NaP} blockade could be compatible with elongated UP states with higher firing rates? While most of the studies cited above consider the behaviour of isolated neurons, here we are dealing with an activity that spontaneously emerges from a network. Therefore, we should consider that the consequence of blocking I_{NaP} may be mediated by different mechanisms. On the one hand, the blockade of I_{NaP} reduced GABA release in synaptosomal preparations of both rats and humans (Kammerer et al. 2011b). Glutamate release is also diminished by phenytoin via the inhibition of presynaptic Ca^{2+} and Na^{+} influx in rats and Na^{+} in humans (Kammerer et al. 2011a), an effect that was previously suggested in rat cultured neurons (Stefani et al. 1997a). This suggests a scenario compatible with general disinhibition that may produce increased firing of

both pyramidal neurons and interneurons by means of reduced inhibitory function, leading to an increased excitability of the network. Previous studies showed that $GABA_A$ disinhibition led to the shortening of the UP states and increased firing rate during UP states in the same preparation (Sanchez-Vives et al. 2010) and in rat enthorinal cortex slices (Mann et al. 2009). However, blockade of slow inhibition mediated by $GABA_B$ conductance elongated evoked UP states. Interestingly, when both fast and slow inhibition were blocked, UP states were also elongated (Mann et al. 2009). This suggests that the effect of I_{NaP} blockade could be mediated through its impact on GABA and glutamate release, resulting in a general disinhibition of the network during UP states that would generate an excessive entrance in excitatory synaptic loops, thus elongating UP states with high firing rate.

The effect of I_{NaP} blockade could also be mediated through the activation of the sodium-dependent potassium current (Kaczmarek et al. 1982; Schwindt et al. 1989). This current has been proposed to be a critical mechanism for the termination of UP states (Compte et al. 2003; Sanchez-Vives and McCormick 2000). Both, I_{NaP} and sodium-dependent potassium currents are activated from the initiation of the UP state (see Figure 5 in Compte et al 2003). In this way, a mechanism of UP state termination such as the sodium-dependent current is activity-dependent. If the sodium entry is less through the blocked I_{NaP} channels, there would be lesser activation of the potassium current and therefore a more excitable network during the UP state. That would also explain the elongation of the UP states.

We observed an increase in fast beta-gamma oscillations within the UP state when I_{NaP} was blocked, a change that was correlated with an increase in the network firing rate. Disinhibition plus carbachol has been described to increase fast oscillations in other preparations (Traub et al. 2005; Xiao et al. 2012). These fast oscillations were also found to depend on I_{NaP} in this type of preparation (Oke et al. 2010), where the authors found an increase in power and a shift toward a lower peak frequency. On the other hand, phenytoin decreased 10 Hz resonance in thalamocortical slices of the mouse motor cortex (Castro-Alamancos et al. 2007), however in this case GABAergic synaptic transmission was blocked and it is not comparable. The organization of neuronal firing into fast rhythms is highly dependent on $GABA_A$ time course (Borgers and Kopell 2003; Compte et al. 2008; Traub et al. 2005). We could suggest that the blockade of I_{NaP} raises neuronal impedance, facilitating that neurons engage in the network rhythm. We could thus see I_{NaP} as damping the generation of high rhythms in physiological conditions and therefore playing a role as a modulator of them.

4.2. On the characterization of cortical oscillatory patterns in the mouse

This study is a systematic characterization of the emergent cortical activity in the mouse cerebral cortex during ketamine anesthesia. Continuous infusion of subcutaneous ketamine allowed us to obtain stable anesthesia levels reflected in a regular slow oscillatory frequency along the duration of the experiment (6–7 h). Under these conditions, UP and DOWN states were spontaneously generated by the cortical network, and nine parameters quantifying these were compared across visual, somatosensory, motor, and prefrontal cortices. We also explored the firing of individual neurons with respect to the network activity, wave propagation, and generation of beta and gamma synchronization during UP states. This information should be valuable for understanding cortical network emerging activity in the mouse model. It is also useful as a baseline of spontaneous activity generated in the mouse, allowing us to compare against experimental or genetic manipulations. Given that slow-wave sleep has a role in memory consolidation (Diekelmann and Born 2010; Marshall et al. 2006), it is also relevant to have a quantitative study as a point of reference for behavioral studies.

Slow oscillations recorded in primary sensory cortices (visual and somatosensory) and primary motor cortex were highly similar, and most of the differences found in this study were observed in prefrontal cortex. Interestingly, the mean frequency of occurrence was the same in all areas, coherent with a traveling wave across the cortical network. However, the regularity of this frequency (1/CV of the cycle) was maximal in prefrontal cortex. During slow-wave sleep in humans it has been described that waves preferentially travel from frontal to occipital areas (Massimini et al. 2004). Even though any point in the cortical network can potentially start a new wave, the frontal cortex appears to be the most common initiator of a new wave (Massimini et al. 2004). Our multiple recordings following an anteroposterior alignment also found a preferential propagation from front to back in the mouse (Fig. 22 A). The referential origin of the rhythmic activity in the prefrontal cortex could be due to some of the distinctive features of this area that are discussed next.

In this study we found that UP state duration, the DOWN-to-UP state transition slope, the maximum firing rate, and the CV of UP state duration were significantly different in prefrontal cortex compared with the other three studied regions. These parameters were not statistically different between motor, somatosensory, and visual cortices, a fact perhaps due to all of these being primary areas and thus sharing some structural properties. Not only did we find higher population firing rate in prefrontal cortex, but also single-unit recordings revealed higher firing rates in prefrontal cortex during UP states. Differences in the prefrontal cortical structure or in its connectivity with cortical and subcortical areas could translate functionally into some of the

functional differences detected here. Interestingly some of the differences observed in prefrontal cortex activity (higher population firing rate during UP states, faster DOWN-to-UP state transition) are compatible with a higher interneuronal connectivity and recurrence in this area. The transition from DOWN to UP state reflects the recruitment of the local network for the cortical activation. When the recruitment is faster, there is a steeper transition from DOWN to UP state, as is the case when inhibition is progressively decreased (Sanchez-Vives et al. 2010) or temperature increased (Reig et al. 2010b). That the prefrontal network activates faster than the primary cortices could be explained by different possible mechanisms: higher local connectivity and more efficient reverberation of activity, higher excitability, or less inhibition with respect to primary cortices. The finding of relatively more spinous neurons in prefrontal cortex in macaques and humans is suggestive of higher synaptic connectivity in this area (Elston 2001, 2000).

The DOWN-to-UP transition was then faster in prefrontal than in visual, somatosensory, and motor cortex. The transition from the UP to DOWN state, the silencing of the local network, was significantly faster in prefrontal and motor cortex than in visual and somatosensory cortex. This means that in prefrontal cortex, and partially in motor cortex, the initiation and termination of UP states is more synchronized than in primary sensory cortices. We have observed a correlation between the DOWN-to-UP and UP-to-DOWN slopes previously, for example, in situations with increasingly blocked inhibition (Sanchez-Vives et al. 2010) or with increasing temperatures (Reig et al. 2010b). The link between DOWN-to-UP and UP-to-DOWN slope is population firing rate during the UP state. A fast depolarizing recruitment of the network usually leads to a high firing rate in the population. A high firing rate efficiently recruits the potassium currents that could be terminating UP states and that are activity dependent (Compte et al. 2003; Cunningham et al. 2006; Sanchez-Vives et al. 2010). Indeed, prefrontal and motor cortexes have significantly higher firing rates than primary sensory cortices (Fig. 18 F). In our previous observations, fast DOWN-to-UP and UP-to-DOWN slopes were concurrent not only with higher firing rates during UP states but also with shorter UP states. However, we do not observe in our statistics illustrated in Fig. 3*B* any significant differences in UP state duration across areas.

Our data from prefrontal cortex are in agreement with the complementary hypothesis of an increased dynamical stability of UP states, for example due to a more effective recurrent GABAergic and glutamatergic synaptic coupling (Amit and Brunel 1997; Brunel and Wang 2001). Stronger stability means that changes in time of the firing rates are compelled by “restoring forces” toward the low and high firing states, making them more robust to intrinsic fluctuations in the firing activity. A strong local synaptic reverberation capable of making the high-firing regime a preferred dynamical

state of the network is a way to implement strong restoring forces. Such forces induce the neuronal activity to have highly nonlinear dynamics that could explain why both the drop from the UP states and the chain reaction eliciting high-frequency reverberation from DOWN to UP states are faster in prefrontal than in primary sensory cortices. This is an attractive scenario that suggests the existence along the cortex of a hierarchy of excitability and characteristics of the local circuitry: starting from "caudal" peripheral areas rapidly adapting to fast sensorial stimuli and motor actions and ending with the "rostral" associative areas whose integrative role has to be more stimulus independent, and hence more dependent on local dynamics (Badre and D'Esposito 2009; Braun and Mattia 2010).

The spontaneous activity of individual neurons in the UP states reflects the organization of the recurrent activity in the slow waves (Harris et al. 2010; Steriade et al. 1993c). While the majority of our recorded neurons fired during >90% of the UP states, most neurons participated in the active states sparsely, with <6 spikes per UP state in the majority of cases (see Results section). The PETHs extracted from the firing of individual neurons during slow oscillations showed two main patterns depending on the distribution of spikes of single neurons during the local UP state: those neurons that concentrated their firing at the beginning of the UP state (more common in prefrontal cortex neurons) and those with a peak of their firing rate toward the middle of the UP states (more frequent in motor and somatosensory neurons). Both patterns persisted regardless of UP state duration (Fig. 21, G–I). These firing patterns are comparable to those found in previous studies in rodents (Erchova et al. 2002; Luczak et al. 2007) and explain how firing of neurons collaborates in the generation of the MUA that is present in the UP states.

The slow oscillation is a wave that propagates along the cortical network (Amzica and Steriade 1995; Massimini et al. 2004; Sanchez-Vives and McCormick 2000; Volgushev et al. 2006). In this study we quantified the speed of propagation of the UP states in two cortical areas of the anesthetized mouse: visual and motor cortex. In both of these areas values varied between 6.4 and 74.4 mm/s, with an average value of 18.7 and 24 mm/s in visual and motor cortex, respectively, although the distributions of measures in the two areas are not significantly different (2-tailed Kolmogorov-Smirnov test, $P = 0.42$). Interestingly, such velocities are similar even when the linear arrays of electrodes used to estimate the speeds are placed in orthogonal directions in different cortical areas: sagittal orientation in motor cortex and in the coronal plane in visual cortex. Similar values (10–100 mm/s) were reported in the mouse with the use of voltage-sensitive dyes during the propagation of spontaneous depolarizations or UP states during quiet wakefulness (Petersen et al. 2003a). In multisite recordings from different cortical areas of the cat under ketamine-xylazine anesthesia, the speed of propagation of the slow waves also lies around 100 mm/s (Amzica and Steriade 1995).

However, the speed of propagation of slow waves during slow-wave sleep by highdensity EEG in humans is 1.2–7.0 m/s, the average speed being 2.7 m/s (Massimini et al. 2004). These higher speeds may reflect not only a slight overestimation due to obliquely propagating wave and volume conduction (Massimini et al. 2004) but also a higher speed of propagation in humans secondary to long-range connectivity. In contrast, the speed of propagation in ferret cortical slices is low, around 10 mm/s (Sanchez-Vives and McCormick 2000), given that it relies exclusively on local connectivity. In making the comparison between in vivo and in vitro recordings, the limits of our speed estimate should be considered: a linear array of electrodes was used, allowing an estimation of an upper limit of the velocity. Indeed, under the assumption of quasi-planar waves a correct estimate is available only when the direction of propagation is parallel to the orientation of the multielectrode array.

In the last part of our study, we describe the existence of high-frequency (beta and gamma) synchronization during UP states in different cortical areas of the mouse. Even when beta and gamma frequencies have been functionally associated to cognitive functions like attention (for a review see Wang 2010), these frequencies also emerge spontaneously during UP or activated states. This is the case not only during slow-wave sleep and anesthesia (Steriade et al. 1996) but also in cortical slices in vitro (Compte et al. 2008). We find that in the mouse, the power of beta, and particularly that of gamma, is strikingly higher in prefrontal than in motor and sensory primary cortical areas (Fig. 24). We can only speculate about the cellular or network basis for these differences, but they suggest that the prefrontal circuitry has specific properties to efficiently generate gamma rhythms. These properties may involve networks of fast-spiking inhibitory neurons or specific excitatory-inhibitory loops (Compte et al. 2008; Freund 2003; Hasenstaub et al. 2005; Paik et al. 2009; Tamas et al. 2000; Whittington et al. 1995). Gamma synchronization would then emerge out of the prefrontal circuit during UP states, probably being upregulated in the awake, attentive animal. This trend for the prefrontal circuit to generate beta and gamma frequencies matches its role as the origin of top-down influences during perceptual, attentive, or memory tasks (Engel et al. 2001; Gregoriou et al. 2009; Lachaux et al. 2008; Palva et al. 2010; Womelsdorf et al. 2007).

4.3. Comparison of prefrontal cortex oscillatory patterns and excitatory-inhibitory balance in wild type and TgDyrk1A mice

This study aimed to elucidate the role of the *DYRK1A* gene in the neurophysiological profile of Down syndrome (DS) individuals and to disclose the cortical network basis for the deficits of executive function in DS. In the current study we provide the first evidence that overexpression of the *DYRK1A* is sufficient to impair higher order neurocognitive functions including executive functions and to alter spontaneous rhythmic activity generated by the mPFC. These alterations include a decrease of network firing rate as well as decay in the power of gamma rhythms, changes compatible with a decreased network excitability.

DS individuals exhibit a wide spectrum of cognitive alterations among which deficits in various executive functions such as planning, inhibitory control and shifting and sustaining attention (Ball et al. 2010; Djonlagic et al. 2012; Molle and Born 2011; Rowe et al. 2006) are a major factor contributing to intellectual disability, and some of these features are present in DS trisomic mice (Belichenko et al. 2004; Best et al. 2007; Hanson et al. 2007; Kurt et al. 2000; Perez-Cremades et al. 2010). We here explored to the possible contribution of *DYRK1A* to these phenotypes, using two different behavioral paradigms: spontaneous alternation in a Y-maze, and problem solving in the puzzle box, a test revealing executive function that requires synchronization between prefrontal cortex and hippocampal activities(Ben Abdallah et al. 2011). TgDyrk1A mice showed impaired working memory, as revealed by a reduced percentage of alternation. Working memory is a complex cognitive system designed to retain information until a certain problem has been solved (Baddeley et al. 1986) which relies on the prefrontal cortex function.

In the puzzle box, TgDyrk1A mice showed a clear deficit in solving the problem that got worse with the increasing difficulty of the task. Decreased motivation is unlikely to explain the poor performance of TgDyrk1A mice since they were equal to their WT littermates in the easiest trial of the puzzle box. Thus, behavioral results suggested prefrontal deficits as consequence of Dyrk1A overdosage.

A major finding obtained in the emergent prefrontal activity of TgDyrk1A was a significant decrease of population firing rate during the periods of persistent activity of the slow oscillation. Further, the recruitment of the local network that leads to UP states was decreased in the TgDyrk1A with respect to the control while the variability of the UP states duration was increased. We also observed that the propagation of slow waves in the motor cortex was slowed down in the TgDyrk1A mice. Finally, the power of oscillations in the gamma range, an activity strongly associated to cognitive functions (Buzsaki and Wang 2012; Siegel et al. 2012; Whittington et al. 2011), was decreased. Each one of these changes points towards a more inhibited prefrontal

network (Sanchez-Vives et al. 2010). Futher, that spontaneous slow waves are altered during anesthesia suggests that there are probably equivalent differences in the structure of cortical activity during slow wave sleep, what could lead to failures in memory consolidation (Djonlagic et al. 2012; Molle and Born 2011). Indeed, polysomnographic studies in DS subjects, including children (Babiloni et al. 2009; Clausen et al. 1977; Velikova et al. 2011) showed changes in sleep patterns, as well as shown in other DS mouse models (Colas et al. 2004; Colas et al. 2008). A relevant finding in this study is the synchronization decrease in the high gamma frequency band of the local field potential in mPFC. Fast cortical oscillations in the beta-gamma range are involved in several cognitive processes in which the prefrontal cortex is implicated such as attention, decision making, learning and working memory (for a review see Wang 2010). High gamma frequency band (60-90 Hz) was prominently decreased in the prefrontal cortex, which could underlie the impaired performance of frontal-dependent behavioral tasks detected in TgDyrk1A mice (Fig. 1).

Alterations in oscillatory patterns have also been observed by means of EEG recordings in DS humans (Babiloni et al. 2009; Clausen et al. 1977; Velikova et al. 2011). Several authors (Murata et al. 1994; Velikova et al. 2011) have detected shifts toward lower frequencies in mean EEG signals up to the beta band, as well as decreased low beta (13-18 Hz) oscillatory activity in adults and aged DS individuals. Babiloni et al. found decreased beta and gamma waves in DS adolescents, even correlating this frequency change to cognitive psychometric measurements (Babiloni et al. 2009). Nevertheless, none of them referred to frequency bands beyond 45 Hz and they focused in awake states. Thus, the present study represents the first evidence of a decreased generation of gamma power, accompanied by electrophysiological signs of a decreased excitability in the cortex.

According to previous work on travelling waves, the frontal cortex is the cortical area where slow waves preferentially originate, showing major focuses of wave initiation in humans (Massimini et al. 2004; Mohajerani et al. 2010). This is compatible to the results from mice, where the preferred direction of propagation is from frontal to posterior areas (Ruiz-Mejias et al. 2011; Stroh et al. 2013). We did not detect differences in the propagation patterns in the prefrontal cortex between control and TgDyrk1A mice. In both genotypes an equal fraction of backward and forward propagations was observed in the prefrontal cortex, while in motor cortex propagation was preferentially from front to back. This is highly suggestive that the slow waves orginate most often in local prefrontal region centered around the position in mPFC of our electrodes. On the other hand, in the nearby motor cortex slower propagation was found in transgenic mice. Reduced speed can be due to a stronger inhibition which acts as a brake on wave propagation speed (Sanchez-Vives et al. 2010). Such brake would imply a progressive deceleration of the wavefront propagation across a less

excitable cortical tissue, yielding to measure slower speeds at longer distances from the place where waves originate. This would explain why in mPFC no speed differences were apparent: simply because too close or part of the neural circuitry underlying wave onset.

Post-mortem studies in individuals with DS reveal a reduction in the number of calbindin D-28k and parvalbumin interneurons in elderly individuals (Kobayashi et al. 1990) as well as a reduction in the number of interneurons in layer II and IV (Ross et al. 1984). In DS models a number of studies have pointed out to an unbalanced excitation and inhibition in the hippocampus (Belichenko et al. 2004; Best et al. 2012; Hanson et al. 2007; Kurt et al. 2000; Perez-Cremades et al. 2010) and the possibility of reverting this unbalance as a therapeutic strategy (Begenisic et al. 2011; Braudeau et al. 2011; Fernandez et al. 2007). Ts65Dn mice display a reduction in the number of calbindin D-28k-expressing neurons but not calretinin- and parvalbumin-expressing interneurons in the hippocampus (Hunter et al. 2004), and an increment of calretinin-inmunoreactive cells among them the ones with bipolar morphology in the somatosensory cortex (Perez-Cremades et al. 2010), but the effect of the trisomy in the prefrontal cortex is totally unknown. In our study, TgDyrk1A mice did not show differences in the number of inhibitory interneurons in the prefrontal cortex. However, the proportion of excitatory *versus* inhibitory presynaptic puncta (Vglut1/Vgat ratio) was significantly increased due to the reduced number of presynaptic inhibitory vesicles in parvalbumin interneurons, which represent 80% of cortical interneurons. The net effect would be a reduced inhibitory input to parvalbumin interneurons (PV, Fig. S1) which is compatible with a more inhibited network, so PV neurons would inhibit more efficiently pyramidal neurons, in agreement with our functional findings. In turn, the reduced connectivity over PV cells would produce a lack of capability of interneurons to synchronize network activity, a relevant role of inhibitory-inhibitory synapses (Borgers and Kopell 2003; Compte et al. 2008), and also perisomatic inhibition is essential for gamma oscillations (reviewed in Buzsaki and Wang 2012; Whittington et al. 2011)). We propose that disinhibition of parvalbumin positive neurons would result in an overinhibited functional network. The resulting aberrant spontaneous gamma oscillations suggest that the normal upregulation of gamma waves may be impaired when constructing cognitive assemblies through rhythmic activity in prefrontal-dependent tasks (Fitzgibbon et al. 2004; Siegel et al. 2012). The results described above support our hypothesis that overexpression of *DYRK1A* gene alters the balance of excitation and inhibition towards a more inhibited network. Understanding the function of *DYRK1A* in the development of cortical circuits in the mouse may contribute to elucidate some of the pathophysiological mechanisms underlying DS.

4.4. Comparison of somatosensory cortex oscillatory patterns and excitatory-inhibitory balance in wild type and TgDyrk1A mice

When exploring the functional effects of *DYRK1A* overdosage, we found an increased inhibitory synaptic transmission in the somatosensory cortex. In spite of that, we did not see any change in oscillatory activity in our analysis. In addition, our observations showed that *DYRK1A* overexpression directly affects inhibitory system, either altering neurogenesis of interneurons or by decreasing inhibitory connectivity, which may be understood as a network compensatory mechanism. Dendritic arbor morphology and number of spines are altered in cortical pyramidal neurons in this mouse model (Martinez de Lagran et al. 2012), suggesting alterations in the excitatory system. Here is shown evidence of alterations in the inhibitory system, which may provide an evidence of a homeostatic regulatory effect on synaptic function that is traduced by the reorganization of network connectivity elements such as inhibitory post-synaptic contacts. Thus, while alterations in the excitatory-inhibitory balance may produce an altered function, further modifications of this relationship at other levels that may appear at different times within life, and can be summated to produce a compensated effect that maintains a cortical function in a regulated homeostatic equilibrium.

A major result in this study relies on the increased inhibitory synaptic activity, mediated by $GABA_A$ receptor-associated conductances (Agmon and Connors 1991; Gil and Amitai 1996; Silberberg and Markram 2007). Our results of thalamocortical stimulation show that dysinaptic inhibition is increased in the L4 of somatosensory cortex of TgDyrk1A mice. However, the histological analysis revealed that either the number of PV neurons and synaptic contacts are decreased in L4. For that reason, further experiments wil need to be carried out in order to address this issue.

Nevertheless, the present results may show that the somatosensory cortex is presenting compensatory changes in order to counterbalance the alterations due to the overexpression of *DYRK1A* that may be expressed as homeostatic structural mechanisms. Network structural plasticity has been reported in transgenic mice (Jung et al. 2011; Ventura-Clapier et al. 2004), and also in other species such as flies, where there was evidence of structural compensatory mechanisms (Tripodi et al. 2008; Yuan et al. 2011). In addition, some studies report the importance between the balance of a brain disorder such as neurodegeneration and compensatory mechanisms during life (Berchtold et al. 2008; Kleen et al. 2011), which will set the final phenotype at a given age. Here we show a homeostatic regulation of excitability which is developed within lifetime, resulting in a balanced excitability that remains at physiological levels despite the alterations in the circuitry.

4.5. GENERAL DISCUSSION

From the work of this Thesis, we demonstrated some mechanistic aspects that control the emergence of rhythmic patterns from cortical circuits, with a striking role on the mechanisms which control excitability or cortical connectivity that underlies oscillations. Formerly, this study presents de dependence of Slow and fast rhythms on an intrinsic mechanism of neurons that governs cortical oscillations which is the persistent sodium current. Secondly, here is presented the role of cortical excitability in the expression of those rhythms across different cortical areas. And finally, this study shows the changes in cortical network function in a model of Down syndrome by means of analyzing oscillatory activity, as this represents a network activity and reflects the altered cellular and connectivity elements which are critical for the expression of cortical rhythms. These findings can all be understood within frame of altered balance between excitation and inhibition, and in the following sections a discussion about those issues is presented.

4.5.1. Comparison of the expression of slow and fast rhythms between cortical networks regarding network components and connectivity in vivo*.*

First, differences of expression of slow and fast oscillations between areas can be explained by differential interneuronal composition (Fig. 31 A for prefrontal cortex and 37 A for somatosensory cortex). The proportion of each subclass of interneurons, especially parvalbumin-positive cells, may be a first key to understand the emergence of fast rhythms with special features depending on the area (somatosensory cortex shows a density of ~3.10^{-4} vs ~2.10^{-4} cells/μm^2 in prefrontal cortex). Different density in interneuron population may mean different degree of excitability of the network, if we take into account its connectivity. So, differences in excitatory and inhibitory connections (115 *vs* 185 excitatory mean connections per field in somatosensory and prefrontal cortex, respectively, and 200 vs 270 of mean inhibitory connections, Fig. 38) would explain a different degree of excitability, as it is shown in somatosensory and prefrontal cortex. Thus, somatosensory cortex may have a more inhibited network, less excitability and a reduced network firing rate when compared to prefrontal cortex. As is stated in the beginning of the introduction, prefrontal cortex shows in general a special connectivity when compared to primary cortices that can be illustrated by an increased number of spines (Elston 2001). These findings may help to explain why slow and fast oscillations in deep layers of prefrontal cortex are differentially expressed from the ones in deep layers of somatosensory cortex, in terms of network excitability, as shown in the results section 3.2.

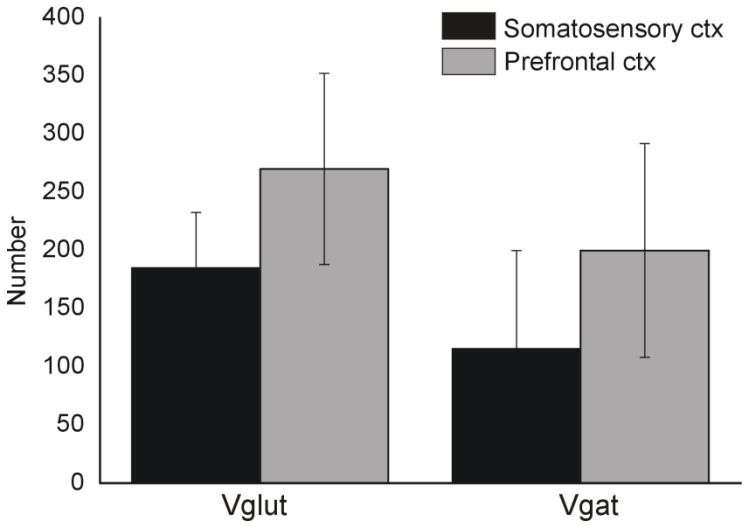

Figure 38. Comparison of the number of L5 synaptic contacts in somatosensory and prefrontal cortex.

Section 3.3 of the results section show the effect of changes in connectivity on fast oscillations *in vivo,* and how these changes affect directly to cognitive function. A striking issue is that fast oscillations are differently expressed across areas, as well as in altered cortical networks such as in TgDyrk1A mice. In cortical networks of TgDyrk1A mice slow and fast oscillations present changes with respect to controls. The connectivity underlying those emerging rhythms is altered in prefrontal cortex at different levels in terms of network excitability. In prefrontal cortex, inhibitory terminals are decreased, but we found it to affect specifically to the parvalbumin-positive interneuron population, where we counted synapses contacting somas, which may drive the network to a more inhibited state. With these results, it may be feasible that the changes in fast oscillations may be explained by the alterations on perisomatic inhibition over parvalbumin-positive cells in the prefrontal cortex of TgDyrk1A mice. Despite of a missing measure of direct synaptic function, these results are undoubtedly in tight relationship with the changes in network firing rate: if the overall effect of structural connectivity connectivity is to reduce network synaptic activity, network firing rate may also be decreased. Both phenomena account for the alterations in fast rhythms that emerge from altered cortical circuits, which may be directly related to cognitive function, as shown by prefrontal-dependent behavioral tasks.

On the other hand, somatosensory cortex shows a decreased number of parvalbumin-positive interneurons in L4 and also both decreased size and number of postsynaptic inhibitory terminals in L4 and 5, while cortical inhibitory synaptic function is shown to be increased in L4. Surprisingly, the network may find the way to compensate the effects and to present no changes in slow and fast rhythms in the

output L5. Because both changes in network connectivity and functional inhibitory synaptic activity are present in somatosensory cortex, here is proposed that the inexistence of changes in the Slow and fast rhythms in L5 may be explained by the presence of a homeostatic regulatory process which allows the network to provide optimal function despite the alterations, as explained in the discussion section 4.4.

Undoubtedly, future work for assessing alterations in fast rhythms that may underlie cognitive deficits will go in the direction of obtaining evidence of those alterations in the awake state, either in open field mazes or while performing prefrontal-dependent cognitive tasks.

4.5.2. Regarding excitatory-inhibitory balance and its alteration in the cortical network.

The *in vitro* study presented here showed the dependence of cortical oscillatory patterns on intrinsic mechanisms such as the persistent sodium current. Here is proposed that a role for that conductance may be to prevent excessive excitatory reverberation with increased network excitability. This is shown to be dependent on synaptic activity of the network, accounting for a network mechanism in regulating excitability. From this point of view, the role of persistent sodium current may be to maintain a stable balance between excitation and inhibition, as this delicate equilibrium is what maintains the physiological slow waves.

In addition to the regulation of slow waves, the persistent sodium current also dampens other cortical oscillatory rhythms, such as fast oscillations, controlling the expression of both slow and fast rhythms.

Another aspect which stands out about the expression of a balanced network is the development of slow oscillations in physiological and altered cortical networks *in vivo.* The results of this Thesis show that in physiological -wild type- networks *in vivo* slow waves and fast waves are differentially expressed across cortical areas. Also, the finding that slow and fast waves are altered in the prefrontal cortical network of a Down syndrome model by result of both altered connectivity and perisomatic inhibition highlights the striking role of those network features in the emergence of oscillatory activity in physiologic or altered cortical networks (Freund and Katona 2007; Molaee-Ardekani et al. 2010, Fig. 39).

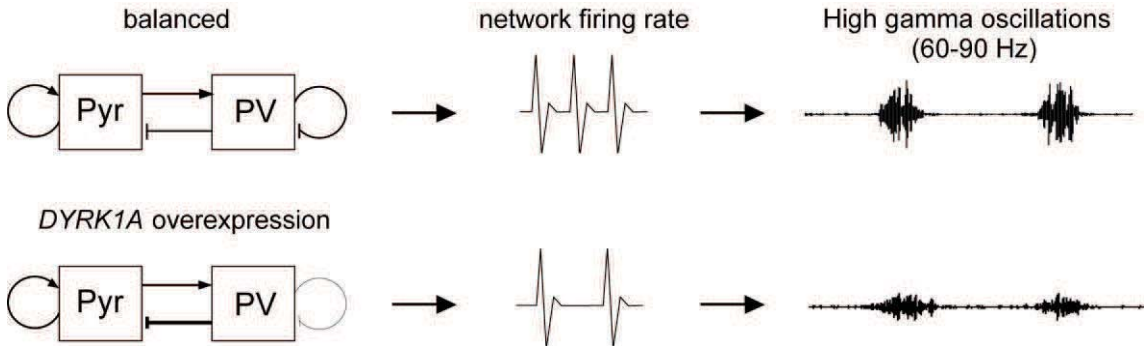

Figure 39. Scheme of a summary of DYRK1A overexpression effect in prefrontal network.

The particularities found in different areas in the same animal imply that each network may express this balance according to its function, and that alterations in the overall gene expression in the cortex can affect different cortical areas at different levels and independently. Thus, a balanced network is crucial for the expression of cortical patterns and prevents aberrant oscillatory activity, which may lead to incorrect function of slow and fast rhythms for the proposed role of these oscillatory patterns during awake and sleep cognitive performance.

4.5.3. Perspectives on therapeutical treatments and the modulation of cortical patterns for cognitive improvement.

In this Thesis is proposed that changes in cortical oscillatory patterns may result from alterations in the underlying circuitry that lead to cognitive disability (Molle and Born 2011; Uhlhaas and Singer 2010; Verret et al. 2012). Restoring the expression of these cortical rhythms to a physiological level may be a key to improve cognitive function in humans with altered expression of those rhythms in several brain disorders, such as Down syndrome, Alzheimer's disease or schizophrenia.

In this direction, brain stimulation approaches have been undertaken to address this question, which include the use of neuroprosthetic devices for stimulating neuronal populations, or different types of external brain stimulation including Transcranial Magnetic Stimulation (TMS) in prefrontal areas. An interesting approach already tested in rodents and monkeys comes from a collaboration between R.E. Hampson and T.W. Berger -and others- in the USA, where they used a neuroprosthesis to recover cognitive function of damaged prefrontal cortex (Berger et al. 2011; Berger et al. 2012; Hampson et al. 2012a; Hampson et al. 2012b; Hampson et al. 2012c).

TMS has shown recognisable benefits for cognitive function in addition to be a non-invasive technique. Some of such improvements rely on language performance in Alzheimer's disease (Cotelli et al. 2011), treatment of resistant depression (Pallanti et al. 2012), improving memory impairment (see Manenti et al. 2012 for a review) or restoring cognitive function and gamma oscillations in schizophrenia (Farzan et al. 2012). This last study resulted of special interest as they recorded EEG oscillatory patterns while stimulations, and observed a concomitant modulation of gamma oscillations (30-50 Hz) which led to correct cognitive performance. Furthermore, TMS has been shown to improve cognitive performance in healthy adult or aging subjects (reviewed in Guse et al. 2010; Kim et al. 2012), extending the cognitive improvement beyond brain disorders. As a general rule in TMS experiments, a particular human prefrontal cortex area, which is the Dorso-Lateral Prefrontal Cortex (DLPFC), has resulted to be a critical target for the improvement of cognitive function.

Despite all that uses of stimulation, there are no studies about cognitive improvement with means of TSM or any kind of brain stimulation in DS humans, but further to conventional pharmacologic approaches, new therapeutic treatments are under investigation in DS. One of those treatments, which is already tested in animal models, is the use of viral infections which carry engineered genetic material to compensate over-expression of candidate genes involved in cognitive function, such as *DYRK1A* (Fillat et al. 2012; Ortiz-Abalia et al. 2008). Very recently, a group in the USA also published a promising therapeutic approach, in where the authors take advantage of the expression of the *XIST* gene in order to silence the extra chromosome 21 in cell cultures, as it naturally happens with the extra chromosome X in mammal females (Jiang et al., 2013). Another promising therapeutic approach tested in animals is the use of polyphenols, which are present in green tea leaves, for restoring *DYRK1A* expression levels and cognitive function (Guedj et al. 2009). Lastly, a new pharmacological approach consists on the reduction of DYRK1A kinase activity with specific inhibitors, such as harmine, in trisomic mice (Mazur-Kolecka et al. 2012).

Given that technology will be able to miniaturize and simplify the devices for a personal use, it would be feasible that in the nearby future everyone had a TMS device at home and would self-administrate brain stimulation protocols for improving their cognitive function, either being healthy or affected by a brain disorder. Or better than that, health centres may administer TSM as a conventional treatment under medical supervision, once its mechanisms of action are disclosed.

CONCLUSIONS

Conclusions of Objective 1, about the role of I_{Nap} in slow oscillations

1. The persistent sodium current is critical for the correct development of slow oscillations, and is necessary for the generation of UP states at a physiological frequency and duration, but not for the maintenance of the UP state plateau.

2. Paradoxically, the blockade of this conductance produces an increase of network firing rate and synchronization of beta-gamma frequencies, suggesting an increase in excitability during UP states.

3. The persistent sodium current regulates the network level of excitability that generate and maintain UP states.

Conclusions of Objective 2, about the baseline of cortical oscillatory activity in WT mice

4. The prefrontal cortex shows network firing properties that are unique and different from the other analyzed primary cortical areas, being an area with higher excitability. In addition, it shows an increased regularity in the duration of UP states.

5. The prefrontal cortex generates oscillatory patterns in the range of beta-gamma frequencies (15-90 Hz) with an increased power compared to the other analyzed primary cortical areas, compatible with its role in top-down signalling and where beta-gamma oscillations would up-regulate for constructing cognitive assemblies.

6. Slow oscillations propagate mainly from frontal areas to posterior zones, and travel through motor cortex at speeds between 6 and 75 mm/s, although they contain more complex patterns of propagation,

Conclusions of Objective 3, about the alterations in cortical oscillatory activity in TgDyrk1A mice

7. The TgDyrk1A mice show executive function deficit associated to prefrontal cortex in behavioural tasks that involve problem solving.

8. The network firing rate and the Upward transitions are decreased in prefrontal cortex in TgDyrk1A mice. This indicates that prefrontal cortex in TgDyrk1A mice is less excitable.

9. Fast gamma frequencies in the prefrontal cortex are decreased in TgDyrk1A mice. In addition, the power of gamma frequencies in each low (30-60 Hz) and high bands (60-90 Hz) are uncorrelated to the peak of network firing rate in the prefrontal cortex of TgDyrk1A mice.

10. There is a decrease in the speed of propagation in frontal cortex in TgDyrk1A mice as long as waves move away from prefrontal cortex. This and the previous two conclusions are compatible with a more inhibited network and would suppose a possible explanation for the cognitive deficits observed in the behaviour.

11. The decrease in excitability and in gamma power in prefrontal cortex of TgDyrk1A mice can be explained by an observed decrease in perisomatic inhibitory connectivity over interneurons that would produce an increase of network inhibition.

12. Synaptic inhibition is increased in somatosensory of TgDyrk1A cortex evoked by result of thalamic stimulation, while excitatory synaptic transmission remains unaltered. This demonstrates alterations of the balance between excitation and inhibition in L4 in this model.

13. The emergent oscillatory pattens of somatosensory cortex of TgDyrk1A mice remain unaltered. This suggests the existence of compensatory mechanisms relative to homeostatic processes.

Bibliography

Abbeduto L, Warren SF, and Conners FA. Language development in Down syndrome: from the prelinguistic period to the acquisition of literacy. *Ment Retard Dev Disabil Res Rev* 13: 247-261, 2007.

Acuna MA, Perez-Nunez R, Noriega J, Cardenas AM, Bacigalupo J, Delgado R, Arriagada C, Segura-Aguilar J, Caviedes R, and Caviedes P. Altered voltage dependent calcium currents in a neuronal cell line derived from the cerebral cortex of a trisomy 16 fetal mouse, an animal model of Down syndrome. *Neurotox Res* 22: 59-68, 2012.

Aghajanian GK and Rasmussen K. Intracellular studies in the facial nucleus illustrating a simple new method for obtaining viable motoneurons in adult rat brain slices. In: *Synapse*, 1989, p. 331-338.

Agmon A and Connors BW. Thalamocortical responses of mouse somatosensory (barrel) cortex in vitro. In: *Neuroscience*. England, 1991, p. 365-379.

Ahn KJ, Jeong HK, Choi HS, Ryoo SR, Kim YJ, Goo JS, Choi SY, Han JS, Ha I, and Song WJ. DYRK1A BAC transgenic mice show altered synaptic plasticity with learning and memory defects. *Neurobiol Dis* 22: 463-472, 2006.

Altafaj X, Dierssen M, Baamonde C, Marti E, Visa J, Guimera J, Oset M, Gonzalez JR, Florez J, Fillat C, and Estivill X. Neurodevelopmental delay, motor abnormalities and cognitive deficits in transgenic mice overexpressing Dyrk1A (minibrain), a murine model of Down's syndrome. *Hum Mol Genet* 10: 1915-1923, 2001.

Altafaj X, Ortiz-Abalia J, Fernandez M, Potier MC, Laffaire J, Andreu N, Dierssen M, Gonzalez-Garcia C, Cena V, Marti E, and Fillat C. Increased NR2A expression and prolonged decay of NMDA-induced calcium transient in cerebellum of TgDyrk1A mice, a mouse model of Down syndrome. *Neurobiol Dis* 32: 377-384, 2008.

Alzheimer C, Schwindt PC, and Crill WE. Modal gating of Na+ channels as a mechanism of persistent Na+ current in pyramidal neurons from rat and cat sensorimotor cortex. *J Neurosci* 13: 660-673, 1993.

Amit DJ and Brunel N. Model of global spontaneous activity and local structured activity during delay periods in the cerebral cortex. *Cereb Cortex* 7: 237-252, 1997.

Amzica F and Steriade M. Disconnection of intracortical synaptic linkages disrupts synchronization of a slow oscillation. *J Neurosci* 15: 4658-4677, 1995a.

Amzica F and Steriade M. Short- and long-range neuronal synchronization of the slow (< 1 Hz) cortical oscillation. *J Neurophysiol* 73: 20-38, 1995b.

Aracri P, Colombo E, Mantegazza M, Scalmani P, Curia G, Avanzini G, and Franceschetti S. Layer-specific properties of the persistent sodium current in sensorimotor cortex. *J Neurophysiol* 95: 3460-3468, 2006.

Arriagada C, Astorga C, Atwater I, Rojas E, Mears D, Caviedes R, and Caviedes P. Endosomal abnormalities related to amyloid precursor protein in cholesterol treated cerebral cortex neuronal cells derived from trisomy 16 mice, an animal model of Down syndrome. *Neurosci Lett* 423: 172-177, 2007.

Babiloni C, Albertini G, Onorati P, Vecchio F, Buffo P, Sara M, Condoluci C, Pistoia F, Carducci F, and Rossini PM. Inter-hemispheric functional coupling of eyes-closed resting EEG rhythms in adolescents with Down syndrome. *Clin Neurophysiol* 120: 1619-1627, 2009.

Baddeley A, Logie R, Bressi S, Della Sala S, and Spinnler H. Dementia and working memory. *Q J Exp Psychol A* 38: 603-618, 1986.

Badre D and D'Esposito M. Is the rostro-caudal axis of the frontal lobe hierarchical? *Nat Rev Neurosci* 10: 659-669, 2009.

Bal T and McCormick DA. Mechanisms of oscillatory activity in guinea-pig nucleus reticularis thalami in vitro: a mammalian pacemaker. *J Physiol* 468: 669-691, 1993.

Ball SL, Holland AJ, Watson PC, and Huppert FA. Theoretical exploration of the neural bases of behavioural disinhibition, apathy and executive dysfunction in preclinical Alzheimer's disease in people with Down's syndrome: potential involvement of multiple frontal-subcortical neuronal circuits. *J Intellect Disabil Res* 54: 320-336, 2010.

Barnet AB and Lodge A. Click evoked EEG responses in normal and developmentally retarded infants. *Nature* 214: 252-255, 1967.

Barnet AB, Ohlrich ES, and Shanks BL. EEG evoked responses to repetitive auditory stimulation in normal and Down's syndrome infants. *Dev Med Child Neurol* 13: 321-329, 1971.

Bartos M, Vida I, and Jonas P. Synaptic mechanisms of synchronized gamma oscillations in inhibitory interneuron networks. *Nat Rev Neurosci* 8: 45-56, 2007.

Bazhenov M, Timofeev I, Steriade M, and Sejnowski TJ. Model of thalamocortical slow-wave sleep oscillations and transitions to activated States. *J Neurosci* 22: 8691-8704, 2002.

Becker L, Mito T, Takashima S, and Onodera K. Growth and development of the brain in Down syndrome. *Prog Clin Biol Res* 373: 133-152, 1991.

Begenisic T, Spolidoro M, Braschi C, Baroncelli L, Milanese M, Pietra G, Fabbri ME, Bonanno G, Cioni G, Maffei L, and Sale A. Environmental enrichment decreases GABAergic inhibition and improves cognitive abilities, synaptic plasticity, and visual functions in a mouse model of Down syndrome. *Front Cell Neurosci* 5: 29, 2011.

Belichenko NP, Belichenko PV, Kleschevnikov AM, Salehi A, Reeves RH, and Mobley WC. The "Down syndrome critical region" is sufficient in the mouse model to confer behavioral, neurophysiological, and synaptic phenotypes characteristic of Down syndrome. *J Neurosci* 29: 5938-5948, 2009.

Belichenko PV, Masliah E, Kleschevnikov AM, Villar AJ, Epstein CJ, Salehi A, and Mobley WC. Synaptic structural abnormalities in the Ts65Dn mouse model of Down Syndrome. *J Comp Neurol* 480: 281-298, 2004.

Beltramo R, D'Urso G, Dal Maschio M, Farisello P, Bovetti S, Clovis Y, Lassi G, Tucci V, De Pietri Tonelli D, and Fellin T. Layer-specific excitatory circuits differentially control recurrent network dynamics in the neocortex. *Nat Neurosci* 16: 227-234, 2013.

Ben Abdallah NM, Fuss J, Trusel M, Galsworthy MJ, Bobsin K, Colacicco G, Deacon RM, Riva MA, Kellendonk C, Sprengel R, Lipp HP, and Gass P. The puzzle box as a simple and efficient behavioral test for exploring impairments of general cognition and executive functions in mouse models of schizophrenia. *Exp Neurol* 227: 42-52, 2011.

Benchenane K, Tiesinga PH, and Battaglia FP. Oscillations in the prefrontal cortex: a gateway to memory and attention. *Curr Opin Neurobiol* 21: 475-485, 2011.

Benita JM, Guillamon A, Deco G, and Sanchez-Vives MV. Synaptic depression and slow oscillatory activity in a biophysical network model of the cerebral cortex. *Front Comput Neurosci* 6: 64, 2012.

Berchtold NC, Cribbs DH, Coleman PD, Rogers J, Head E, Kim R, Beach T, Miller C, Troncoso J, Trojanowski JQ, Zielke HR, and Cotman CW. Gene expression changes in the course of normal brain aging are sexually dimorphic. *Proc Natl Acad Sci U S A* 105: 15605-15610, 2008.

Berger TW, Hampson RE, Song D, Goonawardena A, Marmarelis VZ, and Deadwyler SA. A cortical neural prosThesis for restoring and enhancing memory. *J Neural Eng* 8: 046017, 2011.

Berger TW, Song D, Chan RH, Marmarelis VZ, LaCoss J, Wills J, Hampson RE, Deadwyler SA, and Granacki JJ. A hippocampal cognitive prosThesis: multi-input, multi-output nonlinear modeling and VLSI implementation. *IEEE Trans Neural Syst Rehabil Eng* 20: 198-211, 2012.

Best J, Park C, Terman D, and Wilson C. Transitions between irregular and rhythmic firing patterns in excitatory-inhibitory neuronal networks. *J Comput Neurosci* 23: 217-235, 2007.

Best TK, Cramer NP, Chakrabarti L, Haydar TF, and Galdzicki Z. Dysfunctional hippocampal inhibition in the Ts65Dn mouse model of Down syndrome. *Exp Neurol* 233: 749-757, 2012.

Bigum HB, Dustman RE, and Beck EC. Visual and somato-sensory evoked responses from mongoloid and normal children. *Electroencephalogr Clin Neurophysiol* 28: 576-585, 1970.

Blundell J, Tabuchi K, Bolliger MF, Blaiss CA, Brose N, Liu X, Sudhof TC, and Powell CM. Increased anxiety-like behavior in mice lacking the inhibitory synapse cell adhesion molecule neuroligin 2. *Genes Brain Behav* 8: 114-126, 2009.

Borg J and Chereul E. Differential MRI patterns of brain atrophy in double or single transgenic mice for APP and/or SOD. *J Neurosci Res* 86: 3275-3284, 2008.

Borgers C and Kopell N. Synchronization in networks of excitatory and inhibitory neurons with sparse, random connectivity. *Neural Comput* 15: 509-538, 2003.

Borselli L and Sferlazzo R. [Considerations on the Problem of Epilepsy in Mongolism]. *Riv Clin Pediatr* 72: 45-53, 1963.

Boutajangout A, Quartermain D, and Sigurdsson EM. Immunotherapy targeting pathological tau prevents cognitive decline in a new tangle mouse model. *J Neurosci* 30: 16559-16566, 2010.

Bouyer JJ, Montaron MF, and Rougeul A. Fast fronto-parietal rhythms during combined focused attentive behaviour and immobility in cat: cortical and thalamic localizations. *Electroencephalogr Clin Neurophysiol* 51: 244-252, 1981.

Bouyer JJ, Montaron MF, Rougeul A, and Buser P. [Parietal electrocortical rhythms in the cat: their relation to a behavior of focused attention and possible mesencephalic control through a dopaminergic pathway]. *C R Seances Acad Sci D* 291: 779-783, 1980.

Branchi I, Bichler Z, Minghetti L, Delabar JM, Malchiodi-Albedi F, Gonzalez MC, Chettouh Z, Nicolini A, Chabert C, Smith DJ, Rubin EM, Migliore-Samour D, and Alleva E. Transgenic mouse in vivo library of human Down syndrome critical region 1: association between DYRK1A overexpression, brain development abnormalities, and cell cycle protein alteration. *J Neuropathol Exp Neurol* 63: 429-440, 2004.

Braudeau J, Dauphinot L, Duchon A, Loistron A, Dodd RH, Herault Y, Delatour B, and Potier MC. Chronic Treatment with a Promnesiant GABA-A alpha5-Selective Inverse Agonist Increases Immediate Early Genes Expression during Memory Processing in Mice and Rectifies Their Expression Levels in a Down Syndrome Mouse Model. *Adv Pharmacol Sci* 2011: 153218, 2011.

Braun J and Mattia M. Attractors and noise: twin drivers of decisions and multistability. *Neuroimage* 52: 740-751, 2010.

Bremer F. The arousal of the brain. *J Nerv Ment Dis* 130: 467-471, 1960.

Brumberg JC, Nowak LG, and McCormick DA. Ionic mechanisms underlying repetitive high-frequency burst firing in supragranular cortical neurons. *J Neurosci* 20: 4829-4843, 2000.

Brunel N and Wang XJ. Effects of neuromodulation in a cortical network model of object working memory dominated by recurrent inhibition. *J Comput Neurosci* 11: 63-85, 2001.

Buzsaki G, Anastassiou CA, and Koch C. The origin of extracellular fields and currents--EEG, ECoG, LFP and spikes. *Nat Rev Neurosci* 13: 407-420, 2012.

Buzsaki G and Wang XJ. Mechanisms of gamma oscillations. *Annu Rev Neurosci* 35: 203-225, 2012.

Caltagirone C, Nocentini U, and Vicari S. Cognitive functions in adult Down's syndrome. *Int J Neurosci* 54: 221-230, 1990.

Cardin JA, Carlen M, Meletis K, Knoblich U, Zhang F, Deisseroth K, Tsai LH, and Moore CI. Driving fast-spiking cells induces gamma rhythm and controls sensory responses. *Nature* 459: 663-667, 2009.

Castaldo V. Down's syndrome: a study of sleep patterns related to level of mental retardation. *Am J Ment Defic* 74: 187-190, 1969.

Castro-Alamancos MA, Rigas P, and Tawara-Hirata Y. Resonance (approximately 10 Hz) of excitatory networks in motor cortex: effects of voltage-dependent ion channel blockers. *J Physiol* 578: 173-191, 2007.

Chabert C, Jamon M, Cherfouh A, Duquenne V, Smith DJ, Rubin E, and Roubertoux PL. Functional analysis of genes implicated in Down syndrome: 1. Cognitive abilities in mice transpolygenic for Down Syndrome Chromosomal Region-1 (DCR-1). *Behav Genet* 34: 559-569, 2004.

Chakrabarti L, Best TK, Cramer NP, Carney RS, Isaac JT, Galdzicki Z, and Haydar TF. Olig1 and Olig2 triplication causes developmental brain defects in Down syndrome. *Nat Neurosci* 13: 927-934, 2010.

Chao TI and Alzheimer C. Effects of phenytoin on the persistent Na+ current of mammalian CNS neurones. *Neuroreport* 6: 1778-1780, 1995.

Chapman RS and Hesketh LJ. Behavioral phenotype of individuals with Down syndrome. *Ment Retard Dev Disabil Res Rev* 6: 84-95, 2000.

Chauvette S, Crochet S, Volgushev M, and Timofeev I. Properties of slow oscillation during slow-wave sleep and anesthesia in cats. *J Neurosci* 31: 14998-15008, 2011.

Chauvette S, Volgushev M, and Timofeev I. Origin of active states in local neocortical networks during slow sleep oscillation. *Cereb Cortex* 20: 2660-2674, 2010.

Chen JY, Chauvette S, Skorheim S, Timofeev I, and Bazhenov M. Interneuron-mediated inhibition synchronizes neuronal activity during slow oscillation. *J Physiol* 590: 3987-4010, 2012a.

Cheng A, Haydar TF, Yarowsky PJ, and Krueger BK. Concurrent generation of subplate and cortical plate neurons in developing trisomy 16 mouse cortex. *Dev Neurosci* 26: 255-265, 2004.

Chen-Hwang MC, Chen HR, Elzinga M, and Hwang YW. Dynamin is a minibrain kinase/dual specificity Yak1-related kinase 1A substrate. *J Biol Chem* 277: 17597-17604, 2002.

Clausen J, Sersen EA, and Lidsky A. Sleep patterns in mental retardation: Down's syndrome. *Electroencephalogr Clin Neurophysiol* 43: 183-191, 1977.

Colas D, London J, Gharib A, Cespuglio R, and Sarda N. Sleep-wake architecture in mouse models for Down syndrome. *Neurobiol Dis* 16: 291-299, 2004.

Colas D, Valletta JS, Takimoto-Kimura R, Nishino S, Fujiki N, Mobley WC, and Mignot E. Sleep and EEG features in genetic models of Down syndrome. *Neurobiol Dis* 30: 1-7, 2008.

Collins DR, Pelletier JG, and Pare D. Slow and fast (gamma) neuronal oscillations in the perirhinal cortex and lateral amygdala. *J Neurophysiol* 85: 1661-1672, 2001.

Colombo E, Franceschetti S, Avanzini G, and Mantegazza M. Phenytoin inhibits the persistent sodium current in neocortical neurons by modifying its inactivation properties. *PLoS One* 8: e55329, 2013.

Compte A, Reig R, Descalzo VF, Harvey MA, Puccini GD, and Sanchez-Vives MV. Spontaneous high-frequency (10-80 Hz) oscillations during up states in the cerebral cortex in vitro. *J Neurosci* 28: 13828-13844, 2008.

Compte A, Reig R, and Sanchez-Vives MV. *Timing excitation and inhibition in the cortical network. In: Coherent Behavior in Neuronal Networks*. New York: Springer, 2009.

Compte A, Sanchez-Vives MV, McCormick DA, and Wang XJ. Cellular and network mechanisms of slow oscillatory activity (<1 Hz) and wave propagations in a cortical network model. *J Neurophysiol* 89: 2707-2725, 2003.

Contreras D, Timofeev I, and Steriade M. Mechanisms of long-lasting hyperpolarizations underlying slow sleep oscillations in cat corticothalamic networks. *J Physiol* 494 (Pt 1): 251-264, 1996.

Cossart R, Aronov D, and Yuste R. Attractor dynamics of network UP states in the neocortex. *Nature* 423: 283-288, 2003.

Cotelli M, Calabria M, Manenti R, Rosini S, Zanetti O, Cappa SF, and Miniussi C. Improved language performance in Alzheimer disease following brain stimulation. *J Neurol Neurosurg Psychiatry* 82: 794-797, 2011.

Coyle JT, Oster-Granite ML, and Gearhart JD. The neurobiologic consequences of Down syndrome. *Brain Res Bull* 16: 773-787, 1986.

Crunelli V, Cope DW, and Hughes SW. Thalamic T-type Ca2+ channels and NREM sleep. *Cell Calcium* 40: 175-190, 2006.

Crunelli V and Hughes SW. The slow (<1 Hz) rhythm of non-REM sleep: a dialogue between three cardinal oscillators. In: *Nat Neurosci*. United States, 2010, p. 9-17.

Csercsa R, Dombovari B, Fabo D, Wittner L, Eross L, Entz L, Solyom A, Rasonyi G, Szucs A, Kelemen A, Jakus R, Juhos V, Grand L, Magony A, Halasz P, Freund TF, Magloczky Z, Cash SS, Papp L, Karmos G, Halgren E, and Ulbert I. Laminar analysis of slow wave activity in humans. *Brain* 133: 2814-2829, 2010.

Cunningham MO, Pervouchine DD, Racca C, Kopell NJ, Davies CH, Jones RS, Traub RD, and Whittington MA. Neuronal metabolism governs cortical network response state. *Proc Natl Acad Sci U S A* 103: 5597-5601, 2006.

Davisson MT, Schmidt C, Reeves RH, Irving NG, Akeson EC, Harris BS, and Bronson RT. Segmental trisomy as a mouse model for Down syndrome. *Prog Clin Biol Res* 384: 117-133, 1993.

Descalzo VF, Nowak LG, Brumberg JC, McCormick DA, and Sanchez-Vives MV. Slow adaptation in fast-spiking neurons of visual cortex. *J Neurophysiol* 93: 1111-1118, 2005.

Desmedt JE and Tomberg C. Consciousness. *Electroencephalogr Clin Neurophysiol Suppl* 44: 227-234, 1995.

Destexhe A, Hughes SW, Rudolph M, and Crunelli V. Are corticothalamic 'up' states fragments of wakefulness? *Trends Neurosci* 30: 334-342, 2007.

Devinsky O, Sato S, Conwit RA, and Schapiro MB. Relation of EEG alpha background to cognitive function, brain atrophy, and cerebral metabolism in Down's syndrome. Age-specific changes. *Arch Neurol* 47: 58-62, 1990.

Diekelmann S and Born J. The memory function of sleep. *Nat Rev Neurosci* 11: 114-126, 2010.

Dierssen M, Benavides-Piccione R, Martinez-Cue C, Estivill X, Florez J, Elston GN, and DeFelipe J. Alterations of neocortical pyramidal cell phenotype in the Ts65Dn mouse model of Down syndrome: effects of environmental enrichment. *Cereb Cortex* 13: 758-764, 2003.

Dierssen M, Ortiz-Abalia J, Arque G, de Lagran MM, and Fillat C. Pitfalls and hopes in Down syndrome therapeutic approaches: in the search for evidence-based treatments. *Behav Genet* 36: 454-468, 2006.

Djonlagic I, Saboisky J, Carusona A, Stickgold R, and Malhotra A. Increased sleep fragmentation leads to impaired off-line consolidation of motor memories in humans. *PLoS One* 7: e34106, 2012.

Dragomir A, Akay YM, and Akay M. Modeling carbachol-induced hippocampal network synchronization using hidden Markov models. *J Neural Eng* 7: 056012, 2010.

Elston GN. Cortex, cognition and the cell: new insights into the pyramidal neuron and prefrontal function. *Cereb Cortex* 13: 1124-1138, 2003.

Elston GN. Interlaminar differences in the pyramidal cell phenotype in cortical areas 7 m and STP (the superior temporal polysensory area) of the macaque monkey. *Exp Brain Res* 138: 141-152, 2001.

Elston GN. Pyramidal cells of the frontal lobe: all the more spinous to think with. *J Neurosci* 20: RC95, 2000.

Elston GN, Benavides-Piccione R, and DeFelipe J. The pyramidal cell in cognition: a comparative study in human and monkey. *J Neurosci* 21: RC163, 2001.

Ema M, Ikegami S, Hosoya T, Mimura J, Ohtani H, Nakao K, Inokuchi K, Katsuki M, and Fujii-Kuriyama Y. Mild impairment of learning and memory in mice overexpressing the mSim2 gene located on chromosome 16: an animal model of Down's syndrome. *Hum Mol Genet* 8: 1409-1415, 1999.

Engel AK, Fries P, and Singer W. Dynamic predictions: oscillations and synchrony in top-down processing. *Nat Rev Neurosci* 2: 704-716, 2001.

Epstein CJ, Avraham KB, Lovett M, Smith S, Elroy-Stein O, Rotman G, Bry C, and Groner Y. Transgenic mice with increased Cu/Zn-superoxide dismutase activity: animal model of dosage effects in Down syndrome. *Proc Natl Acad Sci U S A* 84: 8044-8048, 1987.

Epstein CJ, Cox DR, and Epstein LB. Mouse trisomy 16: an animal model of human trisomy 21 (Down syndrome). *Ann N Y Acad Sci* 450: 157-168, 1985.

Erchova IA, Lebedev MA, and Diamond ME. Somatosensory cortical neuronal population activity across states of anaesthesia. *Eur J Neurosci* 15: 744-752, 2002.

Farzan F, Barr MS, Sun Y, Fitzgerald PB, and Daskalakis ZJ. Transcranial magnetic stimulation on the modulation of gamma oscillations in schizophrenia. *Ann N Y Acad Sci* 1265: 25-35, 2012.

Fernandez F, Morishita W, Zuniga E, Nguyen J, Blank M, Malenka RC, and Garner CC. Pharmacotherapy for cognitive impairment in a mouse model of Down syndrome. *Nat Neurosci* 10: 411-413, 2007.

Fillat C, Dierssen M, de Lagran MM, and Altafaj X. Insights from mouse models to understand neurodegeneration in Down syndrome. *CNS Neurol Disord Drug Targets* 9: 429-438, 2012.

Fitzgibbon SP, Pope KJ, Mackenzie L, Clark CR, and Willoughby JO. Cognitive tasks augment gamma EEG power. *Clin Neurophysiol* 115: 1802-1809, 2004.

Fleidervish IA, Friedman A, and Gutnick MJ. Slow inactivation of Na+ current and slow cumulative spike adaptation in mouse and guinea-pig neocortical neurones in slices. *J Physiol* 493 (Pt 1): 83-97, 1996.

Fleidervish IA and Gutnick MJ. Kinetics of slow inactivation of persistent sodium current in layer V neurons of mouse neocortical slices. *J Neurophysiol* 76: 2125-2130, 1996.

Freund TF. Interneuron Diversity series: Rhythm and mood in perisomatic inhibition. *Trends Neurosci* 26: 489-495, 2003.

Freund TF and Katona I. Perisomatic inhibition. *Neuron* 56: 33-42, 2007.

Friend WC, Clapoff S, Landry C, Becker LE, O'Hanlon D, Allore RJ, Brown IR, Marks A, Roder J, and Dunn RJ. Cell-specific expression of high levels of human S100 beta in transgenic mouse brain is dependent on gene dosage. *J Neurosci* 12: 4337-4346, 1992.

Fries P, Nikolic D, and Singer W. The gamma cycle. *Trends Neurosci* 30: 309-316, 2007.

Fuchs EC, Doheny H, Faulkner H, Caputi A, Traub RD, Bibbig A, Kopell N, Whittington MA, and Monyer H. Genetically altered AMPA-type glutamate receptor kinetics in interneurons disrupt long-range synchrony of gamma oscillation. *Proc Natl Acad Sci U S A* 98: 3571-3576, 2001.

Fukuma E, Umezawa Y, Kobayashi K, and Motoike M. Polygraphic study on the nocturnal sleep of children with Down's syndrome and endogenous mental retardation. *Folia Psychiatr Neurol Jpn* 28: 333-345, 1974.

Ghazanfar AA, Chandrasekaran C, and Logothetis NK. Interactions between the superior temporal sulcus and auditory cortex mediate dynamic face/voice integration in rhesus monkeys. *J Neurosci* 28: 4457-4469, 2008.

Gil Z and Amitai Y. Properties of convergent thalamocortical and intracortical synaptic potentials in single neurons of neocortex. *J Neurosci* 16: 6567-6578, 1996.

Gilbert CD and Wiesel TN. Morphology and intracortical projections of functionally characterised neurones in the cat visual cortex. *Nature* 280: 120-125, 1979.

Golden JA and Hyman BT. Development of the superior temporal neocortex is anomalous in trisomy 21. *J Neuropathol Exp Neurol* 53: 513-520, 1994.

Gray CM and McCormick DA. Chattering cells: superficial pyramidal neurons contributing to the generation of synchronous oscillations in the visual cortex. *Science* 274: 109-113, 1996.

Gray CM and Singer W. Stimulus-specific neuronal oscillations in orientation columns of cat visual cortex. *Proc Natl Acad Sci U S A* 86: 1698-1702, 1989.

Gregoriou GG, Gotts SJ, Zhou H, and Desimone R. High-frequency, long-range coupling between prefrontal and visual cortex during attention. *Science* 324: 1207-1210, 2009.

Guatteo E, Franceschetti S, Bacci A, Avanzini G, and Wanke E. A TTX-sensitive conductance underlying burst firing in isolated pyramidal neurons from rat neocortex. In: *Brain Res*. Netherlands, 1996, p. 1-12.

Guedj F, Sebrie C, Rivals I, Ledru A, Paly E, Bizot JC, Smith D, Rubin E, Gillet B, Arbones M, and Delabar JM. Green tea polyphenols rescue of brain defects induced by overexpression of DYRK1A. *PLoS One* 4: e4606, 2009.

Guimera J, Casas C, Estivill X, and Pritchard M. Human minibrain homologue (MNBH/DYRK1): characterization, alternative splicing, differential tissue expression, and overexpression in Down syndrome. *Genomics* 57: 407-418, 1999.

Guimera J, Casas C, Pucharcos C, Solans A, Domenech A, Planas AM, Ashley J, Lovett M, Estivill X, and Pritchard MA. A human homologue of Drosophila minibrain (MNB) is expressed in the neuronal regions affected in Down syndrome and maps to the critical region. *Hum Mol Genet* 5: 1305-1310, 1996.

Guse B, Falkai P, and Wobrock T. Cognitive effects of high-frequency repetitive transcranial magnetic stimulation: a systematic review. *J Neural Transm* 117: 105-122, 2010.

Haider B, Duque A, Hasenstaub AR, and McCormick DA. Neocortical network activity in vivo is generated through a dynamic balance of excitation and inhibition. *J Neurosci* 26: 4535-4545, 2006.

Hamaguchi H, Hashimoto T, Mori K, and Tayama M. Sleep in the Down syndrome. *Brain Dev* 11: 399-406, 1989.

Hampson RE, Gerhardt GA, Marmarelis V, Song D, Opris I, Santos L, Berger TW, and Deadwyler SA. Facilitation and restoration of cognitive function in primate prefrontal cortex by a neuroprosThesis that utilizes minicolumn-specific neural firing. *J Neural Eng* 9: 056012, 2012a.

Hampson RE, Song D, Chan RH, Sweatt AJ, Riley MR, Gerhardt GA, Shin DC, Marmarelis VZ, Berger TW, and Deadwyler SA. A nonlinear model for hippocampal cognitive prosThesis: memory facilitation by hippocampal ensemble stimulation. *IEEE Trans Neural Syst Rehabil Eng* 20: 184-197, 2012b.

Hampson RE, Song D, Chan RH, Sweatt AJ, Riley MR, Goonawardena AV, Marmarelis VZ, Gerhardt GA, Berger TW, and Deadwyler SA. Closing the loop for memory prosThesis: detecting the role of hippocampal neural ensembles using nonlinear models. *IEEE Trans Neural Syst Rehabil Eng* 20: 510-525, 2012c.

Hansel D and Mato G. Asynchronous states and the emergence of synchrony in large networks of interacting excitatory and inhibitory neurons. *Neural Comput* 15: 1-56, 2003.

Hanson JE, Blank M, Valenzuela RA, Garner CC, and Madison DV. The functional nature of synaptic circuitry is altered in area CA3 of the hippocampus in a mouse model of Down's syndrome. *J Physiol* 579: 53-67, 2007.

Hardy J, Irving N, and Kessling A. Down on chromosome 21? *Trends Neurosci* 12: 209-210, 1989.

Harris KD, Bartho P, Chadderton P, Curto C, de la Rocha J, Hollender L, Itskov V, Luczak A, Marguet SL, Renart A, and Sakata S. How do neurons work together? Lessons from auditory cortex. *Hear Res* 271: 37-53, 2010.

Hasenstaub A, Shu Y, Haider B, Kraushaar U, Duque A, and McCormick DA. Inhibitory postsynaptic potentials carry synchronized frequency information in active cortical networks. *Neuron* 47: 423-435, 2005.

Haxby JV. Neuropsychological evaluation of adults with Down's syndrome: patterns of selective impairment in non-demented old adults. *J Ment Defic Res* 33 (Pt 3): 193-210, 1989.

Hernandez S, Gilabert-Juan J, Blasco-Ibanez JM, Crespo C, Nacher J, and Varea E. Altered expression of neuropeptides in the primary somatosensory cortex of the Down syndrome model Ts65Dn. *Neuropeptides* 46: 29-37, 2012.

Hill S and Tononi G. Modeling sleep and wakefulness in the thalamocortical system. *J Neurophysiol* 93: 1671-1698, 2005.

Hoover WB and Vertes RP. Anatomical analysis of afferent projections to the medial prefrontal cortex in the rat. *Brain Struct Funct* 212: 149-179, 2007.

Howard MW, Rizzuto DS, Caplan JB, Madsen JR, Lisman J, Aschenbrenner-Scheibe R, Schulze-Bonhage A, and Kahana MJ. Gamma oscillations correlate with working memory load in humans. *Cereb Cortex* 13: 1369-1374, 2003.

Hsiao K. Transgenic mice expressing Alzheimer amyloid precursor proteins. *Exp Gerontol* 33: 883-889, 1998.

Huang Y, Chen-Hwang MC, Dolios G, Murakami N, Padovan JC, Wang R, and Hwang YW. Mnb/Dyrk1A phosphorylation regulates the interaction of dynamin 1 with SH3 domain-containing proteins. *Biochemistry* 43: 10173-10185, 2004.

Hughes JR, Ikram A, and Fino JJ. Characteristics of travelling waves under various conditions. *Clin Electroencephalogr* 26: 7-22, 1995.

Hughes SW, Cope DW, Toth TI, Williams SR, and Crunelli V. All thalamocortical neurones possess a T-type Ca2+ 'window' current that enables the expression of bistability-mediated activities. *J Physiol* 517 (Pt 3): 805-815, 1999.

Hunter CL, Bachman D, and Granholm AC. Minocycline prevents cholinergic loss in a mouse model of Down's syndrome. *Ann Neurol* 56: 675-688, 2004.

Hunter CL, Bimonte HA, and Granholm AC. Behavioral comparison of 4 and 6 month-old Ts65Dn mice: age-related impairments in working and reference memory. *Behav Brain Res* 138: 121-131, 2003.

Innocenti GM, Manger PR, Masiello I, Colin I, and Tettoni L. Architecture and callosal connections of visual areas 17, 18, 19 and 21 in the ferret (Mustela putorius). *Cereb Cortex* 12: 411-422, 2002.

Jensen O, Kaiser J, and Lachaux JP. Human gamma-frequency oscillations associated with attention and memory. *Trends Neurosci* 30: 317-324, 2007.

Jernigan TL, Bellugi U, Sowell E, Doherty S, and Hesselink JR. Cerebral morphologic distinctions between Williams and Down syndromes. *Arch Neurol* 50: 186-191, 1993.

Jiang J, Jing Y, Cost GJ, Chiang J, Kolpa HJ, Cotton AM, Carone DM, Carone BR, Shivak DA, Guschin DY, Pearl JR, Rebar EJ, Byron M., Gregory PD, Brown CJ, Urnov FD, Hall LL, and Lawrence JB. Translating dosage compensation to trisomy 21. *Nature*, 2013.

Jones MS and Barth DS. Sensory-evoked high-frequency (gamma-band) oscillating potentials in somatosensory cortex of the unanesthetized rat. *Brain Res* 768: 167-176, 1997.

Jung CK, Fuhrmann M, Honarnejad K, Van Leuven F, and Herms J. Role of presenilin 1 in structural plasticity of cortical dendritic spines in vivo. *J Neurochem* 119: 1064-1073, 2011.

Kaczmarek LK, Jennings KR, and Strumwasser F. An early sodium and a late calcium phase in the afterdischarge of peptide-secreting neurons of Aplysia. *Brain Res* 238: 105-115, 1982.

Kammerer M, Brawek B, Freiman TM, Jackisch R, and Feuerstein TJ. Effects of antiepileptic drugs on glutamate release from rat and human neocortical synaptosomes. *Naunyn Schmiedebergs Arch Pharmacol* 383: 531-542, 2011a.

Kammerer M, Rassner MP, Freiman TM, and Feuerstein TJ. Effects of antiepileptic drugs on GABA release from rat and human neocortical synaptosomes. *Naunyn Schmiedebergs Arch Pharmacol* 384: 47-57, 2011b.

Karlsen AS and Pakkenberg B. Total numbers of neurons and glial cells in cortex and basal ganglia of aged brains with Down syndrome--a stereological study. *Cereb Cortex* 21: 2519-2524, 2011.

Kendrick KM, Zhan Y, Fischer H, Nicol AU, Zhang X, and Feng J. Learning alters theta amplitude, theta-gamma coupling and neuronal synchronization in inferotemporal cortex. *BMC Neurosci* 12: 55, 2011.

Kim SH, Han HJ, Ahn HM, Kim SA, and Kim SE. Effects of five daily high-frequency rTMS on Stroop task performance in aging individuals. *Neurosci Res* 74: 256-260, 2012.

Kim U and McCormick DA. Functional and ionic properties of a slow afterhyperpolarization in ferret perigeniculate neurons in vitro. *J Neurophysiol* 80: 1222-1235, 1998.

Kleen JK, Sesque A, Wu EX, Miller FA, Hernan AE, Holmes GL, and Scott RC. Early-life seizures produce lasting alterations in the structure and function of the prefrontal cortex. *Epilepsy Behav* 22: 214-219, 2011.

Kobayashi K, Emson PC, Mountjoy CQ, Thornton SN, Lawson DE, and Mann DM. Cerebral cortical calbindin D28K and parvalbumin neurones in Down's syndrome. *Neurosci Lett* 113: 17-22, 1990.

Koenig T, Prichep L, Dierks T, Hubl D, Wahlund LO, John ER, and Jelic V. Decreased EEG synchronization in Alzheimer's disease and mild cognitive impairment. *Neurobiol Aging* 26: 165-171, 2005.

Kononenko NI, Shao LR, and Dudek FE. Riluzole-sensitive slowly inactivating sodium current in rat suprachiasmatic nucleus neurons. *J Neurophysiol* 91: 710-718, 2004.

Kuo CC and Bean BP. Slow binding of phenytoin to inactivated sodium channels in rat hippocampal neurons. *Mol Pharmacol* 46: 716-725, 1994.

Kurata T, Kawarabayashi T, Murakami T, Miyazaki K, Morimoto N, Ohta Y, Takehisa Y, Nagai M, Ikeda M, Matsubara E, Westaway D, Hyslop PS, Harigaya Y, Kamiya T, Shoji M, and Abe K. Enhanced accumulation of phosphorylated alpha-synuclein in double transgenic mice expressing mutant beta-amyloid precursor protein and presenilin-1. *J Neurosci Res* 85: 2246-2252, 2007.

Kurt MA, Davies DC, Kidd M, Dierssen M, and Florez J. Synaptic deficit in the temporal cortex of partial trisomy 16 (Ts65Dn) mice. *Brain Res* 858: 191-197, 2000.

Lachaux JP, Jung J, Mainy N, Dreher JC, Bertrand O, Baciu M, Minotti L, Hoffmann D, and Kahane P. Silence is golden: transient neural deactivation in the prefrontal cortex during attentive reading. *Cereb Cortex* 18: 443-450, 2008.

Lamb BT, Sisodia SS, Lawler AM, Slunt HH, Kitt CA, Kearns WG, Pearson PL, Price DL, and Gearhart JD. Introduction and expression of the 400 kilobase amyloid precursor protein gene in transgenic mice [corrected]. *Nat Genet* 5: 22-30, 1993.

Lampl I, Schwindt P, and Crill W. Reduction of cortical pyramidal neuron excitability by the action of phenytoin on persistent Na+ current. *J Pharmacol Exp Ther* 284: 228-237, 1998.

Le Bon-Jego M and Yuste R. Persistently active, pacemaker-like neurons in neocortex. *Front Neurosci* 1: 123-129, 2007.

Le Pecheur M, Bourdon E, Paly E, Farout L, Friguet B, and London J. Oxidized SOD1 alters proteasome activities in vitro and in the cortex of SOD1 overexpressing mice. *FEBS Lett* 579: 3613-3618, 2005.

Lima B, Singer W, and Neuenschwander S. Gamma responses correlate with temporal expectation in monkey primary visual cortex. *J Neurosci* 31: 15919-15931, 2011.

Llinas R. *I of the vortex: from neurons to self*, 2001.

Llinas R and Ribary U. Coherent 40-Hz oscillation characterizes dream state in humans. *Proc Natl Acad Sci U S A* 90: 2078-2081, 1993.

Llinas RR. The intrinsic electrophysiological properties of mammalian neurons: insights into central nervous system function. *Science* 242: 1654-1664, 1988.

Llinas RR, Grace AA, and Yarom Y. In vitro neurons in mammalian cortical layer 4 exhibit intrinsic oscillatory activity in the 10- to 50-Hz frequency range. *Proc Natl Acad Sci U S A* 88: 897-901, 1991.

Lopes da Silva FH, van Rotterdam A, Storm van Leeuwen W, and Tielen AM. Dynamic characteristics of visual evoked potentials in the dog. II. Beta frequency selectivity in evoked potentials and background activity. *Electroencephalogr Clin Neurophysiol* 29: 260-268, 1970.

Loring DW and Sheer DE. Laterality of 40 Hz EEG and EMG during cognitive performance. *Psychophysiology* 21: 34-38, 1984.

Luczak A, Bartho P, Marguet SL, Buzsaki G, and Harris KD. Sequential structure of neocortical spontaneous activity in vivo. *Proc Natl Acad Sci U S A* 104: 347-352, 2007.

Manenti R, Cotelli M, Robertson IH, and Miniussi C. Transcranial brain stimulation studies of episodic memory in young adults, elderly adults and individuals with memory dysfunction: a review. *Brain Stimul* 5: 103-109, 2012.

Mann DM and Esiri MM. The pattern of acquisition of plaques and tangles in the brains of patients under 50 years of age with Down's syndrome. *J Neurol Sci* 89: 169-179, 1989.

Mann EO, Kohl MM, and Paulsen O. Distinct roles of GABA(A) and GABA(B) receptors in balancing and terminating persistent cortical activity. *J Neurosci* 29: 7513-7518, 2009.

Marshall L, Helgadottir H, Molle M, and Born J. Boosting slow oscillations during sleep potentiates memory. *Nature* 444: 610-613, 2006.

Martinez de Lagran M, Altafaj X, Gallego X, Marti E, Estivill X, Sahun I, Fillat C, and Dierssen M. Motor phenotypic alterations in TgDyrk1a transgenic mice implicate DYRK1A in Down syndrome motor dysfunction. *Neurobiol Dis* 15: 132-142, 2004.

Martinez de Lagran M, Benavides-Piccione R, Ballesteros-Yanez I, Calvo M, Morales M, Fillat C, Defelipe J, Ramakers GJ, and Dierssen M. Dyrk1A influences neuronal morphogenesis through regulation of cytoskeletal dynamics in mammalian cortical neurons. *Cereb Cortex* 22: 2867-2877, 2012.

Massimini M, Huber R, Ferrarelli F, Hill S, and Tononi G. The sleep slow oscillation as a traveling wave. *J Neurosci* 24: 6862-6870, 2004.

Matsuda Y, Inoue Y, Izumi H, Kaga M, Inagaki M, and Goto Y. Fewer GABAergic interneurons, heightened anxiety and decreased high-frequency electroencephalogram components in Bronx waltzer mice, a model of hereditary deafness. *Brain Res* 1373: 202-210, 2011.

Mazur-Kolecka B, Golabek A, Kida E, Rabe A, Hwang YW, Adayev T, Wegiel J, Flory M, Kaczmarski W, Marchi E, and Frackowiak J. Effect of DYRK1A activity inhibition on development of neuronal progenitors isolated from Ts65Dn mice. *J Neurosci Res* 90: 999-1010, 2012.

McAlaster R. Postnatal cerebral maturation in Down's syndrome children: a developmental EEG coherence study. *Int J Neurosci* 65: 221-237, 1992.

McCrimmon DR, Monnier A, Ptak K, Zummo G, Zhang Z, and Alheid GF. Respiratory rhythm generation: preBotzinger neuron discharge patterns and persistent sodium current. *Adv Exp Med Biol* 499: 147-152, 2001.

McLean MJ and Macdonald RL. Multiple actions of phenytoin on mouse spinal cord neurons in cell culture. *J Pharmacol Exp Ther* 227: 779-789, 1983.

Menghini D, Costanzo F, and Vicari S. Relationship between brain and cognitive processes in Down syndrome. *Behav Genet* 41: 381-393, 2011.

Mohajerani MH, McVea DA, Fingas M, and Murphy TH. Mirrored bilateral slow-wave cortical activity within local circuits revealed by fast bihemispheric voltage-sensitive dye imaging in anesthetized and awake mice. *J Neurosci* 30: 3745-3751, 2010.

Molaee-Ardekani B, Benquet P, Bartolomei F, and Wendling F. Computational modeling of high-frequency oscillations at the onset of neocortical partial seizures: from 'altered structure' to 'dysfunction'. *Neuroimage* 52: 1109-1122, 2010.

Molle M and Born J. Slow oscillations orchestrating fast oscillations and memory consolidation. *Prog Brain Res* 193: 93-110, 2011.

Molnar P and Erdo SL. Vinpocetine is as potent as phenytoin to block voltage-gated Na+ channels in rat cortical neurons. *Eur J Pharmacol* 273: 303-306, 1995.

Morgan HM, Muthukumaraswamy SD, Hibbs CS, Shapiro KL, Bracewell RM, Singh KD, and Linden DE. Feature integration in visual working memory: parietal gamma activity is related to cognitive coordination. *J Neurophysiol* 106: 3185-3194, 2011.

Murakami N, Xie W, Lu RC, Chen-Hwang MC, Wieraszko A, and Hwang YW. Phosphorylation of amphiphysin I by minibrain kinase/dual-specificity tyrosine phosphorylation-regulated kinase, a kinase implicated in Down syndrome. *J Biol Chem* 281: 23712-23724, 2006.

Murata T, Koshino Y, Omori M, Murata I, Nishio M, Horie T, and Isaki K. Quantitative EEG study on premature aging in adult Down's syndrome. *Biol Psychiatry* 35: 422-425, 1994.

Murphy M, Riedner BA, Huber R, Massimini M, Ferrarelli F, and Tononi G. Source modeling sleep slow waves. *Proc Natl Acad Sci U S A* 106: 1608-1613, 2009.

Muthukumaraswamy SD, Edden RA, Jones DK, Swettenham JB, and Singh KD. Resting GABA concentration predicts peak gamma frequency and fMRI amplitude in response to visual stimulation in humans. *Proc Natl Acad Sci U S A* 106: 8356-8361, 2009.

Nadel L. Down's syndrome: a genetic disorder in biobehavioral perspective. *Genes Brain Behav* 2: 156-166, 2003.

Nir Y, Staba RJ, Andrillon T, Vyazovskiy VV, Cirelli C, Fried I, and Tononi G. Regional slow waves and spindles in human sleep. *Neuron* 70: 153-169, 2011.

Nunez A, Amzica F, and Steriade M. Voltage-dependent fast (20-40 Hz) oscillations in long-axoned neocortical neurons. *Neuroscience* 51: 7-10, 1992.

O'Doherty A, Ruf S, Mulligan C, Hildreth V, Errington ML, Cooke S, Sesay A, Modino S, Vanes L, Hernandez D, Linehan JM, Sharpe PT, Brandner S, Bliss TV, Henderson DJ, Nizetic D, Tybulewicz VL, and Fisher EM. An aneuploid mouse strain carrying human chromosome 21 with Down syndrome phenotypes. *Science* 309: 2033-2037, 2005.

Oke OO, Magony A, Anver H, Ward PD, Jiruska P, Jefferys JG, and Vreugdenhil M. High-frequency gamma oscillations coexist with low-frequency gamma oscillations in the rat visual cortex in vitro. *Eur J Neurosci* 31: 1435-1445, 2010.

Olson LE, Roper RJ, Sengstaken CL, Peterson EA, Aquino V, Galdzicki Z, Siarey R, Pletnikov M, Moran TH, and Reeves RH. Trisomy for the Down syndrome 'critical region' is necessary but not sufficient for brain phenotypes of trisomic mice. *Hum Mol Genet* 16: 774-782, 2007.

Ongur D and Price JL. The organization of networks within the orbital and medial prefrontal cortex of rats, monkeys and humans. *Cereb Cortex* 10: 206-219, 2000.

Ono Y. EEG changes with aging in adults with Down syndrome. *Jpn J Psychiatry Neurol* 47: 75-84, 1993.

Ortiz-Abalia J, Sahun I, Altafaj X, Andreu N, Estivill X, Dierssen M, and Fillat C. Targeting Dyrk1A with AAVshRNA attenuates motor alterations in TgDyrk1A, a mouse model of Down syndrome. *Am J Hum Genet* 83: 479-488, 2008.

Paik SB, Kumar T, and Glaser DA. Spontaneous local gamma oscillation selectively enhances neural network responsiveness. *PLoS Comput Biol* 5: e1000342, 2009.

Pallanti S, Di Rollo A, Antonini S, Cauli G, Hollander E, and Quercioli L. Low-frequency rTMS over right dorsolateral prefrontal cortex in the treatment of resistant depression: cognitive improvement is independent from clinical response, resting motor threshold is related to clinical response. *Neuropsychobiology* 65: 227-235, 2012.

Palva JM, Monto S, Kulashekhar S, and Palva S. Neuronal synchrony reveals working memory networks and predicts individual memory capacity. *Proc Natl Acad Sci U S A* 107: 7580-7585, 2010.

Palva S, Palva JM, Shtyrov Y, Kujala T, Ilmoniemi RJ, Kaila K, and Naatanen R. Distinct gamma-band evoked responses to speech and non-speech sounds in humans. *J Neurosci* 22: RC211, 2002.

Park J, Song WJ, and Chung KC. Function and regulation of Dyrk1A: towards understanding Down syndrome. *Cell Mol Life Sci* 66: 3235-3240, 2009.

Partanen J, Soininen H, Kononen M, Kilpelainen R, Helkala EL, and Riekkinen P, Sr. EEG reactivity correlates with neuropsychological test scores in Down's syndrome. *Acta Neurol Scand* 94: 242-246, 1996.

Pedroarena C and Llinas R. Dendritic calcium conductances generate high-frequency oscillation in thalamocortical neurons. *Proc Natl Acad Sci U S A* 94: 724-728, 1997.

Pennington BF, Moon J, Edgin J, Stedron J, and Nadel L. The neuropsychology of Down syndrome: evidence for hippocampal dysfunction. *Child Dev* 74: 75-93, 2003.

Pereira PL, Magnol L, Sahun I, Brault V, Duchon A, Prandini P, Gruart A, Bizot JC, Chadefaux-Vekemans B, Deutsch S, Trovero F, Delgado-Garcia JM, Antonarakis SE, Dierssen M, and Herault Y. A new mouse model for the trisomy of the Abcg1-U2af1 region reveals the complexity of the combinatorial genetic code of down syndrome. *Hum Mol Genet* 18: 4756-4769, 2009.

Perez-Cremades D, Hernandez S, Blasco-Ibanez JM, Crespo C, Nacher J, and Varea E. Alteration of inhibitory circuits in the somatosensory cortex of Ts65Dn mice, a model for Down's syndrome. *J Neural Transm* 117: 445-455, 2010.

Petersen CC, Grinvald A, and Sakmann B. Spatiotemporal dynamics of sensory responses in layer 2/3 of rat barrel cortex measured in vivo by voltage-sensitive dye imaging combined with whole-cell voltage recordings and neuron reconstructions. *J Neurosci* 23: 1298-1309, 2003a.

Petersen CC, Hahn TT, Mehta M, Grinvald A, and Sakmann B. Interaction of sensory responses with spontaneous depolarization in layer 2/3 barrel cortex. *Proc Natl Acad Sci U S A* 100: 13638-13643, 2003b.

Petre-Quadens O and Jouvet M. Sleep in the mentally retarded. *J Neurol Sci* 4: 354-357, 1967.

Pinter JD, Eliez S, Schmitt JE, Capone GT, and Reiss AL. Neuroanatomy of Down's syndrome: a high-resolution MRI study. *Am J Psychiatry* 158: 1659-1665, 2001.

Poulet JF, Fernandez LM, Crochet S, and Petersen CC. Thalamic control of cortical states. *Nat Neurosci* 15: 370-372, 2012.

Ray S, Niebur E, Hsiao SS, Sinai A, and Crone NE. High-frequency gamma activity (80-150Hz) is increased in human cortex during selective attention. *Clin Neurophysiol* 119: 116-133, 2008.

Raz N, Torres IJ, Briggs SD, Spencer WD, Thornton AE, Loken WJ, Gunning FM, McQuain JD, Driesen NR, and Acker JD. Selective neuroanatomic abnormalities in Down's syndrome and their cognitive correlates: evidence from MRI morphometry. *Neurology* 45: 356-366, 1995.

Reig R, Gallego R, Nowak LG, and Sanchez-Vives MV. Impact of cortical network activity on short-term synaptic depression. *Cereb Cortex* 16: 688-695, 2006.

Reig R, Mattia M, Compte A, Belmonte C, and Sanchez-Vives MV. Temperature modulation of slow and fast cortical rhythms. *J Neurophysiol* 103: 1253-1261, 2010a.

Reig R, Mattia M, Compte A, Belmonte C, and Sanchez-Vives MV. Temperature Modulation of Slow and Fast Cortical Rhythms. *J Neurophysiol* 103: 1253-1261, 2010b.

Reig R and Sanchez-Vives MV. Synaptic transmission and plasticity in an active cortical network. *PLoS One* 2: e670, 2007.

Reinhart RM, Heitz RP, Purcell BA, Weigand PK, Schall JD, and Woodman GF. Homologous mechanisms of visuospatial working memory maintenance in macaque and human: properties and sources. *J Neurosci* 32: 7711-7722, 2012.

Reynolds GP and Warner CE. Amino acid neurotransmitter deficits in adult Down's syndrome brain tissue. *Neurosci Lett* 94: 224-227, 1988.

Rigas P and Castro-Alamancos MA. Impact of persistent cortical activity (up States) on intracortical and thalamocortical synaptic inputs. *J Neurophysiol* 102: 119-131, 2009.

Rigas P and Castro-Alamancos MA. Thalamocortical Up states: differential effects of intrinsic and extrinsic cortical inputs on persistent activity. *J Neurosci* 27: 4261-4272, 2007.

Risser D, Lubec G, Cairns N, and Herrera-Marschitz M. Excitatory amino acids and monoamines in parahippocampal gyrus and frontal cortical pole of adults with Down syndrome. *Life Sci* 60: 1231-1237, 1997.

Rockland KS. Complex microstructures of sensory cortical connections. *Curr Opin Neurobiol* 8: 545-551, 1998.

Ross MH, Galaburda AM, and Kemper TL. Down's syndrome: is there a decreased population of neurons? *Neurology* 34: 909-916, 1984.

Roubertoux PL and Carlier M. Mouse models of cognitive disabilities in trisomy 21 (Down syndrome). *Am J Med Genet C Semin Med Genet* 154C: 400-416, 2010.

Rougeul A, Bouyer JJ, Dedet L, and Debray O. Fast somato-parietal rhythms during combined focal attention and immobility in baboon and squirrel monkey. *Electroencephalogr Clin Neurophysiol* 46: 310-319, 1979.

Roux F, Wibral M, Mohr HM, Singer W, and Uhlhaas PJ. Gamma-band activity in human prefrontal cortex codes for the number of relevant items maintained in working memory. *J Neurosci* 32: 12411-12420, 2012.

Rowe J, Lavender A, and Turk V. Cognitive executive function in Down's syndrome. *Br J Clin Psychol* 45: 5-17, 2006.

Ruiz-Mejias M, Ciria-Suarez L, Mattia M, and Sanchez-Vives MV. Slow and fast rhythms generated in the cerebral cortex of the anesthetized mouse. *J Neurophysiol* 106: 2910-2921, 2011.

Sago H, Carlson EJ, Smith DJ, Kilbridge J, Rubin EM, Mobley WC, Epstein CJ, and Huang TT. Ts1Cje, a partial trisomy 16 mouse model for Down syndrome, exhibits learning and behavioral abnormalities. *Proc Natl Acad Sci U S A* 95: 6256-6261, 1998.

Sago H, Carlson EJ, Smith DJ, Rubin EM, Crnic LS, Huang TT, and Epstein CJ. Genetic dissection of region associated with behavioral abnormalities in mouse models for Down syndrome. *Pediatr Res* 48: 606-613, 2000.

Sakata S and Harris KD. Laminar structure of spontaneous and sensory-evoked population activity in auditory cortex. *Neuron* 64: 404-418, 2009.

Sanchez-Vives MV, Mattia M, Compte A, Perez-Zabalza M, Winograd M, Descalzo VF, and Reig R. Inhibitory modulation of cortical up states. *J Neurophysiol* 104: 1314-1324, 2010.

Sanchez-Vives MV and McCormick DA. Cellular and network mechanisms of rhythmic recurrent activity in neocortex. *Nat Neurosci* 3: 1027-1034, 2000.

Sarsoza F, Saing T, Kayed R, Dahlin R, Dick M, Broadwater-Hollifield C, Mobley S, Lott I, Doran E, Gillen D, Anderson-Bergman C, Cribbs DH, Glabe C, and Head E. A fibril-specific, conformation-dependent antibody recognizes a subset of Abeta plaques in Alzheimer disease, Down syndrome and Tg2576 transgenic mouse brain. *Acta Neuropathol* 118: 505-517, 2009.

Schwindt PC, Spain WJ, and Crill WE. Long-lasting reduction of excitability by a sodium-dependent potassium current in cat neocortical neurons. *J Neurophysiol* 61: 233-244, 1989.

Scott-McKean JJ, Chang B, Hurd RE, Nusinowitz S, Schmidt C, Davisson MT, and Costa AC. The mouse model of Down syndrome Ts65Dn presents visual deficits as assessed by pattern visual evoked potentials. *Invest Ophthalmol Vis Sci* 51: 3300-3308, 2010.

Sebrie C, Chabert C, Ledru A, Guedj F, Po C, Smith DJ, Rubin E, Rivals I, Beloeil JC, Gillet B, and Delabar JM. Increased dosage of DYRK1A and brain volumetric alterations in a YAC model of partial trisomy 21. *Anat Rec (Hoboken)* 291: 254-262, 2008.

Segal MM and Douglas AF. Late sodium channel openings underlying epileptiform activity are preferentially diminished by the anticonvulsant phenytoin. *J Neurophysiol* 77: 3021-3034, 1997.

Seo H and Isacson O. The hAPP-YAC transgenic model has elevated UPS activity in the frontal cortex similar to Alzheimer's disease and Down's syndrome. *J Neurochem* 114: 1819-1826, 2010.

Seppalainen AM and Kivalo E. EEG findings and epilepsy in Down's syndrome. *J Ment Defic Res* 11: 116-125, 1967.

Sheppard O, Plattner F, Rubin A, Slender A, Linehan JM, Brandner S, Tybulewicz VL, Fisher EM, and Wiseman FK. Altered regulation of tau phosphorylation in a mouse model of down syndrome aging. *Neurobiol Aging* 33: 828 e831-844, 2011.

Shetty HU, Siarey RJ, Galdzicki Z, Stoll J, and Rapoport SI. Ts65Dn mouse, a Down syndrome model, exhibits elevated myo-inositol in selected brain regions and peripheral tissues. *Neurochem Res* 25: 431-435, 2000.

Shu Y, Hasenstaub A, Badoual M, Bal T, and McCormick DA. Barrages of synaptic activity control the gain and sensitivity of cortical neurons. *J Neurosci* 23: 10388-10401, 2003.

Shukkur EA, Shimohata A, Akagi T, Yu W, Yamaguchi M, Murayama M, Chui D, Takeuchi T, Amano K, Subramhanya KH, Hashikawa T, Sago H, Epstein CJ, Takashima A, and Yamakawa K. Mitochondrial dysfunction and tau hyperphosphorylation in Ts1Cje, a mouse model for Down syndrome. *Hum Mol Genet* 15: 2752-2762, 2006.

Siegel M, Donner TH, and Engel AK. Spectral fingerprints of large-scale neuronal interactions. *Nat Rev Neurosci* 13: 121-134, 2012.

Siegel M, Donner TH, Oostenveld R, Fries P, and Engel AK. Neuronal synchronization along the dorsal visual pathway reflects the focus of spatial attention. *Neuron* 60: 709-719, 2008.

Silberberg G and Markram H. Disynaptic inhibition between neocortical pyramidal cells mediated by Martinotti cells. *Neuron* 53: 735-746, 2007.

Silva LR, Amitai Y, and Connors BW. Intrinsic oscillations of neocortex generated by layer 5 pyramidal neurons. *Science* 251: 432-435, 1991.

Singer W and Gray CM. Visual feature integration and the temporal correlation hypothesis. *Annu Rev Neurosci* 18: 555-586, 1995.

Smigielska-Kuzia J, Sobaniec W, Kulak W, Bockowski L, and Solowiej E. Quantitative EEG analysis of REM sleep in children with Down syndrome. *Rocz Akad Med Bialymst* 50 Suppl 1: 20-22, 2005.

Sohal VS, Zhang F, Yizhar O, and Deisseroth K. Parvalbumin neurons and gamma rhythms enhance cortical circuit performance. *Nature* 459: 698-702, 2009.

Soininen H, Partanen J, Jousmaki V, Helkala EL, Vanhanen M, Majuri S, Kaski M, Hartikainen P, and Riekkinen P, Sr. Age-related cognitive decline and electroencephalogram slowing in Down's syndrome as a model of Alzheimer's disease. *Neuroscience* 53: 57-63, 1993.

Solinas S, Forti L, Cesana E, Mapelli J, De Schutter E, and D'Angelo E. Fast-reset of pacemaking and theta-frequency resonance patterns in cerebellar golgi cells: simulations of their impact in vivo. *Front Cell Neurosci* 1: 4, 2007.

Stefani A, Spadoni F, and Bernardi G. Differential inhibition by riluzole, lamotrigine, and phenytoin of sodium and calcium currents in cortical neurons: implications for neuroprotective strategies. *Exp Neurol* 147: 115-122, 1997a.

Stefani A, Spadoni F, and Bernardi G. Differential inhibition by riluzole, lamotrigine, and phenytoin of sodium and calcium currents in cortical neurons: implications for neuroprotective strategies. In: *Exp Neurol*. United States, 1997b, p. 115-122.

Steriade M. Basic mechanisms of sleep generation. *Neurology* 42: 9-17; discussion 18, 1992.

Steriade M. The corticothalamic system in sleep. *Front Biosci* 8: d878-899, 2003.

Steriade M. Grouping of brain rhythms in corticothalamic systems. *Neuroscience* 137: 1087-1106, 2006.

Steriade M and Amzica F. Intracortical and corticothalamic coherency of fast spontaneous oscillations. *Proc Natl Acad Sci U S A* 93: 2533-2538, 1996.

Steriade M, Amzica F, and Contreras D. Synchronization of fast (30-40 Hz) spontaneous cortical rhythms during brain activation. *J Neurosci* 16: 392-417, 1996.

Steriade M, Contreras D, Curro Dossi R, and Nunez A. The slow (< 1 Hz) oscillation in reticular thalamic and thalamocortical neurons: scenario of sleep rhythm generation in interacting thalamic and neocortical networks. *J Neurosci* 13: 3284-3299, 1993a.

Steriade M, Nunez A, and Amzica F. Intracellular analysis of relations between the slow (< 1 Hz) neocortical oscillation and other sleep rhythms of the electroencephalogram. *J Neurosci* 13: 3266-3283, 1993b.

Steriade M, Nunez A, and Amzica F. A novel slow (< 1 Hz) oscillation of neocortical neurons in vivo: depolarizing and hyperpolarizing components. *J Neurosci* 13: 3252-3265, 1993c.

Steriade M and Timofeev I. Neuronal plasticity in thalamocortical networks during sleep and waking oscillations. *Neuron* 37: 563-576, 2003.

Stroh A, Adelsberger H, Groh A, Ruhlmann C, Fischer S, Schierloh A, Deisseroth K, and Konnerth A. Making waves: initiation and propagation of corticothalamic ca(2+) waves in vivo. *Neuron* 77: 1136-1150, 2013.

Suetsugu M and Mehraein P. Spine distribution along the apical dendrites of the pyramidal neurons in Down's syndrome. A quantitative Golgi study. *Acta Neuropathol* 50: 207-210, 1980.

Tahvildari B, Wolfel M, Duque A, and McCormick DA. Selective functional interactions between excitatory and inhibitory cortical neurons and differential contribution to persistent activity of the slow oscillation. *J Neurosci* 32: 12165-12179, 2012.

Takashima S, Ieshima A, Nakamura H, and Becker LE. Dendrites, dementia and the Down syndrome. *Brain Dev* 11: 131-133, 1989.

Tallon-Baudry C. The roles of gamma-band oscillatory synchrony in human visual cognition. *Front Biosci* 14: 321-332, 2009.

Tamas G, Buhl EH, Lorincz A, and Somogyi P. Proximally targeted GABAergic synapses and gap junctions synchronize cortical interneurons. *Nat Neurosci* 3: 366-371, 2000.

Tazerart S, Vinay L, and Brocard F. The persistent sodium current generates pacemaker activities in the central pattern generator for locomotion and regulates the locomotor rhythm. *J Neurosci* 28: 8577-8589, 2008a.

Tazerart S, Vinay L, and Brocard F. The persistent sodium current generates pacemaker activities in the central pattern generator for locomotion and regulates the locomotor rhythm. In: *J Neurosci*. United States, 2008b, p. 8577-8589.

Tejedor FJ and Hammerle B. MNB/DYRK1A as a multiple regulator of neuronal development. *Febs J* 278: 223-235, 2011.

Timofeev I and Chauvette S. Thalamocortical oscillations: local control of EEG slow waves. *Curr Top Med Chem* 11: 2457-2471, 2011.

Timofeev I, Grenier F, Bazhenov M, Sejnowski TJ, and Steriade M. Origin of slow cortical oscillations in deafferented cortical slabs. *Cereb Cortex* 10: 1185-1199, 2000.

Toiber D, Azkona G, Ben-Ari S, TorÃ¡n N, Soreq H, and Dierssen M. Engineering DYRK1A overdosage yields Down syndrome-characteristic cortical splicing aberrations. *Neurobiology of Disease* 40: 348-359, 2010.

Traub RD, Bibbig A, LeBeau FE, Cunningham MO, and Whittington MA. Persistent gamma oscillations in superficial layers of rat auditory neocortex: experiment and model. *J Physiol* 562: 3-8, 2005.

Tripodi M, Evers JF, Mauss A, Bate M, and Landgraf M. Structural homeostasis: compensatory adjustments of dendritic arbor geometry in response to variations of synaptic input. *PLoS Biol* 6: e260, 2008.

Tsodyks M, Kenet T, Grinvald A, and Arieli A. Linking spontaneous activity of single cortical neurons and the underlying functional architecture. *Science* 286: 1943-1946, 1999.

Uhlhaas PJ and Singer W. Abnormal neural oscillations and synchrony in schizophrenia. *Nat Rev Neurosci* 11: 100-113, 2010.

Uhlhaas PJ and Singer W. Neural synchrony in brain disorders: relevance for cognitive dysfunctions and pathophysiology. *Neuron* 52: 155-168, 2006.

Valderrama M, Crepon B, Botella-Soler V, Martinerie J, Hasboun D, Alvarado-Rojas C, Baulac M, Adam C, Navarro V, and Le Van Quyen M. Human gamma oscillations during slow wave sleep. *PLoS One* 7: e33477, 2012.

Velikova S, Magnani G, Arcari C, Falautano M, Franceschi M, Comi G, and Leocani L. Cognitive impairment and EEG background activity in adults with Down's syndrome: a topographic study. *Hum Brain Mapp* 32: 716-729, 2011.

Ventura-Clapier R, Kaasik A, and Veksler V. Structural and functional adaptations of striated muscles to CK deficiency. *Mol Cell Biochem* 256-257: 29-41, 2004.

Verret L, Mann EO, Hang GB, Barth AM, Cobos I, Ho K, Devidze N, Masliah E, Kreitzer AC, Mody I, Mucke L, and Palop JJ. Inhibitory interneuron deficit links altered network activity and cognitive dysfunction in Alzheimer model. *Cell* 149: 708-721, 2012.

Villar AJ, Belichenko PV, Gillespie AM, Kozy HM, Mobley WC, and Epstein CJ. Identification and characterization of a new Down syndrome model, Ts[Rb(12.1716)]2Cje, resulting from a spontaneous Robertsonian fusion between T(171)65Dn and mouse chromosome 12. *Mamm Genome* 16: 79-90, 2005.

Visser FE, Aldenkamp AP, van Huffelen AC, Kuilman M, Overweg J, and van Wijk J. Prospective study of the prevalence of Alzheimer-type dementia in institutionalized individuals with Down syndrome. *Am J Ment Retard* 101: 400-412, 1997.

Volgushev M, Chauvette S, Mukovski M, and Timofeev I. Precise long-range synchronization of activity and silence in neocortical neurons during slow-wave oscillations [corrected]. *J Neurosci* 26: 5665-5672, 2006.

Volman V, Behrens MM, and Sejnowski TJ. Downregulation of parvalbumin at cortical GABA synapses reduces network gamma oscillatory activity. *J Neurosci* 31: 18137-18148, 2011.

Wang XJ. Neurophysiological and computational principles of cortical rhythms in cognition. *Physiol Rev* 90: 1195-1268, 2010.

Wegiel J, Kuchna I, Nowicki K, Frackowiak J, Dowjat K, Silverman WP, Reisberg B, DeLeon M, Wisniewski T, Adayev T, Chen-Hwang MC, and Hwang YW. Cell type- and brain structure-specific patterns of distribution of minibrain kinase in human brain. *Brain Res* 1010: 69-80, 2004.

Whittington MA, Cunningham MO, LeBeau FE, Racca C, and Traub RD. Multiple origins of the cortical gamma rhythm. *Dev Neurobiol* 71: 92-106, 2011.

Whittington MA, Traub RD, and Jefferys JG. Synchronized oscillations in interneuron networks driven by metabotropic glutamate receptor activation. *Nature* 373: 612-615, 1995.

Whittle N, Sartori SB, Dierssen M, Lubec G, and Singewald N. Fetal Down syndrome brains exhibit aberrant levels of neurotransmitters critical for normal brain development. *Pediatrics* 120: e1465-1471, 2007.

Wilson HR and Cowan JD. Excitatory and inhibitory interactions in localized populations of model neurons. *Biophys J* 12: 1-24, 1972.

Wilson TW, Rojas DC, Reite ML, Teale PD, and Rogers SJ. Children and adolescents with autism exhibit reduced MEG steady-state gamma responses. *Biol Psychiatry* 62: 192-197, 2007.

Wisniewski KE. Down syndrome children often have brain with maturation delay, retardation of growth, and cortical dysgenesis. *Am J Med Genet Suppl* 7: 274-281, 1990.

Womelsdorf T, Schoffelen JM, Oostenveld R, Singer W, Desimone R, Engel AK, and Fries P. Modulation of neuronal interactions through neuronal synchronization. *Science* 316: 1609-1612, 2007.

Xiao Y, Huang XY, Van Wert S, Barreto E, Wu JY, Gluckman BJ, and Schiff SJ. The role of inhibition in oscillatory wave dynamics in the cortex. *Eur J Neurosci* 36: 2201-2212, 2012.

Xue S, Li Q, and Khalil Z. Alterations in vascular reactivity in single- and double-transgenic mice coexpressing human APP-C100 and mutant SOD(1) genes. *Chin Med J (Engl)* 115: 696-701, 2002.

Yeterian EH, Pandya DN, Tomaiuolo F, and Petrides M. The cortical connectivity of the prefrontal cortex in the monkey brain. *Cortex* 48: 58-81, 2012.

Yu T, Liu C, Belichenko P, Clapcote SJ, Li S, Pao A, Kleschevnikov A, Bechard AR, Asrar S, Chen R, Fan N, Zhou Z, Jia Z, Chen C, Roder JC, Liu B, Baldini A, Mobley WC, and Yu YE. Effects of individual segmental trisomies of human chromosome 21 syntenic regions on hippocampal long-term potentiation and cognitive behaviors in mice. *Brain Res* 1366: 162-171, 2010.

Yuan Q, Xiang Y, Yan Z, Han C, Jan LY, and Jan YN. Light-induced structural and functional plasticity in Drosophila larval visual system. *Science* 333: 1458-1462, 2011.

Zhang X, Kendrick KM, Zhou H, Zhan Y, and Feng J. A computational study on altered theta-gamma coupling during learning and phase coding. *PLoS One* 7: e36472, 2012.

J Neurophysiol 106: 2910–2921, 2011.
First published August 31, 2011; doi:10.1152/jn.00440.2011.

Slow and fast rhythms generated in the cerebral cortex of the anesthetized mouse

Marcel Ruiz-Mejias,[1] Laura Ciria-Suarez,[1] Maurizio Mattia,[2] and Maria V. Sanchez-Vives[1,3]
[1]*IDIBAPS, Barcelona, Spain;* [2]*Istituto Superiore di Sanità, Rome, Italy; and* [3]*ICREA, Barcelona, Spain*

Submitted 13 May 2011; accepted in final form 31 August 2011

Ruiz-Mejias M, Ciria-Suarez L, Mattia M, Sanchez-Vives MV. Slow and fast rhythms generated in the cerebral cortex of the anesthetized mouse. *J Neurophysiol* 106: 2910–2921, 2011. First published August 31, 2011; doi:10.1152/jn.00440.2011.—A characterization of the oscillatory activity in the cerebral cortex of the mouse was realized under ketamine anesthesia. Bilateral recordings were obtained from deep layers of primary visual, somatosensory, motor, and medial prefrontal cortex. A slow oscillatory activity consisting of up and down states was detected, the average frequency being 0.97 Hz in all areas. Different parameters of the oscillation were estimated across cortical areas, including duration of up and down states and their variability, speed of state transitions, and population firing rate. Similar values were obtained for all areas except for prefrontal cortex, which showed significant faster down-to-up state transitions, higher firing rate during up states, and more regular cycles. The wave propagation patterns in the anteroposterior axis in motor cortex and the mediolateral axis in visual cortex were studied with multielectrode recordings, yielding speed values between 8 and 93 mm/s. The firing of single units was analyzed with respect to the population activity. The most common pattern was that of neurons firing in >90% of the up states with 1–6 spikes. Finally, fast rhythms (beta, low gamma, and high gamma) were analyzed, all of them showing significantly larger power during up states than in down states. Prefrontal cortex exhibited significantly larger power in both beta and gamma bands (up to 1 order of magnitude larger in the case of high gamma) than the rest of the cortical areas. This study allows us to carry out interareal comparisons and provides a baseline to compare against cortical emerging activity from genetically altered animals.

oscillations; in vivo recording; ketamine; up states; sleep; spontaneous activity

SLOW OSCILLATIONS (<1 Hz) occurring during slow-wave sleep and ketamine anesthesia were originally characterized in the neocortex of the cat (Steriade et al. 1993). During this rhythmic activity, the cortical network switches between depolarized, active periods or up states and silent periods or down states. During up states, the recurrency within the network maintains persistent activity with a functional structure that often reproduces that occurring during the cortical processing in the awake state (Destexhe et al. 2007; Luczak et al. 2007; MacLean et al. 2005; Sakata and Harris 2009; Steriade and Timofeev 2003; Tsodyks et al. 1999). One of these features is the synchronization of activity in beta and gamma bands during up states (Compte et al. 2008; Hasenstaub et al. 2005; Steriade et al. 1996). In vivo rhythmic cortical slow oscillations and their propagation have been observed and characterized in different species including humans (Csercsa et al. 2010; Massimini et al. 2004; Nir et al. 2011), cats (Chauvette et al. 2010; MacLean et al. 2005; Volgushev et al. 2006), ferrets (Haider et al. 2006), and rats (Sakata and Harris 2009). Up and down states have been studied as well in the brain of mice in vitro (Ikegaya et al. 2004; Rigas and Castro-Alamancos 2007) and in vivo, both in cortex (Fellin et al. 2009; Petersen et al. 2003) and thalamus (Zhu et al. 2006). However, there has not been a systematic characterization across different cortical areas, despite this being interesting for sleep and memory studies (Diekelmann and Born 2010; Vyazovskiy et al. 2006) as well as for establishing a baseline for cortical function in genetically modified mice.

Here we present a detailed characterization of rhythmic spontaneous activity across different cortical areas in the anesthetized mouse, including patterns of propagation and high-frequency content. We find that prefrontal cortex presents differences with respect to all other studied areas (primary visual, somatosensory, and motor). An analysis of the firing of single units during up states is also included.

EXPERIMENTAL PROCEDURES

In vivo extracellular recordings. Mice were cared for and treated in accordance with Spanish regulatory laws (BOE 256; 25-10-1990), which comply with the European Union guidelines on protection of vertebrates used for experimentation (Strasbourg 3/18/1986). All experiments were approved by the Ethics Committee from the Hospital Clinic (Barcelona, Spain). Adult C57BL6/SJL mice 3–6 mo old were used for extracellular recordings ($n = 40$). Anesthesia was induced with intraperitoneal injection of ketamine (75 mg/kg) and medetomidine (1 mg/kg). Atropine (0.3 mg/kg) was administered to prevent respiratory secretions. Tracheotomy was performed to increase stability during recordings. After this procedure and administration of a maintaining dose of ketamine (37.5 mg/kg ip), the animal was placed in a stereotaxic frame and air enriched with oxygen was delivered through a thin silicon tube placed at 0.5–1 cm from the tracheal cannula. A continuous infusion of ketamine at 40 $mg \cdot kg^{-1} \cdot h^{-1}$ was delivered subcutaneously to maintain a constant level of anesthesia. Methylprednisolone (30 mg/kg) was also administered to prevent inflammation. Body temperature was maintained at 36–37.5°C. Bilateral craniotomies were made at 4 sites: AP 2.3 mm from bregma, L 0.4 mm or AP 2.5 mm, L 0.5 mm (medial prefrontal cortex); AP 0.5 mm, L 1.5 mm (primary motor cortex); AP −1.5 mm, L 2.5 mm (primary somatosensory cortex); and AP −2.5 mm, L 2.5 mm (primary visual cortex) (following Franklin and Paxinos 2008). Extracellular slow wave recordings were obtained with tungsten electrodes with impedances of 1–2 MΩ. Electrodes were placed in infragranular layers (0.4 lateral and 1.0–1.2 mm deep in prefrontal cortex, 0.9–1.1 mm in somatosensory cortex, 0.7–0.9 mm in visual cortex, 1.0–1.2 mm in motor cortex). Extracellular recordings were usually obtained bilaterally, amplified with either a NeuroLog (Digitimer) or a multichannel system (Multi Channel Systems). The signal was digitized at 20 KHz with a CED acquisition board and Spike 2 software (Cambridge Electronic Design).

In vivo slow wave propagation. Arrays of $M = 16$ aligned electrodes separated by 125 μm (Neuronexus) were used to record activity propagation. We computed the speed of up state propagation across the cortex, relying on the time lags between consecutive detected up state onsets from multiunit activity (MUA) of different electrodes. We selected

Address for reprint requests and other correspondence: M. V. Sanchez-Vives, IDIBAPS, Villarroel 170, 08036 Barcelona, Spain (e-mail: msanche3@clinic.ub.es).

time series containing at least $N = 300$ up states. The average of the onset times of the same traveling up state in the multielectrode array was taken as reference for each detected up state to compute the array of relative time lags. In other words, if $T_{s,c}$ is the onset time of the sth up state in the cth electrode, the array of relative time lags is $\Delta T_{s,c} = T_{s,c} - \sum_{c=1}^{M} T_{s,c}/M$. Absolute values $\Delta T_{s,c} > 150$ ms were not considered, because these were very likely due to a failed up state detection. We explored the possible existence of different patterns of activity propagation by sorting the time lag arrays ΔT_s of the detected up states in the low-dimensional space resulting from principal component analysis (PCA) (Jackson 1991). We found that the first three principal components always represented >50% of the total variance. In this three-dimensional subspace each detected up state is a point. We worked out the "principal axis" of the point cloud, minimizing in the least-squares sense the sum of the distances of the points from this axis. Finally, the points are projected on such a principal axis in order to associate a scalar quantity to each up state and to rank them. Sorting $\Delta T_{s'}$ with such ranking, we found gradual but significant changes in the activity propagation patterns. We then pooled the up states in five equally sized groups (at least 60 time lag arrays per group), such that the first pool was $\Delta T^{(1)} = \{\Delta T_{s'}\}_{s'=1}^{N/5}$, the second pool was $\Delta T^{(2)} = \{\Delta T_{s'}\}_{s'=N/5+1}^{2N/5}$, and so on. For each group of arrays we carried out the average time lag $<\Delta T_c^{(n)}> = \sum_{s=1}^{N/5} \Delta T_{s,c}^{(n)}/(N/5)$ and its standard error (SE) for each electrode c. Finally, the speed was computed in those recordings showing a monotonic change with electrode position of the average time lag within each propagation pattern. It was carried out by dividing the distance $D^{(n)}$ between the electrodes showing the maximum and minimum average time lags by their time lag difference: $D^{(n)}/[\max_c <\Delta T_c^{(n)}> - \min_c <\Delta T_c^{(n)}>]$.

In vivo single unit with extracellular recordings. Glass recording electrodes (8–15 MΩ) were pulled on a Sutter Instruments P-97 micropipette puller (Novato, CA) from medium-walled glass and filled up with saline. Electrodes were placed in the primary motor, medial prefrontal cortex, and somatosensory cortex. A tungsten electrode similar to those described above was placed nearby the glass electrode, at <200 μm, to obtain a recording from the local network in the vicinity. Signals were digitized and acquired at 50 kHz for single-unit recordings and at 10 kHz for extracellular recordings. Agar at 4% was used to prevent the cortex from desiccation and to stabilize electrophysiological recordings.

Data analysis. MUA was estimated as the power change in the Fourier components at high frequencies of the extracellular recordings (Reig et al. 2010; Sanchez-Vives et al. 2010). We assume that the normalized MUA spectrum provides a good estimate of the population firing rate, because normalized Fourier components at high frequencies have densities proportional to the spiking activity of the involved neurons (Mattia and Del Giudice 2002). MUAs were logarithmically scaled in order to balance the large fluctuations of the nearby spikes. Up and down states were singled out by setting a threshold in the log(MUA) time series. The threshold was set to 60% of the interval between the peaks in the bimodal distributions of log(MUA) corresponding to the up and down states. The peak related to the down state was used as reference, setting there log(MUA) = 0. Singled-out sets of up and down state durations from each recording were used to estimate the nine parameters reported in Fig. 3. Up and down state durations (Fig. 3, *B* and *C*) were the averages across such sets. Frequency in Fig. 3*A* was the inverse of the average duration of the whole up-down cycles. Down-to-up and up-to-down transitions in Fig. 3, *D* and *E*, were estimated as the slope of the average profile of log(MUA) around a small time interval around the transitions ([−10, 25] ms and [−25, 10] ms for upward and downward transitions, respectively). The maximum relative firing rate in Fig. 3*F* was the maximum average log(MUA) following the down-to-up transition. The coefficient of variation (CV) in Fig. 3, *G–I*, was the fraction between the standard deviation and the mean value of the durations of up and down states and of the whole up-down cycles singled out for each recording, respectively.

All of the MUA off-line estimates and analyses were implemented in MATLAB (The MathWorks, Natick, MA). Data are displayed as means ± SE in all error bars in plots.

Single-unit recordings were analyzed with Spike2 software (Cambridge Electronic Design). Firing patterns were obtained through perievent time histograms (PETHs) triggered to the onset of up states and a bin size of 20 ms. The length of the analyzed periods for the PETHs was 300 s.

To analyze the fast components of oscillations, up and down states were detected and their respective power spectra were calculated. Power spectrum density analysis was carried out by Welch's method with 50% overlapped windows of 2,000 samples. To compare power, an average relative power was calculated by averaging within three frequency bands (beta 15–30 Hz, low gamma 30–60 Hz, and high gamma 60–90 Hz) resulting from the quotient between the power in the up states and in the down states.

Statistical analysis. Unless otherwise stated, all comparisons between means were performed with one-way ANOVA followed by Fischer least significant difference post hoc tests, and their degrees of freedom and F values are shown in Supplemental Tables S1 and S2.[1]

RESULTS

The spontaneous rhythmic activity generated in different regions of the mouse cortex (primary visual, somatosensory, and motor cortex and medial prefrontal) was recorded under ketamine anesthesia. Under these conditions, both slow oscillations and fast rhythms are generated in the thalamocortical network (Steriade et al. 1993, 1996). The slow oscillation (Fig. 1) consisted of periods of neuronal firing or up states (Fig. 1*A*, *bottom*) interspersed with rather silent periods or down states. The recordings showed the low-frequency nature of the slow waves (≤1 Hz). During up states different frequencies were generated, including high-frequency fluctuations (Fig. 1*A*, *top*), as described in detail below. Such up states propagate across the cortical tissue (Luczac et al. 2007; Massimini et al. 2004; Sanchez-Vives and McCormick 2000), and several parameters of these waves were analyzed to describe the features of these oscillations and to compare across different cortical areas.

General description of slow oscillation in the anesthetized mouse. To characterize the slow waves in the anesthetized mouse, extracellular recordings from primary visual, somatosensory, motor, and medial prefrontal cortex were obtained by means of tungsten electrodes placed in the deep cortical layers. The recordings were bilateral, and up states usually occurred concurrently in both hemispheres with a small time lag measurable at the central peak of the waveform cross-correlation (Fig. 1, *B* and *C*). The distribution of time lags between left and right hemispheres is represented in Supplemental Fig. S1 ($n = 29$ bilateral recordings; $n = 16$ mice). It illustrates that there was no significant bias toward one hemisphere to initiate the activity. The average absolute value of the time lag of the peak (mean ± SD) was 7.1 ± 10.9 ms in visual cortex ($n = 7$), 7.9 ± 9.4 ms in somatosensory cortex ($n = 7$), 5.0 ± 4.9 ms in motor cortex ($n = 6$) , and 6.4 ± 3.8 ms in prefrontal cortex ($n = 9$).

To characterize the emergent rhythmic activity, nine parameters of the oscillatory activity were quantified as in Sanchez-Vives et al. (2010): frequency of oscillation, up state duration, down state duration, slope of down-to-up

[1] Supplemental Material for this article is available online at the Journal website.

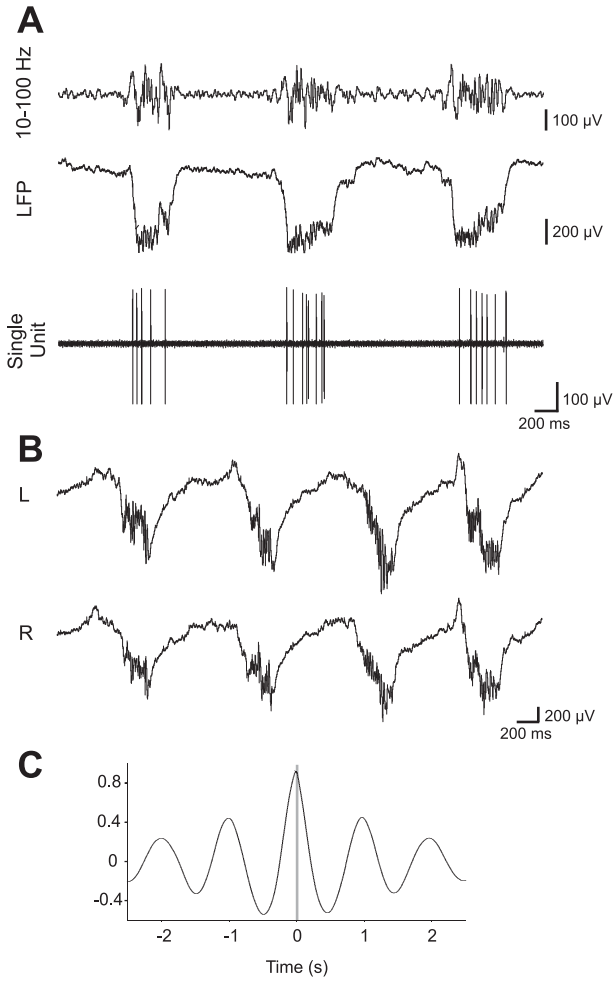

Fig. 1. Oscillatory activity in the mouse cerebral cortex during ketamine anesthesia. *A*, *top*: filtered signal of the recording (band pass 10–100 Hz) illustrating the occurrence of high frequencies in the up state. *Middle*: local field potential (LFP) in the motor cortex. *Bottom*: single-unit recording of a neuron firing in the up states. *B*: simultaneous bilateral extracellular recording in the prefrontal cortex. L, left hemisphere; R, right hemisphere. *C*: waveform cross-correlation of the 2 signals in *B*.

state transition, slope of up-to-down state transition, maximum relative firing rate, CV of the up state duration, CV of the down state duration, and CV of the up state–down state period. An operational definition of each one of these parameters is included in EXPERIMENTAL PROCEDURES.

Figure 2 illustrates representative recordings of all four recorded cortical areas and the analytical methods used to quantify their activity. We were interested in the comparative evaluation of these parameters across cortical areas, and therefore box plots were produced for primary visual ($n = 7$), primary somatosensory ($n = 7$), primary motor ($n = 7$), and medial prefrontal ($n = 10$), displaying the mean and median values (Fig. 3). These numbers of observations refer to the number of recordings included. Given that only one recording was obtained per area in each experiment, the number of recordings per area is equivalent to the number of animals. No significant differences in any of the analyzed parameters were found across hemispheres for the same cortical area.

The average oscillatory frequency of oscillation across all areas was 0.97 Hz; 54.8% of the recordings displayed frequencies between 0.6 and 1 Hz, while 45.8% oscillated at frequencies over 1 Hz. No significant differences across areas were observed between the average duration of either up (Fig. 3*B*; 0.28 s) or down (Fig. 3*C*; 0.8 s) states.

Comparing across areas, prefrontal cortex was the area that exhibited larger differences ($P < 0.05$) compared with the other areas across a variety of parameters. The slope of down-to-up transitions in prefrontal recordings was significantly faster than in the other three cortical regions. The population firing rate was also higher in prefrontal cortex than in the other cortical areas (Fig. 3*F*). Another property of the rhythm in the prefrontal cortex was the higher regularity in oscillations, reflected in a lower CV of the duration of up states compared with the other three areas (Fig. 3*G*).

Some other specific differences between areas were also detected, such as a faster transition from up to down state in motor and prefrontal cortex than in the two primary sensory areas. Further information about the statistics of this section is given in Supplemental Table S1.

Firing properties of cortical neurons during slow waves. Recordings of single units (Fig. 4) were obtained by singling out 37 single neurons from motor, 9 from somatosensory, and 43 from prefrontal cortex. Their firing patterns were analyzed with respect to the population activity in the same location recorded as the local field potential (LFP). Almost all spikes were found to occur during up states, with a few exceptions that are described below. Figure 4, *A–D*, illustrates two different firing patterns that were observed: tonic firing during the whole duration of the up state (mean firing rate 24.7 Hz; $n = 19$ neurons) versus a sparse firing (mean firing rate 5.2 Hz; $n = 70$).

We were interested to determine the number of spikes that single neurons fire per up state. No differences were observed between neurons from motor and somatosensory cortex; thus we grouped them together. Of those 46 neurons, 52.2% fired in >90% of the up states, while 37.0% fired in 50–90% of up states and only 10.9% fired in <50% of active states (Fig. 4*F*). On the other hand, most of the neurons had a sparse firing with <2 spikes per up state in 47.8% of the neurons; 26.1% fired 2–6 spikes, and the same percentage had tonic firing and fired trains of >6 spikes during up states (Fig. 4*E*).

Neurons from prefrontal cortex showed some differences with neurons from primary cortices, and we report these separately. The difference was that prefrontal cortex neurons fired in more up states and with more spikes per up state. This is represented in Fig. 4, *G* and *H*; 72% of prefrontal cortex neurons fired in all up states, while only 3% fired in less than half the up states. On the other hand, 50% of neurons had a discharge of 2–6 spikes per up state.

Taking all neurons together, we conclude that most of the neurons participate with a relatively sparse firing in most of the up states when participating in slow oscillations.

We were interested to know how the firing of individual neurons was distributed during up states. Therefore, the firing rate of all 89 units was analyzed within up states, and PETHs were built around the onset of up states. We observed a different distribution of single units' firing during up states between primary cortices and prefrontal cortex neurons, so they appear separated in the next considerations. The PETHs

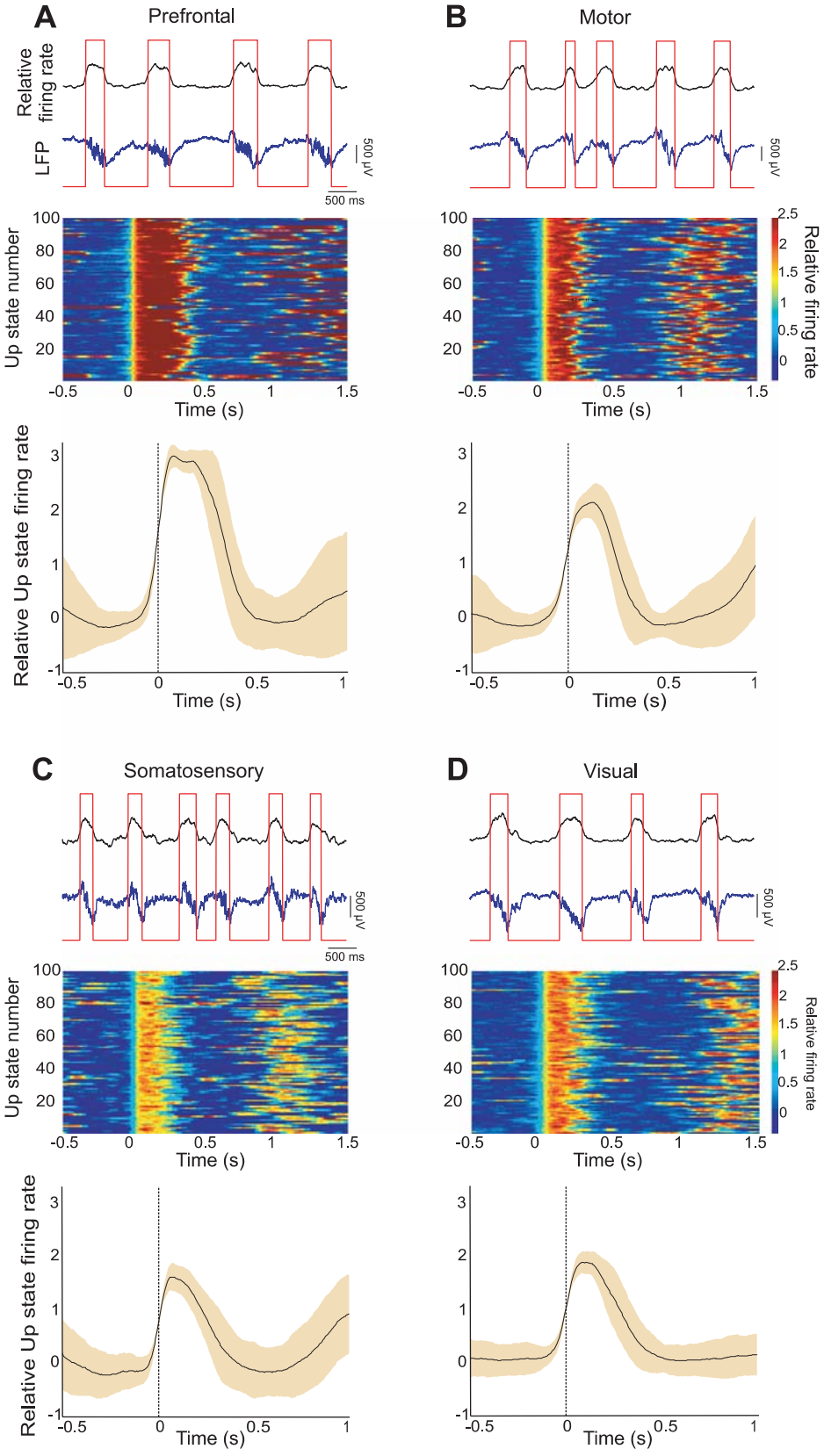

Fig. 2. Analysis of population activity in 4 cortical areas. *A*: prefrontal cortex: from *top* to *bottom*: relative firing rate, LFP, raster plots of 100 aligned up states, and waveform average of the relative firing rate. This average is the one used for the calculation of the down-to-up and up-to-down slopes and the maximum firing rate of the analyzed periods. The shade corresponds to the SD. The red boxes represent the automatically detected up and down states. *B–D*: same as *A* but in motor, somatosensory, and visual cortices, respectively.

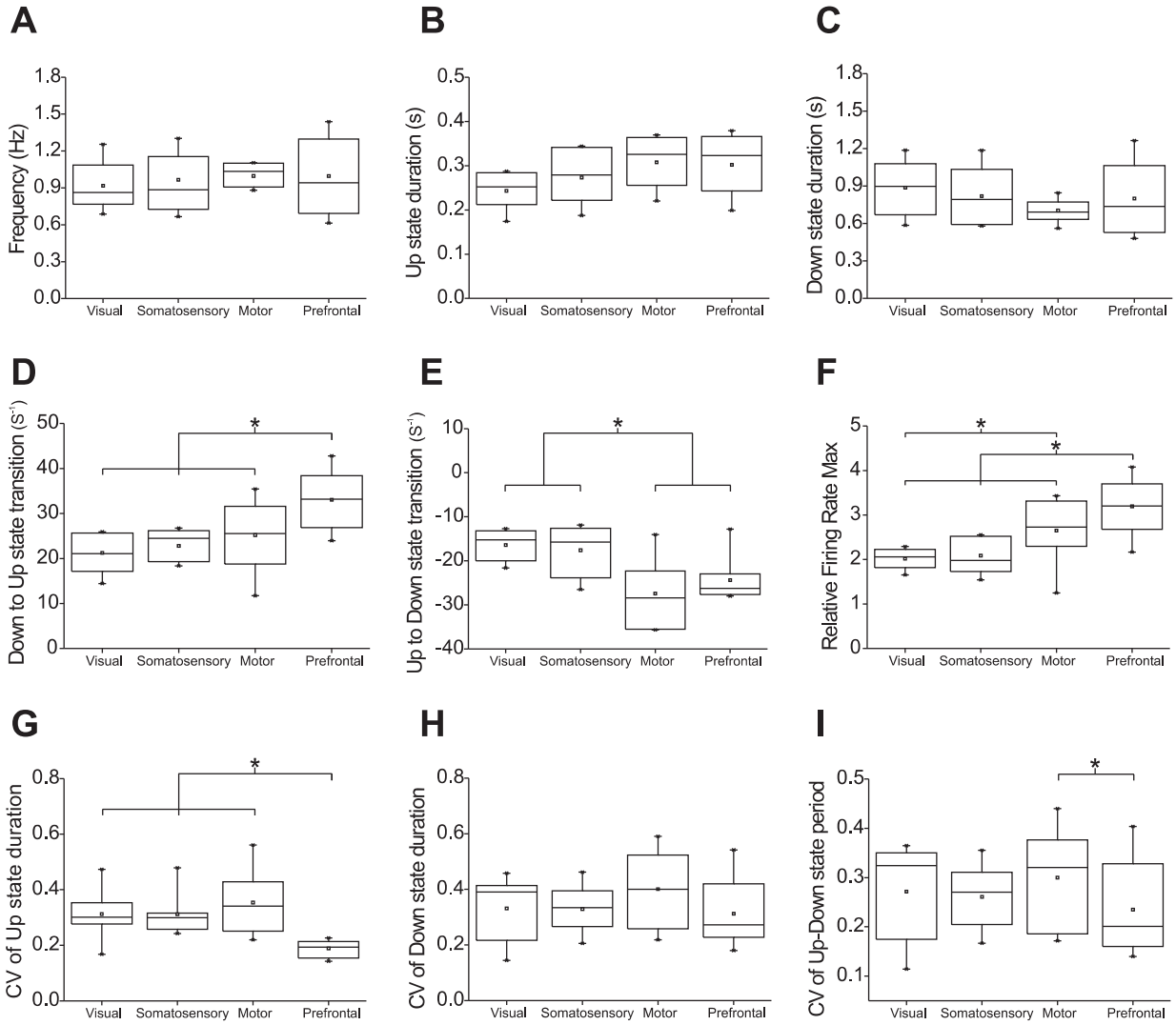

Fig. 3. Box plots representing the statistical values of the 9 parameters (*A–I*) of the slow oscillations in visual, somatosensory, motor, and prefrontal cortex. *A*: frequency of the oscillation. *B*: up state duration. *C*: down state duration. *D*: down-to-up state transition slope. *E*: up-to-down state transition slope. *F*: peak of relative firing rate. *G*: coefficient of variation (CV) of up state duration. *H*: CV of down state duration. *I*: CV of the oscillatory period. Each box represents 50% of the data (from 25% to 75%), the small square inside depicts the mean, and the divisory line is the median. Whiskers represent the 5–95% interval of the data, and asterisks represent 1% and 99% values. Recordings from the right hemisphere were used for the averages.

revealed two main groups of firing patterns: *1*) neurons with a maximum firing rate at the initiation of the up state (primary cortices $n = 15$; prefrontal cortex $n = 23$) (Fig. 5, *A* and *D*) and *2*) neurons with the maximum firing rate toward the center of the up state (primary cortices $n = 28$; prefrontal cortex $n = 15$) (Fig. 5, *B* and *E*). Of the remaining three neurons from primary cortices, one had a tonic firing evenly distributed during the duration of the up state (e.g., Fig. 5*C*) and two showed an increased firing rate preceding the termination of the up state. Of the remaining prefrontal cortex single units, three fired at the end of up states and two had rather a tonic discharge (Fig. 5*F*).

To compare across neurons and to exclude the variations in up state duration, up states were divided into five even windows (Fig. 5, *G–I*), and the firing rate of the unit was estimated for each fifth of the up state. In this way, a grand average of the PETHs for 46 neurons from primary cortices and 43 prefrontal cortex neurons was calculated (see Fig. 5*G*, *inset*). The average distribution of somatosensory and motor single units' firing showed a preferential increase of firing rate toward the center of the up state, given that the most common neuronal pattern was that in Fig. 5*B* and *E*. Prefrontal cortex single units fired toward the beginning of the up state (Fig. 5*G*, *inset*).

To further take into account differences in up state duration, all the up states recorded for each neuron ($n = 100–200$) were split into three groups according to length: short, medium, and large. When the firing rate distribution of single neurons was represented for these three groups (Fig. 5, *G–I*) it showed that the predominance of motor and somatosensory single-unit firing toward the center of the up state was not dependent on the duration of the up states. The same was the case for prefrontal cortex single units, which independently of the duration of up states tended to fire toward the beginning of up states (Fig. 5, *G–I*). In this way the single-unit firing rate distribution was evaluated in a total of 6,764 up states in the case of the primary cortices and 7,695 in the case of the prefrontal cortex.

A small number of neurons (3 of 46) had spikes in the 50-ms window preceding up states. These were the only spikes

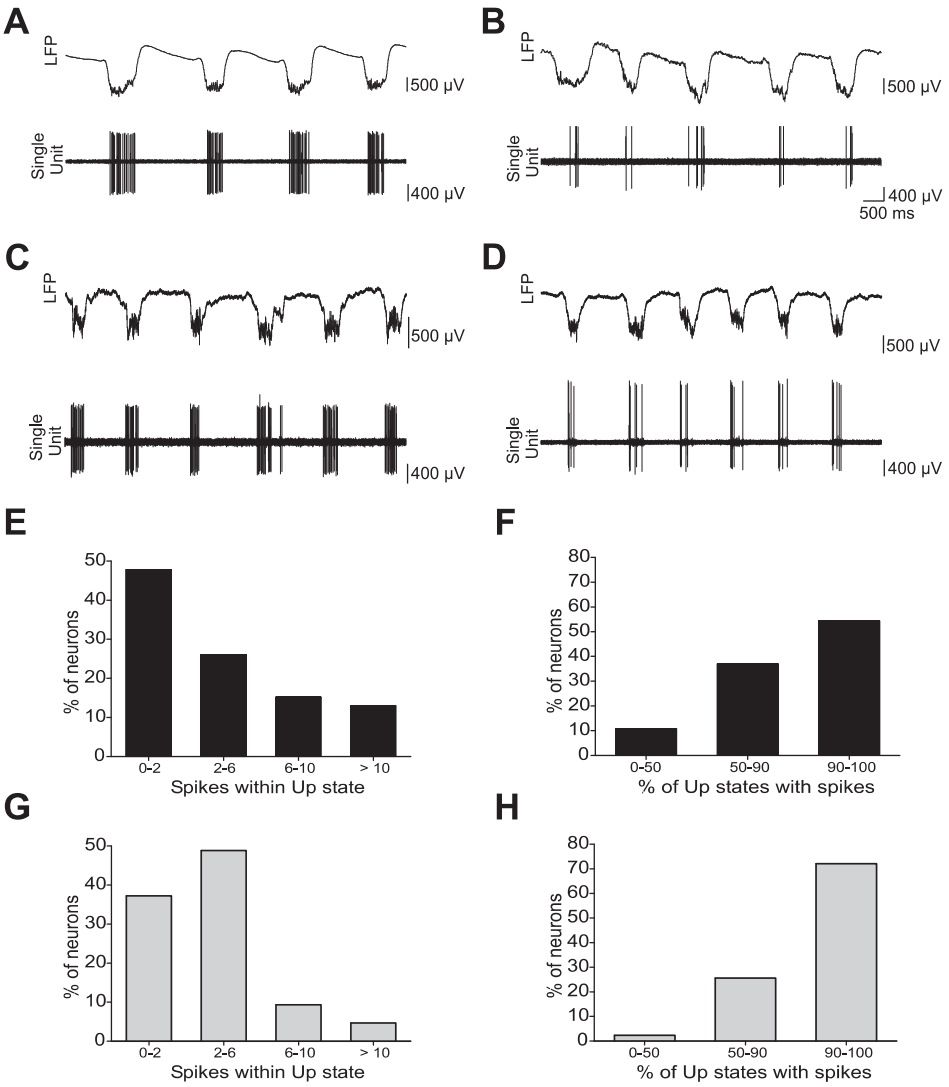

Fig. 4. Firing of single units during up states. *A*: LFP (*top*) and single-unit recording from motor cortex (*bottom*) both obtained through closely located (<200 μm apart) tungsten and glass electrodes, respectively. *B*: recording from motor cortex from a different animal; rest same as in *A*. Neurons fired either tonically during up states (e.g., *A*) or just a few spikes (e.g., *B*). *C* and *D*: as *A* and *B*, but the recording was obtained from prefrontal cortex. Note that the neuron in *C* fires more spikes per up state than the neuron in *D*. *E*: histograms of single units from somatosensory and motor cortex according to the number of spikes fired within up states. *F*: histograms of single units from somatosensory and motor cortex according to % of up states where they displayed spike activity. *G*: histograms of single units from prefrontal cortex according to the number of spikes fired within up states. *H*: histograms of single units from prefrontal cortex according to % of up states where they displayed spike activity.

observed during down states. When analyzing these spikes preceding up states, we should take into account a number of possible sources of error. One of these is the fact that single units and LFP were analyzed with two closely located different electrodes. The maximum separation between the electrodes was 100 μm. If we consider that some up states could be detected earlier in one electrode than in the other, and we consider the slowest detected propagation speed (10 mm/s), we conclude that it would take 10 ms to travel from one electrode to the other, so the firing occurring earlier than 10 ms has to be considered as preceding the up state. Another possible source of error could be the method of detection of the up state in the population. Any method of up state detection requires the determination of a threshold. In the network, though, the up state starts building up before the threshold is reached. We estimate that on average we could consider that up to 30 ms preceding the threshold there could be activity building up. Thus, if we consider both confounds together, there can be a window of 40 ms during which the firing of single units could be considered as occurring during up states. Those occurring earlier are probably spikes actually preceding up states. From this we conclude that the spikes detected in these two neurons that appear to precede up states are probably part of the building up of the activity.

Propagation of slow waves in the mouse cortex. Wave propagation was evaluated with an array of 16 electrodes separated from each other by 125 μm. The electrode was placed at 1 $\pm$ 0.2-mm depth and parallel to the midline in the motor cortex and orthogonal to the midline in the visual cortex (Fig. 6, *A* and *B*, *top insets*). We included in the analysis 20 recordings of wave propagation, 12 from motor and 8 from visual cortex, and the propagation of at least 300 consecutive up states was evaluated.

Up states were detected with the same threshold algorithm for the spectral estimated MUA used previously to determine the properties of slow oscillatory activity (see EXPERIMENTAL PROCEDURES for details; Sanchez-Vives et al. 2010). The relative time lags between up state onsets singled out from the 16 electrodes were used to identify different patterns of activity propagation. Therefore, we performed a PCA that allowed the projection of the time lag patterns of different up states into a subspace suitable for sorting them and capable of retaining the most variance. These ranked up states were pooled into five equally sized groups. The average time lags within each group

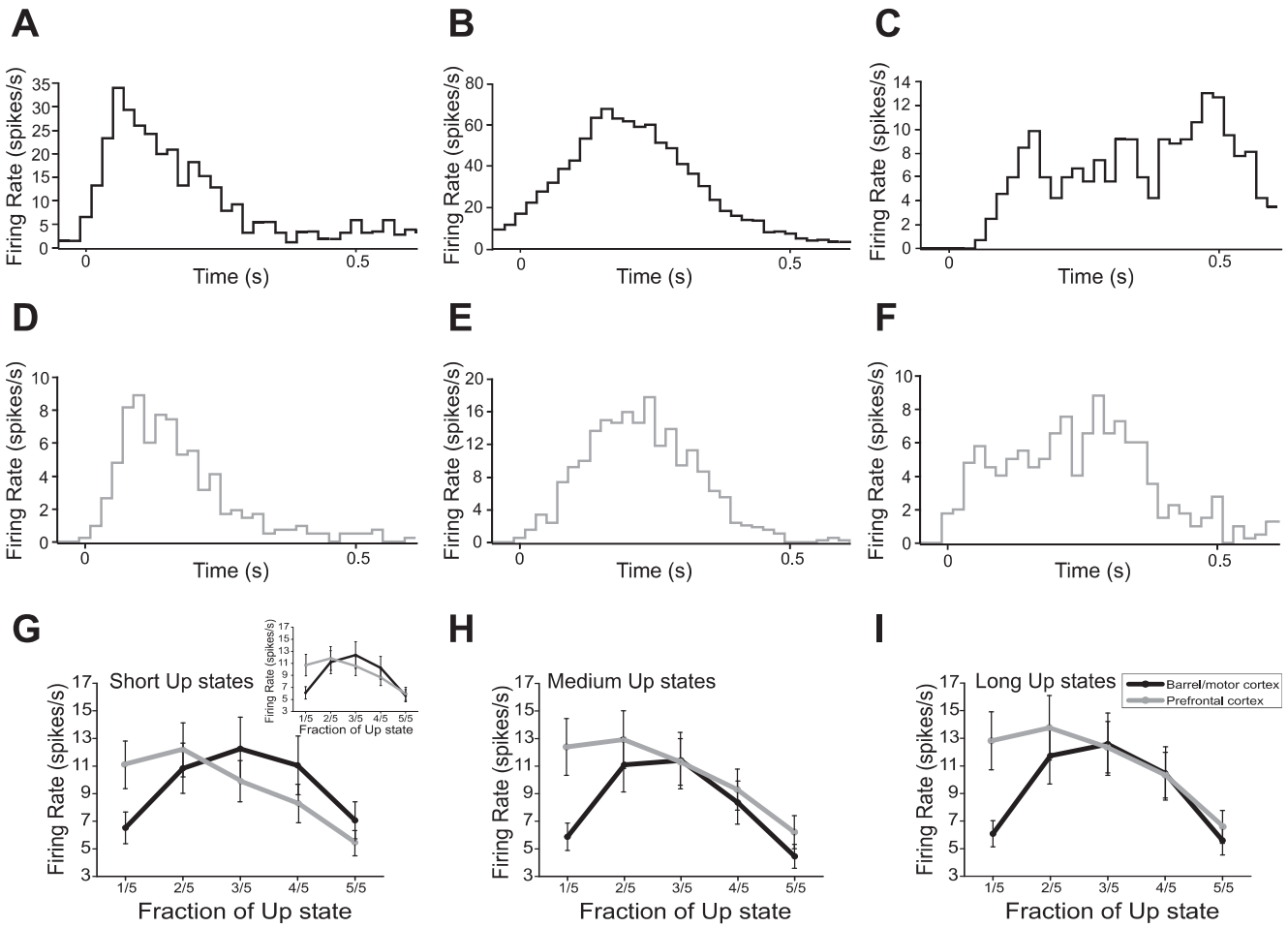

Fig. 5. Distribution of single units' firing rate during up states. *A*: perievent time histogram (PETH) of a motoneuron with the firing rate peak toward the initiation of the up state. *B*: PETH of a motoneuron that reached the peak of its firing rate toward the center of the up state. *C*: example of a motoneuron that fired rather tonically during the duration of the up state, increasing its firing toward the end of the up state. In all cases 200 s has been analyzed and the firing rate in 100–200 up states averaged for each neuron. *D–F*: same as *A–C* but for prefrontal cortex. *G*: distribution of single spikes during up states for "short" (see below) up states. Black, data corresponding to motor and somatosensory units; gray, data corresponding to prefrontal cortex units. *Inset*: grand average of the firing rate of single units ($n = 46$ for somatosensory and motor cortex, $n = 43$ for prefrontal cortex) after dividing each analyzed up state into 5 equal time windows. *H*: distribution of single spikes during up states for "medium" (see below) up states. *I*: distribution of single spikes during up states for "long" (see below) up states. Up states recorded for 200 s in each one of 46 neurons for somatosensory and motor cortex (gray traces) or 43 neurons in prefrontal cortex (black traces) were clustered in short, medium, and long durations (33.3% of analyzed up states for each neuron were classified in each group). Error bars correspond to SE. Note that the distribution of firing rate of single neurons along the up states was independent of their duration.

are shown in Fig. 6 for three typical recordings: the different symbols and related connecting lines clearly display significantly different modes of propagation within the same recording session, which occur randomly in time.

Six of twelve cases showed a clear pattern of propagation from front to back in motor cortex, in agreement with the predominant direction of propagation of oscillations during slow-wave sleep in humans (Massimini et al. 2004). In visual cortex, the majority of cases (6 of 8) showed a monotonic variation of the average time lag along the multielectrode array.

While the direction of the propagation along the axis of the electrode array was constant, the estimated speed of different waves varied continuously within a range of 8–93 mm/s. This is illustrated for both motor and visual recordings in Fig. 6, *A* and *B*. All 12 cases were highly similar to those illustrated here. The motor and visual distributions of velocities (Fig. 6, *A* and *B*, *bottom insets*) across time lag patterns and recordings are not significantly different (2-tailed Kolmogorov-Smirnov test, $P = 0.42$), although the two electrode arrays were placed in orthogonal positions.

The remaining seven cases showed more heterogeneity in the direction of propagation (see, e.g., Fig. 6*C* from a motor cortex recording). These patterns were compatible with waves propagating from other areas, e.g., with lateral propagation or with colliding waves coming from different directions. In these cases we could not confidently estimate the component of the speed of propagation along the axis of the electrode array.

Fast components of mouse neocortical slow oscillations. The frequency content of the LFP in the recordings from the four studied cortical areas (visual, somatosensory, motor, and prefrontal cortex) was analyzed. Spectrogram analysis confirmed the presence of fast rhythms in the up states (Fig. 7*A*). To study frequency content during up and down states in a systematic manner, a power spectrum analysis was carried out on recordings from prefrontal cortex ($n = 10$ mice; Fig. 7, *B* and *C*) and somatosensory ($n = 7$; Fig. 7*E*), motor ($n = 6$; Fig.

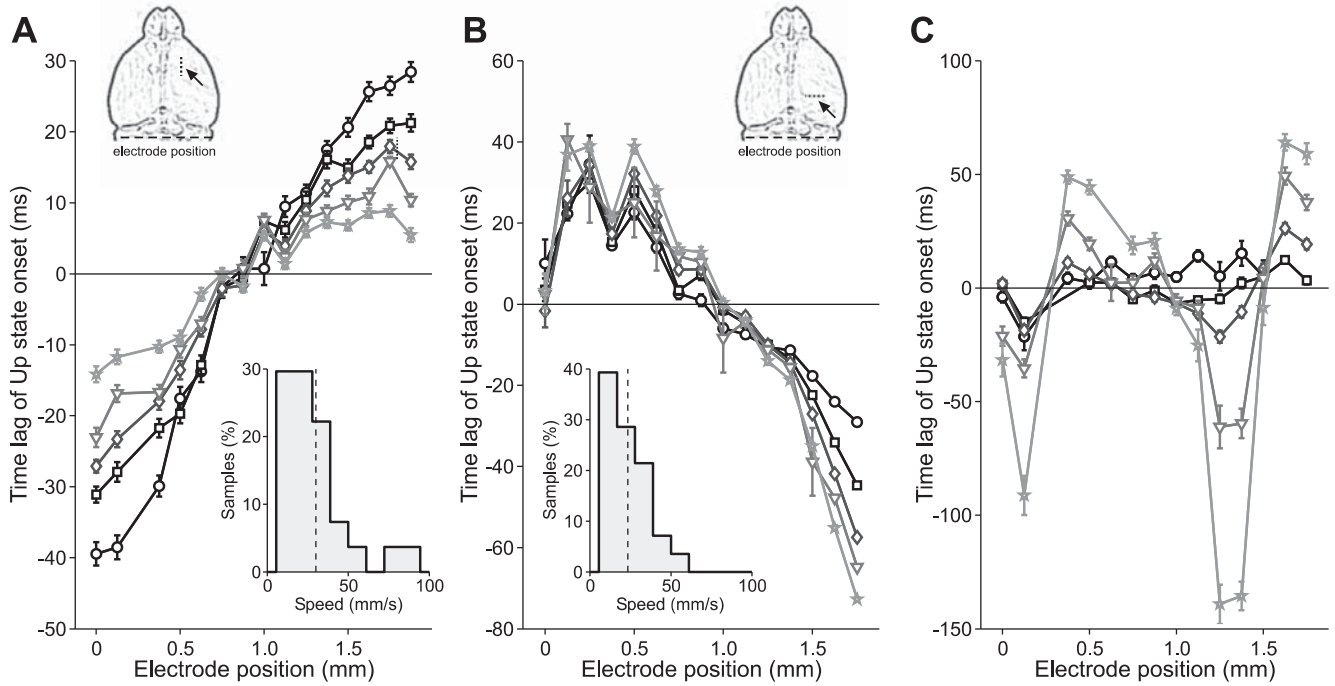

Fig. 6. Speed of propagation of up state onsets in 2 cortical areas (motor and visual) of the mouse. *A*: average time lags of up state onsets recorded with arrays of 16 electrodes in primary motor cortex. *Top inset*: location and position of the recording array (discontinuous line). Time lags were grouped in 5 different pools with similar patterns of activity propagation (each with different symbols and gray levels) obtained with a principal component analysis (see text for details). *Bottom inset*: distribution of speeds estimated from the up state pools with similar time lag patterns in the motor cortex recordings, illustrating a monotonic propagation from front to back ($n = 27$, 6 of 12 recordings). Vertical dashed line is the average propagation speed: 30.0 ± 3.9 mm/s. *B*: same as in *A* for recordings in the visual cortex. Note that in this cortical area the array was placed in the coronal plane (see *top inset*), thus orthogonal to that in *A*. *Bottom inset*: distribution of speeds for the visual cortex recordings showing a monotonic decrease of time lags from medial to lateral positions ($n = 28$, 6 of 8 recordings). Average speed: 23.4 ± 2.1 mm/s. *C*: another motor cortex example showing complex patterns of activity propagation.

7*D*), and visual ($n = 7$; Fig. 7*F*) areas. The analysis focused on the occurrence of fast rhythms that were divided into beta (15–30 Hz), low gamma (30–60 Hz), and high gamma (60–90 Hz). The power of fast rhythms was significantly larger during up than during down states (Fig. 7, *B* and *D–F*). Interestingly, for all the studied frequency bands, beta, low gamma and high gamma, power was consistently higher in prefrontal cortex than in the rest of the areas (Fig. 8, *A*, *B*, and *C*, respectively). The absolute values of beta and gamma power in up (Fig. 8, *D–F*) and down (Fig. 8, *G–I*) states are illustrated in Fig. 8, *D–I*, while the relative beta and gamma power in up versus down states is represented in Fig. 8, *A–C*. Figure 8 shows that the higher beta and gamma power in prefrontal cortex is the result of a specific increase during up states and not of other reasons like a lower power during down states in prefrontal cortex.

The beta band power was 3.5- to 7.2-fold higher in motor, somatosensory, and visual cortex in up with respect to down states. The beta power ratio was 13.2 times larger in prefrontal cortex ($P < 0.005$ with respect to motor cortex, $P < 0.0001$ with respect to somatosensory cortex, and $P < 0.0001$ with respect to visual cortex). Prefrontal cortex showed a markedly higher relative power in the gamma band (Fig. 7, *B* and *C*). We divided the gamma band into high gamma (60–90 Hz) and low gamma (30–60 Hz). In the low gamma range, the relative power in prefrontal cortex was 42.2, significantly larger than in other areas ($P < 0.001$ with respect to motor cortex, $P < 0.0001$ with respect to somatosensory cortex, and $P < 0.001$ with respect to visual cortex), where values ranged from 3.6 to 5.8. Finally, in the high gamma band prefrontal cortex showed a relative power value of 124, which was significantly different from motor ($P < 0.005$), somatosensory ($P < 0.005$), and visual ($P < 0.005$) cortices, where the values ranged from 8.9 to 14. Further information on the statistics of this section is given in Supplemental Table S2.

DISCUSSION

This study is a systematic characterization of the emergent cortical activity in the mouse cerebral cortex during ketamine anesthesia. Continuous infusion of subcutaneous ketamine allowed us to obtain stable anesthesia levels reflected in a regular slow oscillatory frequency along the duration of the experiment (6–7 h). Under these conditions, up and down states were spontaneously generated by the cortical network, and nine parameters quantifying these were compared across visual, somatosensory, motor, and prefrontal cortices. We also explored the firing of individual neurons with respect to the network activity, wave propagation, and generation of beta and gamma synchronization during up states. This information should be valuable for understanding cortical network emerging activity in the mouse model. It is also useful as a baseline of spontaneous activity generated in the mouse, allowing us to compare against experimental or genetic manipulations. Given that slow-wave sleep has a role in memory consolidation (Diekelmann and Born 2010; Marshall et al. 2006), it is also relevant to have a quantitative study as a point of reference for behavioral studies.

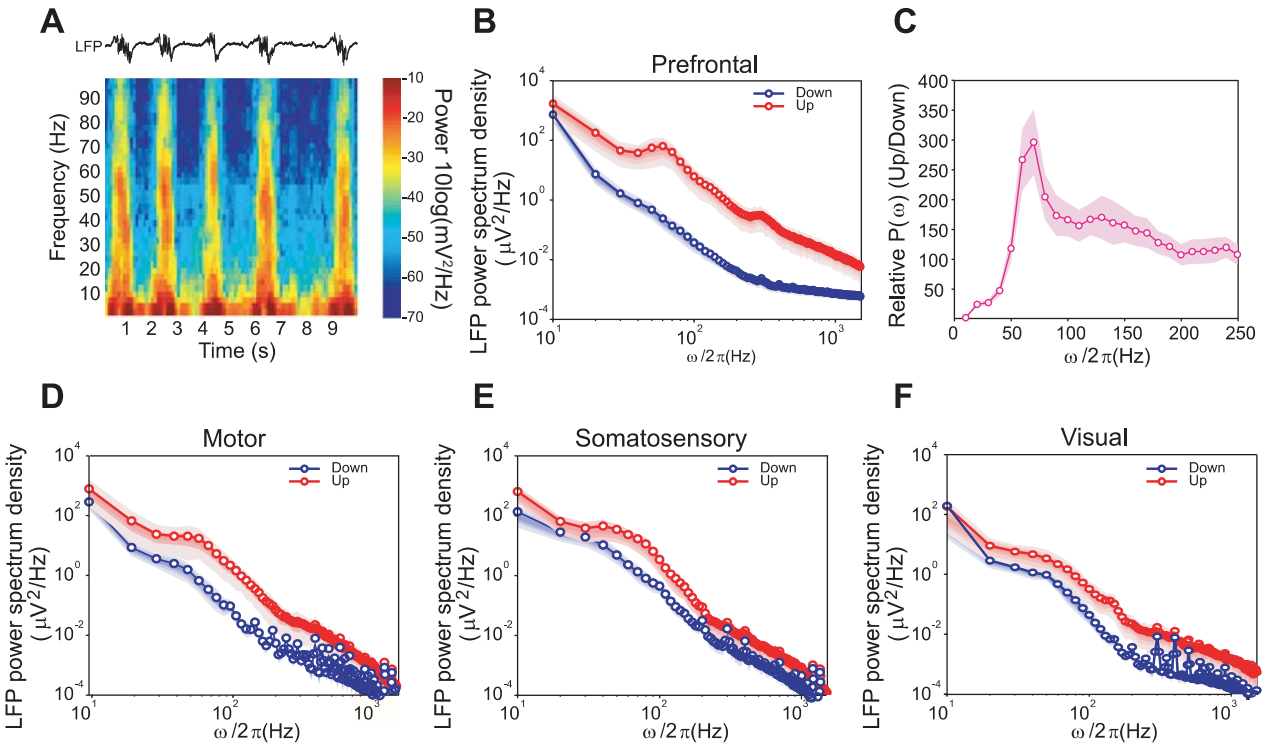

Fig. 7. Oscillatory activity during slow waves in 4 (prefrontal, motor, somatosensory, and visual) cortical areas of the mouse. *A*: spectrogram showing the occurrence of fast rhythms during the up states in prefrontal cortex. *B*: power spectrum of activity in the prefrontal cortex after separating up (red with circles) and down (dark blue with circles) states. *C*: relative power in up vs. down states calculated from the power spectra. *D–F*: power spectra of oscillatory activity in motor, somatosensory, and visual cortex, respectively.

Slow oscillations recorded in primary sensory cortices (visual and somatosensory) and primary motor cortex were highly similar, and most of the differences found in this study were observed in prefrontal cortex. Interestingly, the mean frequency of occurrence was the same in all areas, coherent with a traveling wave across the cortical network. However, the regularity of this frequency (1/CV of the cycle) was maximal in prefrontal cortex. During slow-wave sleep in humans it has been described that waves preferentially travel from frontal to occipital areas (Massimini et al. 2004). Even though any point in the cortical network can potentially start a new wave, the frontal cortex appears to be the most common initiator of a new wave (Massimini et al. 2004). Our multiple recordings following an anteroposterior alignment also found a preferential propagation from front to back in the mouse (Fig. 6*A*). The preferential origin of the rhythmic activity in the prefrontal cortex could be due to some of the distinctive features of this area that are discussed next.

In this study we found that up state duration, the down-to-up state transition slope, the maximum firing rate, and the CV of up state duration were significantly different in prefrontal cortex compared with the other three studied regions. These parameters were not statistically different between motor, somatosensory, and visual cortices, a fact perhaps due to all of these being primary areas and thus sharing some structural properties. Not only did we find higher population firing rate in prefrontal cortex, but also single-unit recordings revealed higher firing rates in prefrontal cortex during up states. Differences in the prefrontal cortical structure or in its connectivity with cortical and subcortical areas could translate functionally into some of the functional differences detected here. Interestingly, some of the differences observed in prefrontal cortex activity (higher population firing rate during up states, faster down-to-up state transition) are compatible with a higher interneuronal connectivity and recurrence in this area. The transition from down to up state reflects the recruitment of the local network for the cortical activation. When the recruitment is faster, there is a steeper transition from down to up state, as is the case when inhibition is progressively decreased (Sanchez-Vives et al. 2010) or temperature increased (Reig et al. 2010). That the prefrontal network activates faster than the primary cortices could be explained by different possible mechanisms: higher local connectivity and more efficient reverberation of activity, higher excitability, or less inhibition with respect to primary cortices. The finding of relatively more spinous neurons in prefrontal cortex in macaques and humans is suggestive of higher synaptic connectivity in this area (Elston 2000; Elston et al. 2001).

The down-to-up transition was then faster in prefrontal than in visual, somatosensory, and motor cortex. The transition from the up to down state, the silencing of the local network, was significantly faster in prefrontal and motor cortex than in visual and somatosensory cortex. This means that in prefrontal cortex, and partially in motor cortex, the initiation and termination of up states is more synchronized than in primary sensory cortices. We have observed a correlation between the down-to-up and up-to-down slopes previously, for example, in situations with increasingly blocked inhibition (Sanchez-Vives et al. 2010) or with increasing temperatures (Reig et al. 2010). The link between down-to-up and up-to-down slope is population firing rate during the up state. A fast depolarizing recruitment of the network usually leads to a high firing rate in

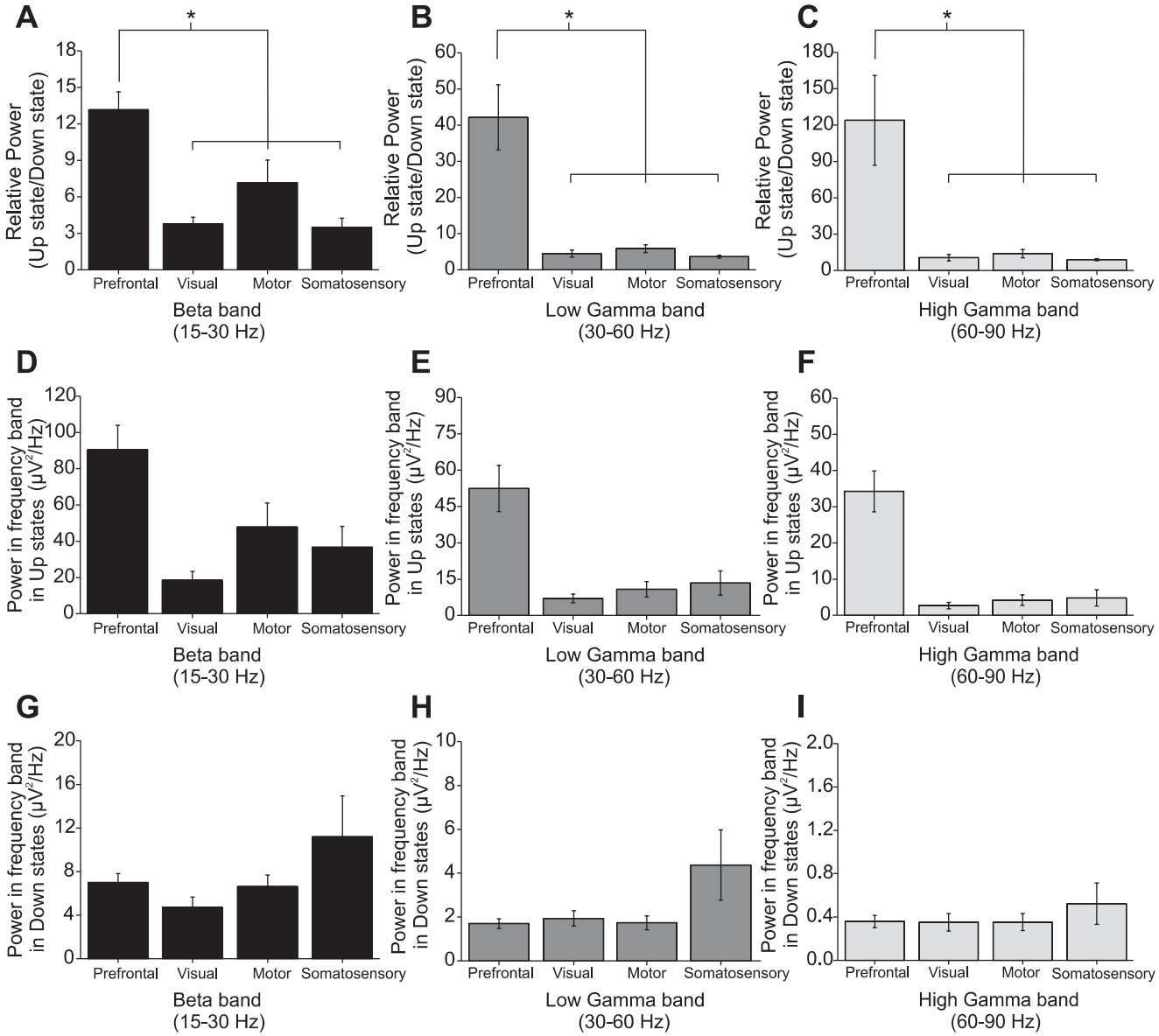

Fig. 8. Fast rhythms in the mouse cerebral cortex during slow oscillations in 4 cortical areas. *A–C*: comparison of relative power in 15–30 Hz (beta), 30–60 Hz (low gamma), and 60–90 Hz (high gamma) frequency bands across the 4 cortical areas (prefrontal, visual, motor, and somatosensory cortex). *D–F*: comparison of absolute power in up states in the beta, low gamma, and high gamma frequency bands across cortical areas. *G–I*: comparison of absolute power across areas in down states for the same frequency bands. Error bars are SE. *Significant difference $P < 0.01$.

the population. A high firing rate efficiently recruits the potassium currents that could be terminating up states and that are activity dependent (Compte et al. 2003; Cunningham et al. 2006; Sanchez-Vives et al. 2010). Indeed, prefrontal and motor cortex have significantly higher firing rates than primary sensory cortices (Fig. 3*F*). In our previous observations, fast down-to-up and up-to-down slopes were concurrent not only with higher firing rates during up states but also with shorter up states. However, we do not observe in our statistics illustrated in Fig. 3*B* any significant differences in up state duration across areas.

Our data from prefrontal cortex are in agreement with the complementary hypothesis of an increased dynamical stability of up states, for example due to a more effective recurrent GABAergic and glutamatergic synaptic coupling (Amit and Brunel 1997; Brunel and Wang 2001). Stronger stability means that changes in time of the firing rates are compelled by "restoring forces" toward the low and high firing states, making them more robust to intrinsic fluctuations in the firing activity. A strong local synaptic reverberation capable of making the high-firing regime a preferred dynamical state of the network is a way to implement strong restoring forces. Such forces induce the neuronal activity to have highly nonlinear dynamics that could explain why both the drop from the up states and the chain reaction eliciting high-frequency reverberation from down to up states are faster in prefrontal than in primary sensory cortices. This is an attractive scenario that suggests the existence along the cortex of a hierarchy of excitability and characteristics of the local circuitry: starting from "caudal" peripheral areas rapidly adapting to fast sensorial stimuli and motor actions and ending with the "rostral" associative areas whose integrative role has to be more stim-

ulus independent, and hence more dependent on local dynamics (Badre and D'Esposito 2009; Braun and Mattia 2010).

The spontaneous activity of individual neurons in the up states reflects the organization of the recurrent activity in the slow waves (Harris et al. 2010; Steriade et al. 1993). While the majority of our recorded neurons fired during >90% of the up states, most neurons participated in the active states sparsely, with <6 spikes per up state in the majority of cases (see RESULTS). The PETHs extracted from the firing of individual neurons during slow oscillations showed two main patterns depending on the distribution of spikes of single neurons during the local up state: those neurons that concentrated their firing at the beginning of the up state (more common in prefrontal cortex neurons) and those with a peak of their firing rate toward the middle of the up states (more frequent in motor and somatosensory neurons). Both patterns persisted regardless of up state duration (Fig. 5, *G–I*). These firing patterns are comparable to those found in previous studies in rodents (Erchova et al. 2002; Luczak et al. 2007) and explain how firing of neurons collaborates in the generation of the MUA that is present in the up states.

The slow oscillation is a wave that propagates along the cortical network (Amzica and Steriade 1995; Massimini et al. 2004; Sanchez-Vives and McCormick 2000; Volgushev et al. 2006). In this study we quantified the speed of propagation of the up states in two cortical areas of the anesthetized mouse: visual and motor cortex. In both of these areas values varied between 8 and 93 mm/s, with an average value of 23.4 and 30.0 mm/s in visual and motor cortex, respectively, although the distributions of measures in the two areas are not significantly different (2-tailed Kolmogorov-Smirnov test, $P = 0.42$). Interestingly, such velocities are similar even when the linear arrays of electrodes used to estimate the speeds are placed in orthogonal directions in different cortical areas: sagittal orientation in motor cortex and in the coronal plane in visual cortex. Similar values (10–100 mm/s) were reported in the mouse with the use of voltage-sensitive dyes during the propagation of spontaneous depolarizations or up states during quiet wakefulness (Petersen et al. 2003). In multisite recordings from different cortical areas of the cat under ketamine-xylazine anesthesia, the speed of propagation of the slow waves also lies around 100 mm/s (Amzica and Steriade 1995). However, the speed of propagation of slow waves during slow-wave sleep by high-density EEG in humans is 1.2–7.0 m/s, the average speed being 2.7 m/s (Massimini et al. 2004). These higher speeds may reflect not only a slight overestimation due to obliquely propagating wave and volume conduction (Massimini et al. 2004) but also a higher speed of propagation in humans secondary to long-range connectivity. In contrast, the speed of propagation in ferret cortical slices is low, around 10 mm/s (Sanchez-Vives and McCormick 2000), given that it relies exclusively on local connectivity. In making the comparison between in vivo and in vitro recordings, the limits of our speed estimate should be considered: a linear array of electrodes was used, allowing an estimation of an upper limit of the velocity. Indeed, under the assumption of quasi-planar waves a correct estimate is available only when the direction of propagation is parallel to the orientation of the multielectrode array.

In the last part of our study, we describe the existence of high-frequency (beta and gamma) synchronization during up states in different cortical areas of the mouse. Even when beta and gamma frequencies have been functionally associated to cognitive functions like attention (for a review see Wang 2010), these frequencies also emerge spontaneously during up or activated states. This is the case not only during slow-wave sleep and anesthesia (Steriade et al. 1996) but also in cortical slices in vitro (Compte et al. 2008). We find that in the mouse, the power of beta, and particularly that of gamma, is strikingly higher in prefrontal than in motor and sensory primary cortical areas (Fig. 8). We can only speculate about the cellular or network basis for these differences, but they suggest that the prefrontal circuitry has specific properties to efficiently generate gamma rhythms. These properties may involve networks of fast-spiking inhibitory neurons or specific excitatory-inhibitory loops (Compte et al. 2008; Freund 2003; Hasenstaub et al. 2005; Paik et al. 2009; Tamas et al. 2000; Whittington et al. 1995). Gamma synchronization would then emerge out of the prefrontal circuit during up states, probably being upregulated in the awake, attentive animal. This trend for the prefrontal circuit to generate beta and gamma frequencies matches its role as the origin of top-down influences during perceptual, attentive, or memory tasks (Engel et al. 2001; Gregoriou et al. 2009; Lachaux et al. 2008; Palva et al. 2010; Womelsdorf et al. 2007).

ACKNOWLEDGMENTS

We thank Maria Perez-Zabalza and David Robbe for their suggestions regarding data analysis.

GRANTS

This work has been funded by the Spanish Ministry of Science and Innovation (BFU2008-01371/BFI to M. V. Sanchez-Vives).

DISCLOSURES

No conflicts of interest, financial or otherwise, are declared by the author(s).

AUTHOR CONTRIBUTIONS

Author contributions: M. R.-M., M. M., and M. V. S.-V. conception and design of research; M. R.-M. performed experiments; M. R.-M., L. C.-S., M. M., and M. V. S.-V. analyzed data; M. R.-M., L. C.-S., M. M., and M. V. S.-V. interpreted results of experiments; M. R.-M., L. C.-S., and M. M. prepared figures; M. R.-M. and M. V. S.-V. drafted the manuscript; M. M. and M. V. S.-V. edited and revised the manuscript; M. V. S.-V. approved the final version of the manuscript.

REFERENCES

Amit DJ, Brunel N. Model of global spontaneous activity and local structured activity during delay periods in the cerebral cortex. *Cereb Cortex* 7: 237–252, 1997.

Amzica F, Steriade M. Short- and long-range neuronal synchronization of the slow (<1 Hz) cortical oscillation. *J Neurophysiol* 73: 20–38, 1995.

Badre D, D'Esposito M. Is the rostro-caudal axis of the frontal lobe hierarchical? *Nat Rev Neurosci* 10: 659–669, 2009.

Braun J, Mattia M. Attractors and noise: twin drivers of decisions and multistability. *Neuroimage* 52: 740–751, 2010.

Brunel N, Wang XJ. Effects of neuromodulation in a cortical network model of object working memory dominated by recurrent inhibition. *J Comput Neurosci* 11: 63–85, 2001.

Chauvette S, Volgushev M, Timofeev I. Origin of active states in local neocortical networks during slow sleep oscillation. *Cereb Cortex* 20: 2660–2674, 2010.

Compte A, Reig R, Descalzo VF, Harvey MA, Puccini GD, Sanchez-Vives MV. Spontaneous high-frequency (10–80 Hz) oscillations during up states in the cerebral cortex in vitro. *J Neurosci* 28: 13828–13844, 2008.

Compte A, Sanchez-Vives MV, McCormick DA, Wang XJ. Cellular and network mechanisms of slow oscillatory activity (<1 Hz) and wave propagations in a cortical network model. *J Neurophysiol* 89: 2707–2725, 2003.

Csercsa R, Dombovari B, Fabo D, Wittner L, Eross L, Entz L, Solyom A, Rasonyi G, Szucs A, Kelemen A, Jakus R, Juhos V, Grand L, Magony A, Halasz P, Freund TF, Magloczky Z, Cash SS, Papp L, Karmos G, Halgren E, Ulbert I. Laminar analysis of slow wave activity in humans. *Brain* 133: 2814–2829, 2010.

Cunningham MO, Pervouchine DD, Racca C, Kopell NJ, Davies CH, Jones RS, Traub RD, Whittington MA. Neuronal metabolism governs cortical network response state. *Proc Natl Acad Sci USA* 103: 5597–5601, 2006.

Destexhe A, Hughes SW, Rudolph M, Crunelli V. Are corticothalamic "up" states fragments of wakefulness? *Trends Neurosci* 30: 334–342, 2007.

Diekelmann S, Born J. The memory function of sleep. *Nat Rev Neurosci* 11: 114–126, 2010.

Elston GN. Pyramidal cells of the frontal lobe: all the more spinous to think with. *J Neurosci* 20: RC95, 2000.

Elston GN, Benavides-Piccione R, DeFelipe J. The pyramidal cell in cognition: a comparative study in human and monkey. *J Neurosci* 21: RC163, 2001.

Engel AK, Fries P, Singer W. Dynamic predictions: oscillations and synchrony in top-down processing. *Nat Rev Neurosci* 2: 704–716, 2001.

Erchova IA, Lebedev MA, Diamond ME. Somatosensory cortical neuronal population activity across states of anaesthesia. *Eur J Neurosci* 15: 744–752, 2002.

Fellin T, Halassa MM, Terunuma M, Succol F, Takano H, Frank M, Moss SJ, Haydon PG. Endogenous nonneuronal modulators of synaptic transmission control cortical slow oscillations in vivo. *Proc Natl Acad Sci USA* 106: 15037–15042, 2009.

Franklin KBJ, Paxinos G. *The Mouse Brain in Stereotaxic Coordinates*. Amsterdam: Elsevier/Academic, 2008.

Freund TF. Interneuron Diversity series: Rhythm and mood in perisomatic inhibition. *Trends Neurosci* 26: 489–495, 2003.

Gregoriou GG, Gotts SJ, Zhou H, Desimone R. High-frequency, long-range coupling between prefrontal and visual cortex during attention. *Science* 324: 1207–1210, 2009.

Haider B, Duque A, Hasenstaub AR, McCormick DA. Neocortical network activity in vivo is generated through a dynamic balance of excitation and inhibition. *J Neurosci* 26: 4535–4545, 2006.

Harris KD, Bartho P, Chadderton P, Curto C, de la Rocha J, Hollender L, Itskov V, Luczak A, Marguet SL, Renart A, Sakata S. How do neurons work together? Lessons from auditory cortex. *Hear Res* 271: 37–53, 2010.

Hasenstaub A, Shu Y, Haider B, Kraushaar U, Duque A, McCormick DA. Inhibitory postsynaptic potentials carry synchronized frequency information in active cortical networks. *Neuron* 47: 423–435, 2005.

Ikegaya Y, Aaron G, Cossart R, Aronov D, Lampl I, Ferster D, Yuste R. Synfire chains and cortical songs: temporal modules of cortical activity. *Science* 304: 559–564, 2004.

Jackson JE. *A User's Guide to Principal Components*. Wiley Online Library, 1991.

Lachaux JP, Jung J, Mainy N, Dreher JC, Bertrand O, Baciu M, Minotti L, Hoffmann D, Kahane P. Silence is golden: transient neural deactivation in the prefrontal cortex during attentive reading. *Cereb Cortex* 18: 443–450, 2008.

Luczak A, Bartho P, Marguet SL, Buzsaki G, Harris KD. Sequential structure of neocortical spontaneous activity in vivo. *Proc Natl Acad Sci USA* 104: 347–352, 2007.

MacLean JN, Watson BO, Aaron GB, Yuste R. Internal dynamics determine the cortical response to thalamic stimulation. *Neuron* 48: 811–823, 2005.

Marshall L, Helgadottir H, Molle M, Born J. Boosting slow oscillations during sleep potentiates memory. *Nature* 444: 610–613, 2006.

Massimini M, Huber R, Ferrarelli F, Hill S, Tononi G. The sleep slow oscillation as a traveling wave. *J Neurosci* 24: 6862–6870, 2004.

Mattia M, Del Giudice P. Population dynamics of interacting spiking neurons. *Phys Rev E* 66: 1–19, 2002.

Nir Y, Staba RJ, Andrillon T, Vyazovskiy VV, Cirelli C, Fried I, Tononi G. Regional slow waves and spindles in human sleep. *Neuron* 70: 153–169, 2011.

Paik SB, Kumar T, Glaser DA. Spontaneous local gamma oscillation selectively enhances neural network responsiveness. *PLoS Comput Biol* 5: e1000342, 2009.

Palva JM, Monto S, Kulashekhar S, Palva S. Neuronal synchrony reveals working memory networks and predicts individual memory capacity. *Proc Natl Acad Sci USA* 107: 7580–7585, 2010.

Petersen CC, Hahn TT, Mehta M, Grinvald A, Sakmann B. Interaction of sensory responses with spontaneous depolarization in layer 2/3 barrel cortex. *Proc Natl Acad Sci USA* 100: 13638–13643, 2003.

Reig R, Mattia M, Compte A, Belmonte C, Sanchez-Vives MV. Temperature modulation of slow and fast cortical rhythms. *J Neurophysiol* 103: 1253–1261, 2010.

Rigas P, Castro-Alamancos MA. Thalamocortical Up states: differential effects of intrinsic and extrinsic cortical inputs on persistent activity. *J Neurosci* 27: 4261–4272, 2007.

Sakata S, Harris KD. Laminar structure of spontaneous and sensory-evoked population activity in auditory cortex. *Neuron* 64: 404–418, 2009.

Sanchez-Vives MV, Mattia M, Compte A, Perez-Zabalza M, Winograd M, Descalzo VF, Reig R. Inhibitory modulation of cortical up states. *J Neurophysiol* 104: 1314–1324, 2010.

Sanchez-Vives MV, McCormick DA. Cellular and network mechanisms of rhythmic recurrent activity in neocortex. *Nat Neurosci* 3: 1027–1034, 2000.

Steriade M, Contreras D, Amzica F, Timofeev I. Synchronization of fast (30–40 Hz) spontaneous oscillations in intrathalamic and thalamocortical networks. *J Neurosci* 16: 2788–2808, 1996.

Steriade M, Nunez A, Amzica F. A novel slow (<1 Hz) oscillation of neocortical neurons in vivo: depolarizing and hyperpolarizing components. *J Neurosci* 13: 3252–3265, 1993.

Steriade M, Timofeev I. Neuronal plasticity in thalamocortical networks during sleep and waking oscillations. *Neuron* 37: 563–576, 2003.

Tamas G, Buhl EH, Lorincz A, Somogyi P. Proximally targeted GABAergic synapses and gap junctions synchronize cortical interneurons. *Nat Neurosci* 3: 366–371, 2000.

Tsodyks M, Kenet T, Grinvald A, Arieli A. Linking spontaneous activity of single cortical neurons and the underlying functional architecture. *Science* 286: 1943–1946, 1999.

Volgushev M, Chauvette S, Mukovski M, Timofeev I. Precise long-range synchronization of activity and silence in neocortical neurons during slow-wave oscillations [corrected]. *J Neurosci* 26: 5665–5672, 2006.

Vyazovskiy VV, Ruijgrok G, Deboer T, Tobler I. Running wheel accessibility affects the regional electroencephalogram during sleep in mice. *Cereb Cortex* 16: 328, 2006.

Wang XJ. Neurophysiological and computational principles of cortical rhythms in cognition. *Physiol Rev* 90: 1195–1268, 2010.

Whittington MA, Traub RD, Jefferys JG. Synchronized oscillations in interneuron networks driven by metabotropic glutamate receptor activation. *Nature* 373: 612–615, 1995.

Womelsdorf T, Schoffelen JM, Oostenveld R, Singer W, Desimone R, Engel AK, Fries P. Modulation of neuronal interactions through neuronal synchronization. *Science* 316: 1609–1612, 2007.

Zhu L, Blethyn KL, Cope DW, Tsomaia V, Crunelli V, Hughes SW. Nucleus-and species-specific properties of the slow (<1 Hz) sleep oscillation in thalamocortical neurons. *Neuroscience* 141: 621–636, 2006.